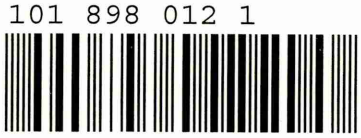

REFERENCE

The Production and Tribology of Hard Facing Coatings for Agricultural Applications

Paul Roffey

2008

A thesis submitted to Sheffield Hallam University for the degree of Doctor of Philosophy.

Collaborating Organisation: Chapmans Agricultural Ltd.

Kirsty

For your unwavering support.

"She walks in beauty, like the night of cloudless climes and starry skies"

Byron

Abstract

This research has been carried out by the author at the Materials and Engineering Research Institute at Sheffield Hallam University in collaboration with Chapmans Agricultural Ltd.

Abrasive wear is a significant issue in many industries but is of particular significance in agriculture. This research is being carried out due to the demand for a hard wearing, economical coating for use in the agricultural industry.

A primary objective has been to review and develop an in depth understanding of the type of wear suffered by metal shares in agricultural soils. The affect of soil properties and abrasive wear environments on the amount of wear that occurs, and the way in which material properties can be used to reduce or prevent this has also been investigated. A review of the diverse range of soil properties, such as the mineral content, moisture content, soils strengths has been carried out in order to create an appropriate wear test procedure.

The coatings developed for testing were modifications to an existing powder metallurgy coating. The modifications were made by the addition of selected hard phases to the powder prior to sintering. The resulting materials were characterised in terms of sinterability, hardness and abrasive wear resistance. Prior to commencing this work little or no data existed on the wear performance of the pre-existing coating.

Wear resistance has been measured using a fixed ball micro-scale abrasive wear test (also known as the ball-cratering wear test) with SiC and SiO_2 abrasives and also using a modified version of the ASTM G65 abrasive wear test which allowed testing in dry and wet modes. Limited field trials were performed to determine the abrasive wear resistance in real soil. Results from wear testing have determined that the optimum modification to the coating can improve performance compared to the unmodified coating.

Detailed scanning electron microscopy (SEM) has been performed on the wear scars and has revealed the resultant wear mechanisms and role that the hard phase additions play in improving the wear resistance. The influence of the hard phase addition on the microstructure has also been studied.

The wear volume and corresponding wear coefficient from laboratory studies have been used to determine the optimum level of addition that can be added to produce an improved wear resistance. The results show the optimum hard phase addition to be 100μm WC/W_2C particles at around 10wt.% with 15 μm WC at 5wt.% also providing improved wear resistance.

Acknowledgements

I would like to express my appreciation to the following for their input and support throughout the course of the work presented in this thesis.

Many thanks are due to my supervisor Dr Hywel Jones, who has shown great faith and belief in myself and provided me with guidance and encouragement, not only throughout this project, but throughout my undergraduate years and time within the MERI.

Thanks to the industrial sponsors, Chapmans Agricultural Ltd, in particular Mr Richard Day, who provided a great deal in terms of producing samples to assist me in my research but also organised and help run the field trials. In addition to the technical support provided by my sponsors, there is also the matter of the financial assistance that they made available; this, together with the research funding from the EPSRC made it possible for me to concentrate on my work by helping to alleviate financial matters.

I would like to say a huge thanks to everyone whom I have worked with, or alongside, both past and present, within the Materials and Engineering Research Institute over the last few years.

Contents

Chapter 4 - Tribological Testing

Chapter 5 - Materials Development and Characterisation

List of Figures

Symbols

B	Degree of wear
E	Young's modulus
Π	Pi
°	Degrees
Å	Angstroms
A'	Volume of material lost
A''	Material flow to groove edges
a_c	Critical attack angle
A_p	Contact area or interaction area
A_s	Surface area
B	Bulk density
D	Diameter
E^*	Poisson's relationship between ball & sample
E_1	Poisson's modulus of wear ball
E_2	Poisson's modulus of sample
F_m	Maximum applied load
G	Grams
H_a	Abrasive hardness
h_c	Contact depth or crater depth
h_f	Final imprint depth
H_{IT}	Nano-indentation hardness
H_b	Hardness of ball
H_m	Tool hardness
h_{max}	Maximum indentation depth
H_s	Hardness of specimen
H_{RC}	Rockwell hardness
H_V	Vickers hardness
K	Wear coefficient
k^{-1}	Wear resistance
Λ	Wavelength
K	Density of wax
Kg	Kilograms
L	Applied load
Mm	Millimetres
mph	Miles per hour
R	Radius
P	Wax-coated weight
P_f	Final contact pressure
P_i	Initial contact pressure
S/S^*	Severity of contact
S_E	Standard error
μ	Coefficient of friction
v	Vol fraction of abrasive
V	Volume
V_1	Volume including wax
V_2	Volume of wax
v_1	Poisson's ratio of wear ball
v_2	Poisson's ratio of sample
$vol.\%$	Volume percent
W	Initial weight
$wt.\%$	Weight percent
ρ	Density
ρ_a	Specific density

R	Radius
RH	Relative humidity
S	Sliding distance or suspended weight

AVL	Adjusted volume loss
BSE	Back scattered electron
CVD	Chemical vapour deposition
DSRW	Dry sand rubber wheel abrasion test
EDX	Energy dispersive x ray analysis
ESEM	Environmental scanning electron microscope/microscopy
MMC	Metal matrix composite
MIM	Metal injection moulding
MLM	Multiple load method
MSAW	Microscale abrasive wear test
PM	Powder metallurgy
PVD	Plasma vapour deposition
RWR	Relative wear resistance
SE	Secondary electron
SEM	Scanning electron microscope/microscopy
WSRW	Wet sand rubber wheel abrasion test
XRD	X ray diffraction
XRF	X ray fluorescence

Candidate's Statement

This thesis is entirely my own work unless otherwise referenced and has not been submitted for the award of a degree at any other university. The work was carried out as part of an industrial collaboration with Chapmans Agricultural Ltd, who provided and manufactured test samples.

1 Introduction

The study of wear, and in particular the prevention of the abrasive wear of soil engaging tools, has been the focus of research for well over 50 years. This peaked between the 1960's and early 1980's, and was carried out mainly by a few key researchers, but then declined and has continued to do so ever since. One of the prominent research groups involved with the study of agricultural wear was the Silsoe Research Institute which was founded in 1924. However, over the last 30 years operations were gradually scaled down and the Institute ceased operating in March 2006.

Whilst soil wear research has experienced a decline, advances in materials science have continued and the availability of lower cost materials has grown, both of which can be applied to agricultural applications. An increasing demand placed on the UK market from European and Asian manufacturers has highlighted the need for soil working tools with improved tool life, allowing companies to continue being competitive within the industry. This research has arisen due to the need for an economical soil working tool with improved efficiency and performance.

1.1 Wear prevention

A study of the literature reveals that efforts to reduce the wear occurring to soil working tools have included the use of white cast irons as a bulk material and the use of wear resistant coatings, ceramic tips and tungsten carbide tiles. The use of welding beads in varied patterns on the surface of tools has also been employed in an attempt to reduce wear by disrupting soil flow.

As might be expected some of the approaches studied showed promising results while others proved unsatisfactory. While a few studies included the use of field trials to measure wear performance, the main body of literature has concerned the testing performed under laboratory conditions. This led to many types of test apparatus being developed or modified in an attempt to recreate the mechanisms of soil wear. More importantly the research has also produced significant developments in the understanding of wear mechanisms and of further advances in laboratory based wear tests, which may allow a more accurate comparison of laboratory results with field data.

1.2 Description of research

This research was performed in collaboration with a Sheffield based agricultural equipment manufacturer, Chapmans Agricultural Ltd. One area of Chapmans expertise is the production of wear resistant powder metallurgy coatings for soil tillage tools. This study focuses on the reduction of wear to tillage tools by the further development of a metal matrix composite (MMC) powder metallurgy coating, known as Armatech™.

The use of coatings is a rapidly developing area, driven by all sectors of engineering. The potential advantages of using coatings include:

- Increased surface hardness
- Increased wear resistance
- Enhanced corrosion resistance

Whilst surface hardness can be increased by the addition of coatings, a common misconception is that an increase in hardness automatically gives rise to an improvement in wear resistance. This however is rarely the case and will be discussed in more detail in Chapter 2.

A pre-requisite of most agricultural tools is the necessity for both toughness and wear resistance, but this combination is difficult to obtain from a single material. However, a hard, wear resistant coating applied to a tough substrate can be employed to achieve this.

The Armatech coating is applied to the leading edge of soil working tools in an attempt to reduce the rate of wear. Chapmans and farmer's experience in the field has provided anecdotal evidence that tool life is extended when compared to uncoated boron steel tools. However, the agricultural sector is a highly competitive and continually expanding market, with UK companies finding ever increasing competition from overseas manufacturers. For this reason Chapmans wanted to develop Armatech to further increase its wear resistant properties and thus, create a market leading product.

1.3 Research objectives

The main objectives of this research are to:

1. **Gain a full understanding of the wear of soil tillage tools.**
2. **Characterise existing coating and manufacturing methods.**
3. **Further improve performance of existing coating technology whilst retaining its commercial viability.**
4. **Develop laboratory based wear test methods that simulate the wear of agricultural tools in soil.**

To achieve this, an in depth review of the research literature into the wear of tools in soil and methods used to reduce, or prevent wear was carried out. The published literature provided an understanding of the factors needed for consideration when investigating the wear of soil working tools. An extensive literature review of tribological testing was also performed. It was

also found that the subject of powder metallurgy (PM) coatings on tools for the prevention of wear was an area poorly understood.

An important initial aim of this study was to examine tools recovered from service to gain an understanding of the wear mechanisms occurring in soil. This was vital in order to enable reliable judgements to be made as to the ability of laboratory wear tests to recreate the wear modes found in service.

In order to further develop the Armatech a full understanding of the coating was needed, along with a review of the manufacturing processes used by Chapmans. Due to this research being part of an industrial collaboration the need to limit the amount of modifications to the existing manufacturing process was important. The coating used by Chapmans Agricultural, which is described in detail in Chapter 5, was a PM coating densified by sintering. Enhancement of the coating was carried out by the addition of several secondary hard phases. Modified coatings were assessed in terms of the quality of sinter and the level of porosity along with density and hardness measurements. Furthermore, X-ray diffraction was used to determine the resultant phases present. Another important aspect was that the resultant materials needed to not only out perform Armatech, but be cost effective.

The modified coatings that showed promising preliminary results from microstructural and hardness studies were subjected to micro-scale wear tests using laboratory based techniques. From these test results, coatings that showed signs of improved wear resistance were then tested using a larger scale laboratory wear test (ASTM G65). Both microscale and macroscale laboratory testing were performed using different environments and abrasives in order to simulate wear mechanisms associated with varied soil conditions.

During this research an opportunity arose to carry out limited field trials which enabled, to some degree, the comparison of the laboratory wear tests to actual field data.

Chapter

2

Literature Review

2 Introduction

2.1 The problem of industrial wear

The objective of this research was to develop an existing powder metallurgy coating, used primarily in agricultural applications, to increase the lifetime of soil working tools. This chapter reviews the mechanisms of wear as experienced in such applications and previous research that has sought to increase the lifetime of soil engaging tools.

2.2 The cost to the economy

A national survey carried out in 1997[1] estimated the process of wear to cost the UK manufacturing industry and public sector around £650 million every year. The costs are associated with the need to replace components due to failures or the premature replacement of parts that suffer a reduced lifespan due to wear.

In agriculture the problems caused by abrasive wear impact in several ways. Plough components subjected to excessive wear by soils are dramatically reduced in size and thus produce a poor tillage quality which can yield a poor crop growth, which affects profit margins. The worn tool also becomes less efficient and causes an increase in the rate of work required, in turn increasing the fuel consumption of the traction unit[2]. The benefits of improving tool life with respect to the agricultural industry include[3]:

- Reduced change over time leading to productivity increase.
- Reduction in change over time so seeding is more likely to occur under optimum conditions possibly leading to an increase in crop yield.
- Better wear rates resulting in shares staying sharper longer, reducing energy requirements, and therefore fuels costs.
- Reduction in wear allowing tools to operate at the required depth for longer, minimising the depth variation and increasing tillage quality.
- If life increase outweighs the extra cost of improvement then the total replacement cost is reduced.

The main area of interest in this research is abrasive wear caused by soils on agricultural tools. The abrasive wear is caused by hard angular abrasive particles present within the soils being dragged over the tool surface which is found to be the dominant wear mechanism. Impact damage may also occur due to larger stones in the soil. However, impact behaviour is not assessed in this work as field data and feedback received by the industrial collaborator showed that the materials tested were not susceptible to excessive impact damage when compared to

other brittle materials such as alumina. Standard wear testers and wear test methods currently available are also not able to assess wear performance of materials in conjunction with impact damage.

2.2.1 Types of wear

The mechanisms responsible for wear can be separated into three distinct primary groupings as follows[1]:

- a*brasive wear,*
- *adhesive and fretting wear,*
- and *erosion and surface fatigue.*

The different wear mechanisms can have different degrees of severity and hence some can incur higher costs with abrasive wear being the highest contributor at over 60%, adhesive and fretting wear 26% and erosion and surface fatigue around 11%[1]. However, this is a very simple approach and through proper examination of the wear surface, it is common to find more than one mechanism of material removal are acting simultaneously. Under corrosive environments for example components containing moving parts may suffer from corrosion and abrasive wear simultaneously (tribo-corrosion) resulting in a further increase in the rate of material removal.

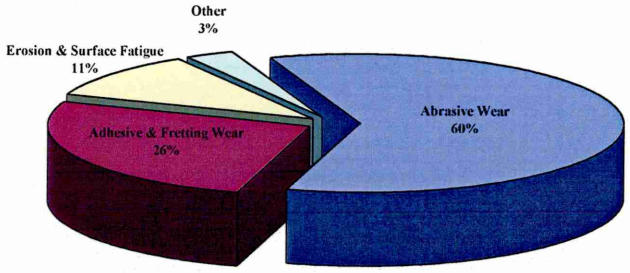

Figure 1: The contribution of wear to industry. Abrasive wear contributes up to 60% of total wear cost.

Previous studies of the most common wear mechanisms associated with agricultural wear have reported adhesion, abrasion, surface fatigue and tribo-chemical reactions[4]. These mechanisms have been subject to many investigations by a large number of researchers. However, due to the complexity of each individual wear mechanism, each worthy a study in itself, this study will focus on the group considered to be dominant in soil engaging applications, this being *abrasive wear*.

Abrasive wear is usually split into two types, (i) *sliding* or *two-body abrasive wear* where the abrasive particle slides across the tool material in a fixed orientation, and (ii) *three-body abrasive wear*, in which abrasive particles become trapped between two independent surfaces and are free to roll and cause multiple indentations on the tool surface. These two wear mechanisms will be discussed in greater detail later.

2.3 The wear of agricultural tools

Abrasive wear is the dominant wear mechanism found in agricultural environments but both two-body and three-body mechanisms are thought to be active in most cases. Whilst both are described as abrasive wear, they also act in very different ways, with varying levels of aggressiveness in respect to material removal. Post-service tools are examined to observe the actual wear mechanisms active in local soils in Chapter 4.

2.3.1 Two-body abrasive wear

This occurs due to the sliding action of two surfaces over each other, i.e. a tool surface and an abrasive particle. It is worth noting that two body abrasion, as described here, includes the action of particles on a substrate, where these particles are acting as the contact and hence only 2 bodies are involved in the wear even if a third body is applying the load to the particles themselves. A definition put forward by Moore[5] states "[two body wear is] the removal of solid material from a surface by the unidirectional sliding action of discrete particles of another material".

Khrushchov and Babichev[6] identified two processes occurring under these conditions:

(1) The formation of plastically impressed grooves that do not involve material removal.

(2) The separation of material particles (from the substrate) in the form of microchips.

The formation of plastically impressed grooves on the tool surface, shown schematically in Figure 2, is created through hard abrasive particles being forced against the tool as it is pulled through the soil. The hard abrasive particle plastically deforms the tool material pushing up the groove edges to produce fins at either side. The amount of material loss is only small from grooves formed but Aghan and Samuels[7] found that these extruded fins may become detached through further rubbing or impacts, creating secondary chips. These secondary chips may also aggravate further wear in certain situations where they either can trapped, or where they come into contact with remainder of tool, acting themselves as abrasive particles. It was concluded however, that the primary mechanism of wear and hence material loss was due to the primary microchips removed from the tool surface.

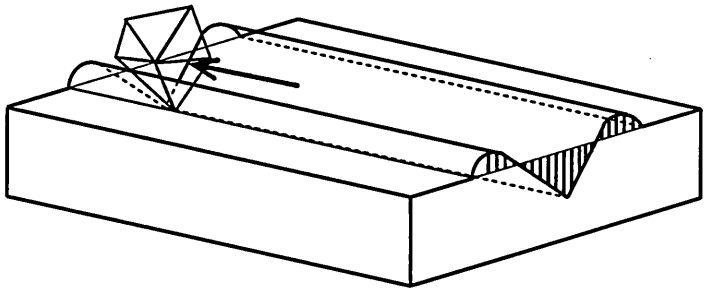

Figure 2: Schematic diagram of plastically deformed impressed wear groove on material surface caused by 'ploughing' or 'grooving' by the abrasive particle.

Kato[8] categorised the mechanisms of abrasive wear further. Three modes were identified and are shown schematically in Figure 3. Firstly *ploughing* or *grooving* wear, previously described by Khrushchov and Babichev[6], involves material displacement to groove edges with no material loss. The second mode identified was *cutting* mode, associated with microchip separation process put forward in Khrushchov and Babichev. The third mode was a transient mode between the ploughing and cutting modes labelled; *wedge forming,* where some of the groove volume is lost with some flow of material to the groove edges occurring.

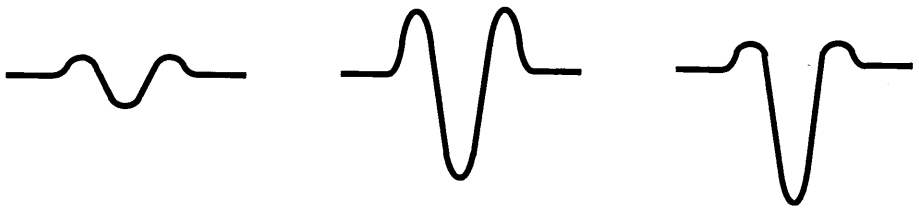

(a) (b) (c)

Figure 3: Schematic diagram of abrasive wear modes, reproduced from Kato[8] (a) *ploughing mode*; (b) *wedge forming mode*; (c) *cutting mode.*

Kato also introduced an equation (Equation 1) to determine the degree of wear occurring at one groove, β, by using the volume of materials lost from the wear groove, A', and the amount by which materials flows to the groove edges, A''.

$$\beta = \frac{\Delta A' - \Delta A''}{\Delta A'}$$

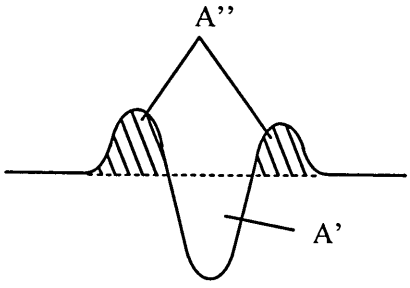

Equation 1: Method of determining the degree of wear at one groove as defined by Kato[8].

Previous estimates suggested that less than 15% of wear is removed as groove volume; these estimates were based on the supposition that all the indenting particles were identical and shared the applied load equally[9]. Work carried out by Stroud and Wilman[10] however, avoided these

assumptions and showed that much of the work done during the process of abrasion causes extreme work hardening of the surface regions and the coefficient of friction is mainly characteristic of the plastic flow of the material around the abrasive particles rather than the removal of metal as wear.

With two-body abrasive wear in agricultural applications, a soil particle is dragged along the tool surface in a ploughing/grooving action, as discussed by Kato, and pressure is applied to the particles from the resistance of the surrounding soil and stones. This pressure depends upon the soil strength and is discussed further in the soil properties and classification section below.

2.3.2 Three-body abrasive wear

Three-body abrasive wear is a mode of abrasive wear in which wear debris or abrasive particles are trapped between two surfaces with the particles not rigidly held in a single orientation as with two-body abrasive wear, but free to roll and/or slide along the surface, resulting in the removal of microchips and/or indentations of the surface[6,11].

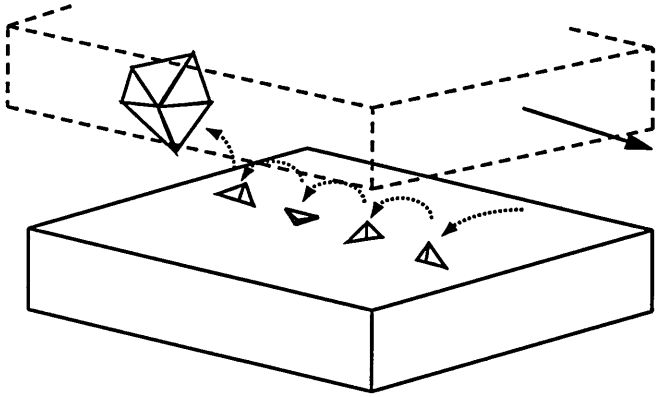

Figure 4: Schematic diagram of three-body indentations caused by 'rolling' of the abrasive particle.

Both two and three-body abrasive wear may occur in one situation due to variable environmental parameters such as applied load, soil moisture content and wear debris.

The effect of three-body abrasion was studied by Rabinowicz *et al.* using a rotating cylinder abrasive wear tester[12], it was suggested that three-body abrasion produces less severe wear rates than two-body by as much as ten times, as it was identified that the abrasive particles which are free to roll spend 90% of the time rolling along the surface and only 10% of the time actually abrading the surface.

2.3.3 Abrasive wear classification errors

Two and three-body abrasive wear mode labels are commonly used and recognised in the UK, however there has been some confusion in classifying wear modes correctly[13]. It appears that the main requirements in classifying two and three-body abrasive wear mechanisms are as follows;

> 'The abrasive of the former [two body wear] is rigidly held in place and forms grooves in the material surface with minimal material losses, while the latter [three body wear] has loose abrasive particles that are free to roll, creating chips in the surface.'

These parameters are readily accepted and are used to determine types of wear mode when discussing wear problems and tests.

However, confusion arises when considering other definitions put forward by other authors, for example Burwell[14] did not use the terms two and three-body wear and instead grouped into *cutting wear* and *abrasive wear.* Burwell defined cutting wear as a hard material causing damage to a softer surface and it was stated that the hard material in this case was the tool or counter face surface itself. Abrasive wear was defined as wear in which a hard material is damaged due to a third body, usually abrasive grit between two surfaces.

Other definitions put forward by Misra and Finnie[15] stated that two-body is a simple mode of wear but that three-body should be further subdivided into 'closed' and 'open' groups. Thus three-body open wear covers cases where a thick bed of abrasive is present or where particles are so large that the two surfaces are too far apart to have any influence on affecting the mechanical properties. It was also stated that in this mode of wear a second counter-face may not be needed at all, as in the case of a shovel digging into loose rock. Therefore, the third body is defined as any loose abrasive material backed by a counter-face or not. Furthermore, some authors argued that open and closed subdivisions should be extended to cover two-body wear also[13].

In light of this information, two- and three-body abrasive wear may be described as:

- *Two-body*; abrasive particles or asperities being rigidly held and able to cut deeply into the first body.
- *Three-body*; abrasive particles that are loose and free to roll and therefore, spend only part of their time cutting into the surface.

Using the previous example of a shovel digging into loose rock, which may be considered to be equivalent to a plough cutting through soil, and employing the wear definitions put forward above, it could be argued that the wear should be considered as three-body wear.

However, evidence from wear scars observed on these types of applications prove this form of wear to be predominantly two-body grooving or ploughing wear and not three-body cutting wear, shown in Chapter 4.

Other research into the wear of metals using abrasive bonded papers as opposed to field trials considered the wear to be two-body on the grounds that the abrasive is rigidly held and not free to roll[16]. However, arguments exist which state the abrasives are held by a backing plate,

which would suggest that three-bodies are involved, with the backing plate making up the third body and the abrasive particles the second body.

Further confusion occurs when attempting to label the wear mechanism of rock crushing and quarrying equipment, closely associated with conditions found in agriculture[13]. The rocks are free to roll and thus considered loose, so the wear mode should be labelled as three-body wear. This appears to be the correct mode as the three bodies are easily identifiable; the jaw plate (first body), the opposite jaw plate (counter-body) and the rocks (third body). However, the large particle size and gripping action of the jaws mean that at the moment of abrasion, the abrasive particles are rigidly held and two-body abrasion grooves are created on the surface.

This present complication in correctly classifying wear modes contributed to other approaches of classification. One such approach attempted to classify by the means of the stresses involved. These are listed as follows; *gouging abrasion*; *high-stress abr*asion such as grinding; *low-stress abrasion* such as scratching; and *solid particle erosion.* With the distinction between low-stress and high-stress applications indicated by whether the abrasive particle fractures during the abrasion process. This approach is favoured in the United States and Australia over the two- and three-body system used commonly in Europe. A drawback to this approach is that the parameter of whether the abrasive particles are free to roll or are constrained is overlooked[13].

It was suggested by Gates[13] that the two- and three-body approach be abandoned and instead a qualitative system of classifying by means of severity of wear should be adopted. For classifications in dividing *low-stress; high-str*ess; and *gouging,* with abrasive wear being subdivided into *mild; severe;* and *extreme* regimes, see Table 1.

Table 1
Proposed severity-based classification for abrasive wear put forward by Gates[13].

Typical Situations	Abrasive wear mode		
	Mild	Severe	Extreme
Particle size	Small	Moderate	Large
Constraint	Unconstrained	Partially constrained by counter face	Strongly constrained
Particle shape	Rounded	Sharp	Sharp
Contact stress	Low – insufficient to fracture particles	Moderate – sufficient to fracture particles	Very high – may cause macroscopic deformation or brittle fracture of material being worn
Dominant mech.	Micro-ploughing	Micro-cutting	Micro-cutting and/or micro-fracture
Equivalent terms	• Low-stress abrasion • Scratching abrasion • Low-stress three-body	• High stress abrasion • Grinding abrasion • High-stress three-body • Low-stress two-body	• Gouging abrasion • High-stress two-body

It was stated that the classification system shown in Table 1 was an initial draft version and needed further discussion to classify each mode more accurately and to eliminate any ambiguities. Once finalised however, it would remove further confusion in labelling wear modes. It was noted that a possible problem with the proposed system could be that it is situation based and suffers from focusing on one aspect of the situation and leads to other potentially important parameters being ignored, and that attempting to describe all the important variables is complex.

The use of the terms two and three-body wear have been applied for long periods of time and in a large body of literature. So, while the argument put forward by Gates is recognised and considered of importance in correctly recognising and labelling wear modes, the common terms used to describe two-body wear (parallel grooving abrasion) and three-body wear (rolling abrasion) will be adopted for ease and continuity throughout this study. Wear exhibiting both grooving and rolling wear will be described as a mixed mode regime.

2.3.4 Material hardness vs. abrasive wear resistance

The relationship between hardness and relative abrasive wear resistance of annealed pure-metals has been explored extensively revealing a linear relationship[6]. However this relationship does not apply to alloyed materials, materials having had surface treatments carried out or materials containing different microstructural phases. A selection of materials all possessing the same hardness perform differently in wear tests due to the differences in microstructure, elemental compositions, dispersed phases and carbides/borides present. There is no simple relationship between hardness and abrasive resistance and therefore materials are not able to be characterised by hardness alone. Work by both Weiss[17] and Khrushchov and Babichev[6] under

laboratory conditions, have shown that while a linear relationship between hardness and abrasive wear resistance may occur with pure metals the introduction of alloys or steels with increased carbon levels means that this relationship no longer applies, as shown in Figure 5.

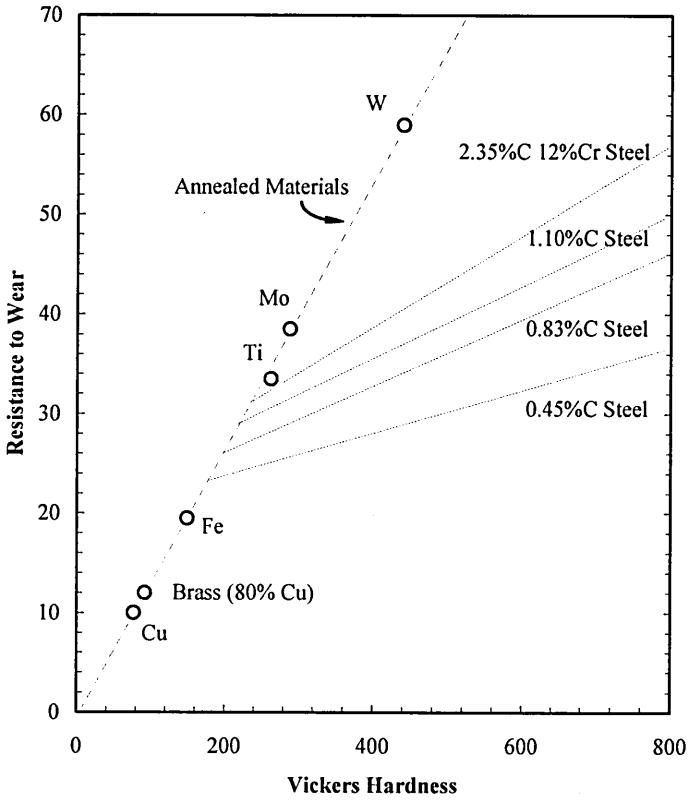

Figure 5: The relative wear resistance of some metallic materials on hard abrasive. Corundum 180grit, 80 μm, $H_a = 2290\ H_V$. After Khrushchov and Babichev 1960[6].

Work carried out by Richardson[18] under two-body grooving conditions showed that wear volume is significantly reduced when tool hardness, H_m, exceeds 80% of the hardness of the abrasive, H_a, at this point deterioration of the abrasive commences. According to this argument, with the hardness of the silica that is commonly found in soils being around 1100 H_V, then the bulk H_m should be 900 H_V or greater to improve wear resistance.

Rabinowicz *et al.* observed the effect of material hardness on the abrasive wear resistance under strictly controlled three-body laboratory conditions[12]. An increasing linear relationship was observed between tool hardness and abrasive wear resistance when the two opposing surfaces were of the same material. Introducing a harder material such as titanium as the opposing surface caused increased relative wear on the opposing softer surface.

Avient, Goddard and Wilman[19] argued that the abrasion process is dependent on the amount that a grit particle can penetrate the wearing surface, which is both a function of material hardness and ductility/strength factors of the wearing surface and the abrasive particle.

In contrast Misra and Finnie stated that work hardening does not increase the wear resistance of a material. Results showed that under two-body abrasion, three-body abrasion and erosive wear

further work hardening did not yield any increases in the wear resistance. This was concluded by the fact that the surface is heavily cold worked during the wearing process, which causes the material to reach its maximum attainable hardness[20].

In further work carried out by Richardson[21] the maximum hardness, H_u, of a range of metals and single phase alloys was determined after having their surfaces heavily strained under three conditions; shot-peening, surface wear in stony soil conditions and by working the surface with a blunt trepanning tool. Measurements were made using a Vickers micro-indenter. This attempted to explain more fully the wear behaviour under different abrasive conditions. It was suggested by the author that previous studies carried out to determine a relationship between tool hardness and relative wear resistance were carried out with materials that had not attained H_u. Richardson's work involved taking hardness measurements directly on the worn surfaces. It was found that generally during abrasion the whole surface does not harden fully to H_u, although local limited regions do so. It was stated, however, that wear resistance is certainly related in a more systematic way to H_u than to surface hardness before wear.

A common misconception is that an increase in hardness directly results in improved wear resistance. However, the research has shown that whilst this may be the case for pure metals it is not the case for alloys or pure metals containing hard phases. It has also been shown that wear is proportional to the amount an abrasive particle can penetrate a surface, the major principle behind hardness determination; however, alloys and multiphase materials possess various phases of differing hardness and bulk hardness alone is not sufficient to determine wear rate.

2.4 The influence of soil condition on wear in agricultural applications

The influence of soil is a major factor in determining the service life of agricultural tools. The properties of the soil can influence the rate at which a tool wears but also the pattern at which a tool will wear, for instance wet soils have been shown to wear the underside of a tool at a higher rate when compared to dry soils. A range of factors are associated with the mechanism of agricultural abrasive wear and thus the life of the tool as stated by Foley[54]. These factors include the following:

- *Soil properties*; hardness, size and shape of abrasive particle will affect the amount and severity of wear occurring.
- *Abrasive behaviour*; whether the abrasive particle shatters and remains sharp when coming into contact with the tool, or whether, the particles deform and become rounded or blunted.
- *Soil strength*; applied loads may be increased caused by stones in soils and/or moisture.

- *Ploughing conditions*; the type of ploughing operation and speed of operation determines the load on the tool.

2.4.1 Soil properties and classification

Although soils differ around the globe, the common abrasive found in all soils is in the form of silica. The earth's continental crust, the source of all rocks, minerals and thus soils is made up of around 60% by weight silica[22]. The different wear mechanisms and rates of wear observed in various soils are caused by factors such as the ratio of stones and abrasive particles present in the soils, the particles sizes and the moisture content.

The common constituents of British soils are various forms of silica such as quartz, flint and chert[52] with varying amounts of stones and water contents, and also oxides of iron and aluminium. The average hardness of British soils is stated to be around 1060 on the Vickers hardness scale[23]. The abrasive nature of soil is related to the abrasive particle size, shape and hardness and the water content which contribute strength of the soil. The load experienced by tools and speed of ploughing are also found to affect wear[2,5,22,24]. The wide variation of soil types across Europe and even across the UK is shown in Figure 6.

Table 2
Distribution of fine particles in a typical soil as classed by the British Soil Association found in BS1377[25].

Soil	Particle size [mm]	
Very coarse soils	Boulders	>200
	Cobbles	60 – 200
Coarse soils	Coarse gravel	20 – 60
	Med gravel	6 – 20
	Fine gravel	2 – 6
	Coarse sand	0.6 – 2.0
	Med sand	0.2 – 0.6
	Fine sand	0.06 – 0.2
Fine soils	Coarse silt	0.02 – 0.06
	Med silt	0.006 – 0.02
	Fine silt	0.002 – 0.006
Clay	Clay	<0.002

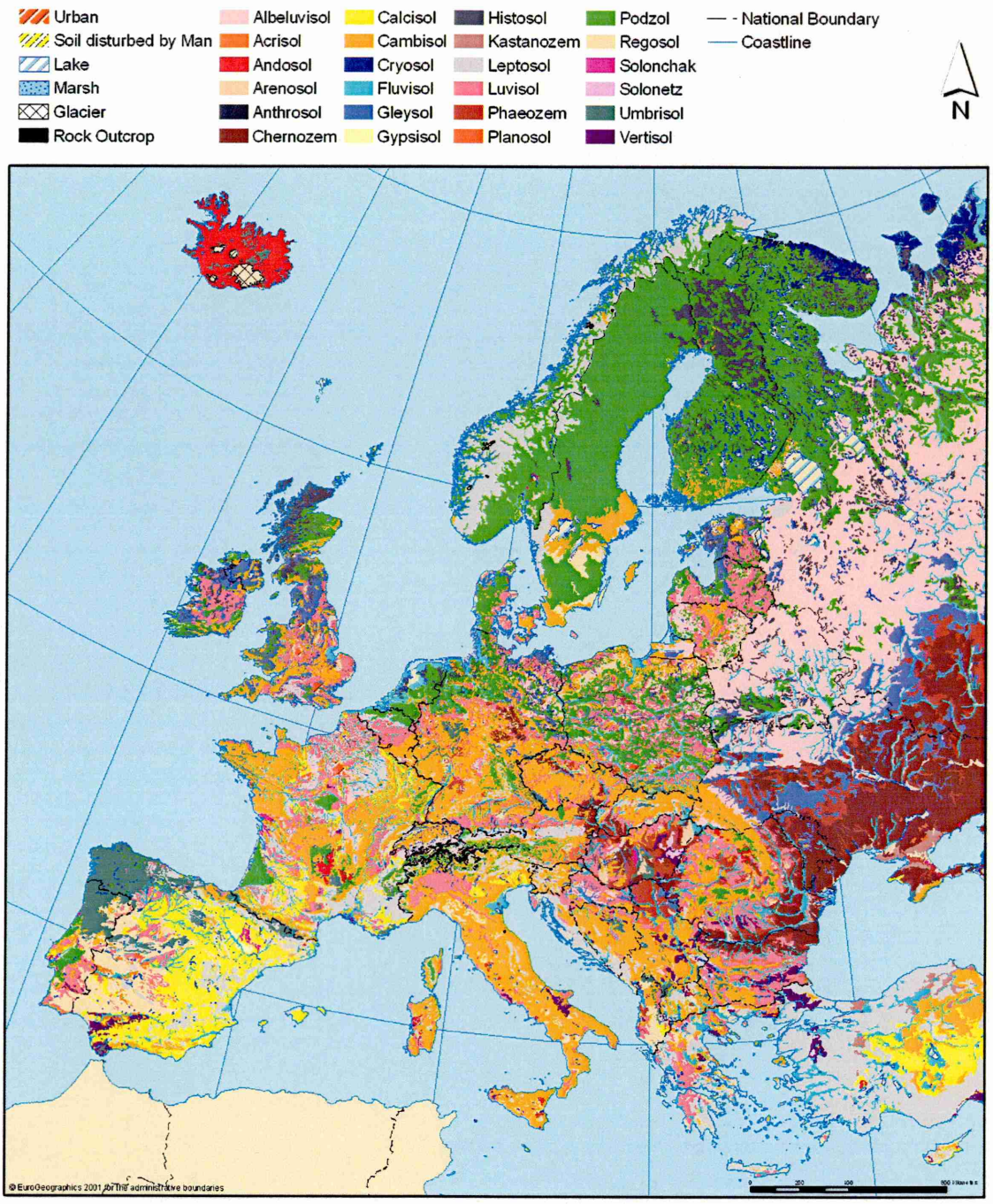

Figure 6: Soil types found across Europe[26].

The classification and distribution of typical soils can be found in Table 2, where it is shown that particles range from <0.002 mm to >200 mm diameter.

Studman stated that stones present in soils gave rise to two types of loading on the tool[27]:

(1) An impact pulse lasting less than a millisecond caused by inertia of the stone.

(2) A 'penetration load' which arises more slowly as the stone is pushed out of the way of the tool.

In work carried out assessing the wear of cultivator shares in south Australian soils, Ferguson, Fielke and Riley found that as gravel content increased up to an optimum level the wear rate of

a tool also increased[3]. It was observed that tool life was greatest when the soil contained no stones larger than 2 mm. Research carried out by Ferguson, Fielke and Riley indicated that Fitzpatrick *et al.*[28] identified an ironstone gravel content of 20% did not yield further increases in wear rate. It was suggested that below 20% gravel content the gravel is held rigidly by the hard-setting soil matrix and above this point there is insufficient soil to hold the gravel, leading to the stable wear rate, Figure 7. However, it is worth noting that this work was conducted in South Australia, and the conditions found in this area differ from those in the northern hemisphere, for example; the annual rainfall is much lower leading to lower soil water contents which would suggest a harder setting soil.

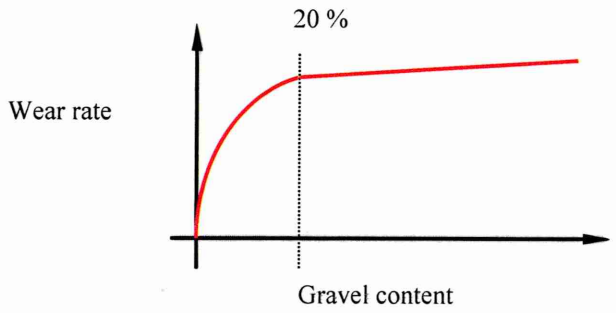

Figure 7: Schematic graph showing the effect gravel content on wear rate. Increases above 20% gravel content yield little increases in wear rate.

In strong soils, weak or large abrasive particles tend to shatter under impacts with a tool creating further sharp facets on the particles which can create further wear of the tool. In weak soils, strong or small particles tend to be blunted by plastic flow under impact from the tool and therefore the chances of material removal from the wearing surface are reduced. In laboratory tests using various abrasives Richardson found that ironstone, a fine-grained, heavy compacted sedimentary rock, the main components being the carbonate or oxide of iron, clay and/or sand, readily fractures due to its weakness. This creates more sharp facets capable of indentation, and it was suggested that it is rendered a more effective abrasive than other constituents of soil such as smooth flint, even though flint produced a deeper wear groove[23].

Research carried out in South Poland showed that carbon steel experienced 40 - 100% higher wear in sandy loam soils then in light clay soils. It was suggested that the sandy loam soil possessed a larger abrasive particle size which increased the load per particle[29].

Richardson has stated that while the amount of wear is expected to be proportional to the load on the tool, wear should be independent of the particle size distribution of the soil[18]. Field tests, however, showed that worn specimens in all types of soils were heavily grooved or scratched perhaps by the stones present within them. It was also found by Richardson that an increase in soil strength did not increase the amount of wear occurring, although there is some uncertainty as tests may not have been carried out over a sufficient range of soils strengths.

A number of previous researchers have concentrated their research on soil properties, and more commonly the effect of the hard abrasive particle within soils on wear. However, it has been shown that soil is a complex composite system with many variables. Abrasive size, shape and hardness all affect the severity of wear along with moisture and gravel content. A fuller understanding of soil as an abrasive system is needed. Soil properties such as size and shape, orientation, hardness, soil moisture levels, the effect of load and speed on wear rate along with other factors will now be considered.

2.4.2 The effect of abrasive properties

Extensive research has been performed to assess the affect of abrasive particle properties on wear. The conditions of the supporting environment and its parameters also contribute to how the particle attacks a material surface. The major factors are considered below.

2.4.3 Particle size and shape

It was found by Khrushchov and Babichev[6], and by Aghan and Samuels[7], that chip cutting and rubbing of a surface depends upon the shape of the indenting particle. More rounded particles tend to slide or roll along the component surface creating plastically deformed grooves, but cause partial chip formation when the indentation strain* exceeds a certain value.

It has been found that volumetric wear increases to some critical point with the increase in abrasive grit size diameter, around 100 μm, Figure 8, it then continues to increase after this point at a reduced rate[30]. This is consistent with findings by Misra and Finnie[31], who used AISI 1020 steel samples at 3 applied loads and silicon carbide (SiC) abrasive. They discovered that the applied load had no affect on the wear rate of the steel and only the size of abrading particle affected the wear rate, with the highest rate occurring at a particle size of 100 μm.

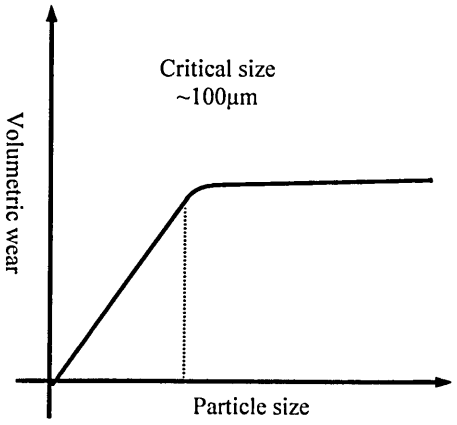

Figure 8: The effect of abrasive particle size on the volumetric wear[30].

The shape of the abrasive particle also affects the amount of volumetric wear occurring, with sharp particles producing more wear due to a cutting and gouging action[31]. Particles that are

* Depth of indentation divided by the diameter of the indenter.

more 'plate-like' reduce wear as they have a tendency to lie flat and not cut into the material surface. This relationship was also observed in work carried out by Rabinowicz *et al.*[12] under three-body conditions and by Mulhearn and Samuel[40] using bonded abrasive papers. It was stated that wear produced by smaller particles, below a critical size (100 μm) was linear, but thereafter the wear rate became nearly independent of abrasive particle size (Figure 8). The abrasive particle diameter at which full abrasion occurs was found to be the same order of magnitude as the average diameter of the loose wear particles of sliding materials, around 100 μm. It was stated, however, by Stroud and Wilman[10] that although practically all particles produce some wear, it is the more acute angular or spade like particles in favourable orientations that are responsible for the main part of wear. This was contradicted however by Rabinowicz, who stated that spade like particles were least likely to cause wear. It is suspected that the comment regarding favourable orientation may be the determining factor.

The effect of abrasive particle size was studied by Sevim and Eryurek[32]. The wear resistance of non heat-treated and heat-treated steels was measured as a function of abrasive particle size. They concluded that an increasing linear relationship exists between abrasive wear resistance and hardness depending on particle size for non-heat treated steels. With a parabolic relationship existing between wear coefficient and abrasive particle size, given by the equation below:

$$\kappa = 9.2\sqrt{d}$$

Equation 2: Relationship between wear coefficient and particle size.

Where d is the abrasive particle size (m). For heat-treated steels they found that the relationship between abrasive wear resistance and hardness showed positive intercepts on the ordinate depending on abrasive particle size, and that heat treated steels have lower resistance to wear than non heat-treated steels of the same hardness. It was also stated that relative wear resistance and hardness related linearly for non heat-treated steels and that abrasive particle size did not affect the relationship between hardness and relative wear resistance. However, it was concluded that relative wear resistance for the heat-treated steels is dependent upon the abrasive particle size.

It was suggested by Avient, Goddard and Wilman[33] that abrasives embedded in the wearing surface may cause an increase in wear resistance against attack from smaller grit sizes effectively acting as a hard phase.

2.4.4 Abrasive hardness

Richardson[34] found that relative wear resistance is dependent upon the abrasive hardness unless the hardness was very much greater than that of the wearing material; as the hardness of the wearing material approaches that of the abrasive then wear decreases rapidly. It was shown

that the wear characteristic of hard and soft abrasives is very similar but with more damage occurring to the softer abrasive grit, and that scratching ceases when the yield stresses of the wearing material and abrasive are equal. An important conclusion from Richardson's research suggested that the volume of wear is constant when H_m/H_a <0.8 and where H_m/H_a is >1.2, the wear volume reduces since deterioration of the abrasive particles commences. In order for soil working tools to experience reduced volume losses, the hardness of the tool would need to be in the region of >900 H_V, which is not acquirable with cast irons and steels alone.

An increasing linear relationship between abrasive hardness and wear rate of AISI 4340 steel under three-body conditions was reported by Misra and Finnie[15,35], furthermore, Wahl and Wellinger and Uetz found the same relationship exists for two-body abrasion and erosive wear.

2.4.5 The effect of soil moisture content on wear rate

Tests carried out by Rabinowicz suggested that high humidity increased the wear rate of tool between 10 and 20%[12]. Experiments carried out during summer months where the humidity was higher saw wear rates increase when compared to identical tests carried out in winter months. To observe this effect fully, Rabinowicz performed a series of test in a controlled humidity chamber, and found that high humidity caused the wear rate to increase by 15%. It was suggested that water vapour acted in a flushing manner removing wear debris and increasing the effectiveness of abrading action. This phenomenon was also observed in previous experiments using oil as a lubricant, which suggested that the action was the same but with a reduced rate in the case of water vapour. However, tests carried out to observe the effect of water content in soil revealed that the effect is small and only considered when observing low wear intensity conditions[6].

Natsis *et al.*[2] found that soil water had different effects subject to soil types. For example it was reported that in loam and clay soils the amount of wear suffered by the tool decreased as the water content increased and in sandy soils an increase in water content led to an increase in volumetric wear, see Figure 9. Upon reflection, this is perhaps due to loamy soils being more porous and being able to take up more water which then acts as a lubricant.

It was stated by Richardson that no evidence existed to show that moisture content has a significant effect on wear, except through its influence on the overall strength of the soil[23].

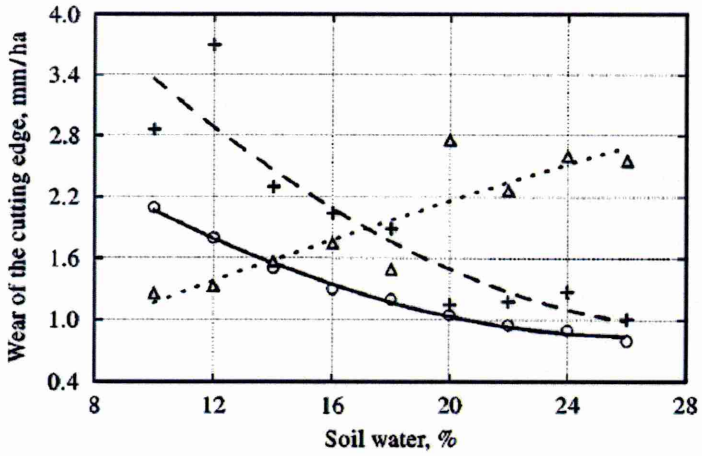

Figure 9: The effect of soil water content on volumetric wear of soil working tools after Natsis *et al.* [2]. The symbols denote; Δ – sandy soil; + - loam soil and ○ – clay soil.

It was found by Ferguson, Fielke and Riley[3] that plough shares suffered from wear on the bottom edge of the tool in dry (~2% water) soil conditions with no thickness reduction while in wet conditions (≥18% water) wear occurred on both the top and bottom of the tool with thickness reduction. Overall the shares wore 4.25 times faster in the dry condition compared to wet.

However, Yu and Bhole[4] stated that based on research carried out by Moore, Foley, Richardson, Swanson and Vetter it has been shown that the stronger the soil or the higher the water content the higher the abrasive losses.

Richardson observed that research by both Weiss, and Khrushchov and Babichev, assessing the effect of moisture on wear mechanism under laboratory conditions, supported the view that the presence of moisture does not necessarily produce important changes in wear mechanism[36].

Research has also shown that the acidity and level of contaminants affect wear resistance. Richardson highlighted that by using a polishing based wear test with carbon and stainless steel test specimens, the volumetric wear was affected by using 4 different fluids which were each allowed to stand over several hours[36]. The four fluids used were river water, tap water, distilled water and a 0.5% solution of K_2CrO_4. The distilled water was used in the test after four standing periods of 1.2, 24, 72, 120 and 5712 hours. The results indicated that this did not have any noticeable effect upon volumetric wear on both the carbon and stainless steel. However, when using tap water that had been stored for 48 hours the volumetric wear of the carbon steel was three times higher than when stood for 1 hour, leaving to stand for 246 hours yielded the same volumetric wear as the 1 hour test. The effect of tap water on stainless steel caused the volumetric wear to reduce from 2.09 to 1.24 to 0.72 mm^3 when storing the water for 1, 48 and 246 hours respectively. This suggests that pH may play an important role in the wearing mechanism of both carbon and stainless steel, although exact pH values were not stated.

The research into the effect of moisture content on the wear of tools in soils has been shown to be of great importance. However, the effect of pH on wear rate is also an important factor for consideration with regards to laboratory based wear tests. Most test involve the use of abrasive slurries, which depending on the water used and the abrasive type will have varying pH levels which may affect wear.

2.4.6 The effect of load and speed on wear rate

Previous research has shown that wear is directly proportional to nominal load up to a critical point, which, is determined by onset of massive deformation[5,37]. Larsen-Badse suggested that failure of the abrasive particle occurs when the applied load on the particle reaches a critical load that corresponds to a critical groove width of 0.17 of the grit diameter[38]. It was also stated that groove widths were approximately constant with respect to load and the load and abrasive particle properties determine the indentation depth. Other research by Richardson found that an increase in ploughing speed during field trials from 0.5 to 5 mph caused an increase in wear rate by around 20% and also affected the distribution of wear on the tools[23].

Studies by Richardson[23], Khrushchov and Babichev[6], and Nathan *et al.* looked at the effect of frictional heating caused by the speed of the component. Richardson and Khrushchov *et al.* concluded that the heat generated is negligible and should be disregarded while Nathan *et al.*[39] suggested an increase in wear rate occurs from the heat generated.

Misra and Finnie studied the effect of applied load on three materials, copper, aluminium and AISI 1020 steel samples using a pin-on-disc wear tester[37]. They found that when using 115 μm SiC abrasive weight loss increased linearly as applied load increased. The effect of sliding speed was also investigated over three orders of magnitude (0.2 – 200 mm/s) using 5 materials: W, Mo, AISI 1020 Steel, Cu and Al. The wear resistance for each material was observed to increase with increases in sliding speed from 1 to 100 mm/s. Beyond this the influence of sliding speed is minimal. Furthermore, the effect of sliding speed on the abrasive particle size showed that a change in speed by three orders of magnitude (0.2 – 200 mm/s) changed only the amount of wear and not the critical particle size (100 μm).

Studman[27] studied the effects of impact loads on soil working tools. Studman stated that previous research had recorded forces of up to 20 kN draught and 10 kN vertically (i.e. the force pushing the plough in to the ground) and up to 8 kN laterally in loamy sand soils. While Soucek (stated in Studman) recorded impacts with large stones of up to 45 kN in stony soils which actually broke a point, it was also seen that a force of 57 kN was recorded by driving the point in to a group of stones. Studman further studied the effect of impact forces from driving a cone shaped probe into objects with known mass and shape. It was found that flints weighing 2.4 kg produced loads in excess of 8 kN and in cases up to 18 kN while smaller flints at only 0.3 kg produced loads up to 7 kN.

2.4.7 *Abrasive particle orientation*

It has been established that the orientation of an abrasive particle is critical in determining whether material is removed from the surface in the form of a chip or not[40]. It was stated by Moore that microchips are only removed from the surface of a material when the abrasive grain achieves the critical angle of attack, a_c[5]. This angle is material dependant and is determined by the coefficient of friction. It is suggested that a chip is cut from the material when this angle is achieved (or greater) and below this angle a groove formed, known as 'cutting' and 'rubbing' respectively.

Research carried out by Mulhearn and Samuels[40] studied the process in which metal is removed from a surface by using bonded abrasive papers. Previous research carried out in this area assumed that the abrasive particles were conical in shape and ignored any particles inclined away from the normal axis of loading as these were deemed unimportant. However, Mulhearn and Samuels showed that in fact the particles being inclined away from this axis are the most important particles and contribute to majority of wear. This research identified that when particles exceed the critical angle to cut a chip large abrasion rates are observed.

2.4.8 *Tillage tool wear*

Field work carried out by Richardson[23] using a range of materials, highlighted that in various soils no wear occurs on the centre point of the cutting edge of a plough share until a parabolic shaped profile is reached (see Figure 10) and after which the wear of a flat plate is proportional to the length of cut made by the blade. In addition the geometry of the stable profile varied with blade thickness, when the thickness of the tool was increased threefold the parabolic profile became 25% more slender measured by the focal length/thickness. It was considered that this relationship was due to the distance a wearing particle slides around the tool edge, and it was estimated that this wear accounted for up to two thirds of the total wear occurring.

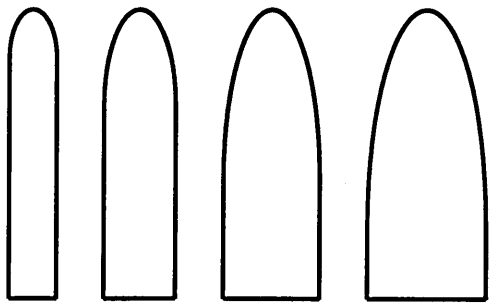

Figure 10: Schematic representation of parabolic profiles of tool edges observed during wear as tool thickness increases. As thickness increases threefold the profile becomes 25% more slender.

Field testing showed that the hard facings applied to the leading edge of the tool had some positive influence on the abrasive wear resistance of the tip in the early stages of the tests, but once a stable profile was achieved then the wear rate was similar to that of points with no hard-

facing. The most promising results appeared to be points having weld beads in the traverse direction of soil flow, possibly due to maximum disruption of soil flow occurring.

2.4.9 Plough position

Owsiak[29] studied the wear of spring tine cultivator points in sandy loam and light clay soils in the Southern Polish region. The points were manufactured from 0.45%C steel hardened on the tips and edges to 400 H_V. It was shown that points working within the tractor wheel track showed between 17 and 40% higher wear than points outside the track. Cultivator points are set up in a three row system normal to the direction of travel, the first row, directly behind the tractor showed wear 26 - 100% higher wear than the rear third row and the second row showed higher wear between 10 - 50%.

From the research discussed in this review it has been shown that there are many factors to be considered when assessing the performance of a soil working tool in its environment. In addition to these factors discussed there are also others that have to be taken into consideration such as the type of ploughing operation, the soil working depth and draught forces created on the tool from these parameters.

2.5 The prevention of wear

The process of wear, in particular abrasive wear, occurs throughout a wide range of industries involving many types of material including metals, polymers and ceramics. In order to minimise wear, a range of techniques may be adopted by designers or manufacturers. These can include modifications of component materials, changes in design and/or the use of lubricants. However, lubricants may only be utilised in specific low-load applications. Various methods have been used in other research to improve wear performance and some examples are discussed later. A common method of protecting against wear for tillage tools is the use of coatings.

A review of literature, focusing on research aimed at improving the wear resistance of soil working tools, will now be presented. The review encompasses a wide range of test methods explored, along with the requirements needed from a soil tillage tool in order to provide adequate wear resistance.

2.5.1 Hardfacing

The objective of hardfacing is to slow down the wear process. Previous research looking at the prevention of wear in agricultural applications has utilised hardfacing techniques. Hardfacing is defined by the American Welding Society simply as; 'an overlay that contributes to wear resistance'[53]. Depending upon soil conditions it may be advantageous to hardface either the

face of the tool or the back. It is wise to observe wear patterns produced by service conditions before hardfacing, to ascertain which point on the tool would benefit most from the hardfacing.

Commonly these are applied by welding as 'beads' in various patterns (see Figure 11) in an attempt to both improve wear resistance and disrupt soil flow around the tool[41,42, 43, 44]. Previous research has found that while certain patterns reduced the wear rate of ploughs in soil, no real cost effective advantage was gained through employing this technique compared with simply using the base material. It was reported that weld beads applied in the transverse direction appeared to suffer reduced wear, most likely by causing the greatest soil disruption and the formation of stationary soil bodies adhered to the tool. It seems more likely, however, that the welds were simply increasing the mass of material and hence prolonging tool life. However, hard-facings have been used extensively with earthmoving machinery, mineral dressing plant and solids handling plant[45].

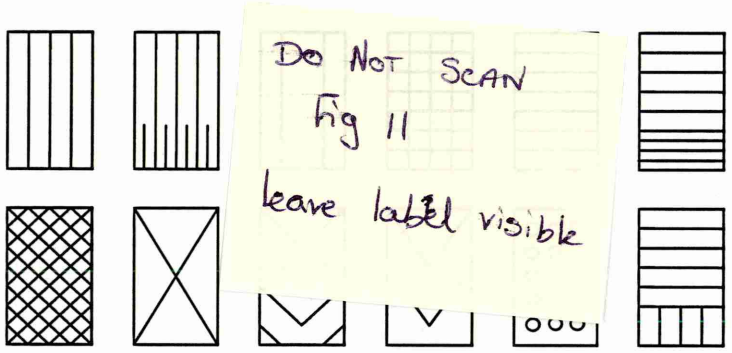

Figure 11: Typical weld bead patterns from work carried out by Moore, McLees and King[41].

When applied as coatings and not as welded beads, hard-facing materials often consist of hard metallic carbides bound in a softer metallic matrix. The overall wear resistance of such a coating is therefore dependent upon the size and hardness of the carbide phases and the load applied. These factors and the hardness of the abrasive affect the amount which the abrasive particle can penetrate the surface and hence cause wear. It has been shown that hard-facings containing hard carbides or other hard phases tend to possess improved wear resistance where the load is low and the abrasive particles are small. As the applied load and abrasive particle size increases, then it is seen that the wear resistance of the matrix determines the wear resistance of the coating[54]. While the size and hardness of any hard phases within a coating are important, it is also necessary for the matrix material to possess some wear resistance to prevent 'plucking out' of the hard phase. It was stated by Angers *et al.* that the abrasive wear of steels containing a large proportion of hard carbides will strongly depend on the level of cohesion the carbides have with the steel matrix as well as the size, shape and brittleness of the carbides[46].

Hardfacings applied to the substrate by welding and/or diffusion treatments are carried out using elevated temperatures and prolonged time-periods and therefore this method can affect substrate properties by effectively carrying out an undesired tempering process thus reducing the hardness

of the base material. It may also cause dilution of the hard-facing coating constituents into the substrate material.

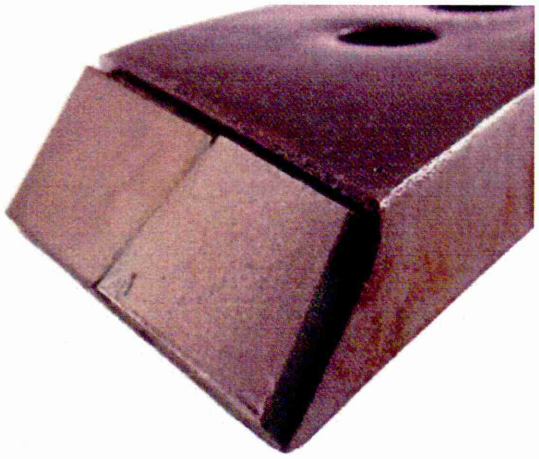

Figure 12: Tungsten carbide tile brazed to leading edge of soil tillage tool in an effort to increase tool life.

The direct application of a hard phase in the form of tungsten carbide (WC-Co) tiles has also been used and a way of protecting against abrasive wear[47,48,49,50]. Figure 12 shows a typical tool with the WC-Co tiles brazed on the leading edge. WC-Co is known for its high wear resistance and is also less brittle than other hard materials such as alumina. The wear resistance of the WC-Co tile is so high that the longevity of the tile can lead to the unprotected steel part behind the leading edge wearing away to the extent that the tile falls off. While this approach has been shown to increase the wear lifetime of a tool considerably there are drawbacks to this method. Due to the effect of thermal stress created during the brazing process several small tiles, as opposed to one large tile have to be applied to the leading edge. Impact damage can also cause failure of the tool, generally by fracture, leading to tile loss. Attempts to improve the joining of the tile (by eliminating the brazing process which can have a detrimental effect on the substrate properties) have led to the introduction of epoxy resins as the joining medium. The early loss of the tile through fracture, substrate wear or adhesive failure is not only expensive but can also introduce further hard wearing bodies into the soil causing increased wear of tools.

2.5.2 Ceramics

Engineering ceramics such as alumina, zirconia, silicon carbide or silicon nitride possess excellent tribological properties, but do not have the required toughness to be used as monolithic materials for ground engaging applications. However, engineering ceramics have been employed in the form of coatings or by additions to metallic coatings in an attempt to improve wear resistance. Ceramic plates have also been used as inserts bonded to the steel substrate by high strength adhesives[51-50]. Alumina has been utilised successfully for applications such as nozzles in sand blasting equipment, textile thread guides and power station equipment[52]. Laboratory studies have revealed that alumina possesses an excellent wear resistance to cost ratio. However, a major problem associated with the use of ceramics such as

alumina in agricultural applications is the inherent brittle properties of the material resulting in fracture under impact damage from stones present in the soils. In cases of loamy† soils with few or no stones present, it was found that ceramic coated tools performed up to four times better than conventional tools with the wear found to be more uniform and consistent[51]. However, a typical British soil possesses a high number of stones that may cause impacts on the tool as it is pulled through the soil creating cracks or chips in the alumina or even total removal of the alumina tile from the tool. For this reason the use of alumina is limited to a number of agricultural situations and geographical locations.

It was stated by Foley[54] that if ceramics were to be used extensively in agriculture then the method of attaching the ceramic to the substrate would need to be addressed; the ceramic must have good support from the substrate to minimise bulk deformation and must allow transmission of applied loads to the substrate. It was found that fixing of the material to the substrate by use of steel bolts yielded premature failure of the ceramic, and the preferred method was the use of adhesives. However, the use of adhesives can be unreliable due to bond failure.

2.5.3 Surface coatings and diffusion treatments

Materials commonly used to produce soil tillage tools are plain high carbon steels or low alloy steels which can be heat-treated and hardened to provide adequate performance. However, the inherent compromise between hardness and ductility means that materials with high hardness are also more prone to brittle failure. This has lead to the use of both coatings and surface engineered materials, technologies which are being developed mainly by the aerospace, prosthetic and engine component industries where the cost/benefit ratio allows the use of more expensive materials and processes. However, it is important to note that there is a clear distinction between surface coatings and surface treatments or modifications.

A surface coating is defined as the deposition of a material substantially different from the substrate on to a surface to obtain desired properties, which can be employed for many reason including corrosion protection, thermal protection and to extend the life of a part which may have been worn[53]. By applying a coating to a substrate material, extra protection against wear or impact may be provided that the substrate material would not be solely adequately able to resist. Coatings may also provide a cost effective method of manufacture by using smaller quantities of often more expensive materials.

The surface of a material can be significantly modified by utilising surface diffusion treatments such as carburising, nitriding or boronising. These surface treatment techniques produce a hardened outer surface layer based upon the substrate material composition which can be up to

† Soil composed of sand, silt, clay, and organic matter in evenly mixed particles of various sizes. High porosity which allows high moisture retention and air circulation.

several millimetres in thickness, while not affecting the tough, substrate core that is desired for a wear and impact resistant part[54]. The depth penetration of these techniques however, is relatively low, typically between 0.5 – 1.0 mm.

2.6 Material requirements

The ability of a material to resist wear also depends upon the microstructure and not merely the bulk (macroscopic) hardness of the material. Any hard constituents of the microstructure such as carbides present contributes to the overall wear resistance. The shape, size and type (chemistry) of any carbide and the support provided to the carbide from the matrix material will determine how a material performs in resisting wear.

Several agricultural grade steels were tested for wear resistance by Bhakat *et al.*[55], these being high carbon steel, boron steel and chromium steel. The high carbon steel was used in the oil quenched and tempered condition whereas the boron and chromium steel was used in the water quenched and tempered condition. Oil quenching is used with high carbon steels as water quenching tends to promote microstructural cracking. Research found the addition of boron and chromium to medium carbon steel (~0.3% C) increased the harden-ability, promoting martensitic and carbide phases. Bhakat highlighted that the chromium steel possessed the greatest wear resistance, followed by the boron steel and then the high carbon steel. It was concluded that the chromium and boron steels were suitable for harder soil conditions.

Richardson[23] stated that under severe wearing conditions materials should contain large carbides or hard phases which should supported by a matrix that becomes harder under abrasion in order for it to perform well. It was observed that the cementite and its surrounding structure was plastically strained and obtained a degree of work hardening, it was also stated that other forms of carbides may also plastically strain even when they are harder than the abrasive material. Richardson concluded that as the contact stress increases, the ratio of scratch depth/carbide diameter increases, leading to the carbides becoming less effective in improving wear resistance due to pullout from the surface in the form of a chip rather than resisting against wear.

Chromium carbides found in some cast irons, that possess hardness values of up to 1400 H_V, may increase the bulk hardness of the material to region of 800 H_V, near to the 'required' $0.8H_a$[56]. However, the low toughness associated with these phases causes the wear resistance to vary with the relative size of the microstructural features and the abrasive particle size. The poor fracture toughness properties of these materials also create problems when under impact from stones in soils.

The use of materials such as WC has been wide spread in industry to improve both abrasion and erosion resistance. Work carried out by Zhou *et al.*[57] studied the effect of increasing the

volume fraction of WC in grey cast iron. Several levels of additives were tested, between 10 and 53 vol.%, it was observed that relative wear decreased as the WC content increased up to 36 vol.%, after which the wear rate then began to increase. Zhou stated that the presence of the hard phase protected the surrounding softer phase of the matrix from wear creating a surface whereby the WC carbides protrude from the surface. It was concluded that loadings above 36 vol.% created a poor bond interface between the carbides and matrix yielding increased wear rates after this point by the mechanism of the carbides being plucked out of the matrix.

In a study carried out by Popov *et al.*, the effect of different carbide phases in a stable austenitic matrix were assessed for wear behaviour[58]. The carbides used were FeC and WC. Examination of the resulting wear scars showed that these carbides presented no resistance to the destructive action of the abrasive, however vanadium (V) and niobium (Nb) carbides resisted the wear better. It was suggested that the resistance of alloys to wear is proportional to the amount of energy needed to rupture the carbides. Further research into chromium (Cr), WC, V and Nb carbides carried out by Popov *et al.* showed that carbide contents of between 5 and 7% of each of the four carbides examined possessed very little difference in wear rates. However, above 7% carbide dispersed within the microstructure, V and Nb carbides resisted abrasive wear better than Cr or WC, whereby no further improvement in wear resistance was seen after 30% content of V and Nb[59].

Work carried out by Oliveira assessed the addition of aluminium oxide particles (20-70 μm) at 10 vol.% to high speed steels[60]. This addition yielded an increase in wear resistance but a drop in bend strength and further additions of Al_2O_3 were made with the particles having had a CVD TiN coating. Results of this study showed that bend strength and hardness increased becoming close to those of the base material with further increase of wear resistance. Microstructural examination showed that the uncoated Al_2O_3 particles were not bonded with the surrounding matrix, whilst the TiN coated particles possessed no porosity and an interficial layer of V rich MC type carbides (carbonitrides) were present. The TiN introduced extra reactivity at the interface between the matrix and ceramic phase improving the sinterability of the composite material. Further additions were studied, these being three batches of TiC (5, 16 and 42 μm nominal mean particle sizes) and two batches of TiN (7 and 12 μm) both materials at each particle size were added at 10 vol.%. Some specimens were tempered at 950°C for 30 min in flowing nitrogen followed by oil quenching followed by a temper for 1h between 450-550 °C. The hardness of the composites reflected the hardness of the matrix due to the low volume fraction of the ceramic but heat treatment was found to provide a significant hardness increase. The bend strength decreased with the ceramic particles acting as crack initiators.

Although the addition of hard carbides to a microstructure in some instances has been shown to increase wear resistance of alloys, improvements in wear resistance can be obtained from a microstructure with a finely dispersed carbide content[61,62,63]. Brittle and continuous carbide

networks are generally found to be undesirable for wear resistance[64,65] as this type of structure has been shown to promote crack propagation[66]. Previous research has shown that the matrix material can play a very important role in wear resistance. The carbides present need adequate support from the matrix and to be well bonded to it, otherwise they may become exposed and not able to offer the full potential of wear resistance [67].

The Armatech material is a powder metallurgy coating that is applied to tool substrates by sintering. The powder production techniques and method of sintering will now be discussed.

2.7 Powder metallurgy

Historically powder metallurgy (PM) and sintering have been around since as early as 1200 B.C. with evidence showing that iron powders, extracted from metal sponge, were fused in to hard tools. Today PM production is used in a wide range of industries, from automotive applications, (the largest producer with around 69% of the market[68]), to lock and door hardware component production. The most common, modern approach to powder metallurgy is via the compaction method which involves powders being mixed with binders prior to being die-pressed under high pressure. The net shapes or 'green' compacts are then heated to remove the binder and sintered to produce a high density part with very little shrinkage which needs little or no machining.

PM in the context of this study encompasses the production of metal coatings by loose powder sintering involving no compaction or injection process with the binder remaining present within the final structure.

2.7.1 Powder production

Various methods exist for the production of metal powders, each having its own advantages such as cost, production time, final powder quality and other requirements such as oxygen content. Some common production methods are:

- Chemical processes
- Electrolysis
- Mechanical processes
- Atomisation

Of the processes listed above atomisation is the most common method of powder production and it utilises high velocity jets of gas or liquids to atomise a melt of the required elements. Some of the common gases used are air, nitrogen or argon with common liquids jets being water, oil and even paraffin. The atomisation approach is the most flexible method of powder production as it allows the production of pre-alloyed powders and provides the greatest control

over final powder properties, see Figure 13(a). Gas atomisation and centrifugal techniques produce a more spherical powder when compared to the other methods and allow smaller particle size to be achieved. The Armatech powder used in this study is a pre-alloyed water atomised powder.

2.7.2 Water atomisation

Water atomisation is a low cost operation when compared to other powder production routes and is mainly carried out when producing Fe based pre-alloyed powders where strict tolerances are not considered necessary. A pre-alloyed powder is one that has all the desired elements in each finished powder particle. Some forms of production do not allow this operation and the final powder has to be manufactured through mixing of elemental powders or by the process of diffusion whereby additional elemental powder is diffused onto the surface of a base powder, see Figure 13(b) and (c). The final powder produced by water atomisation possesses a highly irregular shape due to the increased cooling rate when compared to techniques such as gas atomisation. This irregular shape can be explained by the powder droplets having less time to form a spherical shape before being cooled from the water jets.

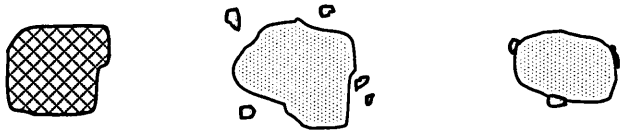

Figure 13: Alloying routes for powder production; a) fully pre-alloyed powder; b) mixed elemental powder; c) diffusion bonded powder.

The stock[‡] is melted using a furnace or by induction heating to form a stream of molten metal. The stream is passed through a tundish at a constant, controlled rate into an atomizing chamber where it is disintegrated by impact from high pressure (5–20 MPa) water jets, see Figure 14. The disintegrated molten stream forms fine droplets which solidify as they fall in the chamber and the solidified particles are collected in the chamber bottom. The droplets size is able to be controlled by adjusting several parameters.

[‡] Elemental, multi element, metallic alloys and/or high quality scrap in the form of ingots or bars.

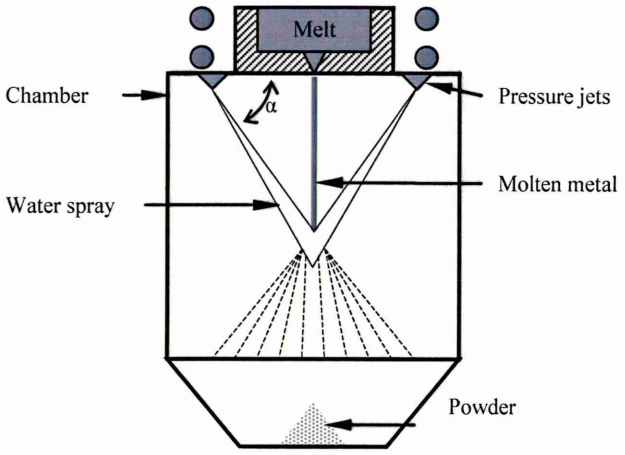

Figure 14: Schematic diagram of the water atomisation process. The melted stock is disintegrated by high pressure water jets. The disintegrated particles solidify during falling and collect in the chamber bottom in the form of a powder.

The powder is separated from the water by using filters or a settling process and dried. Powders produced using this method inevitably acquire a surface oxide film which may be removed by carrying out reduction treatments if required.

2.8 Sintering

For the purpose of this research the materials are manufactured by the sintering of metal powders. The conditions of the sintering process used and manufacturing techniques are provided in Chapter 5. However, a brief introduction into the technique of sintering will be provided here.

2.8.1 Sintering process

The process of sintering enables the production of metallic or ceramic components to be produced at a lower cost than other established and often expensive or wasteful methods such as machining, casting, extrusion and forging. In the case of some ceramics, where melting is not possible, sintering is the only viable method of production. Developments within the last thirty years have been made by technological advancements in producing metallic powders, developing binders and lubricants and in the ability to produce highly dense components. A definition provided by the International Standards Organisation (ISO) states that sintering is:

> "The thermal treatment of a powder or compact at a temperature below the melting point of the main constituent, for the purpose of increasing its strength by bonding together of the particles."

The sintering method for the production of PM components involves the powder, said to be in the 'green' state, being fired into a solid component by utilising temperatures lower than the melting point of the base material. Typical sintering temperatures are around 1000 °C (c.f. melting point of iron, circa 1538 °C). This reduction in temperature, of around a third, reduces

power consumption and helps to increase the lifetime of furnace filaments when compared to other traditional manufacturing methods.

2.8.2 Particle diffusion during sintering

In most cases there are no external forces applied to aid the process of sintering, the driving force is the desire of the system to reach the smallest surface area and hence the lowest level of energy. Sintering occurs through the atomic diffusion stimulated by the temperatures. Various mass transport mechanisms exist which contribute to the process of sintering, these include:

- Evaporation and condensation.
- Volume diffusion.
- Grain boundary diffusion.
- Surface diffusion.

It has been shown that necking occurs on heating, at a point of contact between particles; the neck progressively thickens until the outline of the original particles disappears and re-crystallization and grain growth occurs across the boundaries, Figure 15. This process may be hindered by the presence of surface oxides or impurities which can often be seen to precipitate out at prior particle boundaries.

There are four main diffusion paths that occur between particles during the initial stages of sintering, each occurring over different temperature ranges. In certain cases only one diffusion process may be occurring or, it may be that all paths are diffusing simultaneously.

The Armatech coating used in this research is a pre-alloyed powder and is applied to the tool in the form of aqueous slurry, with a clay based binder. The coating is then sintered onto the substrate at ~1080 °C. A fuller description of the manufacturing process is provided in Chapter 3.

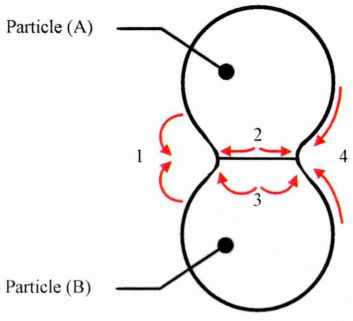

Figure 15: Schematic diagram showing material transfer mechanisms during sintering; 1: evaporation and condensation; 2: grain boundary diffusion; 3: volume diffusion; 4: surface diffusion.

One main focus of this research is the evaluation of materials against wear using several wear test techniques. Each technique will now be discussed along with previous literature regarding these.

2.9 Tribology testing

The most accurate method for determining the wear resistance and lifetime of components is to carry out in-situ based tests using real components under real conditions. However, this is rarely economically and logistically viable, and laboratory based tests which simulate working conditions are preferred in most cases.

Laboratory tests can be employed to test and compare materials quickly and relatively cheaply. Laboratory tests may also be used as a materials selection process prior to further in-situ testing. There are a wide range of wear tests currently in use that vary in the level of the applied load, the type of abrasive used and the resulting wear mechanisms.

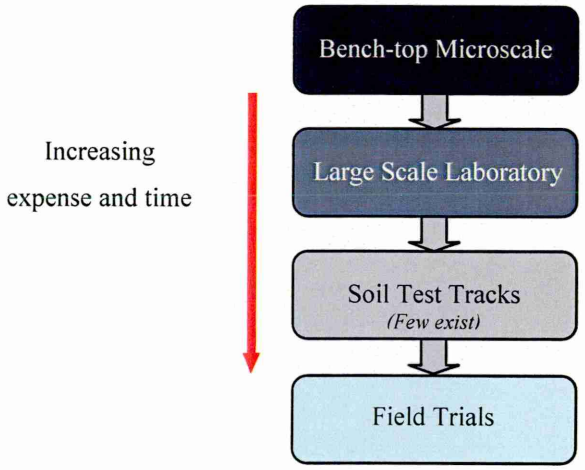

Figure 16: Methods for measuring wear resistance.

Figure 16 shows a series of typical tribological tests that may be used to determine the wear resistance of soil tillage tools. In general the cost of the test increases as it moves down the diagram, with equipment and samples becoming more expensive and generally more time needed to complete a full matrix of tests.

2.10 Field trials

The most informative method of assessing the performance of soil working tools is by field testing. Detailed planning is essential to ensure useful information is gathered and recorded to produce accurate and reliable data. Some of the main advantages to performing field trials include:

- Actual conditions such as plough depth and speed can be replicated.

- Correct abrasive media (to a certain degree).
- Representative load.
- Tools may be assessed for impact damages in conjunction with wear.

The wear rate of a material can be determined using a standard weight loss approach. If desired, several weight loss measurements can be taken at selected intervals to observe the pattern of weight loss occurring throughout the test program. Geometrical measurements may also be taken in order to determine the positions at which the majority of wear is occurring. However, a major drawback of field testing is the amount of time, labour and materials needed and hence the cost. In addition difficulties arise when trying to find suitable land, obtaining permission and cooperation from land owners/farmers.

The majority of arable land is in constant use for farming and crop production. In order to carry out testing in these areas the owner/farmer must first be willing to allow access but may also need to be involved to provide machinery and labour. It is this involvement by the farmer which is difficult to obtain, as the need for accuracy and control over plough speed, depth, the need for weight measurements and other factors involved in carrying out accurate field trials can restrict the farmers who often have little time to spare due to the limited time windows involved in crop rotations and production.

Other drawbacks associated with field testing include the reproducibility of results; often test conditions differ due to seasonal and regional variations. These variations in soil and weather incorporate a wide range of variables which laboratory testing can attempt to reduce. Extensive field trials were preformed both in the UK and Kenya by Richardson [18] and it was stated that in order to obtain useful and informative results from field testing the following should be adhered to:

(a) Experiments should be within an area of land in which soil type and condition is substantially uniform.
(b) Wear test pieces must be homogeneous within the wear zone and a reference material should be used.
(c) Wearing surface should be nearly identical in shape.
(d) Statistical methods should be used to determine the physical layout of experiments in order to reduce error.

It was also stated that for field testing to ensure enough material is lost from the specimens then an area of 100 acres to allow accurate measurement should be used. However, this figure is based on testing uncoated bulk specimens.

The possibility of performing significant wear trials for this research was outside the scope of the project, and more in-depth laboratory wear testing was performed.

2.11 Test tracks

Another method of testing that enables actual working conditions to be replicated, but removes the variability associated field trials, is the use of test tracks[69]. The soil type and condition contained within the test track are able to be closely controlled. By adjusting the stone and water content different geographical regions or seasons can be simulated. However, there are only a small number of known test tracks around the world; the last UK test track was decommissioned in the early 1980's. Other test tracks can be found in the US and South Australia but due to demand and logistical aspects this method also proves an expensive test method.

The obvious benefit to carrying out experiments using field trials or test tracks is that the actual tool, and not a scaled down version can be assessed. Typical cultivation speeds and soil depths are also able to be employed and draft and penetration forces acting on the tool are able to be measured.

2.12 Laboratory testing

Using a small scale laboratory tests significantly reduces the cost and time needed to perform a wear test. Using a laboratory based wear tester allows the use of scaled down samples and allows the test parameters to be carefully controlled in order to understand the influence of any one variable on the wear process. Both micro-scale abrasive wear testing (MSAW) and macroscale laboratory based testing have been carried out in this research and both will be discussed here.

Due to the complexities associated with the field environment, laboratory testing does not attempt to directly reproduce these conditions. In general the parameters that are able to be simulated are abrasive particle type/size, load and speed. For this reason laboratory tests should be used as a comparative ranking test for materials and not used for lifetime prediction, hence field testing will always be a useful method to verify laboratory results.

2.13 Microscale abrasive wear test (MSAW)

The MSAW tester used in this work was a commercially available Plint TE-66 tester manufactured by Phoenix Tribology UK. A schematic diagram is shown in Figure 17. This technique is a 'fixed ball' cratering test which produces an imposed wear scar geometry, which is assumed to reproduce the spherical geometry of the ball. This wear scar can be measured to calculate the volume of material removed and thus yield a wear rate value. This is a rapidly evolving technique for measuring the abrasive wear performance of all types of materials and coatings including polymeric films, hard ceramic coatings, thermally sprayed coatings and metallic coatings[70].

The fixed-ball technique does not allow slippage between the drive shaft and the ball as with the free-ball technique allowing an exact measurement of sliding distance to be made. A further advantage to this technique is the method of applying the load to the sample. Other free ball variants involve using the incline of the sample on the ball to determine load measured by a load cell. The fixed-ball method however employs the use of a pivot arm to apply the load by use of actual weights.

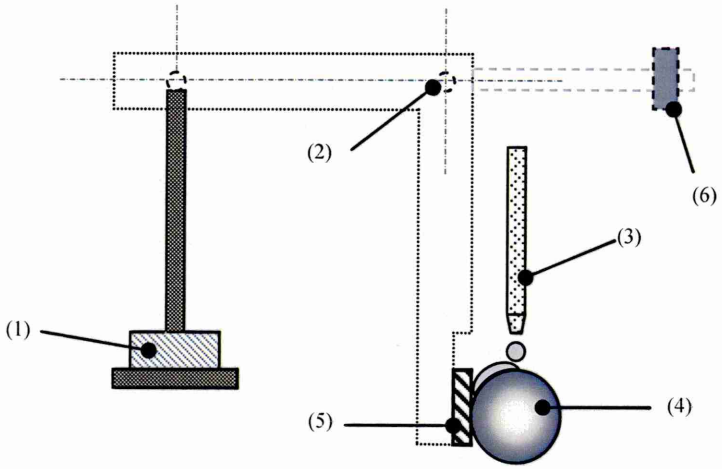

Figure 17: Plint TE 66 abrasive wear tester; (1) applied load; (2) pivots; (3) abrasive slurry drip feed; (4) steel wear ball; (5) the sample and (6) counter balance.

The introduction of slurry to the ball/sample interface has also been improved upon compared to earlier tests. The slurry is fed by a peristaltic pump connected to the drive mechanism used to rotate a co-axial shaft and hence rotate the ball; this produces a constant feed rate relative to the sliding speed. Applied loads of 0.05 to 5 N are able to be used and the ball speed has a range of 30 to 150 rpm.

2.13.1 Wear mechanisms

There is a wide body of literature involving MSAW tests and in particular the Plint TE66 test and a wide range of test conditions have been employed. The MSAW test conditions may be manipulated to produce either two or three-body wear mechanisms by the adjustment of test conditions. Research performed by Trezona *et al.*[71] revealed that both two-body grooving and three-body rolling mechanisms were observed and the occurrence of one mechanism or the other was a function of the applied load, slurry concentration and also abrasive type. High loading and/or low slurry concentration yielded two-body grooving wear and low loading and/or high slurry concentration yielded three-body rolling wear, Figure 18. The transition between the two wear mechanisms occurred at a constant ratio of normal load to slurry volume fraction for both SiC and Al_2O_3 abrasives.

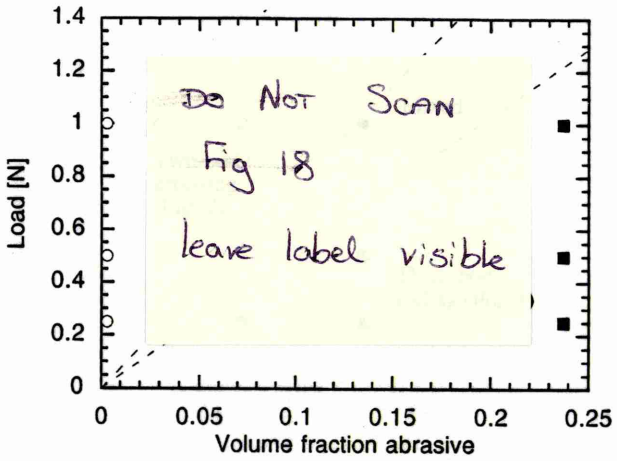

Figure 18: Wear mechanism map for MSAW test on tool steel using F1200 SiC slurry from Trezona et al.[71].

Trezona *et al.*[71] found that the three-body wear volume was proportional to the normal load whilst two-body wear volume is proportional to some power of load lower than one, Figure 19. It was also stated that for the particular method used the wear rate was found to be constant with respect to sliding distance. It was stated that when two-body wear occurs in the microscale abrasion process it is due to the abrasive becoming embedded in the surface of the ball and thus acting as fixed indenters.

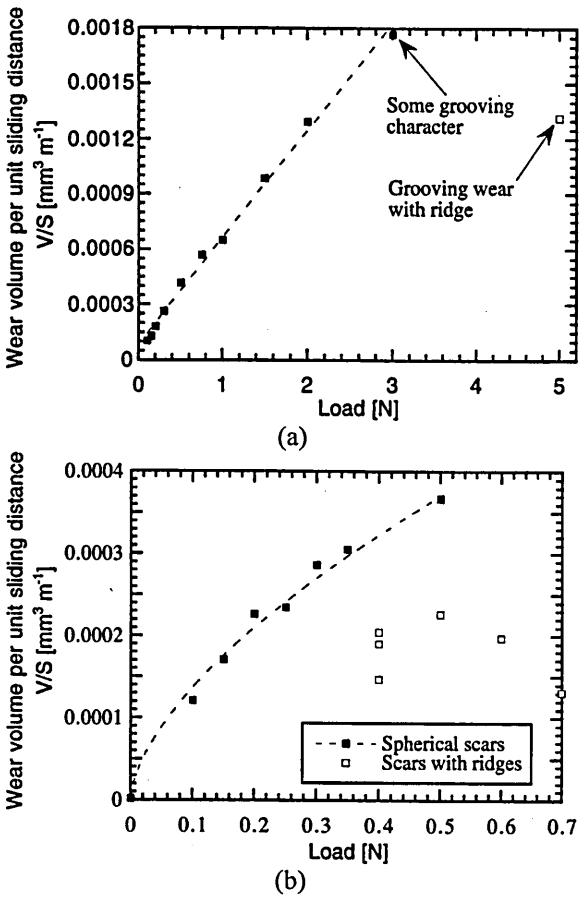

Figure 19: Variation of wear vol. per unit sliding dist. versus load on tool steel using F1200 SiC abrasive; (a) 0.189 volume fraction creating three-body wear (sliding distances from 12 to 24m) and (b) 0.015 volume fraction creating two-body wear at a constant sliding distance of 32m[71].

Research carried out by Stack and Matthews[72] using the MSAW method involved a series of tests on 304 stainless steel. Transitions from three- to two-body and then back to three-body abrasive wear by adjusting both load and sliding distance using 4 μm SiC abrasive was demonstrated as indicated in Figure 20. It was proposed that initially at low loads a pure three-body rolling mechanism is taking place whereas, as the load increases the abrasive particles begin to 'stick', or more likely embed into the abrading surface, in this case the wear ball which begins onset of a mixed mode of wear. As the load continues to increase the dominance of two-body grooving takes over, it was then proposed that as the load increases the asperities of the two surfaces (the ball and sample) come into contact causing ridge formation in the wear groove. The wear regime reverts then back to three body wear as the load is increased.

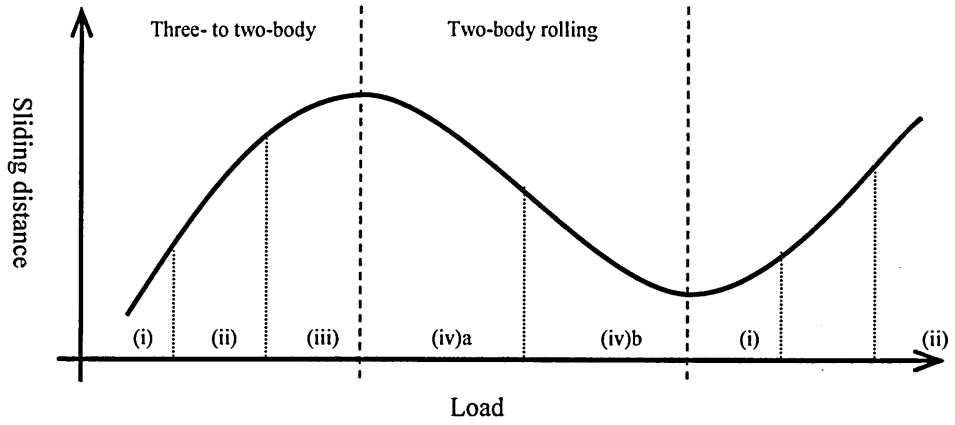

Figure 20: Transition between two- and three-body wear mechanisms observed using wear tester[72].

The standard abrasive used in the MSAW test is SiC, many other abrasives are able to be used such as Al_2O_3 or SiO_2. The abrasive has to be made into slurry however, and the particle size needs to be small, less than 10 μm, in order to obtain a regular flow rate and prevent blockages. For continuity testing was carried out using SiC but also using SiO_2, typically the main constituent of soil.

2.13.2 Sliding speed

Research carried out by Gee *et al.*[73] aimed at standardising the technique of ball cratering as an abrasive wear test showed that the wear volume is largely unaffected by sliding speed (at a constant sliding distance) except at very low speeds.

2.13.3 Wear ball

Research has shown that the condition of the wear ball can affect the amount of wear occurring on the sample. Allsopp *et al.*[74] compared wear using an unused ball and a well-used hard martensitic ball (990 ± 40 H_V). It was stated that the surface condition of the wear ball can greatly influence wear coefficients. The unused ball delayed the onset of wear and showed signs of creating ridging, caused by the inability to draw abrasive particles in the wear interface. It was stated that the rough surface of well used balls allow protuberances on the particle to engage with the ball, which can drag the particles in to the contact area. It was reported that well worn balls obtain highly reproducible wear coefficients.

Allsopp also discussed the possibility of flattening of the wear ball that may affect particle entrainment. Results using new balls that possessed no possibility of flattening gave the same results as tests with previously worn balls. Profilometry of extensively used balls showed they still conformed to a spherical geometry and flattening was insignificant.

2.13.4 Sliding distance and load per abrasive particle

Various researchers[71,75,76] have shown the linear relationship between wear volume and applied load for the MSAW test which is independent of sliding distance, Figure 21.

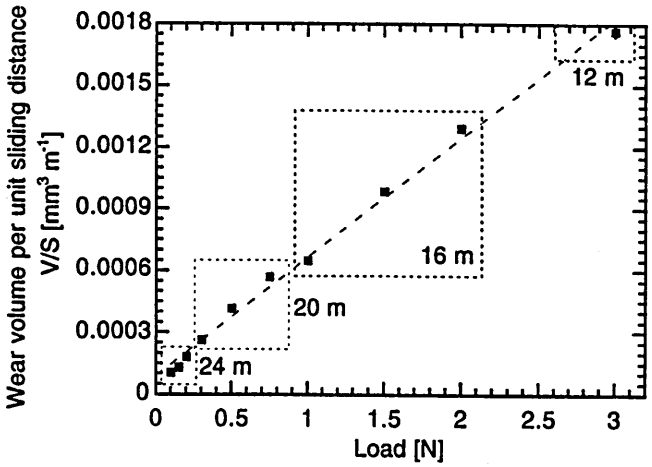

Figure 21: The variation of wear volume per unit sliding distance as a function of load for three-body rolling abrasion using SiC abrasive on tool steel carried out at different sliding distances; after Trezona[71].

A series of tests carried out by Trezona *et al.*[71] at 12, 16, 20 and 24m sliding distances on a Plint TE66 abrasion tester showed a good linear relationship for the wear volume removed per unit sliding distance as a function of load. However, Trezona stated that as a wear scar continually increases throughout a wear test then the apparent contact pressure will continually decrease. So assuming that the concentration of slurry in the wearing interface does not change, one assumption is that the load per abrasive particle will decrease as wear volume increases can be made. Therefore, Trezona stated that for wear volume per unit sliding distance to be independent of sliding distance, it must also be independent of load per abrasive particle. It was concluded that since load per particle is inversely proportional to the volume fraction of the slurry, wear rate is sensitive to it, especially at lower loads, and plots of wear volume against loads are expected to be linear if the wear volumes are small, since the projected area of contact is proportional to the square root of the wear volume.

2.13.5 Abrasive slurry acidity

Work carried out by Gant *et al.*[77] using the MSAW test studied the influence of the corrosive nature of the abrasive slurry on the mechanism and severity of abrasion of WC-Co hardmetals. It was found that the volume loss increased with a decrease in the pH of the abrasive particle carrier medium (a range of solutions from 1.1 to 13 pH were used). The abrasive used was 4 μm SiC at a concentration of 20vol.% and an applied load of 0.2 N. The work also revealed that finer grained hardmetals suffered higher wear rates than coarser grained materials. The materials with coarser grains showed that crater depth increased very little after 500 revolutions (~50 m) of the wear ball, while the finer grained material crater continued to deepen at a steady rate.

2.14 Wear Severity

The effect of wear rate severity on the wear mode was investigated by Adachi and Hutchings with different combinations of ball and bulk specimen materials under different test conditions,

such as load and slurry concentration[78]. It was stated that the dominant mode of particle motion is dependant on the 'severity of contact' *S/S**:

$$S/S^* = L/A_p \upsilon H' * (H_s/H_b)\alpha/\beta$$

Equation 3: Severity of contact

where L is the applied load, A_p is the interaction area (defined by Equation 4), υ the volume fraction of abrasive and H' the effective hardness (defined by Equation 5), related to the hardness of the specimen, H_s, and the ball H_b, and, α and β are empirical constants, which were 0.0076 and -0.49 respectively under Adachi and Hutchings test conditions.

$$A_p = \pi(a^2 + 2RD)$$

Equation 4: Interaction area of wear scar

Where a is the radius of the Hertzian contact area, R is the radius of the ball and D is the diameter of the abrasive particles.

$$1/H' = \alpha (H_s / H_b)^{\beta}$$

Equation 5: Effective hardness

It was stated that when $S/S^* < 1$ three-body rolling abrasion is the dominant wear mode, while $S/S^* > 1$ two-body grooving dominates. It was stated that three-body abrasion was relatively insensitive to test conditions when compared to two-body, suggesting three-body wear is a more appropriate mode to achieve reproducible results, previously stated by Rabinowicz, Dunn and Russell[12]. It should be noted that although the work carried out by Adachi and Hutchings assessed different slurry concentrations it did not investigate the effect of abrasive type and abrasive hardness on the wear mode.

2.15 Dry Sand Rubber Wheel Abrasion Tests (DSRW)

As described previously, laboratory wear testing allows quick and a relatively cheap way to assess a group of materials against each other. Due to the nature of MSAW testing however, only a small area of material is tested and the level of aggressiveness compared to actual working conditions is somewhat reduced and the DSRW may be considered as an intermediary test between MSAW and field trials. DSRW tests use larger samples and produce a much larger wear scar. The applied loads involved are higher and it employs larger particle size abrasives; reducing the possibility of errors associated with sample microstructure.

Like the MSAW test the grit is introduced to the sample interface, which in this test involves a rotating wheel with a rubber rim, see Figure 22. The test specimen is pressed against the wheel under an applied force. The test produces a much larger wear scar compared to the MSAW test and is much more aggressive in nature. The method of determining the wear resistance is carried out by weight loss measurement.

The DSRW test has been around in various forms for a number of years, the first work published using the tester in its current form was in 1949 by Haworth in Stevenson and Hutchings[79]. Since then the test has undergone several modifications and improvements with the first standard test procedure (ASTM G65[80]) being published in 1980. Since this time the standard test procedure has changed very little with only modifications to the actual test apparatus being made.

The ASTM standard test involves abrading a test sample using a controlled size and composition grit abrasive and is currently the most commonly used test for determining abrasive wear resistance. However, various studies have been carried out using different abrasives[81,82,83], along with the standard ~200 μm silica abrasive larger 600 μm SiO_2 and a 200 μm Al_2O_3 have been used.

The DSRW test is commonly referred to as a low stress abrasion test[84,85,86]. Although the loads used in this test are much higher than the ones used in MSAW they are not high enough to crush the abrasive particles as they slide along the wheel/sample interface, giving rise to the term low stress. The test is considered a high stress test when a steel wheel as opposed to a rubber lined wheel is used[84]. While the steel wheel has been found to increase wear loss it has also been found to affect the interaction of the abrasive. Steel wheels have been found to increase the likelihood of particle fracture.

As with the MSAW test, field working conditions are not replicated (although in this test the abrasive is found to be similar to that of common soils), the DSRW test should be used to rank materials against each other in the specific environment and not predict tool life. A further step at recreating aspects of service conditions has seen the adaptation of ASTM G65 by several research groups to allow wet testing, which is now a standard in its own right, ASTM G105. A further restriction of the test is that the applied load and sliding speed are not able to be adjusted, these are set at a normal loading and constant speed. An advantage of this technique over other macroscale tests is that the abrasive passes through the wear contact only once, unlike some other tests where it is re-circulated (ASTM B611 and ASTM G105 are intended more for hard metal mining grades).

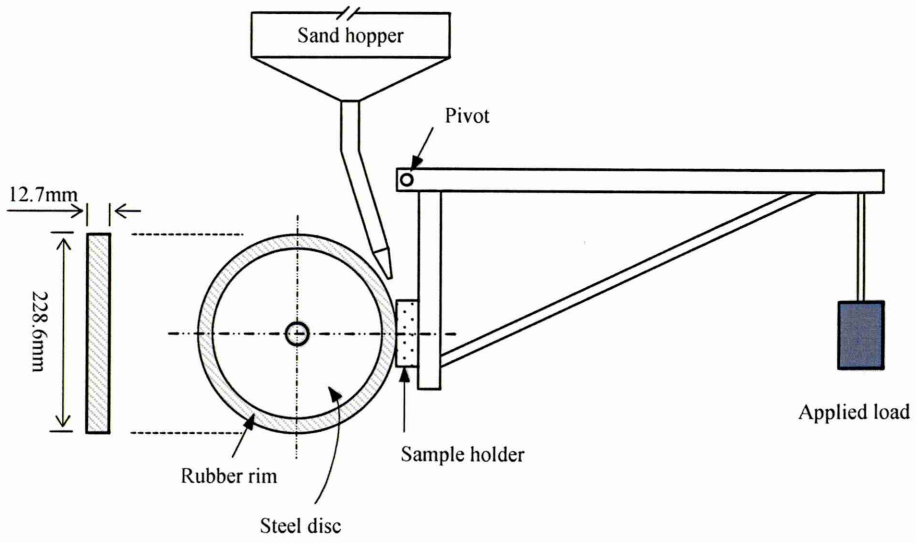

Figure 22: Schematic diagram of DSRW abrasion tester (NB. Not to scale).

When comparing the DSRW test to smaller laboratory tests, such as the MSAW test, the size of the sample required in DSRW testing is relatively large (76 mm long by 25 mm wide with a thickness of 12.7 mm) and only one test can be performed on each sample. Each test is also lengthy in time with a recommendation from ASTM G65 of 5000 wheel revolutions. While this may be considered a disadvantage when comparing it to smaller, cheaper and faster techniques such as the MSAW test, it still provides a cost effective result when compared to field trials.

Swanson[87,88] carried out research comparing laboratory based abrasion tests to field tests using materials used for tillage equipment. It was stated that the relative wear resistance (RWR) of heat treated plain and alloy carbon steels determined by laboratory tests (pin-on-disk and ASTM G65 using both wet and dry abrasive) correlated 'fairly well' with RWR determined by field tests in sandy soils. Swanson found that the RWR of heterogeneous materials, such as brittle hard facings however differed significantly between the laboratory and field. It was concluded that wear scar appearance from the pin-on-disk had closer resemblance to the field wear scars than those produced with the ASTM G65. In the research by Swanson where an attempt to directly compare field trials with DSRW tests it was concluded that DSRW testing adequately simulated the abrasive wear of the materials tested in sandy fields with low moisture content. However, Yu and Bhole[4] stated that the ASTM G65 test was not an entirely satisfactory test for assessing the abrasive wear characteristics experienced by tillage tools. Their argument being that the abrasive used in this test method is dry sand and not representative of field conditions, which has now been addressed by modifications described in section 2.15.1, and that no simple relationship exists between the abrasive wear resistance and common mechanical properties, such as hardness.

Research carried out by Stevenson and Hutchings assessed the effect of load, sliding speed, rubber wheel hardness and frictional force on abrasion[79]. It was found that a linear relationship was observed between wear rate and load (the load was varied between 24.5 and 122.6 N) over

a sliding distance of 71.8 m (100 wheel revolutions). It was also stated in Stevenson and Hutchings that research carried out by Ellis and Armstrong reported that wear rate was linearly proportional to load except at very high loads where the wear rate increases. Stevenson and Hutchings research into the effect of sliding speed reported that tests carried out however showed that under a load of 98.1 N at a range of sliding speeds a maximum wear rate was achieved at around 0.5 m/s. It was concluded that this was caused by a balance between the heating effects decreasing the modulus of the rubber, and the strain rate increasing the modulus.

The effect of wheel hardness was investigated using four polyurethane wheels with hardness's ranging from 46 to 84 IRHD[§] on mild steel specimens over a sliding distance of 359 m (500 wheel revolutions). It was noted that the hardest wheel produced a wear scar with the largest curvature. The wear rate was seen to increase with an increase in wheel hardness. It was reported that the frictional force was found to be independent of both sliding speed and the applied load and also the type and hardness of the rubber wheel.

Doğan *et al.* employed a standard DSRW tester to assess the abrasive wear resistance of TiC reinforced metal matrix composites[89]. It was found that materials with coarse TiC particles suffered higher wear loss than materials with finer TiC particles. It was concluded that that interparticle spacing plays an important role under DSRW testing. Large interparticle spacing (8 μm) in materials with coarser TiC additions gave rise to easier removal of the matrix between the TiC additions; with the finer particles dispersed between the large TiC not providing significant resistance against the abrasive action of the larger silica sand. When interparticle spacing was small (2 μm), found in the materials with finer TiC additions, the matrix is protected by the TiC more efficiently. It was concluded that the primary mechanism of material removal was the removal of matrix material between the TiC particles.

As with any wear tester developed, the conditions of the test will significantly affect the wearing mechanism and rate of wear on a test material. Other conditions include abrasive properties (type, shape, size, hardness etc), properties of the test wheel and the test environment (wet or dry).

2.15.1 Modified ASTM G65 DSRW test system

The DSRW tester used in this work was based at the National Physics Laboratory (NPL), Teddington, UK. In order to improve the standardised equipment several modifications had been made. One problem associated with the standard DSRW equipment is the flow rate of the abrasive feed. The abrasive is fed from a hopper directly down on the interface between the wheel and sample; this can lead to blockages and an uncontrolled feed rate. Modifications have been made after Stevenson and Hutchings[79] whereby the abrasive rate is controlled by a

[§] International Rubber Hardness Degree - The standard test methods for measuring the hardness of rubber and plastics are IRHD or Shore hardness.

motorised notched wheel under the hopper before being passed onto the wheel by an inclined feed which allows for a more even and controlled distribution of the abrasive, see Figure 23. The previous method of controlling the feed rate was by adjusting the nozzle size, shape or position. The modification allows the actual mass flow rate of abrasive abrading the sample to be determined if required, by collection of the sand that falls of the sides of the wheel and subtracting this from the total volume of sand used. The sample position has also been adjusted with the loading being directly above the sample. This modification allows the abrasive to be fed directly onto the wheel further increasing the control of the feed rate. A further modification made by NPL involves a direct fluid feed added behind the abrasive feed close to the wheel to allow wet slurry testing to be performed. As mentioned, a test exists (ASTM G105) that allows wet testing, however the test is very different in design and this modification allows all conditions to be kept constant and allows direct comparison between wet and dry environments.

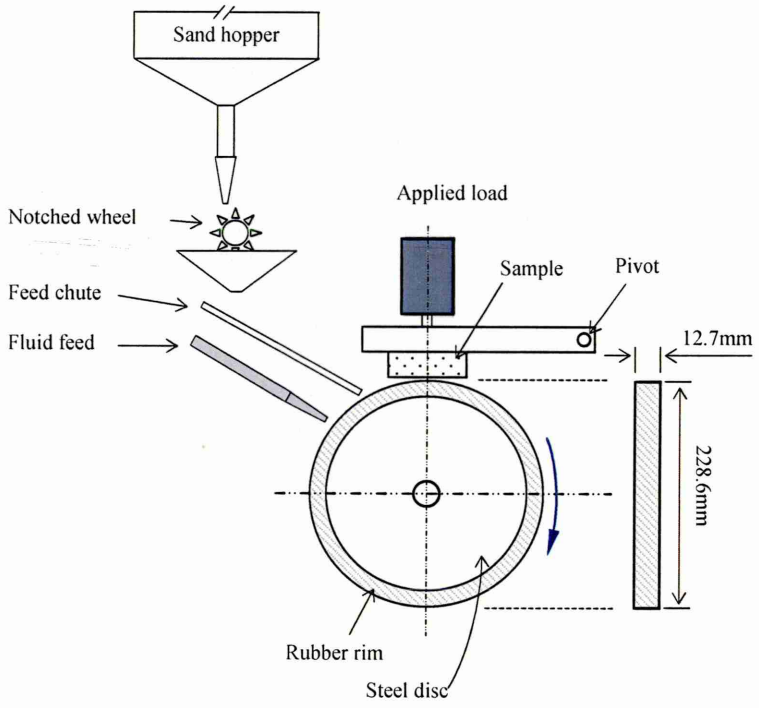

Figure 23: Schematic diagram of modified DSRW test with improved abrasive flow (Not to scale).

The proximity of the fluid feed to the wheel prevents formation of water droplets which allows a constantly wet wheel with no abrasive build up around the sample. The water is pumped from an external deionised water source by a peristaltic pump.

2.15.2 The role of a fluid carrier in abrasion process

Research by Wirojanupatump and Shipway[82,83] involved a comparison of the wet and dry behaviour of mild steel using a modified DSRW tester. It was stated that the abrasive wear rate of mild steel was directly proportional to load when abraded by alumina and silica in both wet and dry environments. It was also concluded that testing carried out in a wet environment using

both alumina and silica abrasives significantly reduces the wear rate of mild steel, more so with rounded silica particles. Smaller angular abrasive powders tended to promote wear by the two-body wear grooving mechanism whereas larger rounded particles promoted three-body wear. It was demonstrated that a linear relationship existed between mass loss and sliding distance.

It is worth noting here that the tester used in this work was also a modified ASTM G65 similar to the NPL tester. There is however one significant difference. The sample position was moved to sit 45 ° to the lowest point of the wheel. The author feels that this may lead to a build up of abrasive, and hence uncontrolled feed rate, at the wheel/sample interface as the abrasive is in effect dropped into the wearing contact as oppose to being fed as with other tests. Further, Wirojanupatump and Shipway[82] carried out testing at relatively low loads, 23 to 75 N, and a low abrasive feed rate was also employed, 70 – 80 g/min. The ASTM G65 standard states that a lower load of 40 N should be used as a variation for the testing of low abrasion resistance materials. The exact sliding distance or test duration used for tests was not stated.

In a study of abrasive wear under three body conditions by Rabinowicz *et al.*[12] suggested that the introduction of a lubricant, in this case oil, to the wearing interface increased the wear rate due to the action of flushing away wear debris and increasing the effectiveness of the abrading action. However, research performed by Swanson showed that plain carbon and low alloy steels experienced a decreased wear rate in the wet environment, between 15 and 30%, it was also reported that both tests produced the same wearing mechanism[87].

Research by Haworth showed that abrasion of steel with angular and rounded silica was lower in a wet environment than under dry conditions[90]. Swanson, in Wirojanupatump and Shipway[82], suggested that the introduction of water as an aqueous carrier in the DSRW test would reduce the temperature of the rubber wheel compared to dry tests thus reducing the loss of rubber hardness. In further work carried out by Wirojanupatump and Shipway[91], they found that specimen temperatures reached up to 65°C in dry conditions whereas in wet conditions the specimen remained at the temperature of the water. Stevenson and Hutchings[79] showed that the hardness of a polyurethane rubber wheel falls from 60 IRHD at 20°C to 50 IRHD at 70°C.

Research carried out by Gant *et al.* using the modified ASTM G65 at NPL assessed the abrasion resistance of WC/Co hardmetals in both wet and dry environments[92]. It was shown that an increase in wear was seen when carrying out tests in the dry environment. It was suggested that the reason for this was possibly due to the lubricating effect reducing the stress between the abrading particle and sample surface.

It was concluded in Shipway and Wirojanupatump[91] that water lubricates the contact between the abrasive particles and specimen which reduces the friction induced deformation, significant in two-body grooving wear.

This literature review has highlighted the dominant wear mechanism responsible for the loss of material on soil working tools. The effect of soil properties in the mechanism and rate of removal has also been discussed along with previous attempts at improving wear lifetimes of such tools. Previous literature involving the wear tests that are to be used in order to evaluate any improvements in wear resistance of modified Armatech coatings was also reviewed along with the techniques used to manufacture and apply Armatech.

Chapter 3 will now provide a review of the analytical techniques used in this research to classify and assess material performance/characteristics and examine resultant wear mechanisms from testing.

Chapter

3

Analytical Techniques

3 Introduction

This chapter describes the methods used for material production and reviews the basic theory of the analytical techniques used to characterise and assess the materials developed within this research.

3.1 Manufacturing method

The pre-existing coating is a powder metallurgy (PM) coating, known as Armatech. The coating is a commercially available product that is currently produced by Chapmans Agricultural Ltd, Sheffield and is described in further detail in Chapter 5. The company developed the method for producing the coating to steel parts from powder slurry. It was a requirement of this research that any modification to the coating composition be compatible with the pre-existing production process.

The powder was mixed with 12wt.% tap water (Sheffield) to form aqueous slurry. The substrates, either a boron or mild steel, were made oxide and grease free by tumbling with S390 round steel shot for 20 – 30 minutes. The process of applying the slurry to the steel substrate can be carried out by either dipping, painting or spraying, depending upon the geometry of the part to be coated. A binder phase of bentonite clay was added to coating to aid the adherence to the substrate material. Typical thickness of the final coating is 1 – 3 mm. The parts are then sent through a conveyor belt furnace process to sinter the coating, a profile of the furnace can be seen in Figure 24 and the parameters are summarised in Table 3. This process consists of a 90°C drying oven, followed by a short cooling chamber. This is followed by 3.3 m sinter furnace with a nitrogen atmosphere (600 litres/min) at a maximum temperature 1083°C** and a belt speed of 5 m/hr. This section is followed by a 7 m water cooled chamber where the tool cools to around 50°C before exiting the chamber. While the maximum temperature through the sinter furnace is 1083°C, the actual temperature that the tool experiences is around 1060 °C. Once the coating has been sintered on to the steel substrate the whole part is subject to a 960 °C heat-treatment (no heat treatment is carried out on mild steel substrate components) and oil or water quenched to achieve a core hardness of 50-55 H_{RC} (513-595 H_{V10}). Following this a temper process is carried out at 200 °C for 6 hours which produces a steel substrate with 48-53 H_{RC} (484-560 H_V10). The heat treatment and tempering do not appear to affect the coating.

** Temperatures measured by thermocouple used to control furnace temperature, accurate to within ± 2°C.

Table 3
Sintering furnace conditions.

Furnace type	Conveyor belt
Belt speed [m/hr]	5
Total belt length [m]	18
Atmosphere	100% N_2 (99.9% purity)
Maximum sinter temp.	1083°C (± 2°C)
Sinter furnace length [m]	3.3
Cooling process	Water cooled chamber, N_2 atmosphere (600 l/min)

The tools exit the water cooled chamber at around 50°C having left Zone 3 at 1062°C, this is a total distance of 7.2 m at a speed of 5 m/hr (72 min) which yields an average cooling rate of 14°C/min.

3.2 Hardness determination

Hardness testing is a process that attempts to measure a materials resistance to plastic deformation by penetrating the surface with an indenter made of very hard material, measuring the amount by which the material has been deformed. Whilst hardness is a key material property that can provide useful information on the ability of a material to resist deformation, the greater the hardness the greater the ability to resist deformation, it is not wholly indicative of wear resistance.

The indenter is pressed into the surface of a test material at a specific applied load (1–50 kg for bulk hardness and 10–1000 g for micro hardness) for a specific amount of time. The Vickers indenter is diamond in shape with an angle of 136° between the faces, Figure 25. After indentation both dimensions of the indentation are measured, *d1* and *d2*, and the average converted in to Vickers hardness value, H_V, using Equation 6.

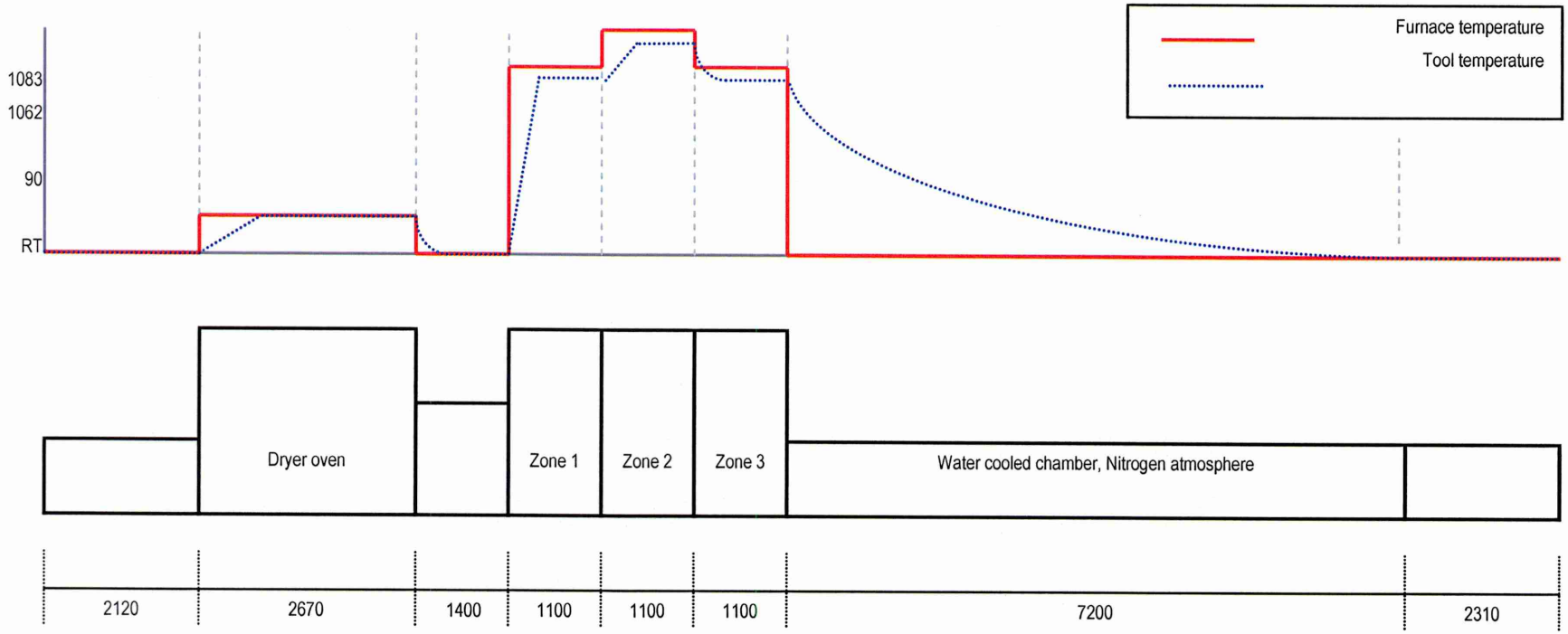

Figure 24: Temperature profile of the sintering furnace as a function of time; a total length of 18 m at a belt speed is 5 m/hr.

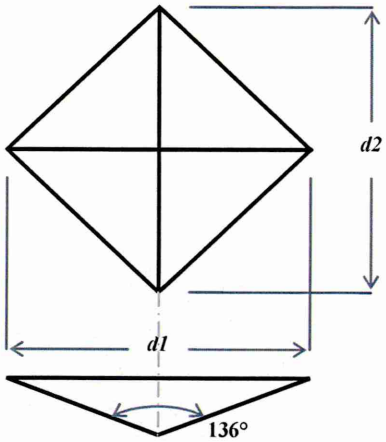

Figure 25: Vickers hardness indenter.

$$H_V = (2F\sin(136°/2)) / D^2$$

Equation 6: Vickers hardness calculation.

H_V = Vickers hardness number, F = Applied load in kg and D = Average of $d1$ and $d2$ in mm.

The hardness of the coatings were determined using two Vickers indentation techniques.

3.2.1 Macrohardness

Bulk hardness measurements were carried out using a Vickers macro-hardness indenter at a load of 20 kg (H_{V20}). Indentations were made to polished (1 µm finish) surfaces and a series of five indentations were made (n=5) and the average calculated. Measurement of indentations was performed using a calibrated optical unit on the tester. Errors within the measurements, generally from the measurement of the indentation, were calculated using the standard deviation (σ) and standard error ($S_E = \sigma / \sqrt{n}$).

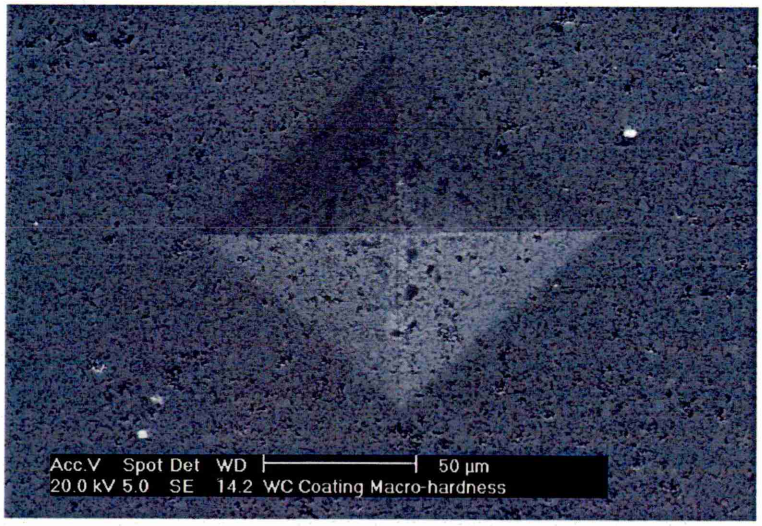

Figure 26: SEM micrograph of a typical 20 kg Vickers indent on a WC-Co tile.

3.2.2 Microhardness

Individual phases in the microstructure were measured where practical. Microhardness results were carried out using a Mitutoyo Microhardness Tester with a load of 25 g and a total indentation time of 20 seconds, including loading and unloading. Microhardness results inherently provide a higher hardness value when compared to standard macro Vickers bulk

hardness testing[93]. Under macro conditions the whole of the material is being tested, for example any hard carbides or secondary phases, softer matrix materials or pores, voids and binders are included in the measurement (unless a manual effort is made to avoid these) and an average of these phases is measured. Microhardness produces a much smaller indent, therefore allows individual phases within a structure to be measured, whilst macro hardness provides an average of all phases.

Indentations were made to polished (1 μm finish) surfaces and a series of five indentations were made (n=5) and the average calculated. The indentations were measured using the calibrated optical eyepiece on the tester. Errors within the measurements were calculated using the standard deviation (σ) and standard error ($S_E=\sigma/\sqrt{n}$).

3.3 Density measurement of sintered materials

The measurement of specific density, ρ_a, was performed using the Archimedes method with a Sartorius density balance and in compliance to the test procedure set out in ASTM C914-95[94].

Since the materials being developed were coatings normally adhered to a steel substrate, specific samples were prepared without a substrate for density measurements. Density samples were produced by sintering each material on an alumina tile; allowing easy removal and measurement without the influence of a substrate. Due to the presence of porosity and cracking, water could penetrate into the sample by capillary action and the need for an impermeable coating of wax was required.

The samples were cleaned and oven dried to remove any excess moisture and the initial weight, W, measured in air. The samples were then coated in beeswax and allowed to cure. The wax weight, P, was then measured. The weight of the coated specimens was then measured suspended in water, S. Weights of the specimens were measured to an accuracy of ±0.0001 g.

The volume of the specimen and wax, V_1, measured in cubic centimetres can be calculated using the following equation (assuming 1 cm^3 of water weighs 1 g):

$$V_1 = P - S$$

Equation 7

The volume of the wax coating, V_2, can be then be calculated (where K is the density of beeswax, 0.961 g/cm^3):

$$V_2 = (P - W) / K$$

Equation 8

The volume of the specimen, V, without the wax can then be calculated from the following:

$$V = V_1 - V_2$$

Equation 9

Allowing the bulk density, B, of the specimen which, includes any pores within the sample but excludes the volume of wax, to be determined by:

$$B = W / V$$

Equation 10

Theoretical densities of the modified coatings were calculated using the measured density of Armatech by the above procedure, and using the density values of the additions that were added as listed in the CRC Handbook[95]. Comparison of the measured density to the theoretical density can provide some idea of the bentonite content and possibly porosity within the material.

3.4 Particle size distribution

The particle size distribution provides information as to the relative amounts of particles present in a powder dispersed in a liquid, sorted according to size. Particle size distribution can be important in understanding physical and chemical properties. It has been shown to affect the strength of soils, discussed in Chapter 2.

The distribution results can be presented in the form of a range, or in cumulative form, in which the total of all sizes retained or passed by a single theoretical sieve is given for a range of sizes. The range is appropriate when a particular ideal mid-range particle size is desired, while cumulative analysis is used where the amount of under-size or over-size particles is required

Particle size analysis was performed using a Malvern Particle Size Analyser. A small amount of each powder was dispersed in water and very small quantities of Teepol detergent were used to break down any agglomerations present. A typical distribution is shown in Figure 27, a bi-modal distribution can be seen by the twin peaked volume distribution series, often seen with powder analysis. The red series plotted is the cumulative distribution. Also provided are the D values, these values provide the particle sizes at which 90, 50 or 10% (D0.9, D0.5 and D0.1 respectively) of particles (by volume) are smaller and the rest larger than this value.

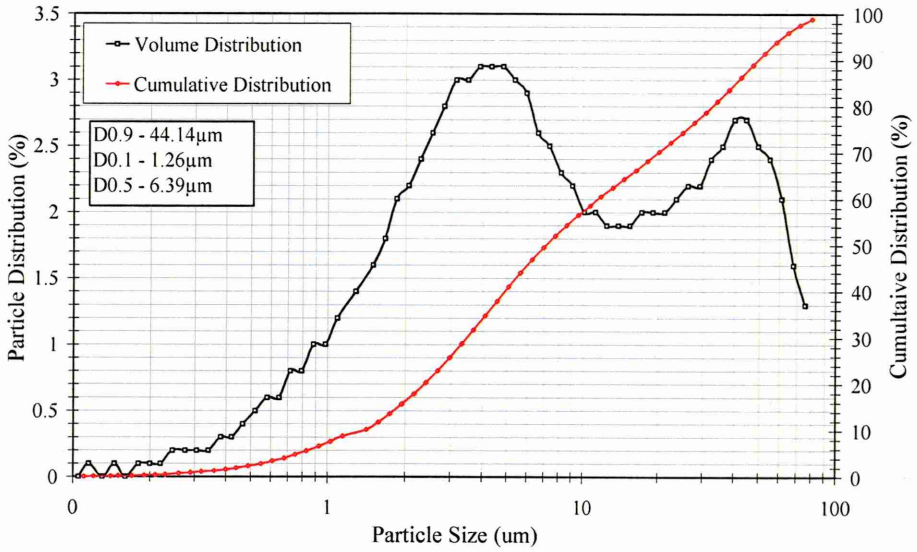

Figure 27: Typical graph from a particle size analysis of a powder.

3.5 pH Analysis

The pH level of abrasive media has been shown to affect the severity of abrasion through a corrosive nature on WC-Co alloys, an increase in volume loss was observed with a decrease in pH[77]. For this reason the acidity of solutions was measured according to BS7755-3.2[96] at room temperature. The mixtures were stirred vigorously for 5 minutes using a mechanical mixer and allowed to settle for 2 hours until a supernatant†† formed. The suspensions were then shaken and the measurement was taken in the settling supernatant allowing the pH meter to stabilise.

3.6 Scanning Electron Microscopy

The existing coating was modified by the addition of secondary phase hard particles in an attempt to manipulate the existing microstructure to increase wear resistance. The particle size of the addition, the degree of interaction between the addition and existing microstructure, the resultant microstructure and the mode of wear exhibited by the newly developed materials all require high magnification microscopy and elemental analysis.

Secondary electron imaging (SE) uses low energy electrons that originate from only a few nanometres surface depth and hence provide topographical information.

Back scattered electron imaging (BSE) uses high energy electrons generated from within the interaction volume of the electron beam, see Figure 29. BSE can be used to show contrast in elemental difference within a microstructure; the higher the atomic number the brighter the contrast[97]. This allows different phases and chemical reactions to be seen.

†† Clear settled solution.

A Philips XL40 Scanning Electron Microscope equipped with both SE and BSE imaging was used to examine wear mode topography and along with energy dispersive X-ray analysis to examine microstructural differences.

3.7 Energy Dispersive X-ray Analysis

The SEM was also equipped with Energy Dispersive X-ray Analysis (EDX) tools. EDX measures the characteristic X-rays given off when the primary electron beam bombards a sample. Electrons from the beam transfer energy to electrons around the atoms of the sample resulting in these electrons gaining enough energy to be ejected from the atom. This vacant position is then eventually occupied by a higher-energy electron from an outer shell losing energy and filling the vacant inner shell. This process of the outer shell electron transferring to the inner shell gives off characteristic energy emitted as an X-ray (Figure 28). The amount of energy given off is dependant on which shell it is transferring from, and which shell it is transferring to. Hence a K_α X-ray is produced by an electron from the L shell replacing a K shell electron and a K_β X-ray is produced by an M shell electron replacing a K shell electron.

Each element releases X-rays with unique amounts of energy and thus elements can be identified by measuring the energies (frequencies) of x-rays emitted from a sample.

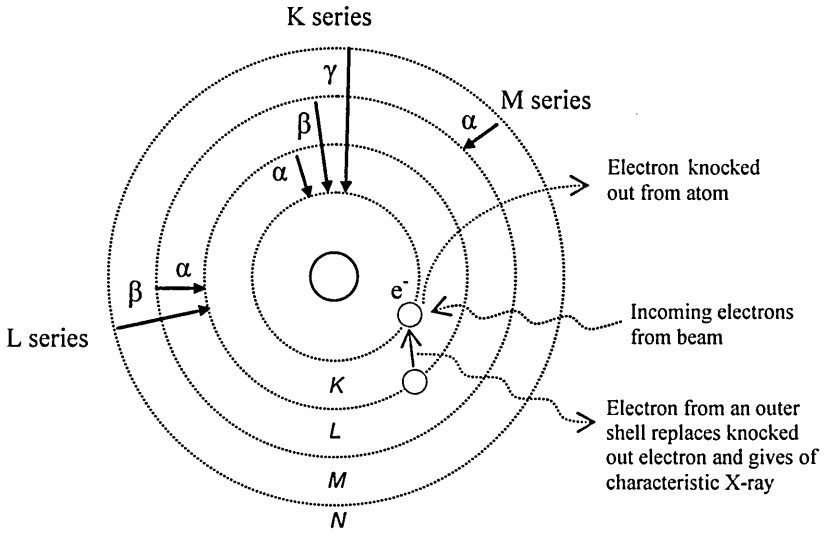

Figure 28: Schematic representation of the identification of an electron transferring from a higher-energy shell to a lower-energy shell.

The nature of EDX analysis allows both qualitative and quantitative compositional data to be collected. Qualitative analysis can be performed using either a spot or area analysis. Spot analysis provides a spectrum of elements present within the interaction volume at the probe position, or by scanning the surface a compositional map can be constructed showing intensity for each element selected.

Quantitative analysis uses ZAF correction (Z = atomic number, A = absorption and F = fluorescence) and can provide data regarding the atomic or weight percentage of elements present and thus specimen composition. The system should be calibrated using a pure standard to ensure accuracy.

3.7.1 Limitations of EDX analysis

A disadvantage associated with EDX analysis is the detection of characteristic X-rays from very light elements. Detectors often use a beryllium or carbon window which absorbs the majority of low energy X-rays making elements of low atomic number difficult to detect. Typically EDX can detect high levels of carbon (C) and oxygen (O) but nitrogen (N) and boron (B) are not detectable unless present at very high concentrations. For this reason it was not possible to map for B in the analysis of the Armatech microstructure.

A further problem with EDX analysis is the detection of carbon. While the system is able to detect the presence of C, quantitative measurements are often inaccurate due to the electron beam depositing carbon on to the sample surface. For this reason quantitative results for carbon often suggest it is present at a higher level.

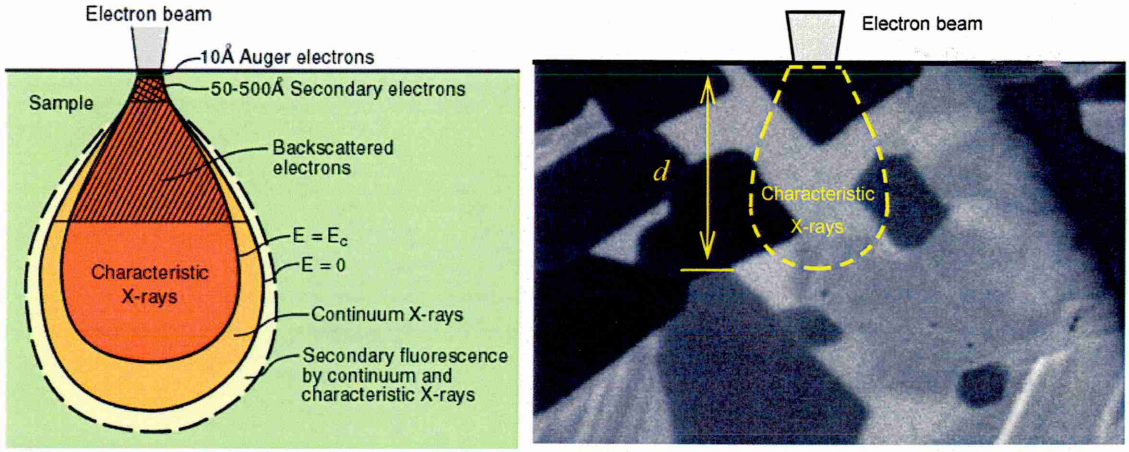

(a) (b)

Figure 29: a) Interaction volume of electron beam [98] and b) possibility of elemental contribution from surrounding phases.

Quantitative results can provide very useful information but may also be misleading due to effects caused by the interaction of the electron beam with the sample. It can be seen from Figure 29(a) that the characteristic X-rays used to determine elemental composition are generated from within the interaction volume beneath the surface of a sample. This volume is a function of the accelerating voltage of the beam and also the atomic weight of the elements present in the sample. For this reason, uncertainty is introduced when selecting an area or spot to analyse as it may appear to the operator that analysis is being acquired from a certain phase on the surface but the phase may only be several nm in thickness, so in actual fact X-rays are being collected from the region below which is of a different composition. An example of this

is shown in Figure 29(b). The micrograph represents a cross-section through the Armatech coating. It can be seen that the electron beam is targeted on the surface, at the point of a hard phase but the volume of interaction is measuring characteristic X-rays from surrounding matrix and other hard phases beneath. To overcome this problem it is best to measure a large quantity of phases from several areas and calculate the average, but caution should be taken when placing any emphasis on EDX quantitative results.

3.8 X-ray Diffraction

Around 95% of all solids may be described as crystalline in nature[99]. X-ray diffraction (XRD) is a non-destructive analytical technique that can provide information about chemical composition and crystallographic structure of a material.

A crystalline structure is one that has a periodic arrangement of atoms in a regular and repeating 3D pattern, atoms arranged irregularly and randomly such as found in liquids are classed as amorphous. Glass is a typical amorphous material. A crystal lattice is a regular three-dimensional distribution (cubic, rhombic, etc.) of atoms in space. The dimensions of a crystalline structure (the unit cell) can be described by three axes; a, b and c and the angles between each; α, β and γ[100]. They are arranged so that they form a series of parallel planes separated from one another by a distance *d*, which varies according to the nature of the material.

When a crystalline structure, pure or a mixture of elements, is bombarded with a monochromatic X-ray, the beam is diffracted in a characteristic manner dependant on the sample. XRD measures the average spacing between the atoms and planes and can determine the orientation of a single crystal or grain.

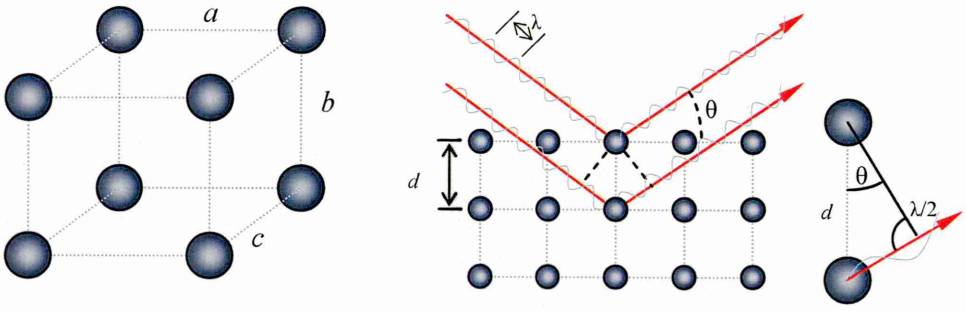

Figure 30: Bragg's Law.

The X-ray beam is generated by an X-ray source generally Mo, Cu, Co or Cr tubes. The beam is passed through a series of filters towards the sample. A detector is then rotated around the sample by and angle of θ, by varying the angle Bragg's Law conditions are satisfied by different *d*-spacings in polycrystalline materials (Equation 11).

$$n\lambda = 2d \sin \theta$$

Equation 11: Bragg's Equation

Where n is an integer, λ is the wavelength of the incident X-ray beam, d is the spacing between the atomic planes and θ is the angle between the incident ray and the scattering planes. Residual stress is also able to be measured by the peak position and width.

A software database can be used to identify peak positions on the trace produced for phase identification.

Although the XRD equipment was subjected to regular calibration procedures to ensure correct peak positioning and remove any error associated with sample preparation or differences in height, a very thin layer of polycrystalline Si (99.9%) was applied to the surface. Pure Si produces a strong peak at 28.44° 2θ and provides a reference point, this allowed for any error in sample preparation or height by correcting 2θ.

X-ray diffraction data was acquired using a Philips PW1830 Diffractometer using a beam Xcelerator with Cu K_α radiation (λ = 1.5418 Å) operated at 40 kV and 40 mA . Incident and diffracted beam slits were 0.5° and 0.25° respectively. The traces were obtained over a range from 10° to 110° 2θ.

Chapter

4

Tribological Testing: Review and Procedures

4 Introduction

A major objective of this study was to establish the relevant wear mechanisms occurring on soil working tools. Assessing and understanding the wearing mechanisms is of paramount importance in order to assess the ability of test rigs to recreate wear modes.

The diversity and variance of field conditions found within soils across the UK, for example abrasive type, soil strength and moisture levels can give rise to significantly different wear rates. However, due to there being no established network of research on soil tillage tools, the means of obtaining post service tools, is reliant upon the willingness of farmers to provide tools for research. Ideally, in the case of coated tools, well before tool lifetime has been reached.

4.1 Tool life

In the agricultural industry there are no strict limits to the life of a tool, the life is generally decided upon by the situation and the farmer. A considerable amount of material loss, up to 95% in some cases, can typically occur before a tool is replaced (more commonly on deep soil working tools), Figure 31. The type of tooling application will also govern when the need to replace a tool occurs, as will the environmental properties of the soil being worked. The life of a tool is commonly quantified by the amount of hectares able to be ploughed. Figure 31 below shows a new reversible point in comparison with a used point following service.

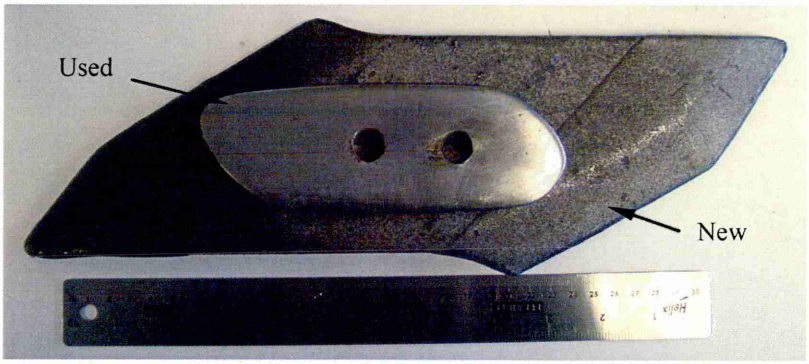

Figure 31: New and used reversible points.

4.2 Post service tool examination

Several tools were obtained which were removed from service for examination. The SEM was used to assess the wear mechanisms. The level of aggressiveness typically means that wear resistant coatings are only present in the early stages of use; once the coating has worn away it is the steel substrate that is working the soil. Due to the lack of test facilities, actual field tools have to be collected from working farms. The constraints associated with farm labouring cause the amount of data received with each tool to be poor or nonexistent. Properties such as geographical location, soil type, time in service and plough position are generally not known.

Though these factors are considered important, especially when comparing the performance of a series of materials, however, it was considered to be negligible for the objective of determining the major wear mechanisms and the tools were considered representative of all soil working tools. The importance here was to determine the type and appearance of wear mechanisms occurring. However, although several tools from different locations were examined, the particular micrographs of the tool surfaces in this chapter were from Trial A of the field tests performed as part of this research (unless stated). So some of the parameters were known and are provided in Chapter 6.

Examination of tools manufactured from the typical material of boron steel and a boron steel coated with Armatech were examined.

4.2.1 Boron steel

A boron steel reversible point removed from service is shown below in Figure 32.

Figure 32: Boron steel reversible point removed from service.

SEM examination of the worn surface of the boron steel point is shown in Figure 33. Heavily worn two-body grooves of varying widths in the direction of travel can be seen (indicated by the dashed yellow arrow). Literature stated that soils contain a wide range of particulate sizes and that groove width is a function of the abrasive particle size. It is also apparent that micro-pitting corrosion has occurred, highlighted by the yellow arrows.

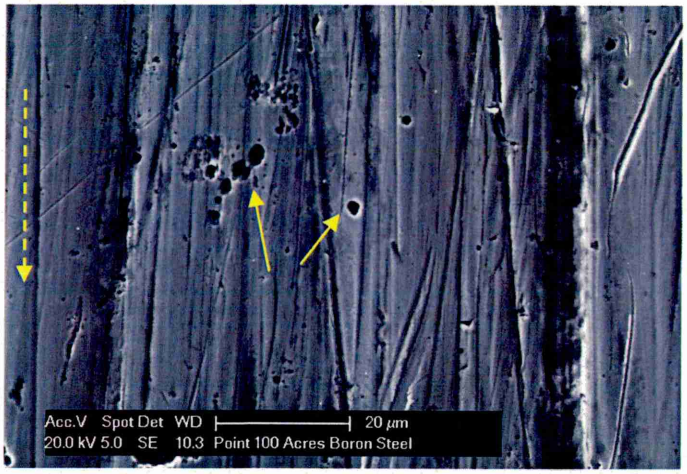

Figure 33: Wear surface of a boron steel reversible point from Field Trial A (see Chapter 6). Evidence of corrosion micro-pitting can be seen.

A second boron steel tool, a tine of unknown service conditions, was also examined. It could be seen that this tool had a 'smoother' appearance and less severe wear mechanism, Figure 34(a).

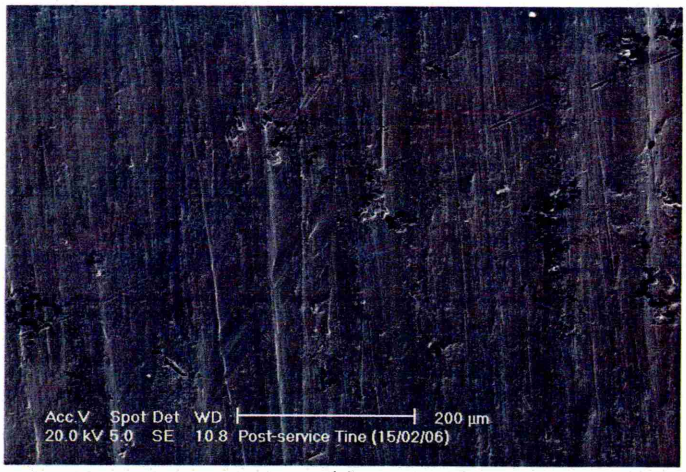

(a)

(b)

Figure 34: Wear surface of a boron steel tine; (a) two-body grooves and surface deformation and (b) at higher magnification clear three-body indentations can be seen.

Signs of intermittent three-body indentations were observed, Figure 34(b). This is most likely due to the tool being a tine as oppose to a point which is a less aggressive tillage operation. A tine is used after ploughing to break up surface clods before seeding occurs. This means that tines experience lower loadings and less severe impacts resulting in the less severe damage.

Examination of the boron tools showed that the ductility of the material produces surface deformation from the wear process. A mixed mode of two-body grooves and three-body indentations could be seen along with micro-pitting caused by corrosion. While the corrosion process is an important factor, the pits are of such a small diameter ($\leq$1 µm) that the amount of material removal created through these must be considered negligible, it may also be the case that the corrosion occurred following removal from service.

4.2.2 Armatech

An Armatech coated reversible point removed during service is shown below in Figure 35. It can be seen that some of the Armatech coating is still present on the boron steel substrate.

Areas of coating can be seen on flat section of the point, highlighted below, with all traces on the leading edges having worn away.

Figure 35: Armatech coated boron steel reversible point soil wear.

Examination of the Armatech coating was performed for wear damage, Figure 36. Figure 36(a) shows large two-body wear grooves around 20 μm in width. Fin edges are clearly distinguishable along the groove edges (indicated by the yellow arrow); it is these fins breaking away that can cause material loss. The micrograph shown in Figure 36(b) again shows a two-body groove but with a much deeper geometry than normally seen, only several microns in diameter. The geometry of the scar suggests that this wear groove may have been caused by a particulate with a very angular morphology or a heavy faceted stone.

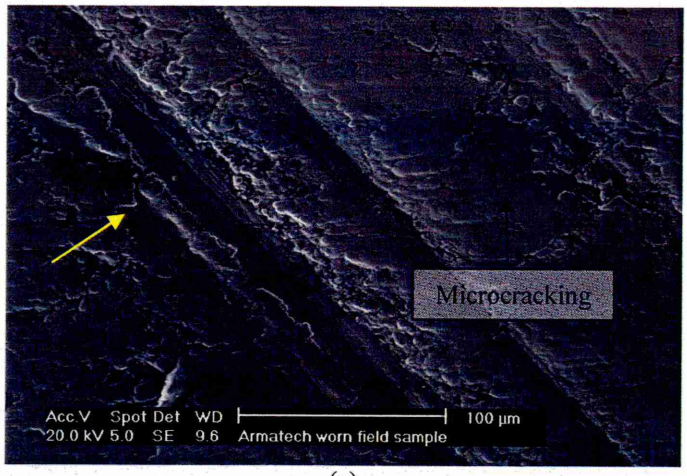

(a)

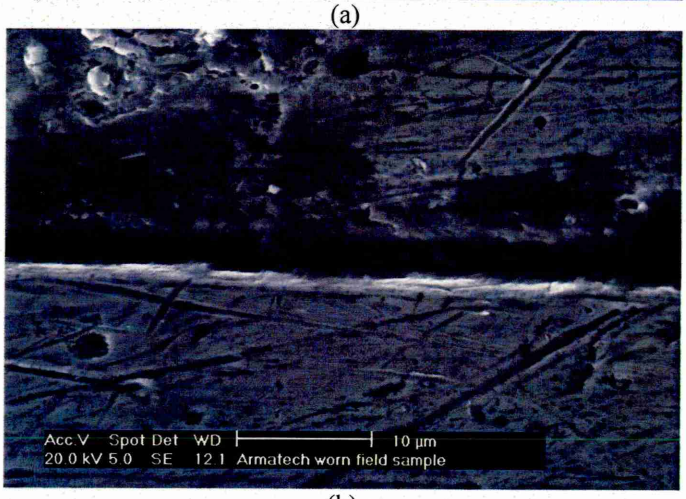

(b)

Figure 36: SEM micrographs of worn tool surfaces showing two-body grooving and microstructural cracking of Armatech.

Closer inspection of the microstructure using BSE imaging, revealed signs of micro-cracking, Figure 37. It can be seen that inter-carbide cracking has occurred within the carbides/borides and also within the interface of the carbide/borides and the matrix. A prominent wear groove that shows signs of the carbides/borides suffering cracking but also plastically deforming.

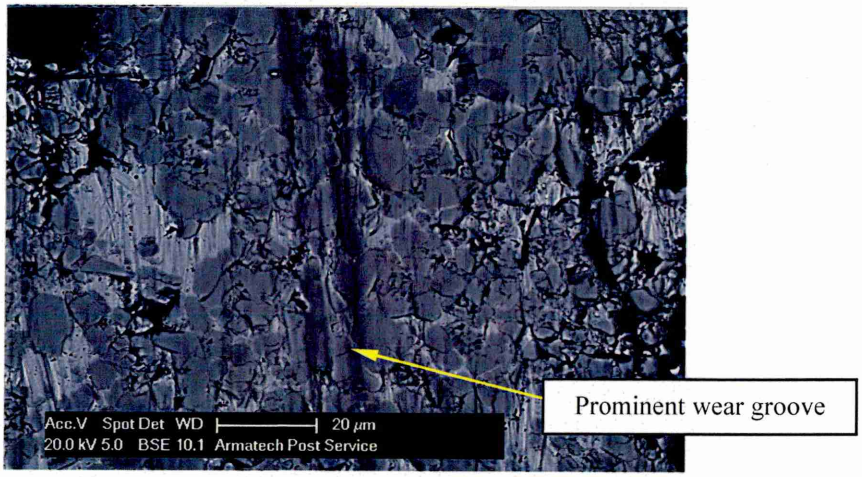

Figure 37: SEM micrograph showing microcracking of microstructure on post-service tool.

A cross-section taken through the tool normal to the direction of the wear was mounted in Bakelite and polished to a one micron finish. The cross-section revealed that around 250 μm of the coating thickness remained on the tool at the point of removal from service, Figure 38(a). The black areas seen in the micrographs are a bentonite clay binder phase (see Chapter 5), which consists of a high percentage of the structure in this particular region, which most likely contributed to a large amount of material loss at the surface.

The microcracking observed in Figure 37 can also be seen in cross-section micrographs in Figure 38(b) and (c). The sub-surface cracking was present along the majority of the surface examined. A higher distribution and depth penetration of cracks appeared to be linked with bentonite areas. In some instances evidence was present that further wear or impacts could cause relatively large amounts of material removal, Figure 38(b) and (c).

Evidence from examination of the Armatech wear surfaces revealed that the dominant wear mechanism was two-body grooving wear. Grooves of varying widths and depth are clearly present. It could also be seen with larger grooves that material may be being pushed to the groove edges causing the likelihood of fin formation, which in turn causes material loss with further wear. However, while some carbides/borides showed signs of resisting against wear by possessing a worn rounded appearance, closer inspection of the microstructure suggested that the primary material removal mechanism was caused by sub-surface microcracking in the more brittle carbides/borides phases. These cracks were present along the whole surface of the coating and in some instances could be seen to penetrate up to 150 μm in depth, especially when associated with bentonite binder phase areas. It is felt that these cracks may be caused by impacts from stones within the soil, or more likely due to the process of wear and applied load experienced by the tool during ploughing.

From the examination of several soil working tools having been removed from service a conclusion can be drawn that the abrasive wear mechanism is overall a mixed mode mechanism with the more dominant wear mode being two-body grooving. The degree of wear and dominance of one wear mode over the other will depend on several conditions previously discussed.

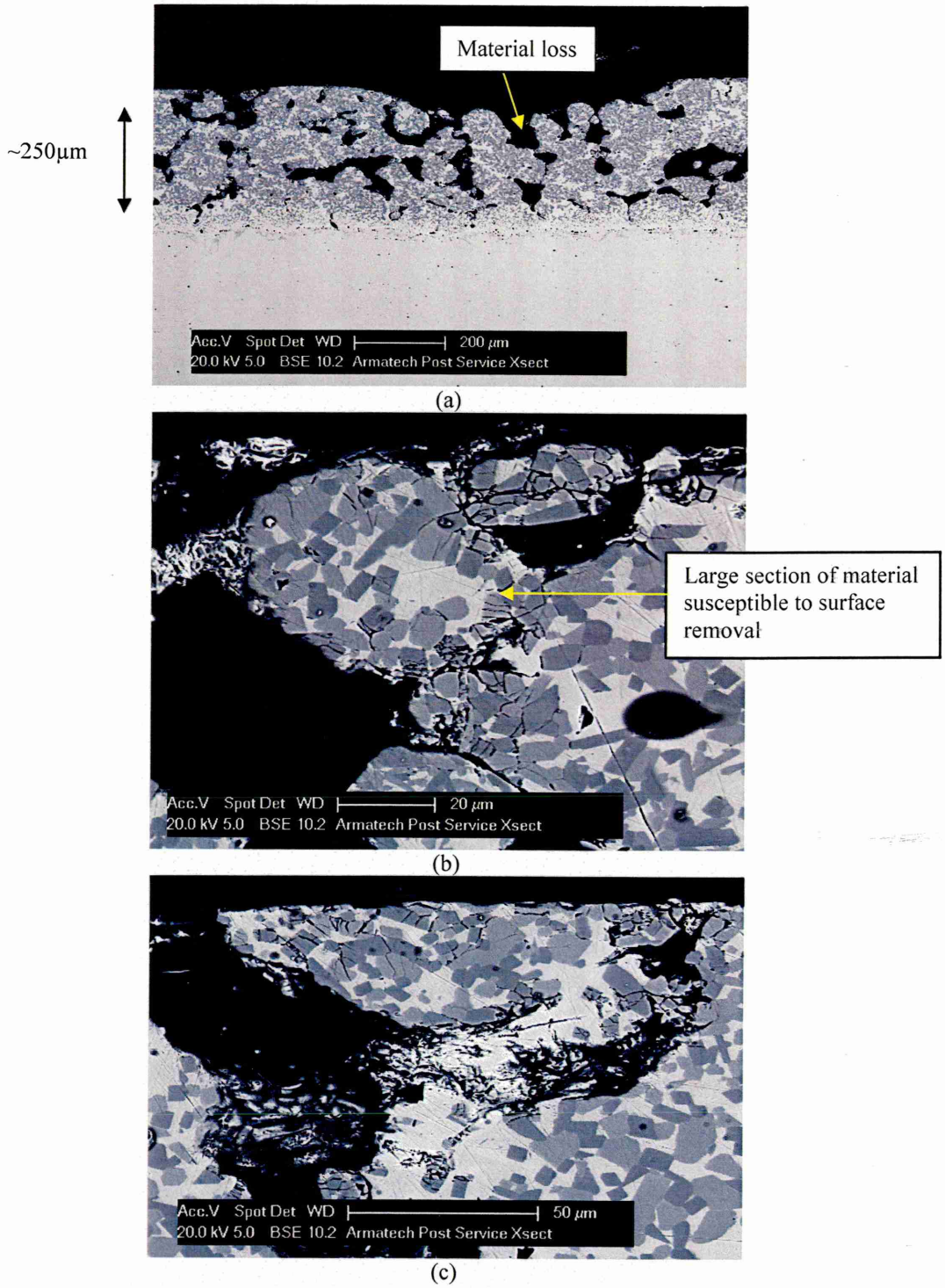

Figure 38: SEM micrographs of cross-section taken normal to the direction of travel; (a) low magnification showing extent of coating thickness remaining and; (b) and (c) evidence of subsurface microcracking.

4.3 Relation of soil wear to laboratory wear tests

It has been shown that soil working tools experience predominantly two-body wear with some signs of three-body indentations. Performing wear tests whereby both wear modes are created in one single test can cause difficulty. Mixed mode wear with the microscale abrasive wear test is considered undesirable and can produce flawed results, see Chapter 6. Wear tests using the

microscale abrasive wear tester (MSAW) to assess the wear resistance of materials for both wear modes independently will be performed. Macroscale testing (DSRW and WSRW) which creates strictly two-body grooving wear at higher loadings will then be performed. Data from basic field trials will also be presented.

4.4 MSAW Test Procedure

4.4.1 Test Specimens

Test samples were manufactured using 32 mm diameter mild steel coupons with a machined recess, Figure 39. The coatings, in slurry form, were poured into the recess, sintered and heat treated according to the manufacturing method described in Chapter 3. The coupons were then ground flat and polished using a final polish with 1 μm diamond paste.

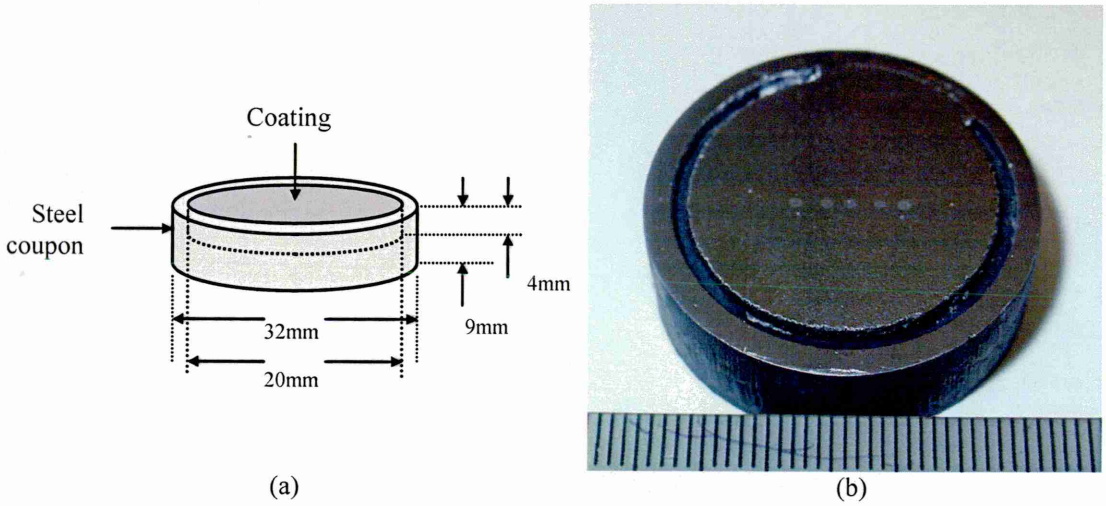

Figure 39: a) Schematic diagram of round test coupons and b) photo.

It was observed upon firing that all samples suffered from a small amount of shrinkage, seen in Figure 39(b), between the coating and inside edge of the coupon. This shrinkage was due the sintering of the powder metallurgy material.

4.4.2 Abrasive media

The particle size distribution of the two abrasives used with the MSAW test in this research along with morphology is shown in Figure 40 and Figure 41. It can be seen from the micrographs that both abrasive powders possess an angular morphology. The particle size distribution revealed that the majority of the SiC particles lie in the size range between 2 and 20 μm with the mean peak at 7 μm. The SiC powder however, was supplied as a 4.5 μm powder and the analysis revealed it to be larger.

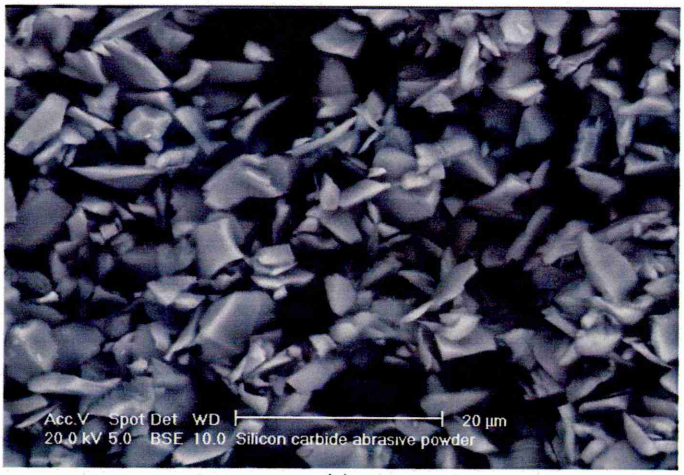

(a)

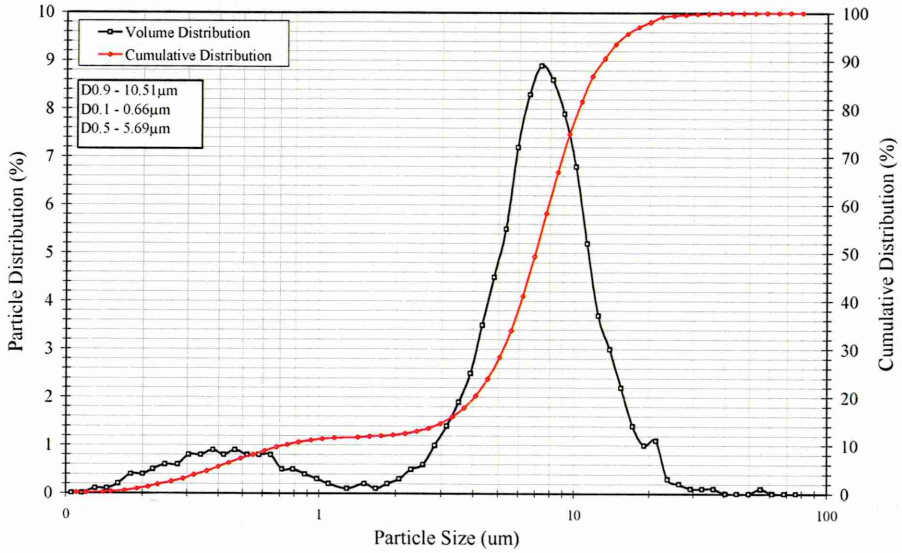

(b)

Figure 40: a) SEM micrograph of SiC abrasive and b) particle size analysis.

The SiO_2 abrasive presents a bimodal distribution, Figure 41. The graph shows the SiO_2 abrasive to be a 1 μm and 2.5 μm powder.

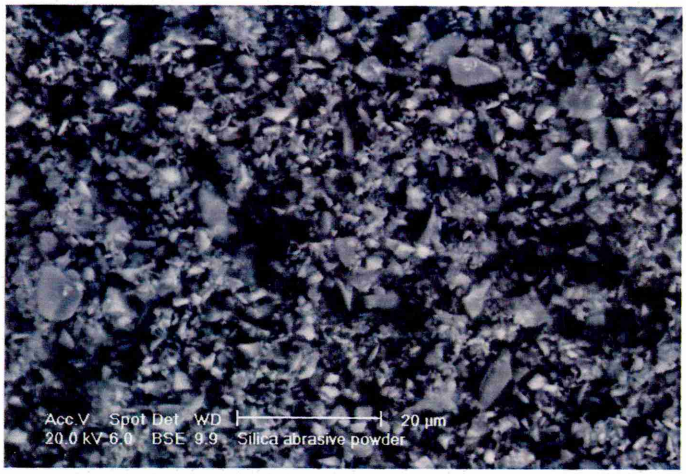

(a)

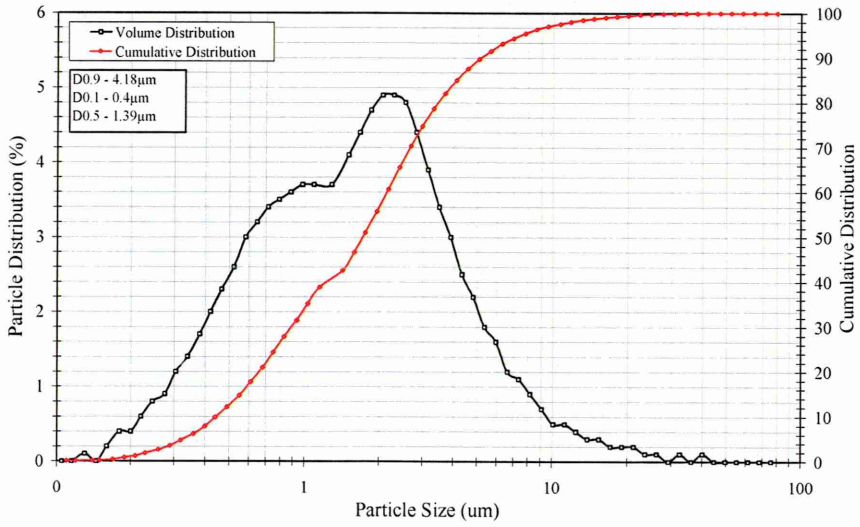

(b)

Figure 41: a) SEM micrograph of SiO_2 abrasive and b) particle size analysis.

The properties of the abrasive powders are provided in Table 4. Aside from the particle size difference the two abrasives have very different hardness values, with the SiC being more than twice that of SiO_2.

Deionised water used in the slurries was allowed to stand in an open container for one hour to allow CO_2 absorption prior to slurry mixing. The water was then added to the abrasive powders in the appropriate ratios.

Table 4
Mass of abrasive particles required for 100 cm^3 of water.

Abrasive	Size [μm]	Hardness [H_V]	Density [g/cm^3]	Mass [g]	Concentration [vol.%]
SiC	7	2500	3.17	80.0	20
SiO_2	2.5 & 1	1050	2.2	65.0	10

The slurries were mixed thoroughly and constantly stirred using a magnetic stirrer throughout the tests to prevent particle sedimentation. The slurry was fed into the ball and sample interface by means of a peristaltic pump on the tester which ensures the ball and sample were well wetted throughout testing. In this work the materials were tested using SiC in order to provide data comparable with other materials in other studies. SiO_2 abrasive was used in an attempt to recreate, to a certain degree, the environment found in typical soils.

4.4.3 Wear scar measurement

The wear scar diameters were measured using a calibrated SEM. The diameters were measured parallel to the direction of ball rotation and at three subsequent forty five degree angles and the average calculated.

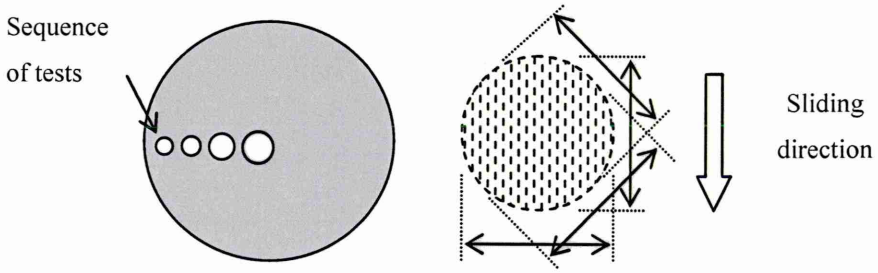

Figure 42: Test sequence and dimensions of crater measurement.

An SEM micrograph of a typical wear scar produced using SiC on Armatech is provided in Figure 43.

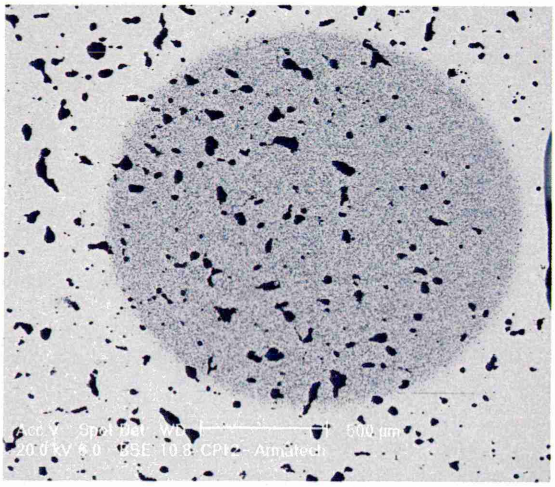

Figure 43: SEM micrograph of a typical MSAW scar produced on Armatech using SiC abrasive and an applied load of 0.4 N.

4.4.4 *Poorly defined wear craters*

Occasionally with MSAW testing the wear crater produced may be non-spherical or show signs of 'ridging'. Shown below in Figure 44(a) is a wear scar produced on a boron steel surface using 7 µm SiC abrasive. It can be seen that the scar is non-spherical in shape and has two protruding areas at the left and right hand edges of the crater. These phenomena are suspected to occur due to slurry starvation in the sample/ball interface. The slurry is pushed out of the interface zone and creates increased wear at the crater edges.

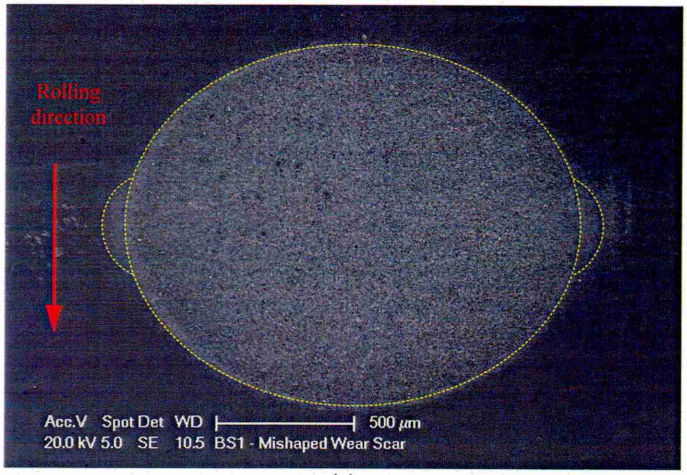

(a)

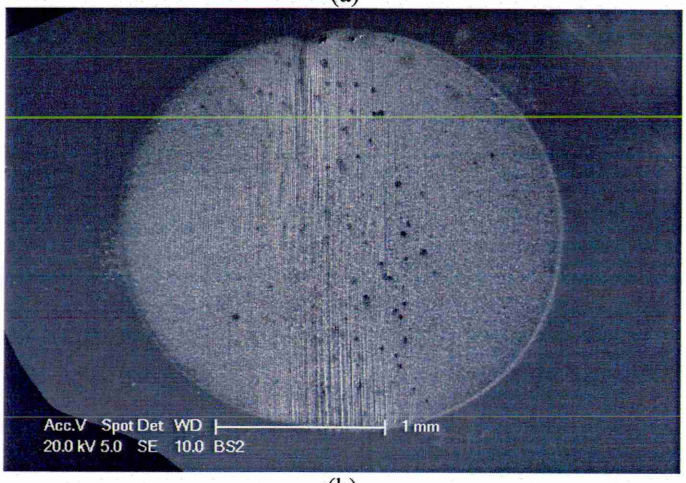

(b)

Figure 44: Boron steel sample worn with 7 µm SiC abrasive; (a) non-spherical wear scar and (b) ridge formation associated with high applied loads (5 N).

A further phenomena is the effect of ridging[73,101,102,72]. High loading causes little or no wear at the centre of a wear scar due to abrasive slurry starvation in the wearing interface from the high contact pressure, Figure 44(b). The lack of abrasive slurry allows the sample and ball to come into direct contact and forms deep wear grooves much larger than the abrasive diameter, early onset of ridging with a distinctive undulation like appearance is shown at low magnification, Figure 45.

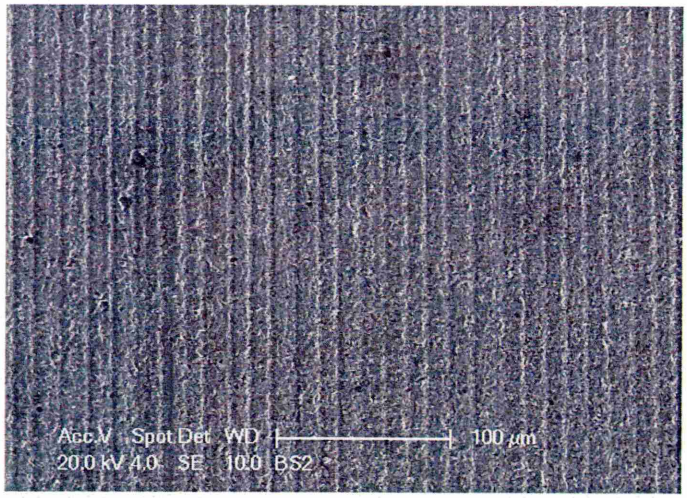

Figure 45: Boron steel sample worn with 7 µm SiC abrasive at 5 N applied load showing surface undulations from the onset of ridging.

Traditionally travelling optical microscopes are used to measure wear scars to calculate wear volumes and rates. As can be seen from Figure 46, there is no distinct edge to the wear scar which can cause problems in defining the real crater edge. Due to this optical microscopy can over estimate crater size, which has been shown through comparison of profilometric wear volume measurements[73].

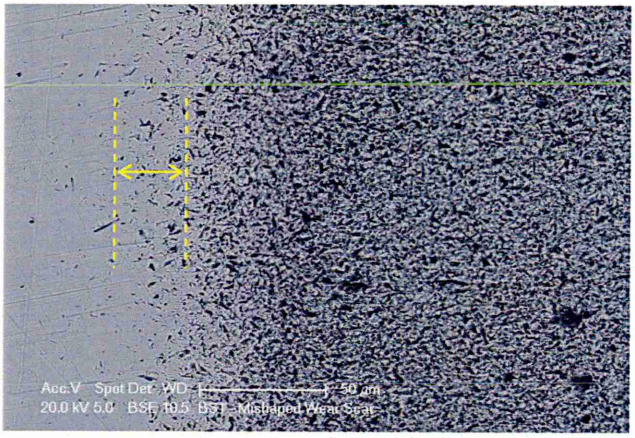

Figure 46: A MSAW scar produced using SiC showing difficulty in determining edge definition.

Figure 46 shows a boron steel surface having been worn using SiC abrasive under a load of 0.8 N. It can be seen that the crater edge has no definable edge, with a boundary of around 30 µm, equating to a 60 µm deviation in the width measurement. The average wear scar diameter is generally between 1000 - 1500 µm, which yields an error of 6 – 9%. Due to this some user judgement has to be made as to where to take measurements.

To eliminate this discrepancy wear craters were measured using a calibrated SEM measuring system to provide more accuracy in measurement, however at high magnification there is still room for error. The MSAW test inter-laboratory exercise carried out, stated a standard deviation in optical measurement of wear scars to be 2% repeatability with in laboratories and 3% reproducibility between laboratories[73].

4.5 Quantitative wear calculation

There have been over 300 proposed wear models and equations in published literature which include over 100 different variables and constants, the most widely used to calculate wear rate however is the Archard equation[103]. It has been shown that load, pressure, force, sliding distance and speed can all affect the rate of wear (Chapter 2). Finding a wear equation that incorporates such a wide range of conditions and materials would have enormous practical value.

4.5.1 Wear volume removed

The wear volume of the spherical wear scar produced in the MSAW test can be calculated using the crater dimensions and geometry of the wear ball:

$$V \approx \pi b^4 / 64R \qquad \text{for } b \ll R \qquad \text{(a)}$$

$$V \approx \pi h^2 R \qquad \text{for } h \ll R \qquad \text{(b)}$$

Equation 12: Spherical wear scar volume.

Where V is the wear volume measured in mm^3, b is the diameter and h the depth of the wear scar and R is the radius of the steel ball all measured in mm. The wear scar is assumed to reproduce the spherical geometry of the ball.

4.5.2 Specific wear rate, κ

From the calculation of the wear volume the specific wear rate coefficient, κ (Nm^{-1}), may be calculated by re-arranging the Archard equation[104] and the wear resistance, κ^{-1}, being inversely proportional to this:

$$V = \kappa SL \qquad (a)$$

$$\text{Re-arranging:} \quad \kappa = V / SL \qquad (b)$$

Equation 13: Archard specific wear rate coefficient equation.

Where S is the sliding distance measured in metres and L is the applied load measured in N. Archard assumed that the material loss was proportional to both the sliding distance and load and the wear rate was independent of contact area for a given load and sliding speed. It is worth noting that the equation assumes that wear rate is independent of contact area and hence pressure and was originally devised for adhesive wear but is now used for abrasive wear. Furthermore, the equation was originally devised for dry abrasives and not wet slurries.

4.5.3 *Relative wear rate, RWR*

The relative wear rate is the ratio of volumetric wear of a reference material divided by the volumetric wear of a test material. In this work, two reference materials have been used, so two separate RWR values will be listed throughout. Firstly boron steel is used as a reference material against all other test materials (RWR_{Boron}), RWR values will then also be stated with respect to Armatech as the reference material ($RWR_{Armatech}$). RWR values >1.0 show better wear performance whilst values <1.0 perform less well. In the case of ASTM G65 tests and field tests direct volumetric wear will be used to calculate RWR, whilst MSAW RWR values will be calculated using κ from the multiple load method.

4.5.4 *Multiple load method, MLM*

The specific wear rate for each crater produced at each load can be calculated using Archard's equation, but adopting the MLM method described in Jones[102] allows a more accurate approach. The Archard equation (Equation 13) is limited to situations in which the wear volume is directly proportional to both the load and sliding distance. Specific wear rate ($mm^3/N/m$) via the MLM method can alternatively be calculated via a plot of wear volume per unit sliding distance (mm^3/m) against varying loads (N), in this case 4 loads (see Figure 47). The resulting gradient of a linear regression analysis then provides κ for the sample, the error is determined from the S_E of the gradient.

The offset in *x*-axis intercepts is regarded as being due to an offset in the applied load caused by the load arm balancing. This method of determining κ for a sample is independent of any uncertainty in the applied load caused by balancing and hence is a more accurate determination of κ than that from individual loads. This method of determining κ, is especially important for tests carried out using low loads, due to any offset in load being a significant fraction of the actual applied load.

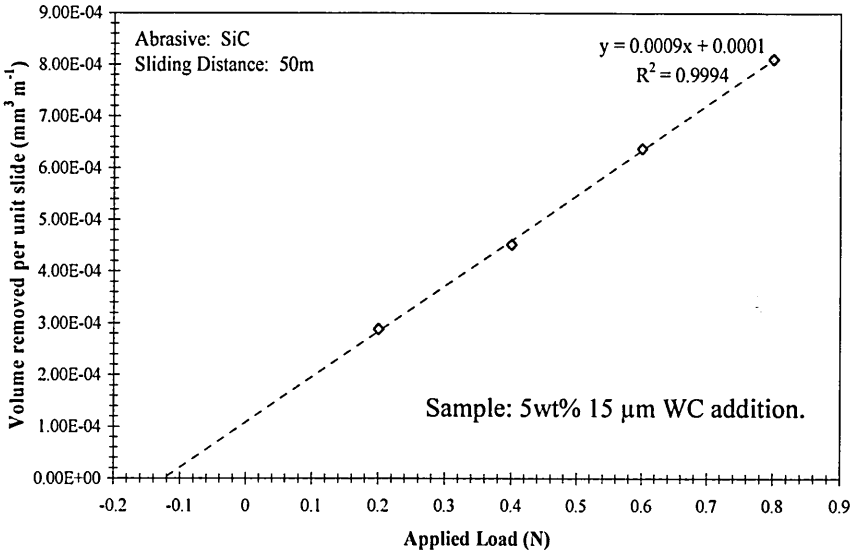

Figure 47: Typical MLM approach for wear resistance calculation.

4.6 Dry Sand Rubber Wheel (DSRW)

Testing was carried out according to conditions listed in procedure A of ASTM G65 but with a reduction in wheel revolutions. Test duration was 20 minutes at a wheel speed of 0.78 ms^{-1}, equating to a sliding distance of 942 m. The complete test conditions are given below in Table 5.

Table 5
Test conditions of ASTM G65 test.

Test parameters	Values
Applied load [N]	130
Speed [m/s]	0.78
Test duration [min]	20
Wheel	12.7mm wide by 228.6mm dia
Rubber	Durometer Shore A-60
Sliding distance	942m
Abrasive media	260μm Silica
Hardness	$1050H_V$
Abrasive flow rate [g/min]	150
Temperature/humidity	22-25°C / 35-45% RH

4.6.1 Test Specimens

Tests specimens were manufactured by the industrial collaborator and were subject to the conditions set out in Chapter 3. Rectangular mild steel coupons (25 mm x 76 mm) with a 5 mm recess were used as a substrate, shown schematically in Figure 48. The slurries were poured into the recess and fired (coating thickness: 3.2 mm min. / 12.7mm max.). After sintering and subsequent heat-treatments the specimens were ground to achieve a 0.8 μm R_a value.

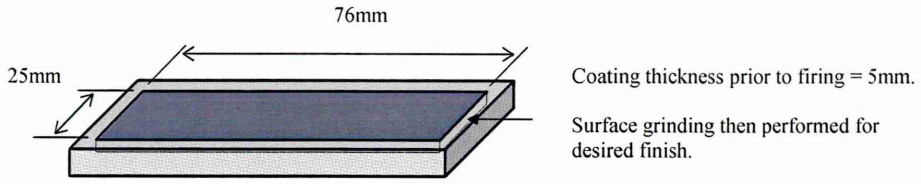

Figure 48: Schematic diagram of DSRW test specimen.

4.6.2 Abrasive media

The DSRW abrasive was rounded silica sand with a stated average particle size of 220 μm (60/85 mesh) obtained from David Ball Group PLC, Cambridge. Particle size distribution and the morphology of the abrasive are shown in Figure 49. It can be seen from the particle size analysis that the silica actually has a mean size (D50) of 260 μm.

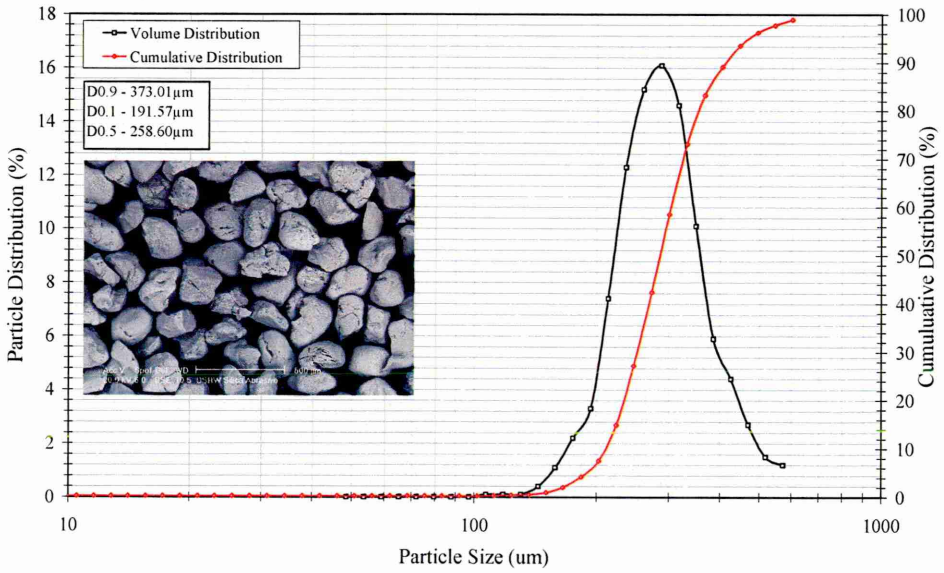

Figure 49: Particle size analysis and morphology of rounded silica sand abrasive used in modified ASTM G65; 220 μm particle size (60/85 mesh).

Closer inspection of the abrasive using SEM microscopy shows that particles possess micro-cracks, promoting the likelihood of fracture upon impact and loading, possibly creating a more angular faceted abrasive, Figure 50.

Figure 50: SEM micrograph of 260 μm silica sand used in ASTM G65 tests.

4.7 Wet Sand Rubber Wheel (WSRW)

In a further attempt to replicate the conditions of abrasive wear in soil, tests were carried out using 'wet' abrasive, made possible by the modifications made to the DSRW test by NPL. The same abrasive and test conditions listed in Table 5 were used with the addition of deionised water being fed onto the wheel by use of the fluid feed. The flow was enough to ensure the wheel was kept constantly wetted during testing using around 2.5 litres over a 20 minute test.

4.7.1 Quantitative wear calculation

Wear in the DSRW/WSRW test is measured by means of mass loss in *g*, which may then be converted into wear volume, mm^3, using bulk density values. Mass measurements were carried out prior to testing after thorough cleaning of the specimens; measurements are taken to an accuracy of 0.005 g. Following testing samples were re-cleaned and a final measurement taken to provide the total mass loss.

$$\text{Volume loss } [mm^3] = (\text{mass loss } [g] \,/\, \text{density } [g/cm^3]) \times 1000$$

Equation 14: Volume loss for DSRW test.

During testing the rubber rim reduces in diameter due to wear. If required wear results can be adjusted for the reduction in rubber volume and hence, wheel diameter. Adjusted volume loss (AVL) is calculated using Equation 15 below:

$$AVL = \text{Volume loss } [mm^3] \times \frac{\text{Wheel dia. before use [mm]}}{\text{Wheel dia. after use [mm]}}$$

Equation 15: Adjusted volume loss

However, measurements of the wheel before and after testing revealed no measurable difference and AVL was considered insignificant.

4.8 Field trials

The initial objectives of this research did not include the funding or time to perform in-depth field trials. However a contact was made in the agricultural industry who agreed to perform basic field trials in a limited area of land for inclusion in this research. Basic field tests were undertaken in two stages; firstly in Trial A, tools coated with Armatech and a modified coating were tested along with boron steel as a reference material. In Trial B only Armatech and the chosen modified coating were compared.

The trials were carried out in Rotherham, South Yorkshire (UK), Trial A in September 2006 and Trial B in March 2007. A map of the area and is shown in Figure 51 and a satellite image of the field is shown in Figure 52.

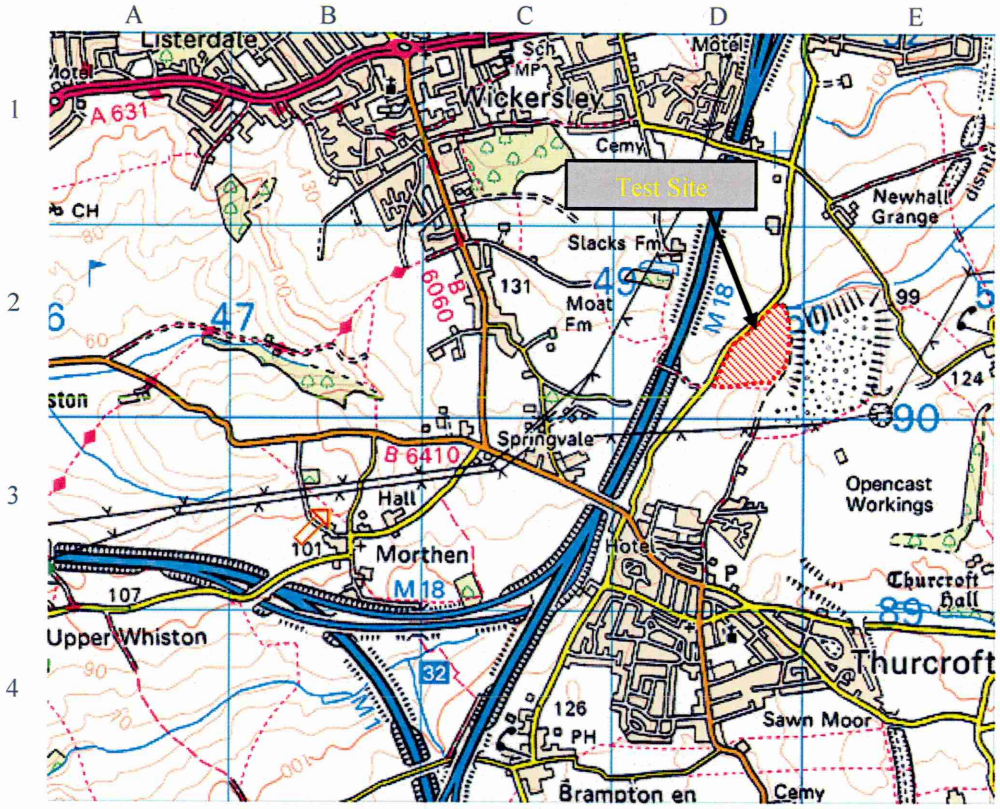

Figure 51: Ordnance survey map of the field used for Trial A and B; grid D2 (53° 24' 27.22" N and 1° 15' 08.56" W).

4.8.1 Soil Analysis

The test field was 20 acres in size and consisted of sandy loam soil which possessed differing clay contents in three areas of the field, detailed in Figure 52. While literature has stated that it should be possible to complete experiments within small areas of land within which the soil and its condition are nearly uniform, this is not always possible to achieve[16].

Soil samples were collected from the field at the typical working depth in the three areas shown to assess for moisture content, pH level and particle distribution. The soil properties are provided in **Table 6**.

Table 6
Soil properties of field trial March 2007.

Soil	Soil Texture	Soil weight [g]	After drying [g]	Moisture [%]	Acidity [pH]
A	Sandy Loam	351	326	7.1%	6.28
B	Sandy Clay Loam (Higher clay)	356	292	18%	6.06
C	Sandy Clay Loam (Lower clay)	252	210	16.7%	5.78

The appearance of Soils B and C in the field suggested higher clay contents than Soil A, clays promotes water retention, which was confirmed by the level of moisture present in this soil (**Table 6**).

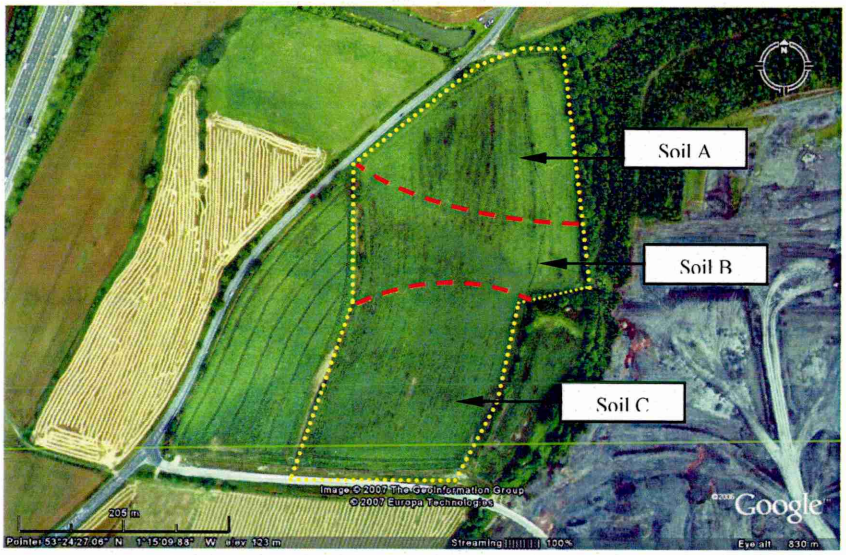

Figure 52: Satellite image of field used for field trial highlighted by yellow dashed line. The field consisted of three soil types, labelled A, B and C.

4.8.2 SEM Soil examination

A 20 g sample from each soil was taken from the small fraction (less than 5 mm) for examination. The sample was repeatedly rinsed and drained to remove debris, small particulates and any organic matter including clay. An ultrasound bath was used to break down agglomerates and binding clays. Following several repeated cycles the particles were allowed to settle and the remaining water was evaporated off at room temperature. Following rinsing the three soils all possessed very similar appearances. The abrasive content in each soil appeared the same with the difference in soil type being the level of clay and hence moisture level. Any affect on wear of the tools would most probably be through the loading on the tool caused by soil strength.

A photograph of the processed Soil A is shown below in Figure 53(a), it can be seen to be made up of a wide range of particulates. An attempt was made to obtain a representative sample to include particulates of all sizes for SEM examination.

(a) (b)

Figure 53: Photograph of dried soil and SEM Micrograph of silica particles.

SEM revealed that the small fraction abrasives were angular silica grains, Figure 53(b). The average particle size of the fine fraction was ~200 µm, the abrasive type and particle size of the fine fraction was very similar to the abrasive used in the DSRW test but possessed a more angular morphology.

4.8.3 Trial A - September 2006

Field testing was carried out in September 2006 to assess the performance of three materials under service conditions. An economical selection from the materials tested under laboratory conditions was made. Laboratory tests revealed Armatech with an addition of 10wt.% 100 µm WC coated materials provided good performance so these were selected for comparison against boron steel as a reference material.

The plough system employed was a mounted 4 furrow reversible Kverneland unit, consisting of a reversible point, share, skim and mouldboard, shown below in Figure 54. Diagrams of the points and shares are provided in the Appendix. The coatings were applied to the leading edges of the reversible points and the shares. It is worth noting here that the reversible point is coated on two edges where one edge is worn and the tool is then turned around to wear the other edge. The total area ploughed during this trial was 110 acres, the point was rotated after 50 acres and the second edge ploughed the remaining 60 acres.

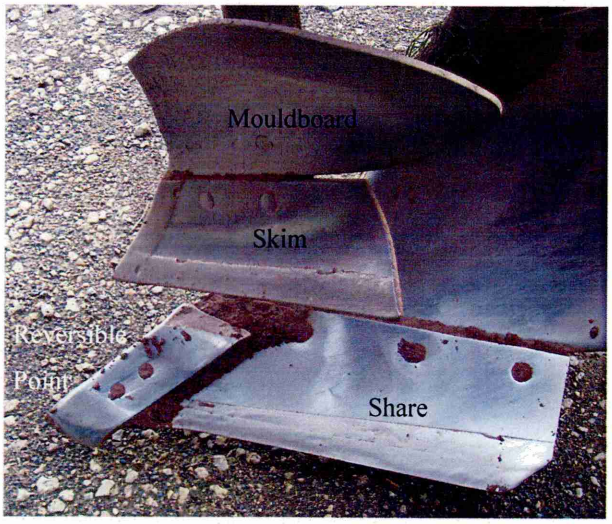

Figure 54: Three part plough body; point, share and skim.

The plough system consisted of two sets of 4 furrows, one left hand side and one right hand side, Figure 55. A simplified schematic drawing of a five furrow plough system is illustrated in Figure 56. The two sets each have an opposite curvature to enable the soil to be turned in a constant direction regardless of direction of travel, between each single pass the system is rotated between the left and right hand sets by a mechanical unit.

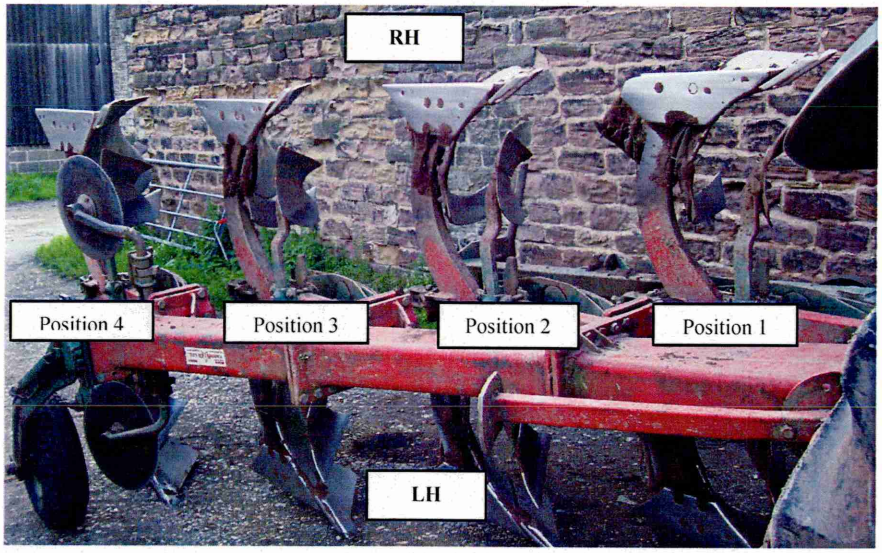

Figure 55: Plough showing the four positions of the left hand and right hand systems.

Due to limitations of time and acreage, it was not possible to test three complete sets of each material so only one complete set of left and right hand parts could be used for testing (8 skims, mouldboards, points and shares). For this reason it was decided to disregard plough position and only three furrows, Position 2-4, were used. Research has shown that the forefront furrow nearest to the tractor wheel suffers increased amounts of wear, in order to assess this fully a complete test matrix would have been needed to assess each material in each position, for which restraints did not allow. Armatech coated points and shares were positioned on both left and right hand side at furrow 2, standard boron steel points and shares were positioned at furrow 3 and points and shares coated with 10wt% 100 μm WC modified Armatech were positioned at

the rear in furrow 4. This configuration had the Armatech at the forefront position for testing, the more aggressive of the three positions, any improvement in wear of Armatech over boron steel would be enhanced when taking position into consideration.

4.8.4 Trial B - March 2007

The plough used in Trial B was a mounted RABE Raven 5 furrow reversible plough (Type 1500 V80-39/47; No. 97771-1) simplified schematically in Figure 56. The system comprised of a left hand and right hand side set as per Trial A.

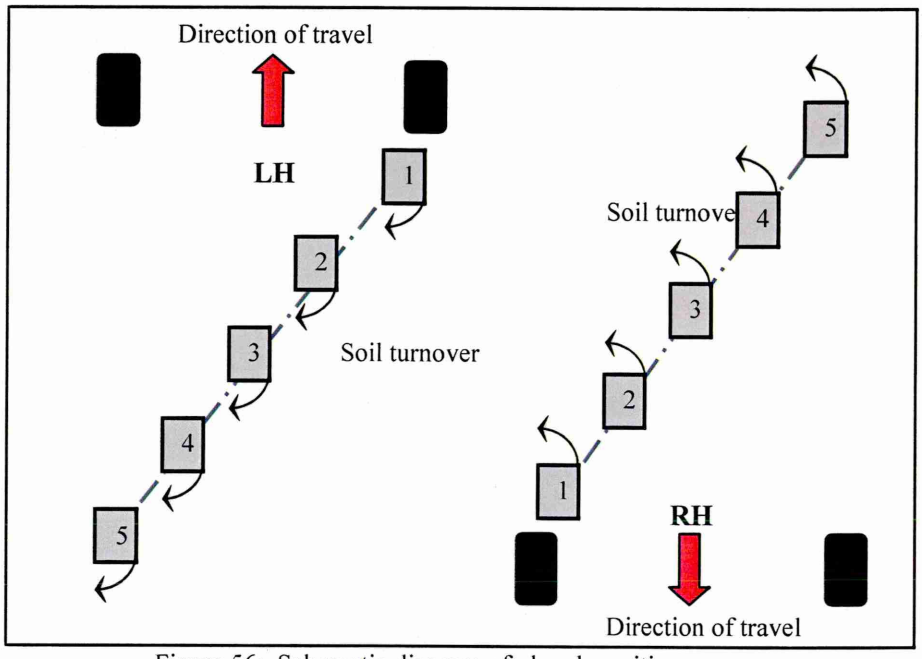

Figure 56: Schematic diagram of plough positions.

Due to time and acreage constraints and from results of Trial A only Armatech and 10wt% 100 μm WC modified Armatech coated samples were assessed. The reduced test matrix allowed plough position to be assessed, a complete LH set was used for Armatech samples and a complete RH set for the 10wt% 100 μm WC modified Armatech coated samples.

4.8.5 Field trial procedure – Trial A and B

The test samples were cleaned to remove grease and debris and allowed to air dry, Figure 54. The reversible points were weighed to an accuracy of ±0.5 g, but due to the unit weight of the shares, these were weighed on larger scales with a lower accuracy of ±50 g. Following the field trials the samples were thoroughly cleaned to remove all soil and debris and re-weighed to calculate material loss. The ploughing speed was around 15 mph and the mean working depth between 250 and 300 mm in both trials.

The proceeding Chapter, *Material Development and Characterisation*, will now investigate the standard materials such as boron steel and Armatech. It will then go on to develop and

characterise Armatech with the addition of several hard phases prior to assessing the modified materials for wear resistance using the approaches reviewed in this Chapter.

Chapter

5

Material Development and Characterisation

5 Standard materials

This chapter will focus on the characterisation of the existing material of boron steel, the powder metallurgy based Armatech and also a tungsten carbide (WC) tile used in plough share production by Chapmans Agricultural Ltd.

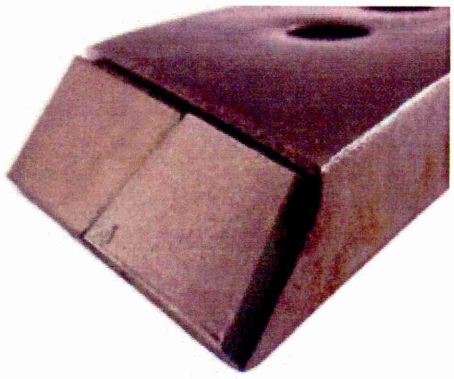

Figure 57: Soil working tool with Tungsten carbide tile brazed to leading edge.

In order to understand how these materials perform in service it is necessary to understand their properties such as chemical composition, microstructure, hardness and the methods of their production. The modified coatings will then be assessed in terms of sinterability and microstructure.

5.1 Boron steel

Boron steel is a relatively cheap and readily available material which has been used effectively for decades to produce soil working tools. Boron steels are able to be hardened through quenching, obtaining a very uniform microstructure. They have improved wear resistance over many carbon steels. With boron steel being a standard material for plough shares it was used as a bench mark for tribological assessment of other materials.

The chemical composition of cast boron steel used by Chapmans Agricultural Ltd. is provided below in Table 7[‡‡].

[‡‡] Obtained from Fundia Ltd, Lubor, Sweden. Grade SB27M12CB.

Table 7
Chemical composition of cast boron steel.

Element	[wt.%]
Carbon (C)	0.25 - 0.32
Silicon (Si)	0.15 - 0.45
Manganese (Mn)	1.0 - 1.45
Sulphur (S)	0.035 max
Phosphor (P)	0.035 max
Chromium (Cr)	0.3 - 0.6
Boron (B)	0.001 - 0.006
Iron (Fe)	Balance

The addition of boron to steel improves the hardenability by retarding the formation of ferrite and pearlite enabling martensite, the hardest metallurgical microstructure, to form on rapid cooling. Adding boron at around 0.002-0.003wt.% can have the same effect on hardness comparable to adding 0.7% Cr or 1% Ni, with the advantage being that boron is much less expensive. This effect of increased hardness however, can be retarded as the C content of the steel increases, the greatest increases are seen with carbon levels below 0.25% C but it is still very effective up to 0.4% C content.

The boron steel tools produced by Chapmans are forged and oil quenched to achieve the desired hardness (50-55 H_{RC} or XX-XX H_V), this is then followed by a heat treatment and temper to achieve the desired toughness whilst lowering the hardness to 48-53 H_{RC} (XX-XX H_V).

5.1.1 Hardfacing tiles

One method used to increase tool life in soil working conditions is to braze a hard wearing material in the form of a tile onto the leading edge of a tool, as discussed in Chapter 1. A typical material used in hardfacing is WC known for its excellent hardness, impact resistance and wear resistance. A typical hardfacing WC tile was provided by Chapmans to allow the comparison of Armatech and the modified materials with a known hard, wear resistant material.

The results of an analysis of the WC material using SEM and EDX examination are shown below in Figure 58. SEM analysis of the WC tile revealed it to be a ~2.5 μm carbide WC with 6% cobalt (Co) binder. The tile possessed a hardness of around 1050 H_{V20}.

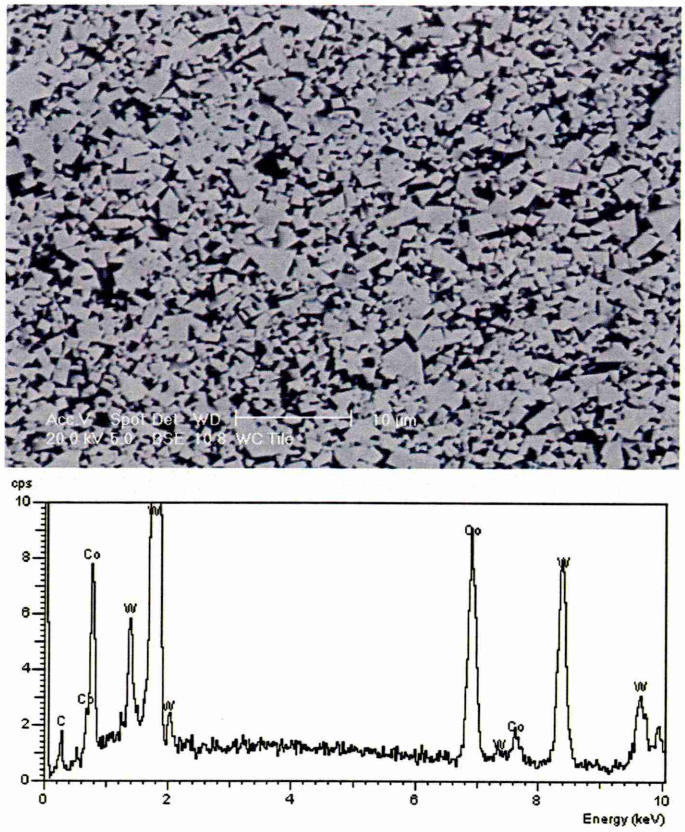

Figure 58: SEM micrograph of WC/Co tile and EDX analysis.

5.2 Existing wear resistant coating - Armatech

The addition of a wear resistant coating to a tool, in most cases applied around the leading edge, can increase the life of a tool. The coating essentially retards the rate of wear for the lifetime of the coating. They are normally applied to a boron steel substrate or mild steel if the application is not considered aggressive. The wear resistance will then revert back to the wear rate of the substrate once all the coating has worn away.

However, since agricultural coatings are typically only a few mm thick and parts are typically a few cm thick then the wear rate of the coating needs to be several multiples of that of the substrate or little benefit will be gained. For example a 2 mm coating with a 5x lower wear rate than the substrate will be the equivalent of 10 mm extra thickness of substrate material.

The coating employed by Chapmans, known as Armatech, has been in use for several years prior to this collaboration. It had been introduced specifically for the company from an outside consultant with whom no contact now remains. Due to this, not every aspect of the coating is fully understood; an element of reverse engineering was required to gain a fuller understanding. The chemical composition, microstructure, and mechanical properties are presented in section 5.3.

The coating is a powder metallurgy (PM) alloy containing Fe-Ni-Cr-C-B as the primary constituents. The nominal composition is given in Table 8. The coating is considered 'thick',

with a typical coating depth between 1 to 3 mm, and is applied to the leading edges of various shaped and sized agricultural tools, see Figure 59.

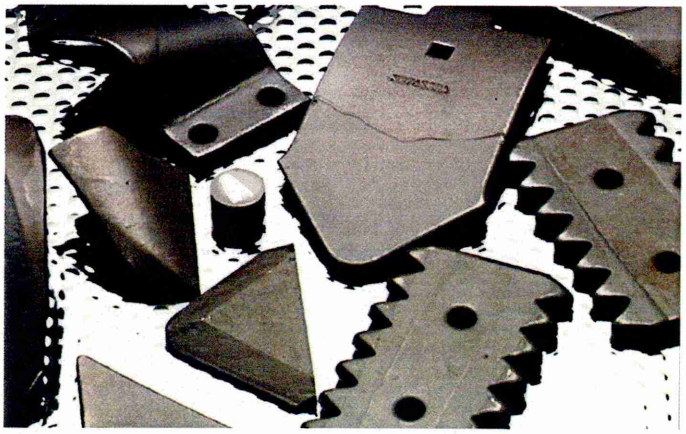

Figure 59: Photograph of several Armatech coated tools.

5.2.1 Production

The powder is manufactured by water atomisation as described in Chapter 3, the morphology is shown by BSE imaging in Figure 60(a). The powder had an average particle size of 100 μm, see 5.2.3.

Table 8: Chemical analysis of Armatech powder[§§].

Element	Mass [wt.%]	[at.%][***]	Melting Point [°C]
C	1.8 - 2.1	6.9 – 7.7	3527
Si	2.8 - 3.1	4.6 – 4.9	1414
Cr	11.5 - 14.5	10.2 – 12.3	1907
Ni	10.0 - 12.0	7.9 – 9.0	1455
V	0.08 - 0.12	0.07 – 0.10	1910
Mn	0.30 - 0.50	0.25 – 0.40	1246
S	0.04 max	0.06 max	115
B	2.75 - 3.75	11.7 – 15.3	2076
Fe	Balance	58.4 – 50.3	1538

5.2.2 Binder phase

A binder is added to the Armatech powder to perform a twofold purpose. Firstly, the binder aids the sinter process by bonding together the powder particles to form a dense sintered structure. The presence of the binder also acts as a suspension agent, enabling the coating to bond to the substrate in the wet slurry form, allowing it to remain on the tool during firing regardless of geometry. The binder is a montmorillonite sodium bentonite clay[†††], is added (1wt.%) to the metal powder prior to forming a slurry with tap water (12wt.%), Figure 60(b).

[§§] Provided by Chapmans Agricultural Ltd.

[***] Calculated using the atomic weights.

[†††] $(Na)_{0.33}(Al,Mg)_2Si_4O_{10}(OH)_2(H_2O)_n$

Bentonite clays are a thixotropic[‡‡‡] material that can absorb up to several times their dry mass in water. The clay binder is not removed during the firing process and remains present in the final sintered microstructure; although the bentonite is irreversibly changed by the firing process. X-ray fluorescence was carried out on a sample of the bentonite clay powder to determine the composition, the results are provided in Table 9.

Table 9
XRF results from bentonite powder.

Compound	Mass [%]
SiO_2	51.9
Al_2O_3	19.1
Na_2O	3.5
MgO	2.2
Fe_2O_3	2.0
CaO	1.3
K_2O	1.10
SO_3	0.2
TiO_2	0.2
BaO	0.1
P_2O_5	0.02

To aid densification and sintering a sodium metaborate ($NaBO_2$) antioxidant or flux (0.4wt.%) is also added with the bentonite. The flux acts to break down any oxides present, by effectively lowering the melting point of the iron oxide.

[‡‡‡] Becomes a fluid or less viscous when shaken or stirred.

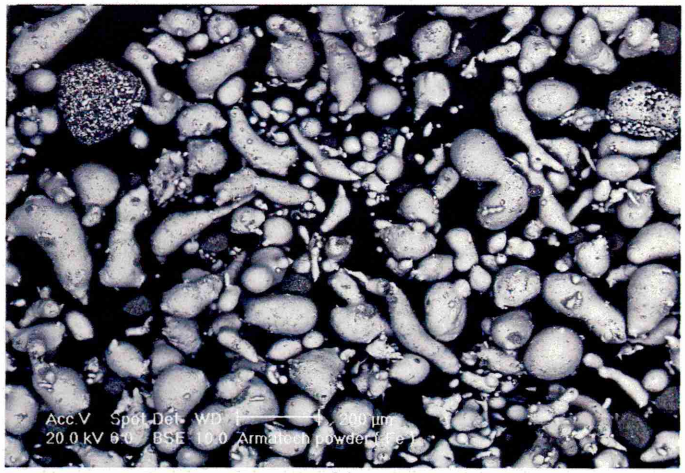

(a)

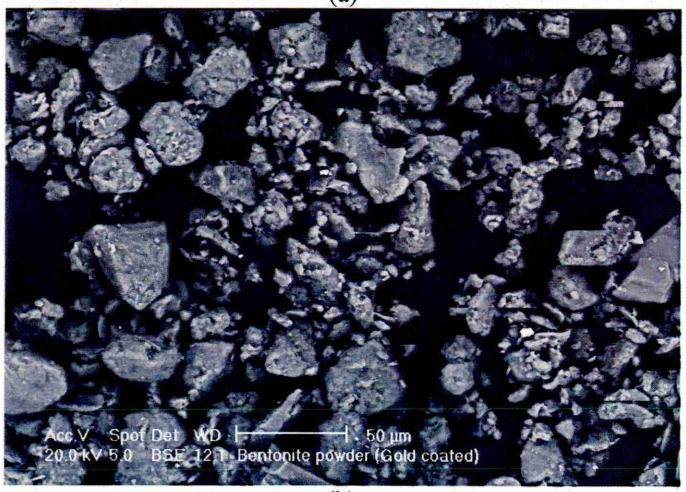

(b)

Figure 60: SEM images of (a) Armatech powder particles and; (b) bentonite binder phase. (Note different scale marker bars.)

5.2.3 Particle size analysis

The results of particle size analysis of the Armatech powder and bentonite clay is shown below in Figure 61. It can be seen the metal powder had a particle size of D0.5=100 µm while the bentonite clay had a bimodal distribution with means at 4 and 40 µm but a D0.5=6 µm.

The bimodal distribution of the clay binder may have been caused by agglomeration of the particles, a common problem when attempting to determine the distribution of clay materials. The micrograph shown in Figure 60(b) however confirmed the likelihood of two common particle sizes.

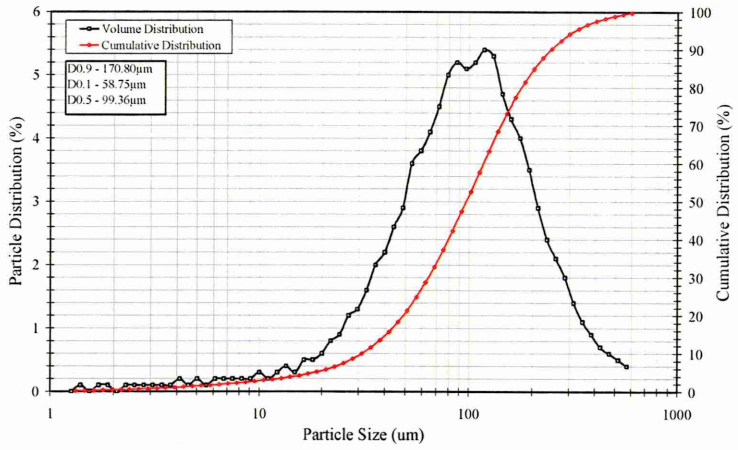

(a)

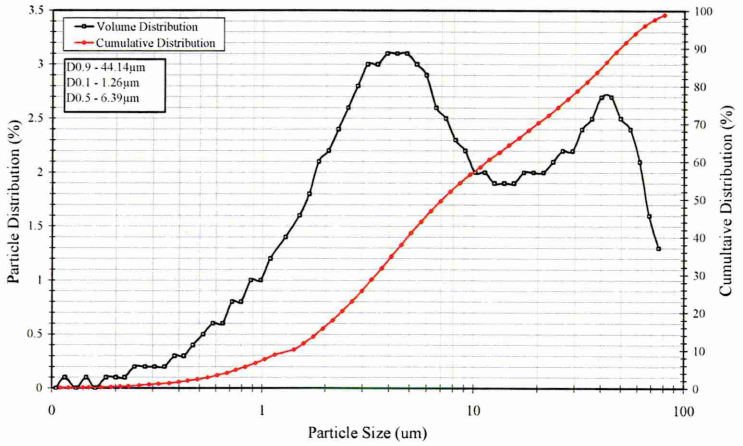

(b)

Figure 61: Particle size analysis of (a) Armatech powder and (b) bentonite clay.

5.2.4 Sintering temperature trials

Since this research was carried out in conjunction with an industrial collaborator, it was vital that new materials could be manufactured using the current methods employed by the collaborator. It was essential not to dramatically change any of the operations in use so as not to affect product output or significantly increase production costs.

Prior to carrying out the experimental work of developing and testing new coating materials the existing method of firing the materials was explored to ensure the optimum material properties were being achieved.

A series of tests were carried out using the existing Armatech material to explore the sintering temperature of the furnace with the aim of finding a more economical method of manufacture or the possibility of improving Armatech properties. However, results from these tests showed that the material would not fully sinter at lower temperatures producing a highly porous material and it was concluded that 1083 °C was the optimum temperature.

5.3 Microstructural examination of Armatech

A full understanding of the properties and microstructural features of Armatech was needed in order to then understand the way in which the coating resisted wear. It was also necessary to understand the Armatech structure before making any modifications in an attempt to increase wear resistance.

SEM examination of the sintered microstructure was carried out on a polished surface of Armatech to determine the phases present, the distribution of phases and the elemental composition of the phases. BSE imaging and energy dispersive X-ray analysis (EDX) were used to observe and analyse the microstructure of the material.

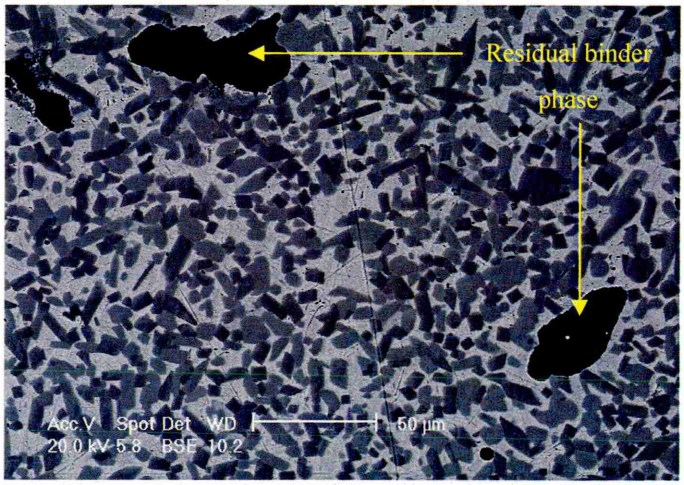

(a)

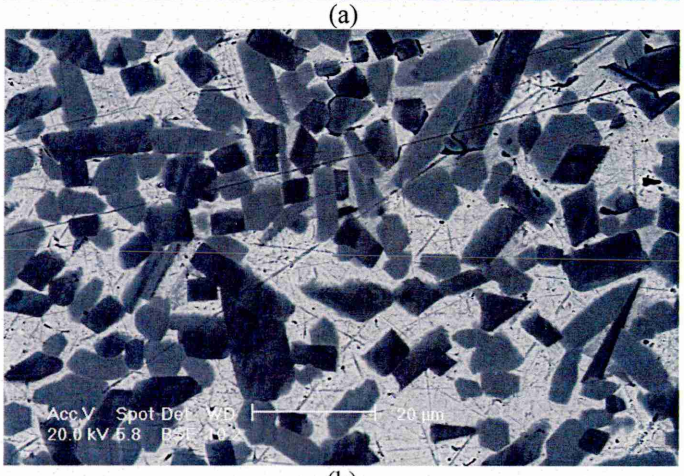

(b)

Figure 62: SEM micrographs of a typical region of Armatech microstructure; a) showing residual binder phase and b) shows BSE contrast between the two primary hard phases with high aspect ratio and random orientation.

SEM examination using BSE revealed that Armatech possessed three distinct phases; a matrix phase and two primary hard phases. The black areas seen in Figure 62(a) were the residual phase of what remained of the bentonite after firing. The two tone angular phases were elongated in shape and around 20-40 µm in length, evident in Figure 62(b). The ranges of sizes seen in the micrograph were most likely attributed to the high aspect ratio and the random

orientation of the primary hard phases. The network of hard phase suggested a good level of distribution; important for wear resistance. The interparticle spacing is relatively small which can protect the more ductile matrix phase with the hard phases providing the wear resistance. An SEM micrograph taken of a cross-section through an Armatech coated boron steel substrate is shown in Figure 63.

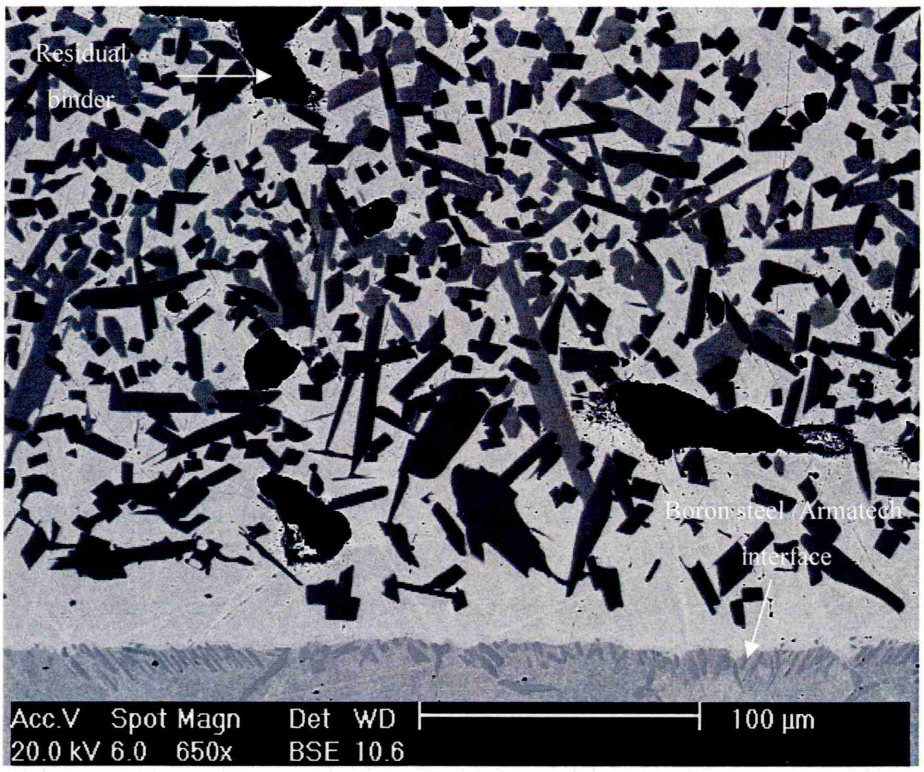

Figure 63: BSE SEM micrograph of cross-section through Armatech coated boron steel substrate showing a good interface reaction.

The coating/substrate interface appeared to be good with no pores or voids, the substrate material had a well bonded reaction with the Fe-Ni matrix. No coating fall off or 'spalling' was observed. The two primary hard phases appeared to be distributed well throughout the microstructure. It was also evident from SEM examination that the primary hard phases near to the substrate/coating interface undergo a change, being more angular in shape and generally of a larger size.

5.4 Energy dispersive X-ray analysis, EDX

EDX analysis shows that matrix phase is predominantly Fe-Ni-Si rich, Figure 64. The two primary hard phases, shown by elemental contrast in the electron image, are most notably distinguished by the level of Cr. The phases that appeared lighter in BSE mode showed a higher Cr content, this also appears to be the case, to a lesser extent for the content of manganese (Mn). The levels of boron and carbon however could not be analysed accurately using EDX.

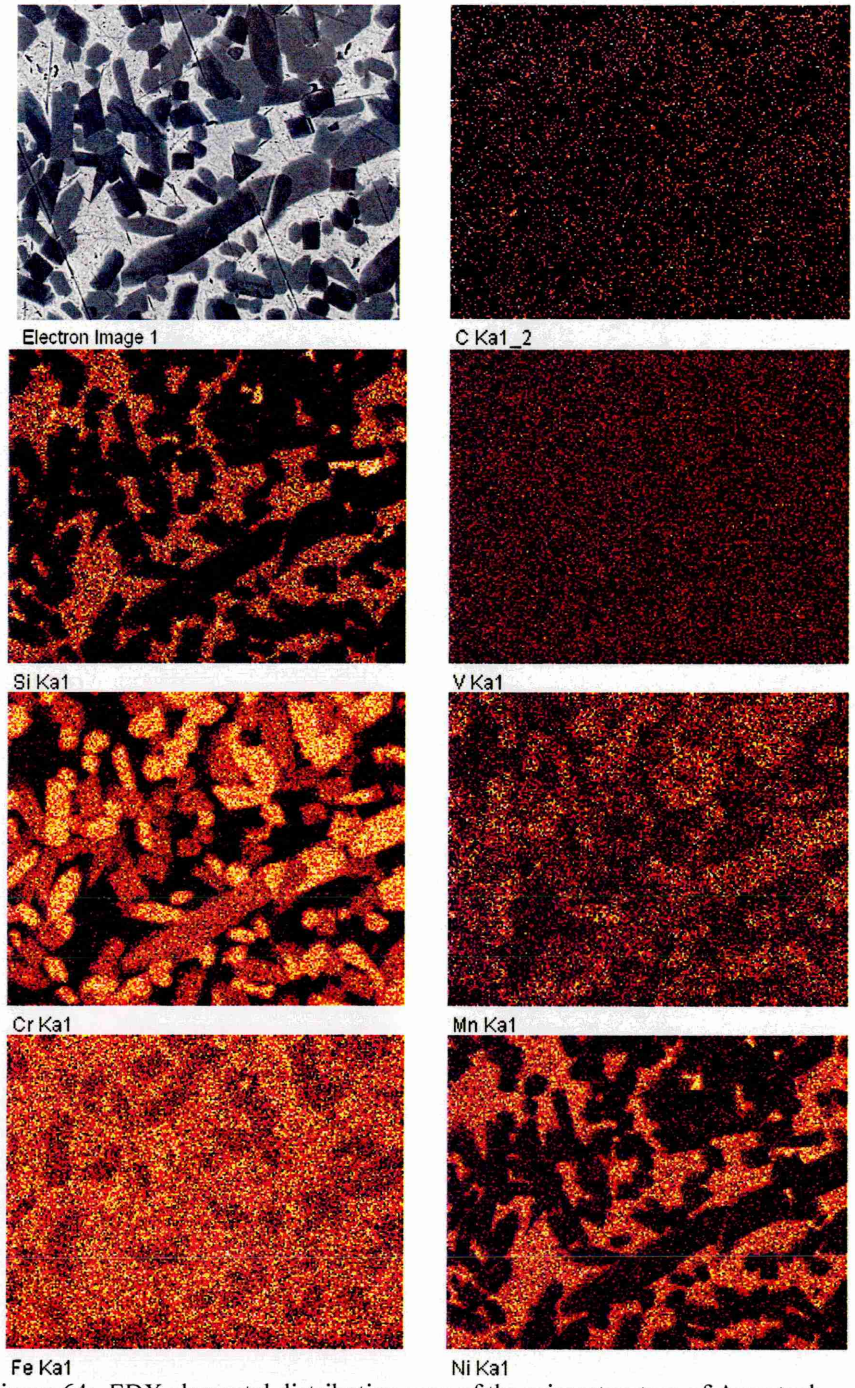

Figure 64: EDX elemental distribution map of the microstructure of Armatech.

5.4.1 Quantitative X-ray analysis

INCA EDX software was used to quantitatively measure the elemental composition of each phase. This was carried out using ZAF correction technique, (Z) atomic number affect, (A) absorption and (F) fluorescence, with a cobalt standard. The weight percentages are provided in Table 10 and the atomic percentages in Table 11.

Table 10: EDX quantitative ZAF results of the three Armatech phases (wt%)

	Matrix	Light	Dark
C	5.5 ± 1.5	11.8 ± 1.7	6.0 ± 1.5
Si	6.3 ± 0.3	0.1 ± 0.1	0.2 ± 0.2
V	0.1 ± 0.1	0.4 ± 0.1	0.1 ± 0.1
Cr	2.9 ± 0.2	27.9 ± 1.2	17.3 ± 1.3
Mn	0.3 ± 0.1	0.5 ± 0.1	0.5 ± 0.1
Fe	62.9 ± 1	57.2 ± 0.9	72.6 ± 1.5
Ni	21.0 ± 0.6	2.2 ± 0.1	3.4 ± 1.0

Table 11: EDX quantitative ZAF results of the three Armatech phases (at%)

	Matrix	Light	Dark
C	23.3 ± 5.1	37.6 ± 3.8	22.3 ±4.4
Si	9.7 ± 0.8	0.1 ± 0.1	0.2 ± 0.3
V	0.05 ± 0.1	0.3 ± 0.1	0.1 ± 0.04
Cr	2.4 ± 0.3	20.7 ± 1.7	15.1 ± 1.5
Mn	0.2 ± 0.1	0.3 ± 0.1	0.4 ± 0.1
Fe	48.8 ± 3	39.5 ± 2.1	59.2 ± 3.5
Ni	15.5 ± 1.1	1.5 ± 0.1	2.6 ± 0.5

Although the C content had been analysed in the above analysis, it can often be a misleading result. As described in Chapter 3, the system is unable to measure B and while the presence of C can be detected, quantitative measurements are often inaccurate due to the electron beam depositing carbon on to the sample surface, which can yield a higher level. The analysis revealed that all phases possessed high Fe contents with the matrix phase rich in Ni. The two primary phases were rich in Cr, with the light phase possessing a higher Cr content. The analysis suggested the presence of Fe-Cr carbides, however due to incongruity of the system measuring C and the inability to measure B, especially as B is present in a relatively high level compositionally, it was impossible to determine the exact nature of the primary hard phases. The analysis combined with X-ray diffraction data would allow a more in depth phase identification.

5.5 X-ray Diffraction (XRD) of Armatech Phases

XRD was performed to determine the exact nature of the phases present within the Armatech microstructure using the equipment described in Chapter 3. Scans were carried out over the range, 20 to 110° 2θ collected at 500 seconds per step at 0.008 [2θ] steps. A typical trace from a sample of Armatech is shown in Figure 65. In order to ensure correct peak positioning and to eliminate any error from differences in sample height, a Si standard was used. A small quantity of pure Si powder was mixed with acetone and painted onto the surface of the samples. The

acetone was allowed to evaporate leaving a thin layer of Si behind. This produces a peak at 28.44° 2θ, allowing the whole trace to be shifted to this if necessary.

The Armatech matrix is a complex structure and not a pure binary system for example Fe-Ni or Fe-Cr. The matrix was shown, through EDX to be a Fe-Ni-Cr system, with Si and C also present. The XRD reference database used to match identified peaks does not contain exact matches. However, the crystal structure is similar and was a close match with other Fe-Ni systems such as Taenite or Kamacite (the mineral names for the Fe-Ni binary phases).

In reality, and when considering the EDX data, the phase most likely had Cr and Si substituted for Fe at certain positions resulting in this actually being a Fe-Ni-Cr-Si phase, with the same crystal structure as Taenite or Kamacite, albeit with slight shifts in the lattice parameters.

The XRD data from the two primary hard phases within the Armatech matched closely with the boride, Fe_2B, although EDX analysis revealed it be more likely $(Fe,Cr)_2B$. Similarly for the second hard phase, a close match with a Cr_7C_3 phase was observed, but again EDX suggests that in fact it is probably $(Fe,Cr)_7C_3$.

Despite SEM showing that there was some residual binder phase present (i.e. fired bentonite) it did not show in the XRD trace, probably due to its low level.

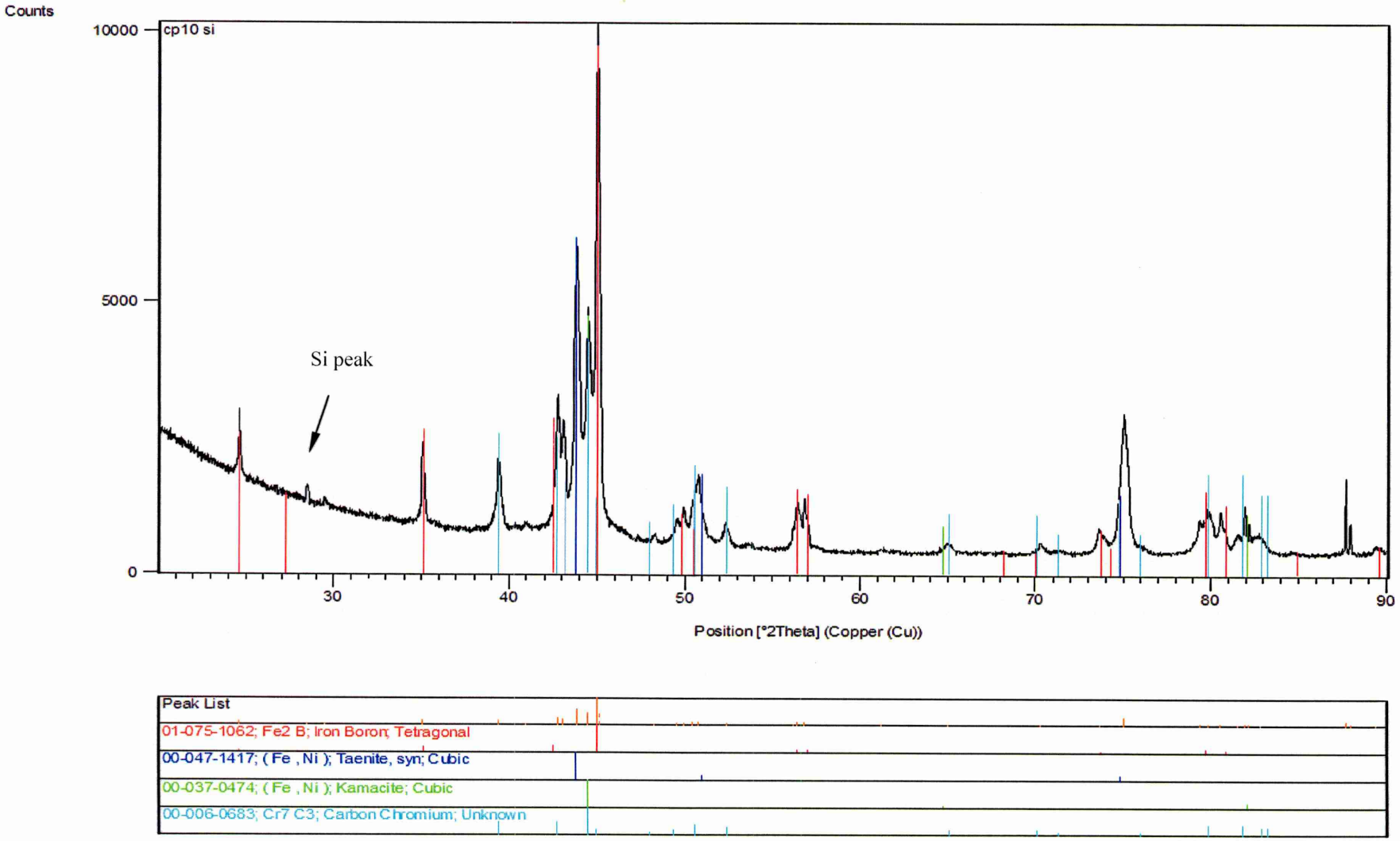

Figure 65: X-ray diffraction (Cu Kα) of phases present in Armatech coating.

5.6 Phase volume

The volumes of the three phases in Armatech were determined using SEM image analysis software. Ten random areas were selected and each phase in view measured using elemental greyscale contrast separation, from these an average was calculated, Table 12.

Table 12
Phase volumes (areas) of Armatech microstructure.

Phase	Average area [%]	S_E
Matrix	35	2.50
Carbide	39	3.1
Boride	26	2.6

The results show that the carbide possessed the highest proportion of surface area at nearly 40% with the matrix around 35%. The boride phase was lower at 25%, notably, the two primary hard phases constituted over 50% of the material surface, an important factor in wear resistance. The residual binder phase remaining within the final structure was around 4%.

5.7 Hardness determination

Microhardness indentations were made in a linear pattern, the results are given below in Table 13. SEM and BSE imaging enabled phase identification following hardness measurement, which was not possible under normal light microscopy. Typical SEM micrographs of indentations and phase identification are shown in Figure 66.

Table 13
Microhardness of Armatech phases.

Phase	Hardness [$H_{V0.25}$]	S_E
Matrix	715	170
Boride	1536	261
Carbide	1556	70

In total five indentations from each phase were selected to calculate the average hardness. The results showed that the carbides and borides both possessed very similar hardness, around 1500 H_V, with the matrix ~700 H_V. The regions of residual binder yielded no hardness. Due to the size and nature of indentations, and the method of measurement, i.e. through an optical eye piece fixed to the indenter, large errors were seen.

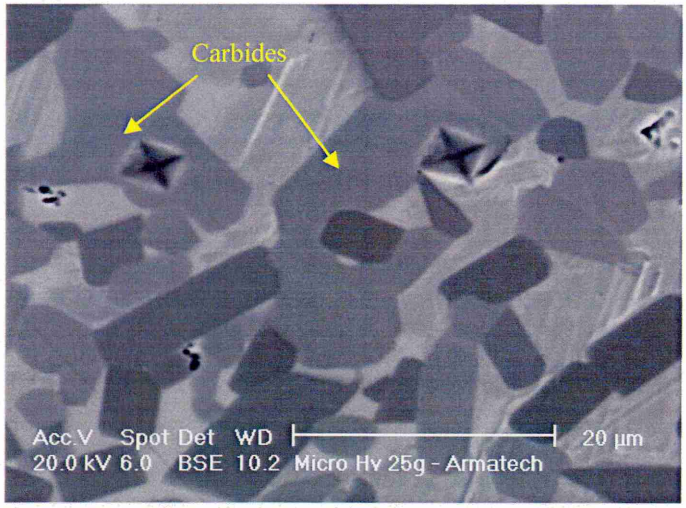

(a)

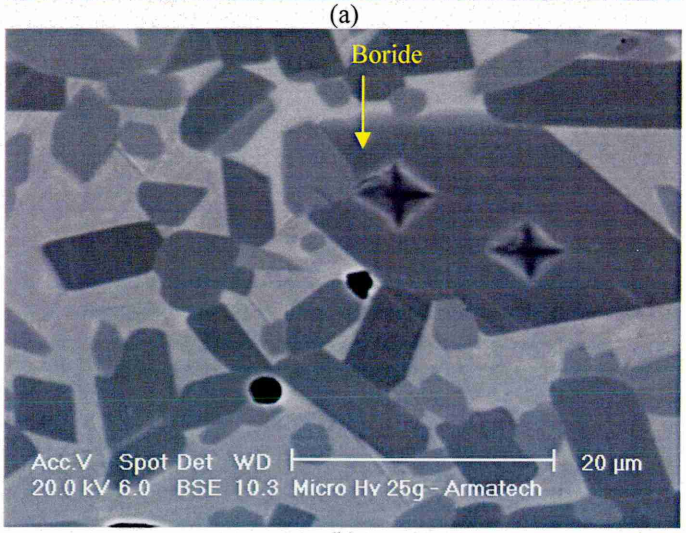

(b)

Figure 66: SEM (BS) micrographs of 25g Vickers microhardness indentations on distinct phases in Armatech coating.

It was interesting to note that other research suggested that for a soil working tool to perform well in its environment it needs to possess 80% hardness of the abrasive, in the case of soils this would be around 900 H_V. It has been shown from the microhardness results that the carbides and borides are well above this limit and the matrix very near to it. However, microhardness is inherently higher than a bulk measurement.

5.8 Coating development

A widely used approach to improve wear resistance of a metallic substrate is by the addition of hard phases. Often materials that contain hard dispersed carbides are known as metal matrix composites (MMC).

This approach was employed in an attempt to improve the wear resistant properties of Armatech. Various commercially available hard phases were selected in several particle sizes to introduce to the Armatech powder.

The additions were selected on the basis of either having a high hardness level, or due to similar additions having been used in other research. Although published literature, reviewed in Chapter 2, involved additions of materials such as WC or Al_2O_3 to a steel matrix in an attempt to increase wear resistance, it was not known if these additions, or other materials, would fully sinter with the Armatech composition prior to experimentation.

The economic viability of the additions were assessed, it was vital that the final material would not increase the costs of the resulting coating to such an extent that it was deemed too expensive to be readily marketable in the agricultural sector.

A full list of the secondary additions along with their particle size, loading level, hardness and density values are provided in Table 14. The hard phase powders were ball milled with zirconium balls for 20 minutes with the appropriate quantity of Armatech powder, prior to being mixed with 12wt.% water. All possessed a hardness of around 2000 H_V or much greater, considerably harder than the carbide and boride phase in the Armatech structure. Whilst hardness is not fully indicative of wear resistance it is a good property for a hard phase held in a ductile matrix. The theory was that the addition of these hard phases would not only increase the bulk hardness of Armatech but would improve the wear resistance by providing a secondary hard phase. Most were known for their wear resistant properties and the ruling factor would be the ability of the Armatech to fuse and 'hold in place' the introduced hard phases. A weakly bonded hard phase suffers 'fallout' and is prone to fracture under loading due to lack of matrix support.

5.8.1 Material designation

For convenience, materials will be referred to in the text by abbreviated designations. The elemental addition is provided with the level of loading in brackets (wt.%) along with the particle size [μm] stated in subscript parenthesis. For example, an addition of 15 μm WC at 5wt.% to Armatech will be designated:

$$WC(5)_{[15]}$$

Table 14
Hard phase additions.[§§§]

Addition	Particle Size [μm]	Hardness* [MH_V]	Theoretical Density [g/cm^3]	Loading (wt.%)
TiN	5	2500	5.22	5
TiB_2	45	3400	4.51	5
TiC	75	3200	4.94	5 & 10
TaC	5	2000	13.9	5
Mo_2C	45	1950	8.2	5 & 10
Al_2O_3	10	2720	3.97	3 & 6
Al_2O_3	50	2720	3.97	3, 6 & 9
WC/W_2C	100	2400	15.7	5, 8, 10, 12, 15, 20, 25, 50 & 70
WC	15	2400	15.7	5, 8, 10, 15 & 20
WC & WC/W_2C[****]	15 & 100	2400	15.7	1 & 4, 3 & 7, 5 & 5, 7 & 3

[§§§] Theoretical density and hardness values obtained from CRC Materials Science and Engineering Handbook, 3rd Edition.

[****] Mixed ratios of 15 μm WC and 100μm WC/W_2C.

5.9 Microstructural examination

Initial assessment of the coatings was carried out by macro (visually) and microscopic (optical and SEM) examination to assess the sinter quality and level of densification.

5.9.1 Titanium nitride, TiN

The addition of TiN as a secondary hard phase was investigated using 5μm particle size powder obtained from Sigma Aldrich at 5wt.%. It can be seen from the SEM micrograph that the powder had a large particle size distribution with the larger particles being up to 20 μm, Figure 67.

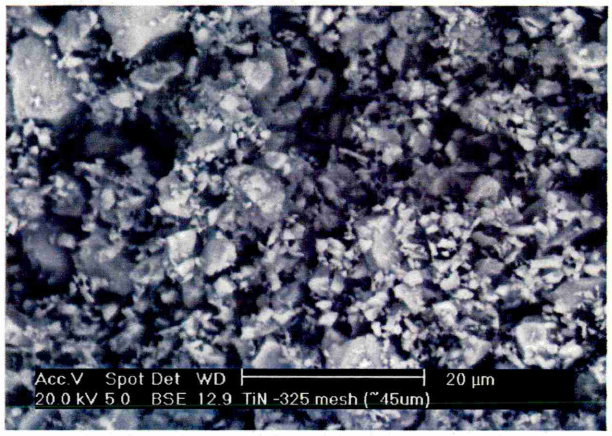

Figure 67: SEM micrograph of 5 μm TiN powder obtained from Sigma Aldrich. The micrograph shows a large particle size distribution.

It is clear from SEM that the final sintered structure was not fully dense and had a high level of porosity, Figure 68. The level of porosity also prevented the Armatech matrix from forming a good diffusive bond with the boron steel substrate. In areas where the Armatech powder had sintered without the TiN, the original three phase structure of Armatech was present. The level of porosity may also have increased due to the polishing carried out to the sample prior to examination, the hard phase most likely suffered pullout of the hard phase due to the lack of bonding.

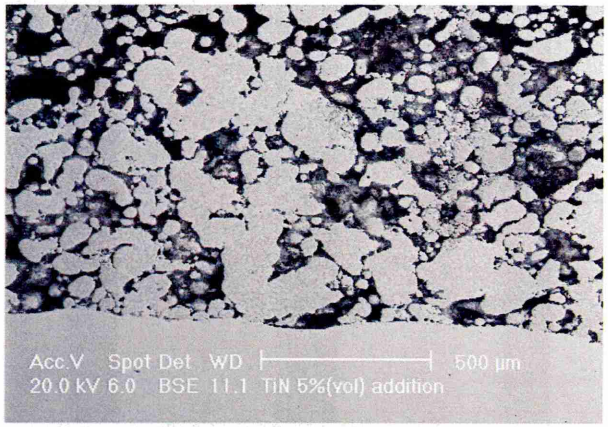

(a)

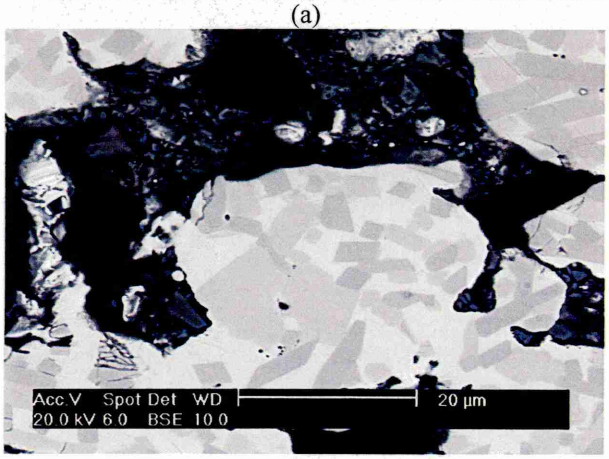

(b)

Figure 68: SEM micrographs of Armatech with 5wt.% addition of 5 µm TiN; a) cross-section through coating and substrate showing porosity and b) high magnification showing poor sinter quality.

5.9.2 Titanium diboride, TiB_2

The second material produced was by the addition of 5µm average particle size TiB_2 powder obtained from Sigma Aldrich at 5wt.%. SEM examination of the sintered material showed that the powder had a rounded morphology and a dual distribution size of around 2 and 10 µm, Figure 69.

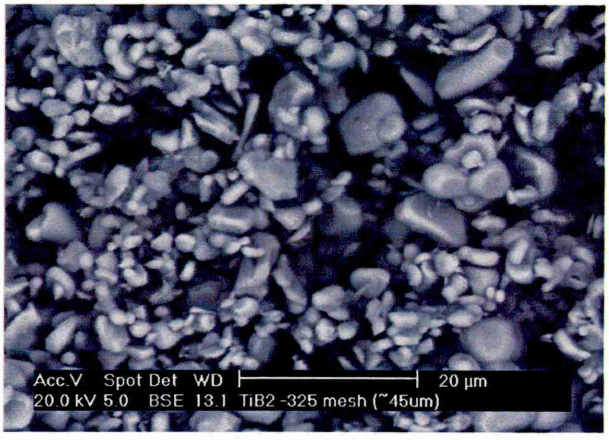

Figure 69: SEM micrograph of TiB_2 45 µm powder showing a rounded morphology.

SEM examination revealed that the hard phase addition underwent no reaction with the Armatech coating. This resulted in a very porous material with pockets of Armatech that

appeared to have sintered fully, Figure 70. It was again clear that the material had suffered pullout of the hard phase during polishing, leaving behind empty voids, shown by the dark regions in the micrographs. The regions of Armatech however appeared to not have been affected by the addition, with the matrix and three phases, matrix, carbides and borides still present.

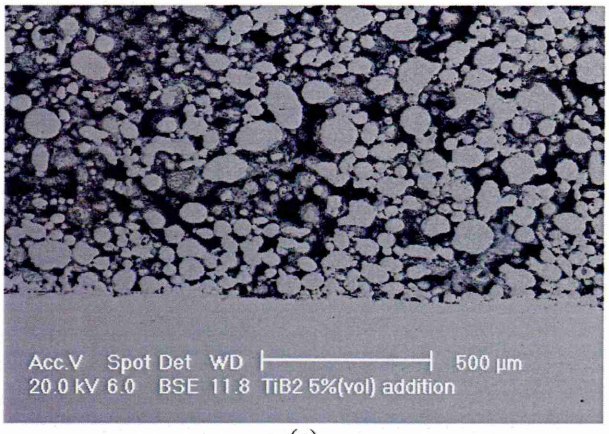

(a)

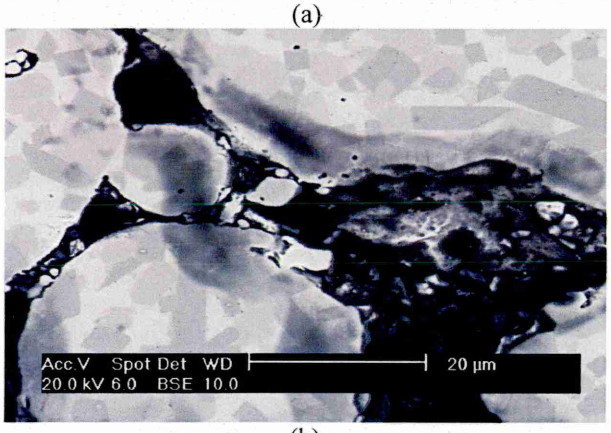

(b)

Figure 70: SEM examination of Armatech with 5wt.% addition of 45 µm TiB_2; a) cross-section through coating and substrate and b) high magnification of poor sinter quality.

5.9.3 Titanium carbide, TiC

The addition of TiC was investigated using a 75 µm powder. An SEM micrograph of the powder morphology can be seen below in Figure 71. The TiC had a very angular nature and possessed a varied particle size distribution.

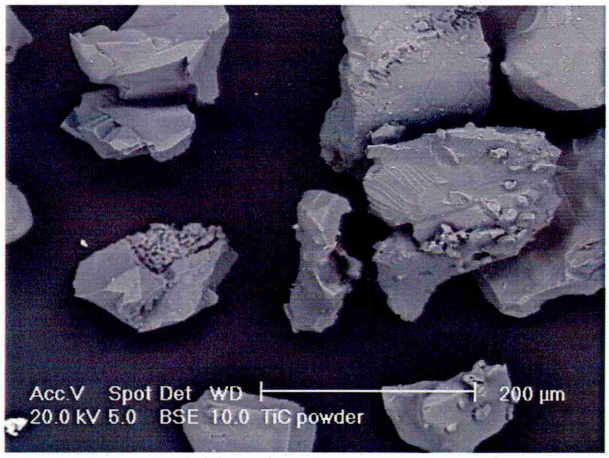

Figure 71: SEM micrograph of 75 µm TiC powder.

The TiC did not affect the sinter of the Armatech material but no reaction with the TiC occurred, Figure 72. The particles of TiC had not fused with the coating but only a small amount of fallout had occurred and particles were being held by the Armatech structure, Figure 72(b). However, this microstructure would most likely suffer fallout under loading and present no improved wear resistance or even reduced wear resistance when compared to Armatech alone.

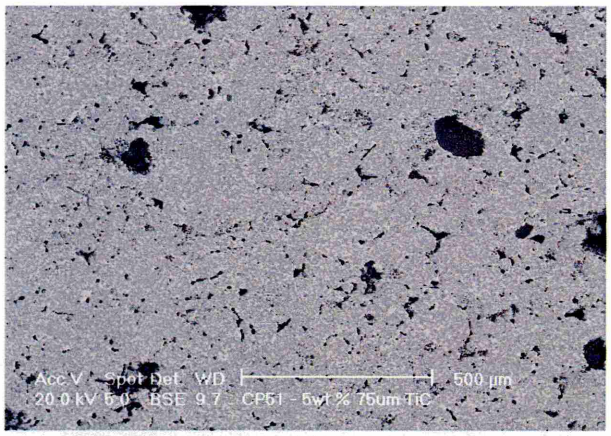

(a)

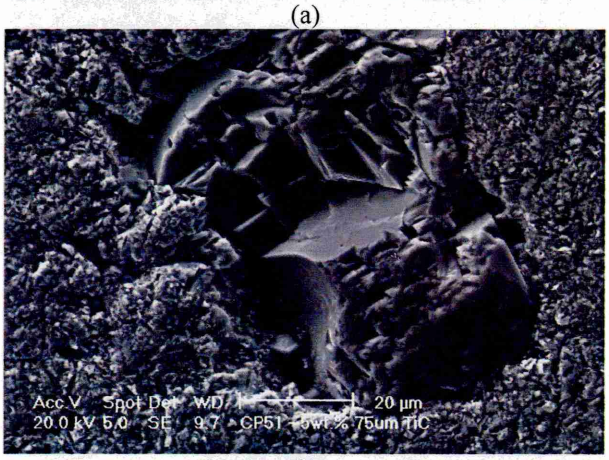

(b)

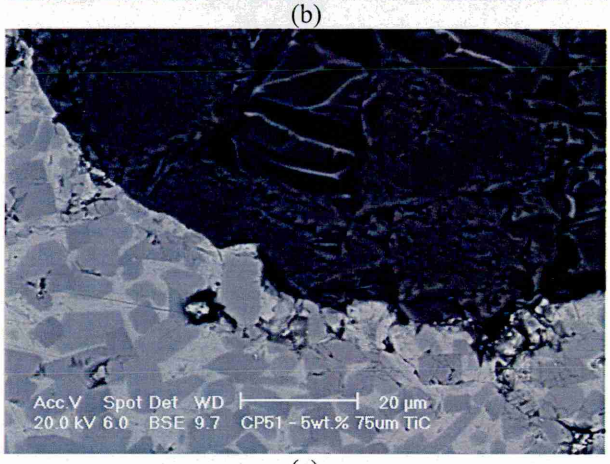

(c)

Figure 72: SEM micrographs of $TiC(5)_{[75]}$ showing the lack of fusion between the Armatech structure and TiC and high magnification SEM micrograph showing lack of fusion of TiC particle in Armatech.

5.9.4 Alumina, Al_2O_3

Two additions of Al_2O_3 at 10 µm and 50 µm (-200 - +325 mesh) were added (obtained from Sigma Aldrich Ltd). The powders had an angular morphology and were plate like in shape, shown by the SEM micrographs below in Figure 73.

(a)

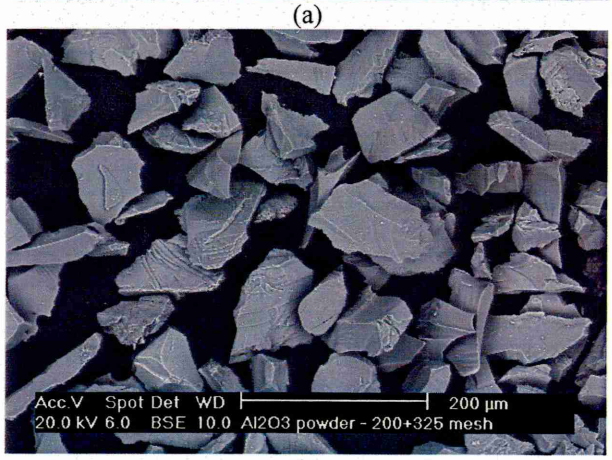

(b)

Figure 73: SEM micrographs of Al_2O_3 powder morphologies; a) 10 µm and b) 50 µm.

The powders were added to the coating at 3, 6 and 9wt.%. SEM images of the 10 and 50 µm materials can be seen below in Figure 74 and Figure 75 respectively.

Cross-sectional SEM examination of the 10 µm addition to Armatech showed that the coating had fused with the substrate material with no pores or voids seen at the interface, Figure 74(a). Inspection of the particles within the coating however revealed a high degree of fallout and no diffusion with the coating occurred leaving a large amount of porosity behind, Figure 74(b). The surrounding Armatech structure however appeared to sinter well.

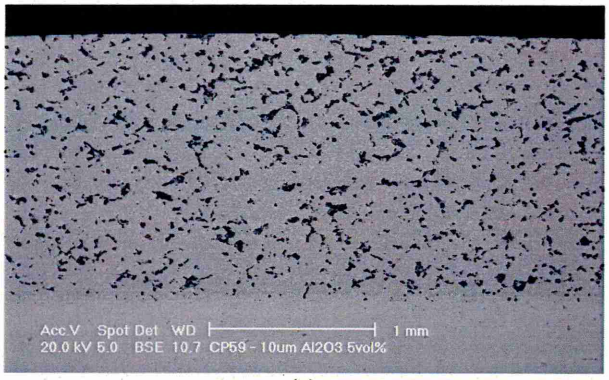

(a)

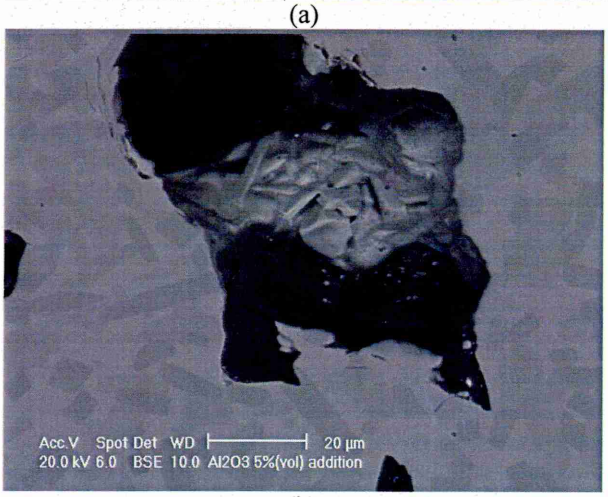

(b)

Figure 74: SEM micrograph of a) a cross-section though $Al_2O_3(10)_{[10]}$ showing a good reaction with substrate and b) fallout of a 10 µm Al_2O_3 particle and surrounding Armatech structure.

SEM examination of the coating with the larger 50 µm Al_2O_3 addition showed a small amount of porosity at the coating/substrate interface, Figure 75(a). Examination of the particles revealed that whilst direct diffusion of the Al_2O_3 with the Armatech structure had not occurred, the majority of the particles were being held by the Armatech structure, Figure 75(b). A small amount of fallout was observed but to a much lesser extent than seen with the smaller Al_2O_3 particle.

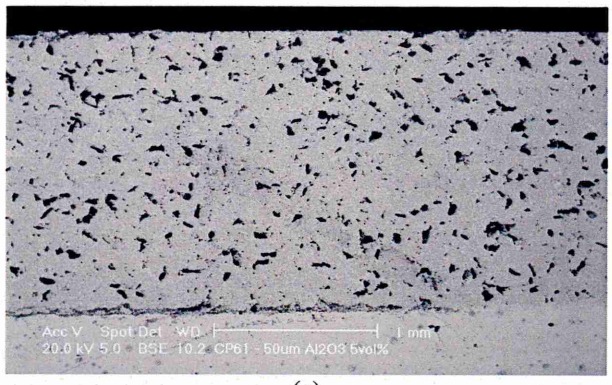

(a)

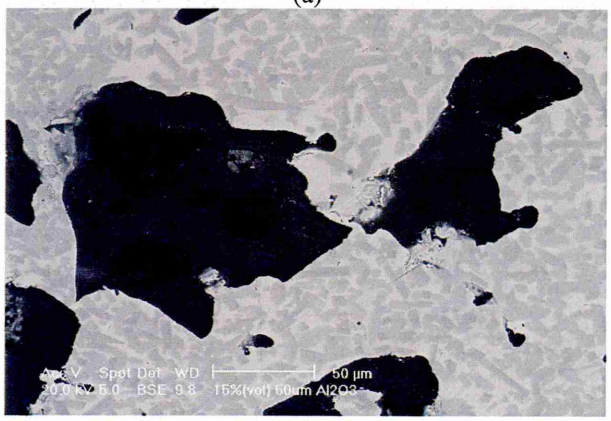

(b)

Figure 75: SEM micrograph of a) a cross-section though $Al_2O_3(15)_{[50]}$ showing reaction with substrate and b) particles being held by surrounding Armatech structure.

5.9.5 Molybdenum carbide, Mo_2C

The addition of Mo_2C as a secondary hard phase was made at 5 and 10wt.% using a 45 µm particle size powder supplied by Chapmans Agricultural Ltd. It could be seen from SEM, that the morphology of the powder was very porous in nature and appeared to be 45 µm agglomerates of nanoscale particles rather than solid 45 µm particles.

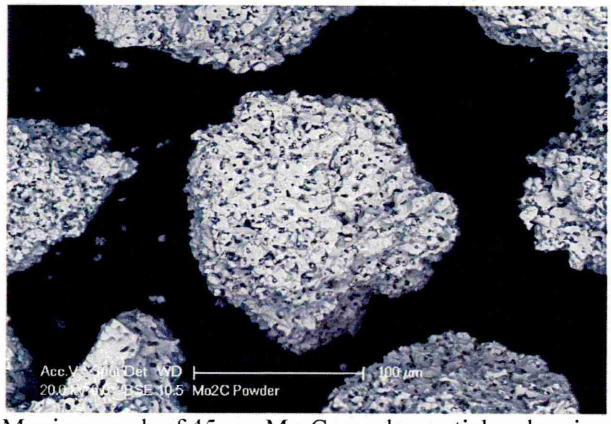

Figure 76: SEM micrograph of 45 µm Mo_2C powder particles showing porous nature.

SEM micrographs of the sintered microstructure are shown below in Figure 77. The Mo_2C appeared to have some degree of sinterability with the Armatech powder. Although the process of polishing caused some fallout the addition. The process of sintering also 'broke down' the porous 45 µm particles.

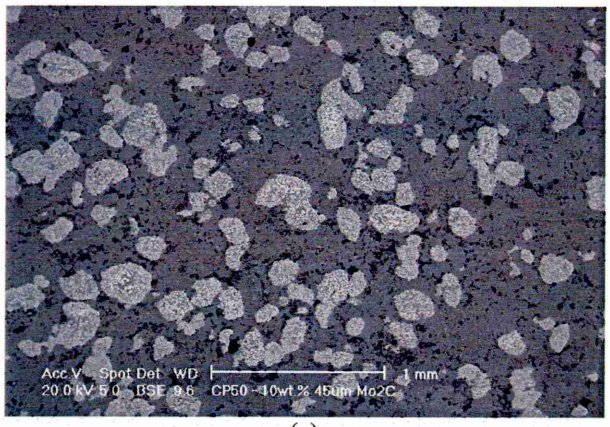

(a)

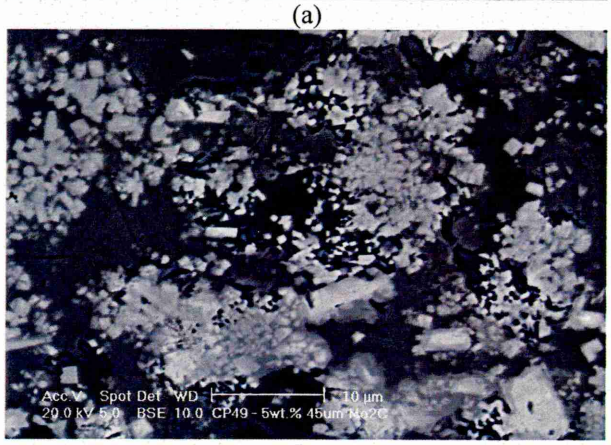

(b)

Figure 77: SEM micrographs of sintered Armatech microstructure with a) 10wt.% addition of 5 µm Mo_2C and b) high magnification of a 45 µm agglomerate.

5.9.6 Tantalum carbide, TaC

A addition of 5 µm TaC was made at 5wt.%, the micrographs can be seen in Figure 78. It could be seen from SEM examination that the TaC particles had no reaction with the Armatech structure and the particles appeared low in density and quite porous. The addition appeared not to affect the sinter quality of the surrounding material but no reaction the particles suggested the coating would be prone to pullout.

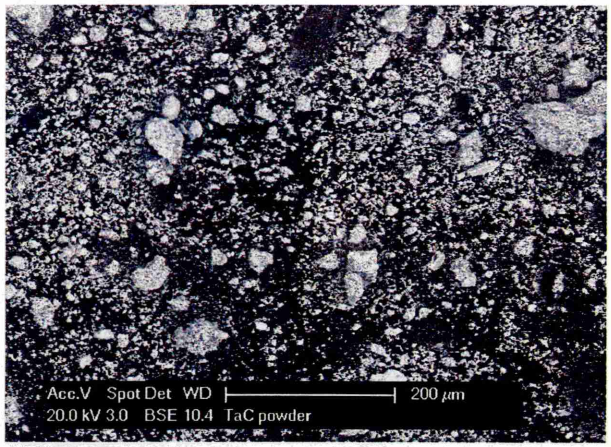

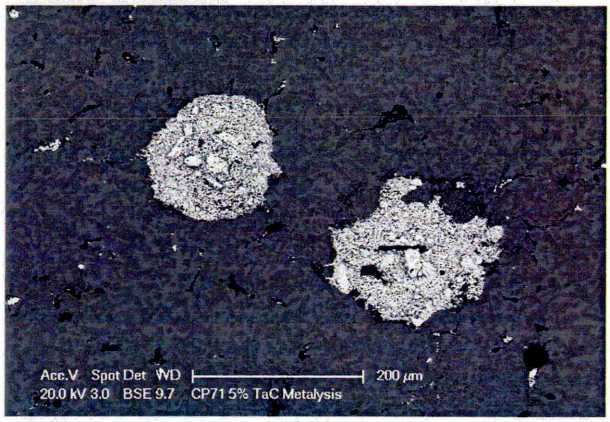

(a)

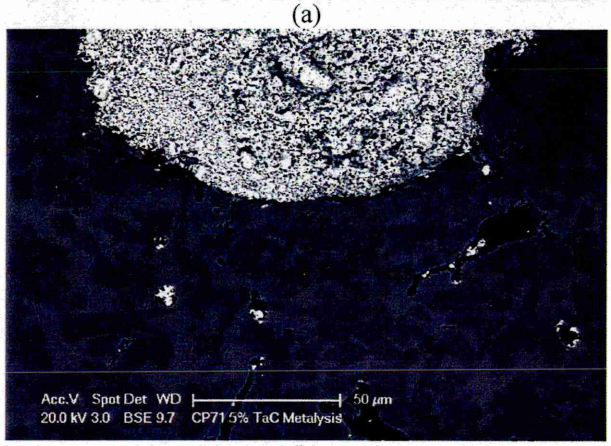

(b)

Figure 78: SEM micrographs of a) TaC 5 µm powder and b) sintered Armatech microstructure with 5wt.% addition of 5 µm TaC and c) high magnification of particle showing poor diffusion.

5.9.7 Tungsten carbide, WC

The addition of WC as a hard phase was explored using two particle sizes. Firstly a 10 µm particle size powder (obtained from Sigma Aldrich Ltd) was investigated at 6 levels of addition (5, 8, 10, 12, 15 & 20wt.%) and a 100 µm powder (originally assumed to be only WC) at 9 levels of addition (5, 8, 10, 12, 15, 20, 25, 50 & 70wt.%). Particle size analysis and SEM micrographs of the powders are shown below in Figure 79.

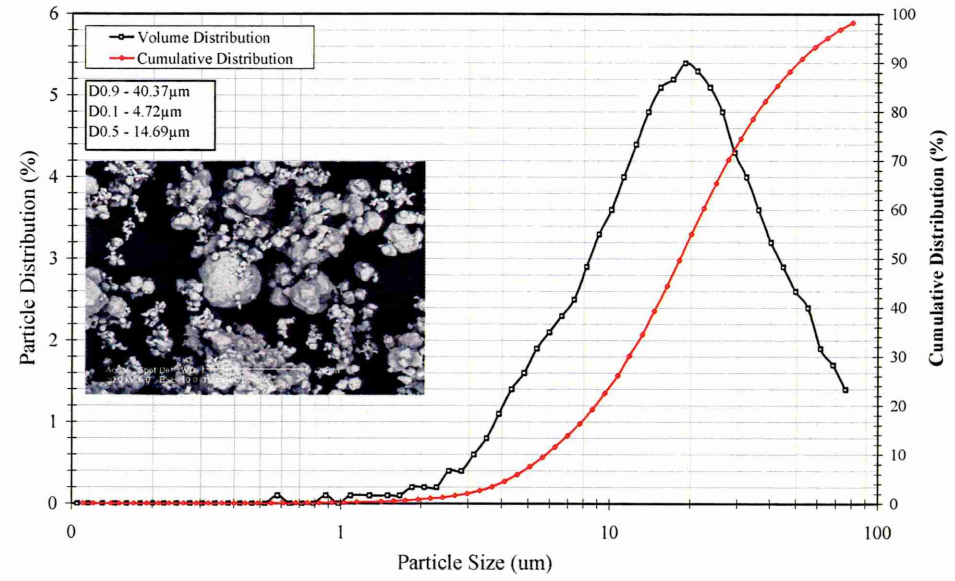

(a)

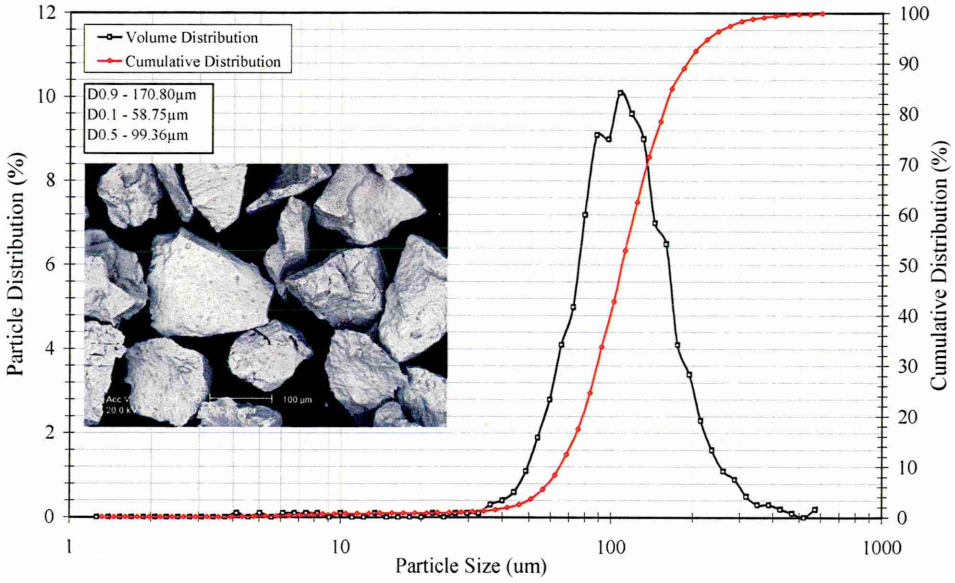

(b)

Figure 79: Particle size distribution and morphology of a) small and b) large WC powders.

Particle size analysis revealed the 10 µm powder possessed a varied particle size, ranging from ~1 to 20 µm. The analysis actually showed the powder to have an average particle size of ~D0.5=15 µm. Analysis of the larger powder showed a distribution of D0.5=99 µm. The morphology of the larger powder was angular in nature and the small powder had a rounded appearance.

A sample of the 100 µm WC powder was set in epoxy resin and polished back to reveal a cross-section of the particles. SEM revealed the particles were a complex dual phase structure shown by BSE imaging, Figure 80.

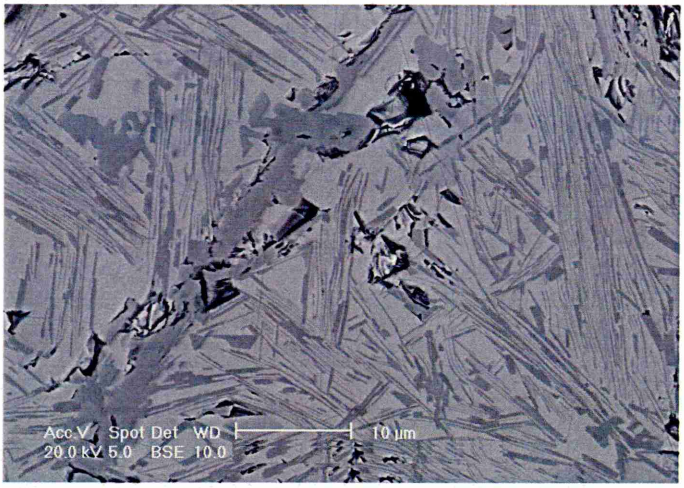

Figure 80: SEM micrograph of cross-section of large WC powder.

X-ray diffraction was employed to determine the nature of the two WC powders. The trace from the 15 µm powder revealed it be solely mono-tungsten carbide, WC, Figure 81. The trace of the 100 µm powder however, confirms that these particles consist of two separate phases, WC and di-tungsten carbide (W_2C), Figure 82. Both WC and W_2C possess hexagonal crystallographic structures, Figure 84.

EDX results showed that the powder consisted of ~75% W_2C and 25% WC.

Table 15: Crystallographic structures of hard phase additions.

Addition	Crystallographic structure
TiN	Rhombohedral
TiB_2	Cubic
TiC	Cubic
TaC	Hexagonal
Mo_2C	Hexagonal or Orthorhombic
Al_2O_3	Cubic
WC	Hexagonal

5.10 XRD data for WC materials and WC modified Armatech

The 15 µm WC and the 100 µm WC powders used as had phase additives were analysed using XRD (Figure 81 and Figure 82 respectively). The XRD data revealed the 15µm particle size material to consist solely of WC. The results from the larger 100µm particle addition confirmed the observation made by SEM and EDX analysis, a dual phase of WC and di-tungsten carbide (W_2C) was seen – from this point onwards described as WC/W_2C.

XRD diffraction data was obtained from WC/$W_2C(10)_{[100]}$ modified Armatech. The trace revealed that the Armatech phases identified earlier through XRD were still present with no obvious changes. The hexagonal structure of the WC and W_2C (the 100µm addition) was observed. Thus it can be seen that both the Armatech and the WC phases are unchanged, in

terms of crystal structure, following firing. Again, no evidence of residual bentonite phase was evident from the XRD trace.

While SEM examination of the WC phases incorporated in the Armatech show some level of reaction between the WC and the Armatech the XRD data does not show the presence of any significant reaction products. Such reaction products are thus either of the same crystal structure as the original phases or they are present at too low a level to be detectable by XRD.

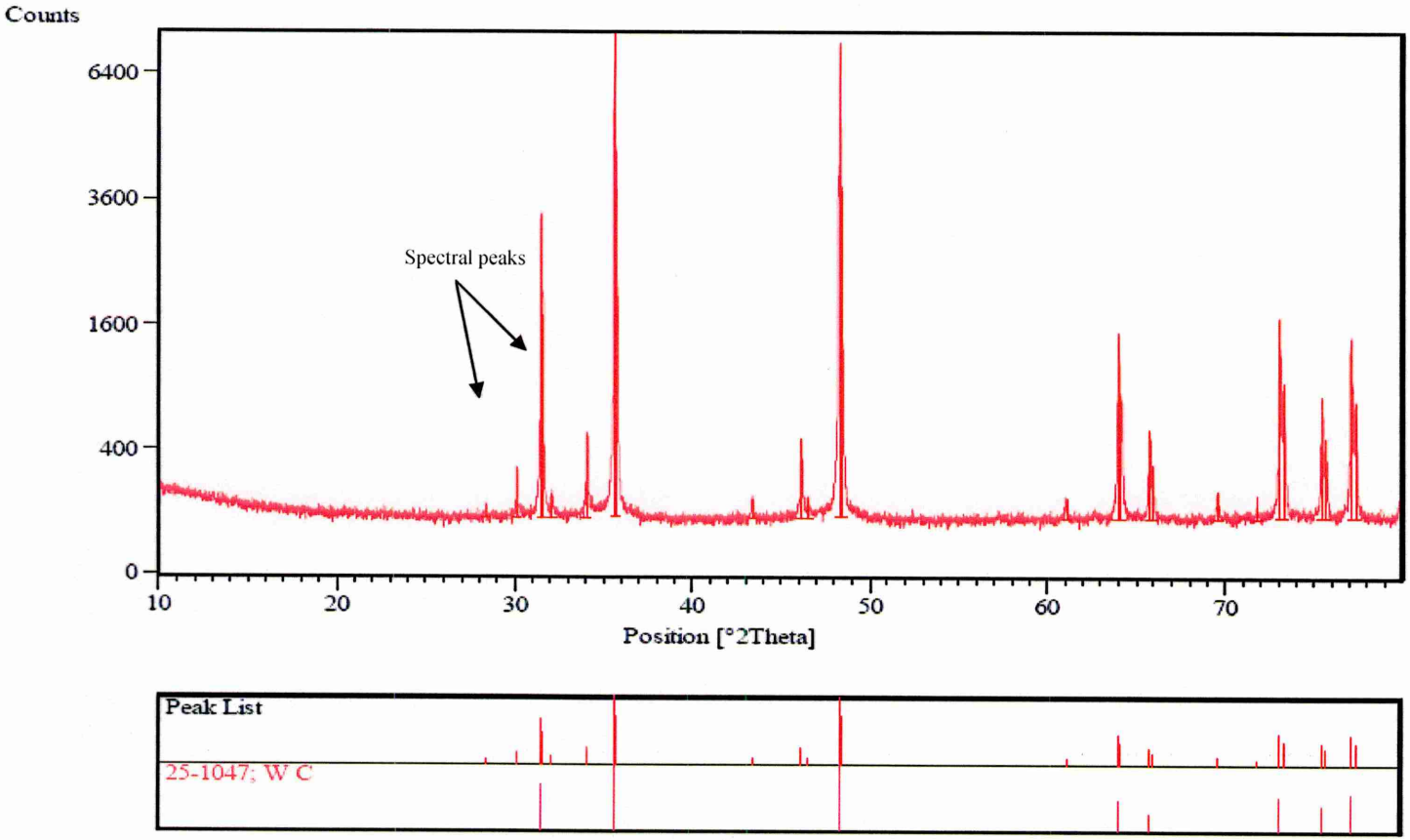

Figure 81: XRD trace (Cu Kα) of 15 μm WC powder.

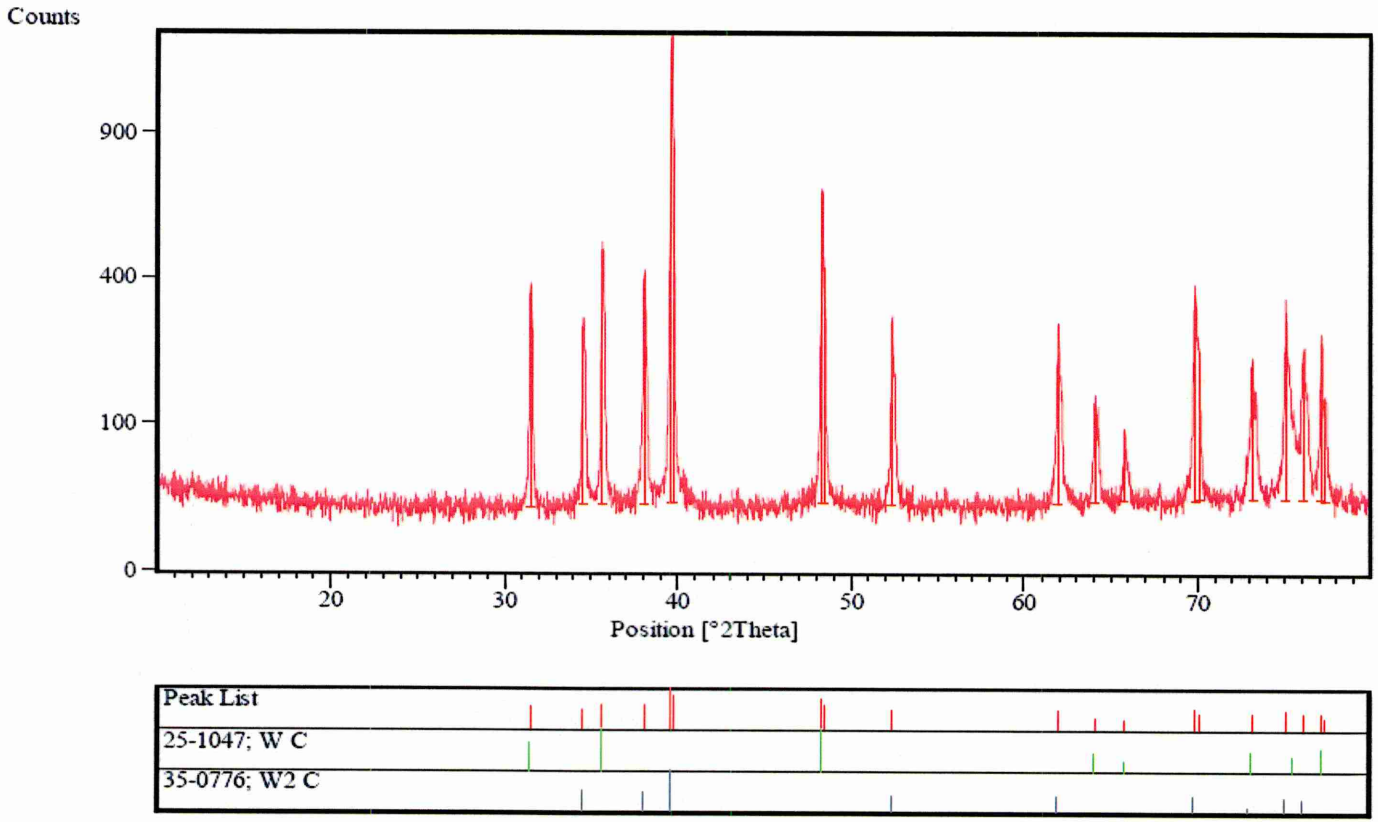

Figure 82: XRD trace (Cu Kα) of 100 μm WC/W_2C powder.

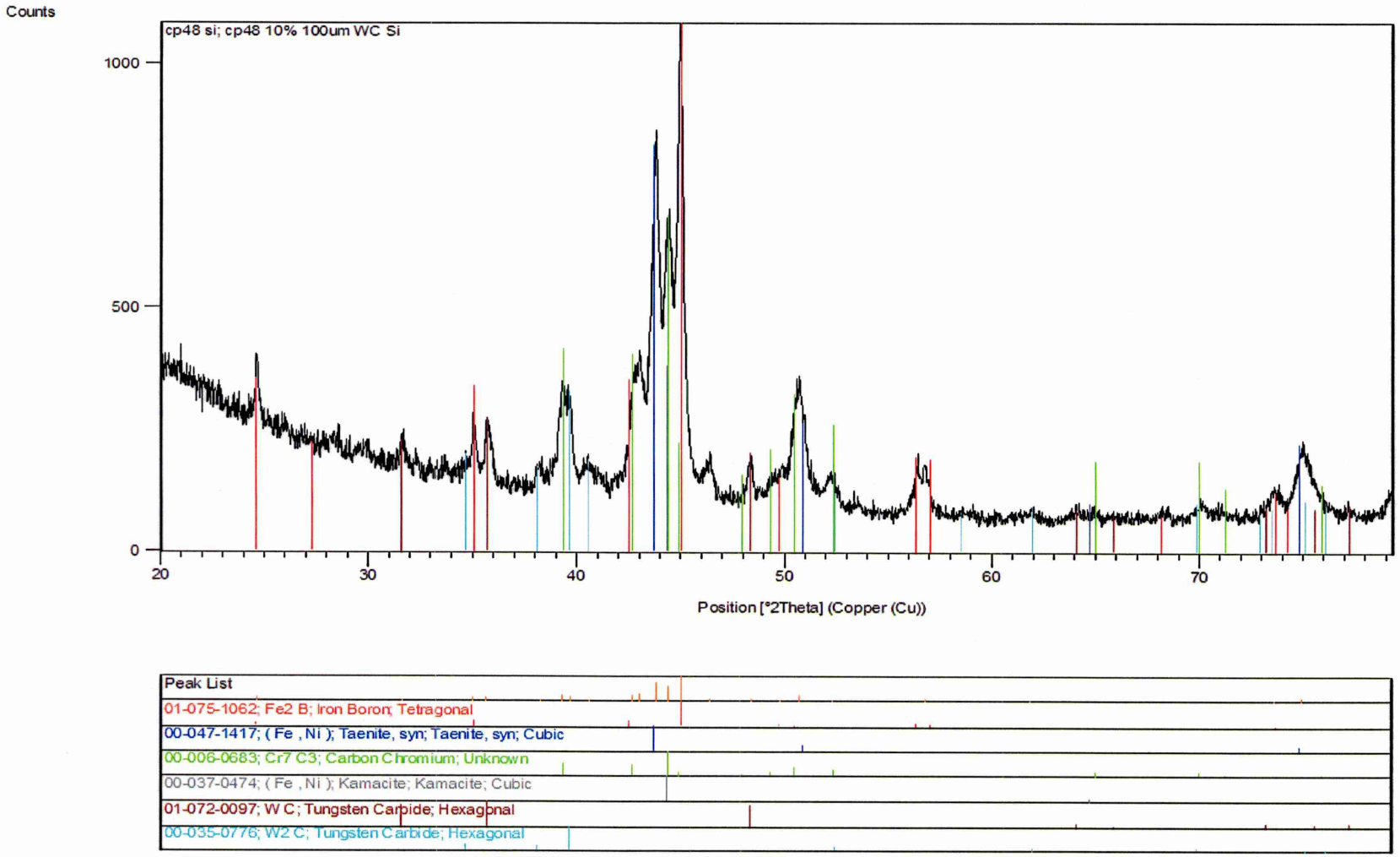

Figure 83: XRD trace (Cu Kα) of Armatech with an addition of 100 µm WC/W_2C powder at 10wt.%.

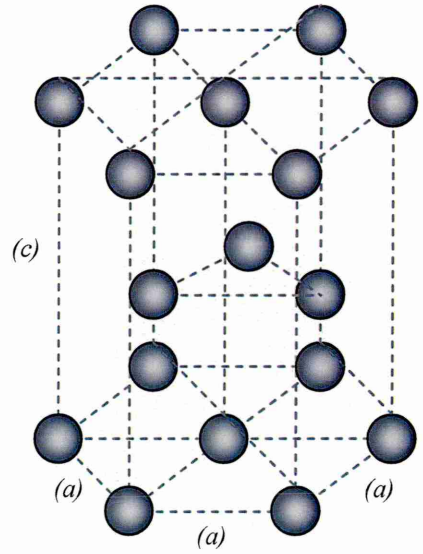

WC
(a) = 2.901 Vol. = 20.76
(c) = 2.838

W_2C
(a) = 2.997 Vol. = 36.78
(b) = 4.728

Figure 84: Hexagonal crystal structure.

5.10.1 SEM examination of mono-tungsten carbide addition

The micrographs below show a cross-section through the $WC(5)_{[15]}$ coated substrate and a polished surface. The residual binder can be seen in the cross-section along with the dispersed WC phase. There appeared to be a good reaction with the coating and substrate and the addition of the WC did not appear to affect the sinter quality of the Armatech. A change in size and shape of the carbides and borides near to the interface could be seen, observed previously with Armatech alone, Figure 85(a). The WC appeared phase to form a good reaction with the Armatech and had diffused in to the coating structure, clear in Figure 85(b).

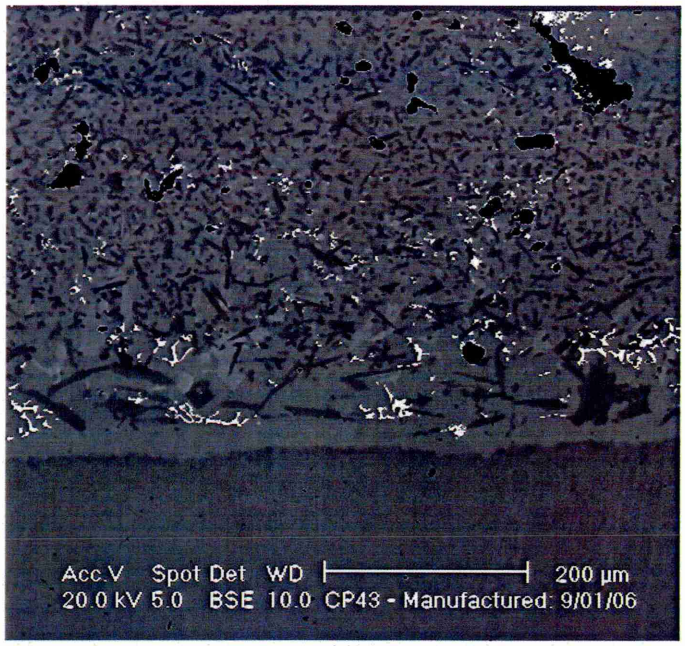

(a)

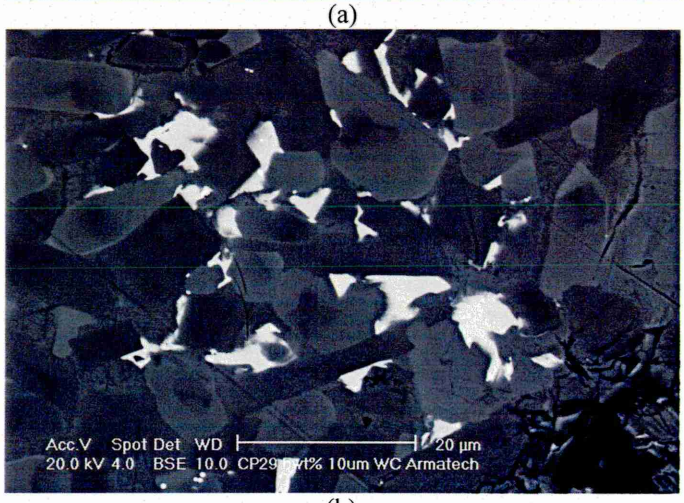

(b)

Figure 85: SEM micrographs of $WC(5)_{[15]}$ coating; a) showing substrate/coating interface and b) high magnification of diffused WC particles.

At low level loadings very little fallout of the WC phase was observed, increasing the loading above 10wt.% however, saw increases in WC fallout and some of the WC began to agglomerate in the residual binder phase. This suggested a possible overloading of WC in the Armatech, all loadings however formed a good reaction with the substrate material.

5.10.2 SEM of mono-tungsten/di-tungsten carbide addition

The addition of the larger 100 µm WC/W_2C powder showed a good distribution of hard phase throughout the coating, Figure 86(a). In some areas pockets of porosity were observed above the substrate/coating interface. The porosity appeared to be residual binder, the exact reason for this was not clear.

The reaction of the powder with the Armatech appeared to very strong, it can be seen that each individual particle possessed an outer reaction zone that diffused into the Armatech structure. A

central core region was also observed in each particle that consisted of a needle like structure, observed previously from SEM examination of a powder particle. This is revealed more clearly in Figure 86(c) where the central core and outer reaction zone is highlighted by BSE imaging.

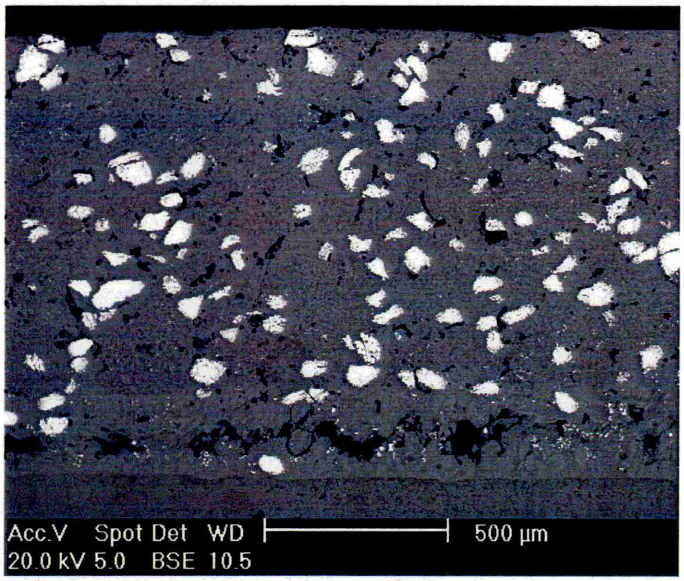

(a)

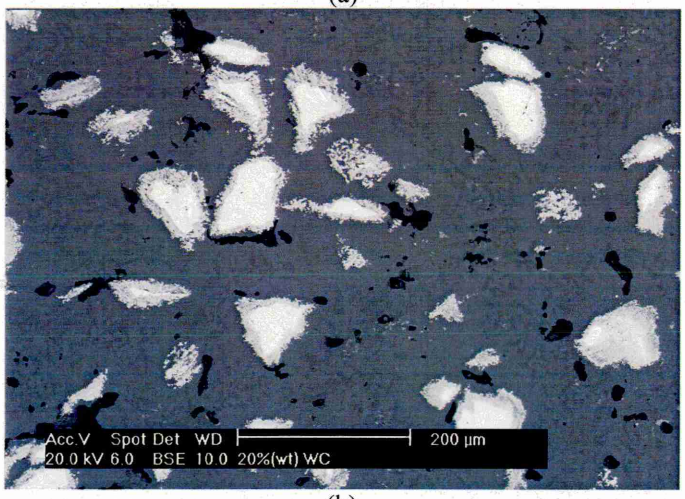

(b)

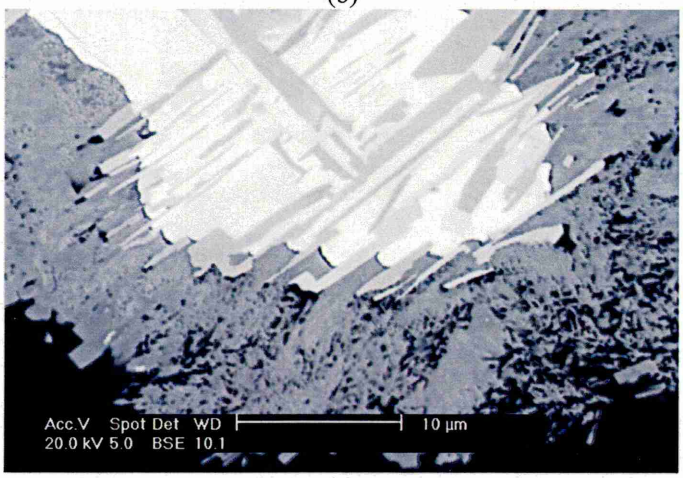

(c)

Figure 86: SEM micrographs of WC/W_2C addition coatings at three magnifications.

It was also seen from SEM examination of the WC/W_2C developed coatings that the reaction of the particle with the Armatech altered the existing microstructure, not previously seen with other additions. Each WC/W2C particle possessed a ~20 µm region where the primary Armatech carbides and borides did not exist in their usual form, highlighted below in Figure 87.

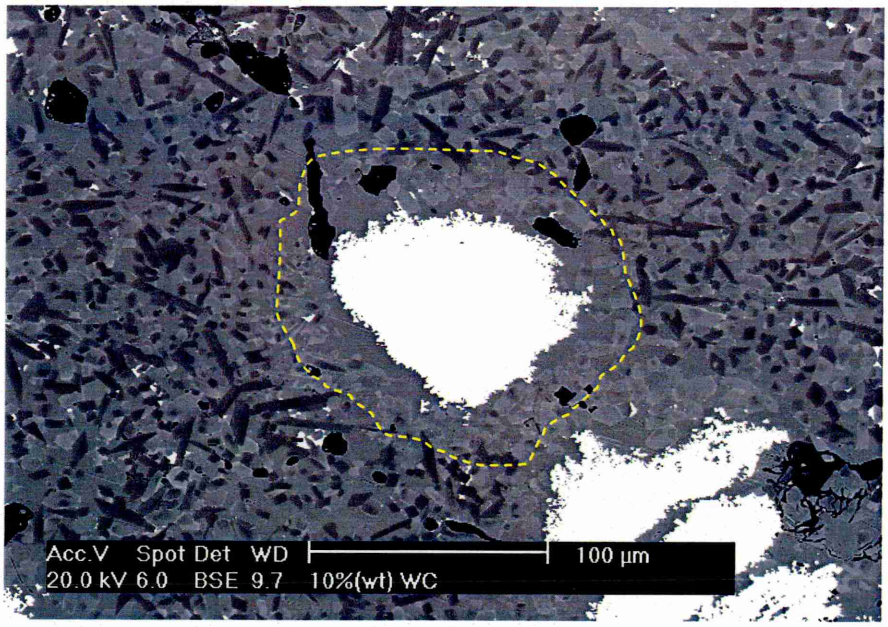

Figure 87: SEM micrograph of $WC/W_2C(10)_{[100]}$ microstructure. Highlighted line shows reaction zone around particles.

Closer inspection of this region, Figure 88, showed that the primary hard phases in this zone had a rounded morphology and BSE contrast suggested a chemical change. WC (unable to determine whether mono- or di-tungsten carbide) could be seen interstitially in this zone at carbide/boride boundaries.

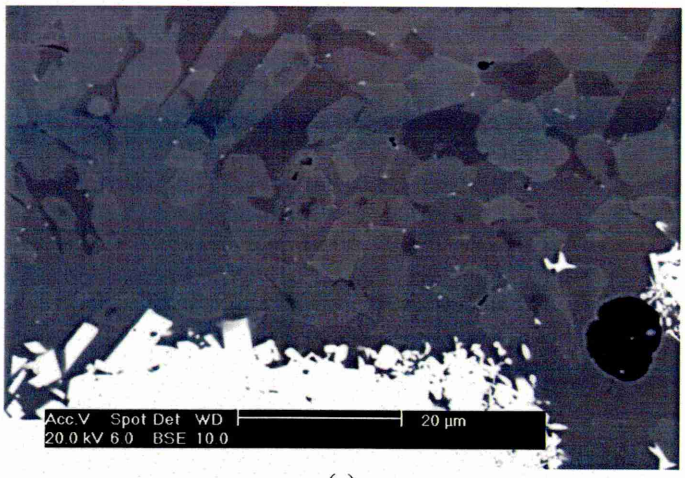

(a)

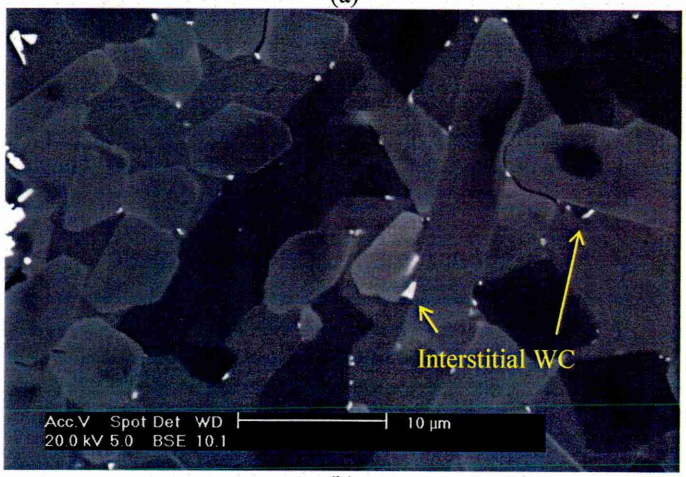

(b)

Figure 88: High magnification SEM micrographs of reaction zones of WC/W_2C particle and Armatech; a) showing change in Armatech structure around WC/W_2C particles and b) interstitial WC at carbide/boride boundaries.

EDX analysis of these regions was performed in order to elementally map the reaction, Figure 89. The analysis revealed the outer reaction zone of the WC/W_2C particles to be W rich with Cr and Ni diffused into the zone, it could also be argued that this zone had a depleted C content. The ~20 µm of Armatech structure surrounding the reaction zone proved to be Ni rich, when compared to the 'normal' structure. It also appeared that the Cr carbides were predominantly within this zone with less Fe borides present.

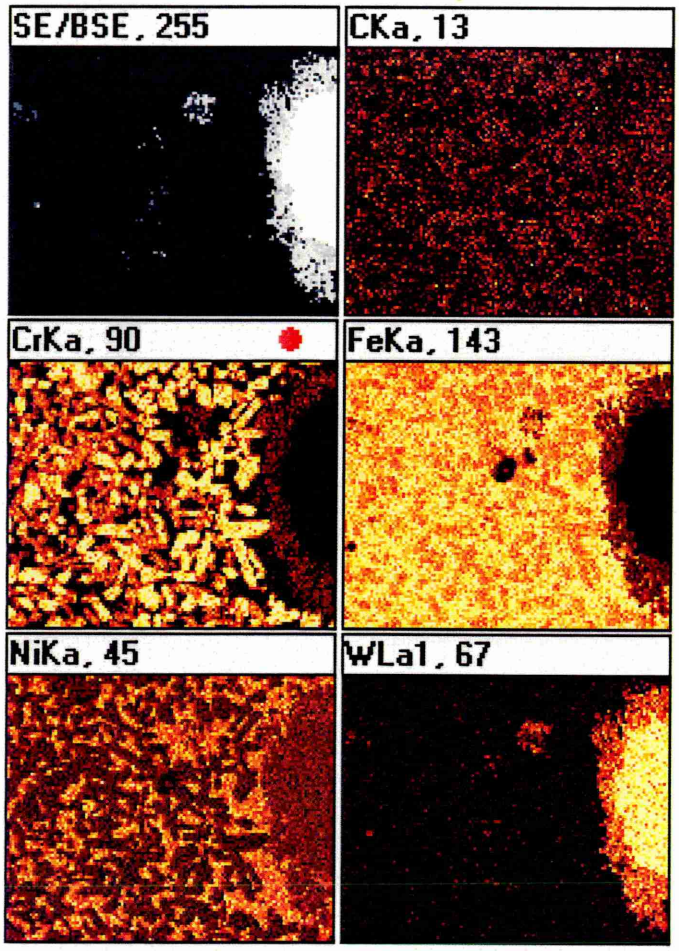

Figure 89: EDX map of 100 μm particle size WC/W_2C phase with surrounding Armatech matrix.

5.10.3 Mixed particle size WC

A series of materials were produced using a combination of ratios using the WC and WC/W_2C powders. Four coatings were developed, each having a total loading of 10wt.%, Table 16.

Table 16
Ratios of mixed WC and W_2C powders

Designation	15 μm WC loading [wt.%]	100 μm WC/W_2C loading [wt.%]
$WC(1\&4)_{[15\&100]}$	1	4
$WC(3\&7)_{[15\&100]}$	3	7
$WC(5\&5)_{[15\&100]}$	5	5
$WC(7\&3)_{[15\&100]}$	7	3

SEM examination of the coatings showed a mix of both reactions seen with the sole additions of 15 μm WC and 100 μm WC/W_2C. The WC particles were evenly disbursed throughout the structure, with each WC/W_2C particle having its own outer reaction zone and zone of reaction with Armatech.

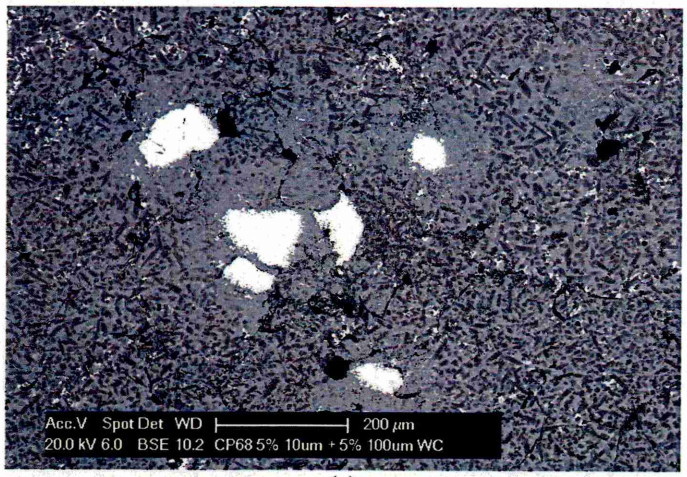

(a)

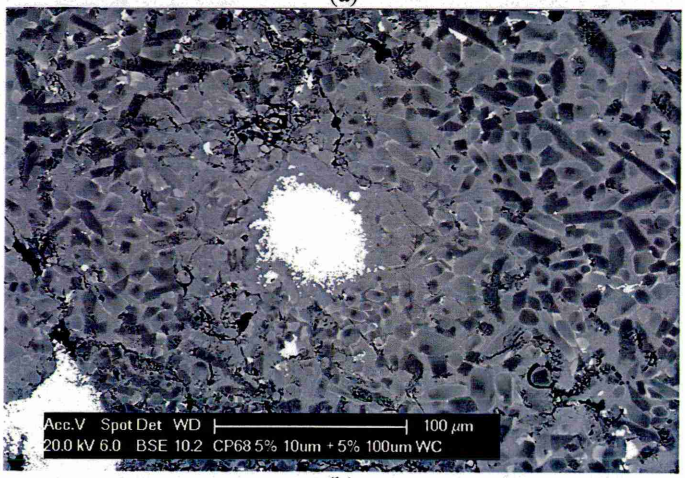

(b)

Figure 90: SEM micrographs of mixed ratio of $WC/W_2C(5+5)_{[15\&100]}$ modified Armatech.

5.11 Summary

It has been shown that the existing coating possesses a primary dual hard phase (carbides and borides) in a more ductile (Ni rich) matrix, a desirable microstructure for the property of wear resistance. From a selection of secondary hard phases and various particle sizes the existing coating has been successfully modified and the sinterability in most cases has not been affected. The hardness, density and tribological testing of the boron steel, Armatech and modified coatings will now be addressed in the following Chapter.

6 Introduction

The results in this Chapter are separated into three main sections;

- Coating hardness (macro and micro)
- Coating density and sinterability
- Tribological properties; microscale, macroscale and field trials

The microscale abrasive wear test section is itself subdivided into abrasive type and the macroscale tests are subdivided into environment type, i.e. dry and wet. The results of basic field trials carried out in September 2006 and March 2007 are included at the end of this chapter.

6.1 Hardness

6.1.1 Macrohardness

The bulk hardness of the materials developed during this work, determined by the method described in Chapter 3, are plotted in Figure 91 in descending order and by material groupings in Figure 92.

Modifications made to Armatech using additions of TiN and TiB_2 were not able to be measured accurately for bulk hardness due to the final sinter quality being porous in nature which resulted in very large and poorly defined indentations. These materials were excluded from further laboratory tests and field trials.

The average bulk hardness measured on Armatech was 485 H_{V20}, slightly higher than boron steel at 477 H_{V20}, although the error in measurement for boron steel was only ±1 whilst the error for Armatech was ±48. The exact reason for the larger standard error for Armatech is not entirely understood. Whilst the multiphase microstructure and residual binder phase most likely contributed to the error, all other coatings produced by the addition of secondary hard phases, did not yield such a large error.

The addition of 5wt.% 15 μm WC resulted in a higher hardness when compared to boron steel and Armatech. Above this level of addition the hardness reduced significantly despite the higher levels of hard phase particles.

The 100 μm WC/W_2C additions resulted in improved hardness values up to 15wt.% above which there was no further improvement. The largest increase in hardness was seen for 8wt.% of 100μm WC additive ($WC/W_2C(8)_{[100]}$) with H_{v20}= 635 H_{V20} ±2.

Improvements in hardness were also observed with low level additions (3wt.%) of 50 μm Al_2O_3 with the smaller 15 μm addition yielding no discernable increase. Higher levels of both additions reduced the hardness by around 100 points on the Vickers scale.

Additions of both TiC and Mo_2C reduced the hardness significantly. The failure of the TiC to bond with the Armatech may have been the cause of the low hardness. The exact reason for the low hardness with the Mo_2C addition is not fully understood. The addition appeared to fuse with the Armatech and was homogenously dispersed throughout the coating so an increased or similar hardness to Armatech was expected.

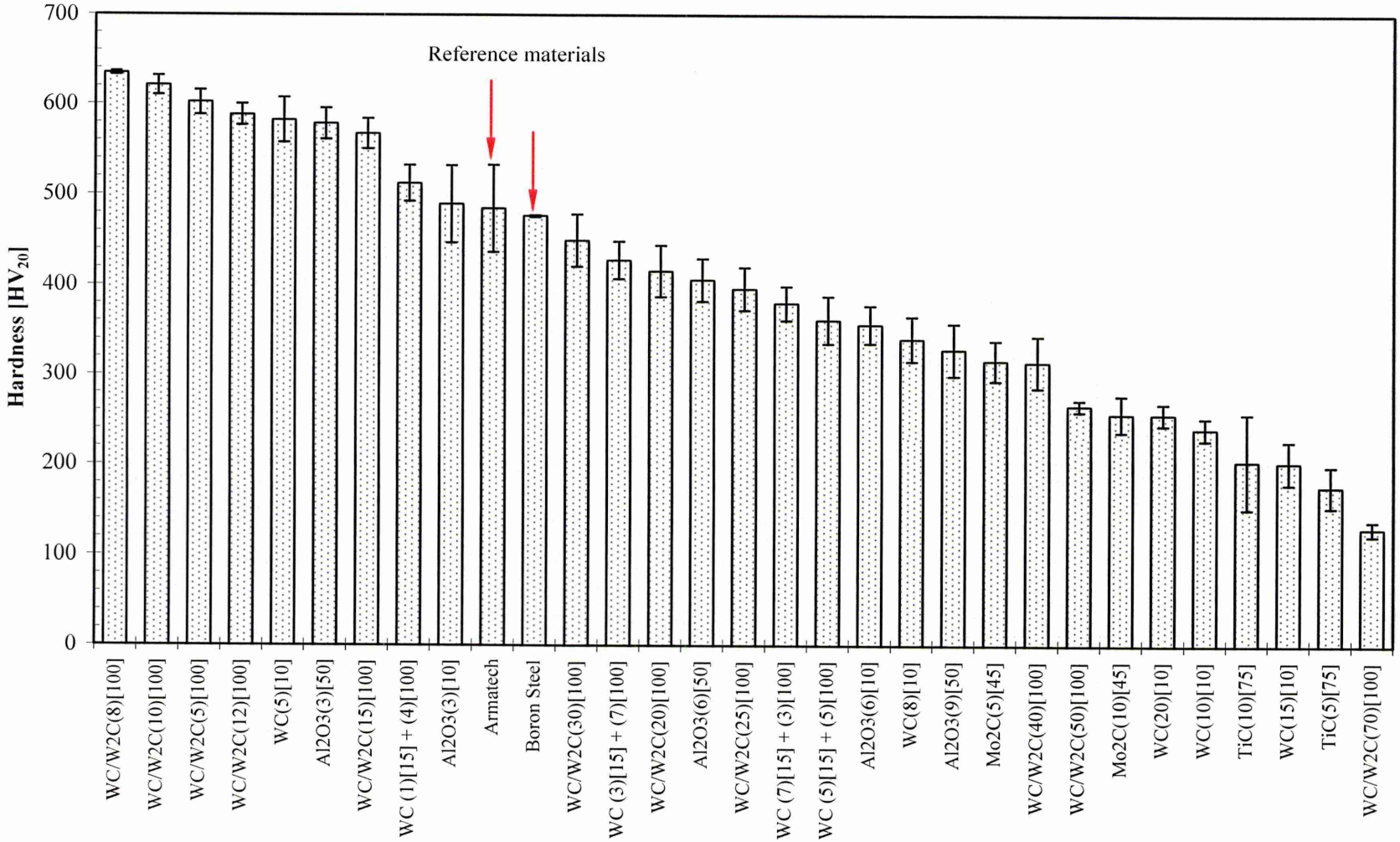

Figure 91: Graph showing Vickers bulk hardness results of final sintered material, presented in descending hardness order.

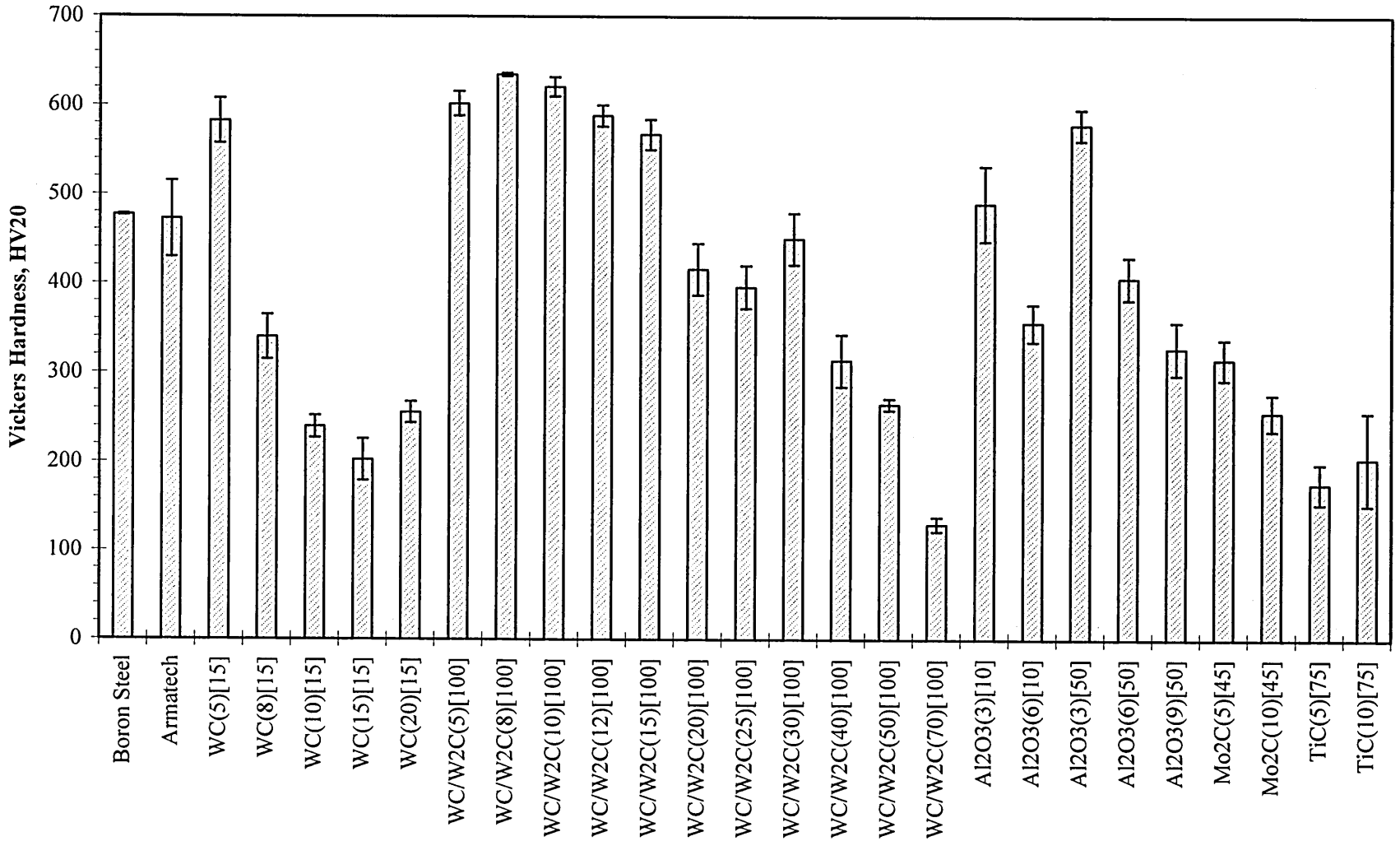

Figure 92: Graph showing Vickers bulk hardness results of final sintered material, presented in material groups.

6.1.2 Microhardness

Microhardness measurements were carried out to determine the inherent hardness of the phases present within the Armatech microstructure. The Fe-Ni rich matrix hardness was measured at ~700 $H_{V0.1}$ and the two distinct hard phases ~1500 $H_{V0.1}$.

The central region of the 100 μm WC/W_2C additions was considerably harder at ~2050 $H_{V0.1}$. The reaction zones surrounding the large particles were too small for meaningful microhardness measurements to be carried out.

Other additions made to Armatech included Al_2O_3, Mo_2C and TiC, which possess hardnesses of 2720, 1950 and 3200 H_V respectively. For a number of reasons such as small particle size, poor sinter quality or poor wetting it was not possible to accurately measure microhardness for other additions.

6.2 Density

Samples from a selection of the test materials were produced for density measurement by sintering a small amount of material on an alumina tile. Results are given below in Table 17 along with the theoretical density values and the values of measured density as a percentage of theoretical.

The average mass of the samples used to calculate densities were ~10 g and each was coated in wax to avoid air bubbles affecting results. The boron steel was measured at 7.86 g/cm^3, 0.01 higher than the theoretical value which may be explained by the error associated with the technique, ±0.01 g/cm^3.

The Armatech sample provided a lower density than the theoretical figure, it may be argued that this could have been due to not only the error of the technique but also the level of residual binder phase in the sample used. However, the remainder of the results that exhibited <90% theoretical density can not be explained by this alone. In particular this is true for materials with very low values such as $WC/W_2C(10)_{[100]}$ which appeared dense from SEM examination and provided good improvement in hardness.

Bulk hardness values were plotted against both theoretical density and measured density, however there was no strong correlation between the two. Certain measured density values did not correspond with the quality of sinter observed from materials characterisation. For this reason it was decided to use a 95% theoretical density value in later calculations of volumes removed in the DSRW test and field trials. It is worth noting that small changes in density, such as 1 - 5% only cause small changes when calculating volume. However, plotting these values as a function of hardness also produced no relationship.

Table 17
Density measurement [g/cm^3]

	Theoretical	Measured Density†††† [*B*]	Percentage of Theoretical	95% of Theoretical
Boron Steel	7.85	7.86	100.13	**6.55**
$Mo_2C(5)_{[45]}$	6.94	7.00	100.86	**6.59**
$Mo_2C(10)_{[45]}$	7.00	6.96	99.43	**6.65**
$TiC(5)_{[75]}$	6.75	6.70	99.26	**6.41**
$WC(1\&4)_{[15\&100]}$	7.08	6.96	98.31	**6.73**
Armatech	6.89	6.73	97.68	**6.55**
$WC(5\&5)_{[15\&100]}$	7.29	7.11	97.53	**6.93**
$Al_2O_3(3)_{[10]}$	6.74	6.45	95.70	**6.40**
$WC(3\&7)_{[15\&100]}$	7.29	7.09	97.26	**6.93**
$WC(7\&3)_{[15\&100]}$	7.29	7.06	96.84	**6.93**
$WC/W_2C(5)_{[100]}$	7.08	6.79	95.90	**6.73**
$Al_2O_3(3)_{[50]}$	6.74	6.46	95.85	**6.4**
$WC(5)_{[15]}$	7.08	6.77	95.62	**6.73**
$WC(15)_{[15]}$	7.52	7.09	94.28	**7.14**
$Al_2O_3(6)_{[50]}$	6.59	6.21	94.23	**6.26**
$WC(10)_{[15]}$	7.29	6.57	90.12	**6.93**
$TiC(10)_{[75]}$	6.62	5.94	89.73	**6.29**
$Al_2O_3(6)_{[10]}$	6.59	5.61	85.13	**6.26**
$WC/W_2C(10)_{[100]}$	7.29	6.19	84.91	**6.93**
$WC/W_2C(15)_{[100]}$	7.52	6.13	81.52	**7.14**

6.3 Development of MSAW test procedure

An initial study was carried out to assess the optimum parameters to be used for the MSAW test. The aim was to ascertain the optimum applied loads and sliding distances that should be used to obtain the wear regimes discussed previously, to produce good quality craters, and to provide reproducible results using SiC and SiO_2 abrasive (see Table 19 for abrasive information).

It is important to note that with MSAW testing, and indeed all laboratory tests, various assumptions have to be made. Assumptions associated with the fixed-ball MSAW test used in this research include:

- Adequate slurry entrainment into the wear interface.
- The wear scar reproduces the spherical geometry of ball.
- The load applied to the samples remains constant throughout the test.

†††† Error ± 0.01 g/cm^3.

- The wear ball remains the same diameter throughout.

The test method followed was set out in a European report produced by NPL with an aim to standardising and hence increasing reproducibility in ball cratering wear tests[105].

6.3.1 Tests with SiC abrasive

The plot below in Figure 93 shows the average crater diameter in μm as a function of applied load between 0.2 and 5 N, over a sliding distance of 50 m using SiC abrasive. It reveals a relationship between crater diameter and load that obeys a power law.

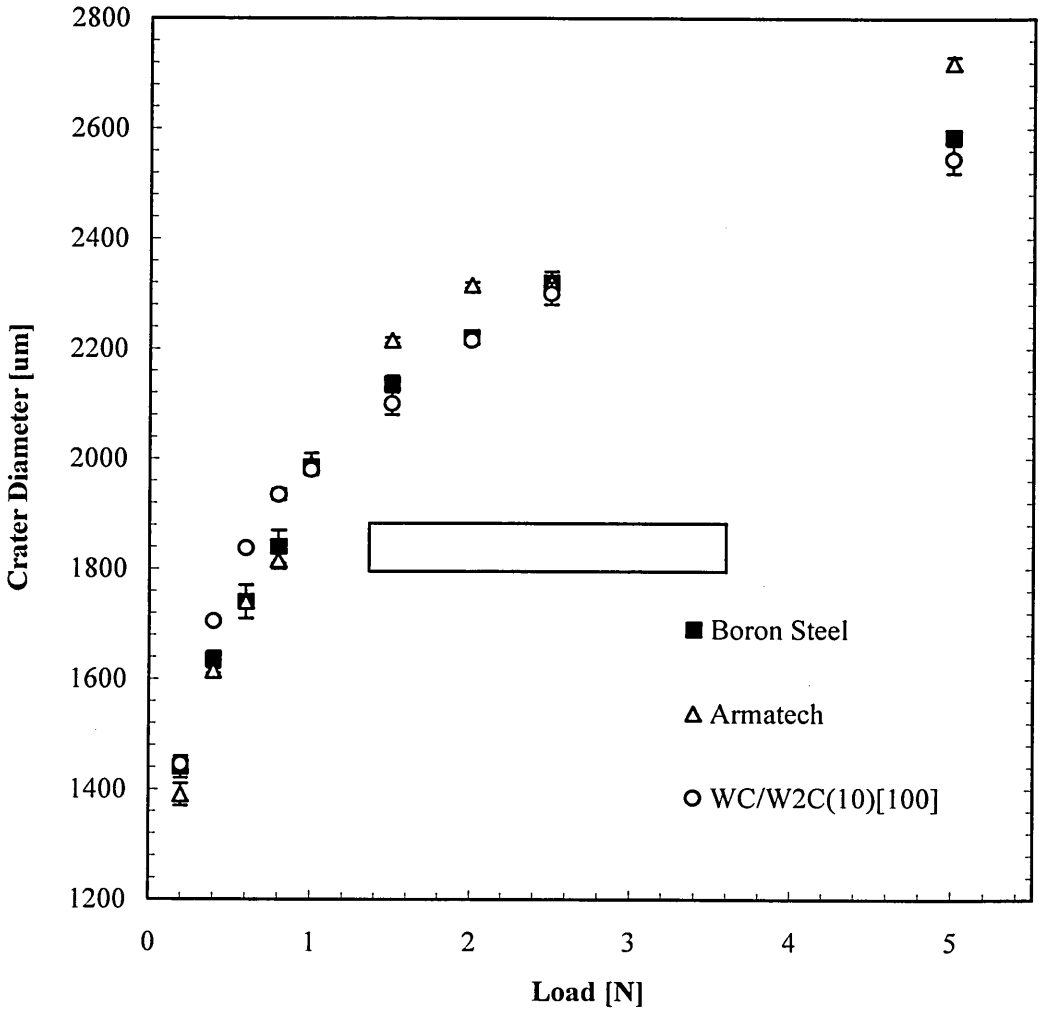

Figure 93: Average crater diameter (μm) vs. load (N) over a sliding distance of 50 m using 7 μm SiC abrasive for 3 types of material.

Figure 94 is a plot of the wear volume per unit sliding distance as a function of applied load. The boron steel wear scars displayed three-body rolling wear from 0.2 to 1.5 N. At 2 N applied load the onset of ridging was observed which increased up to 5 N applied load, Figure 97. This same trend occurred with Armatech and $WC/W_2C(10)_{[100]}$ material, although at 0.2 N two-body grooving was observed but disappeared between 0.4 to 1.5 N applied load. The ridges at high loads did not appear to correlate to the size of the SiC abrasive and signal the onset of ridge

formation due to contact of the sample with the wear ball (see Chapter 4). Wear scars produced using the maximum test load of 5 N showed clear signs of ridging.

The relationship between wear volume and applied load appears to be an increasing linear one until the ridging occurs at around 2 N. A similar relationship was observed in work by Trezona[71] using a similar abrasive, Figure 19 in Chapter 2.

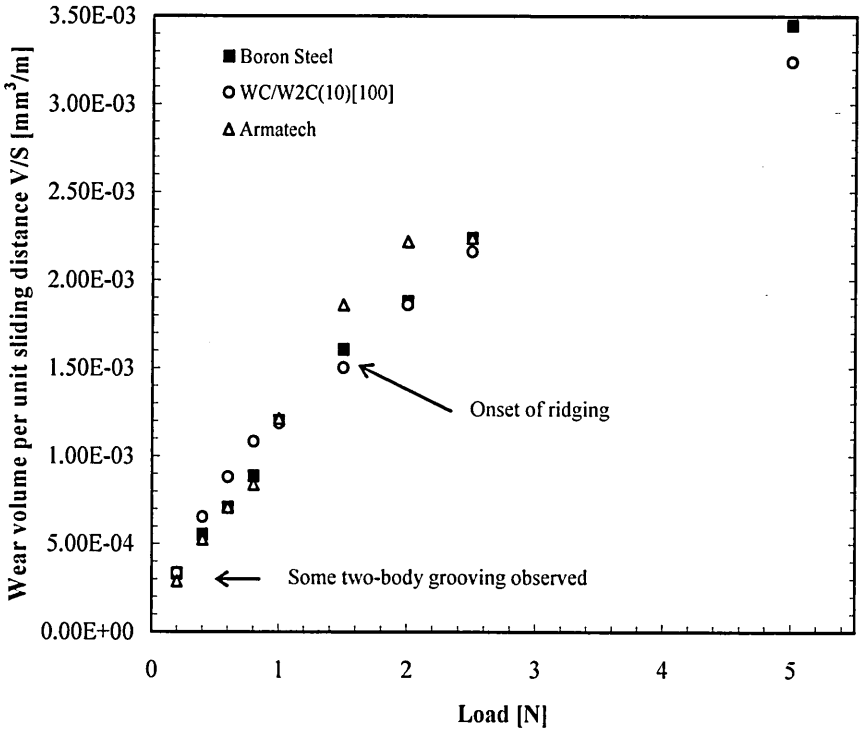

Figure 94: Variation of wear volume per unit sliding distance (mm^3/m) as a function of load (N) using 7 μm SiC abrasive at a sliding distance of 50m.

Archard's equation (see Chapter 4), predicts that the wear volume removed is linearly proportional to the applied load, which could be argued is the case in Figure 94, certainly up to a load of 2 N. The results in Figure 94 however, revealed that in this case, for three-body wear obtained using a 20% volume fraction 7 μm SiC abrasive on these test materials; it is proportional to a power of the load less than one up to 2 N and falls off after this load.

Figure 95 presents a plot of κ (expressed as volume removed per unit sliding distance per unit load), as a function of applied load. κ can be seen to reduce with an increase in applied load, an effect also observed in other research using the same abrasive[72,76,78,]. This is an interesting observation and is discussed briefly in Chapter 7.

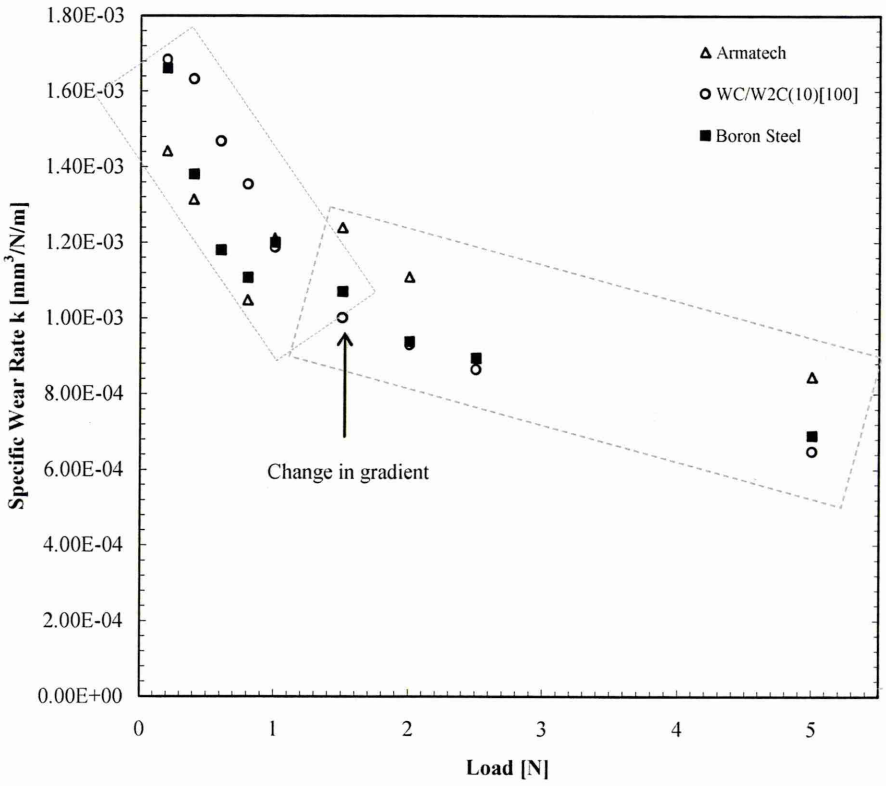

Figure 95: Plot of κ ($mm^3/N/m$) vs. load (N) at a sliding distance of 50 m using 7 μm SiC abrasive.

The variation of κ as a function of applied load appears to show two regimes each with a linear relationship as shown in Figure 95. Between 0.2 to 0.8 N there is a steep negative gradient while between 1.5 to 5 N, the gradient is still negative but less steep. It is this latter region that signs of ridging were observed.

If the data points that exhibited signs of mixed mode wear (0.2 N) and ridge formation (>0.8 N) are removed then it can be said that the specific wear rate decreases linearly from 0.2 to 0.8 N, as is shown below in Figure 96.

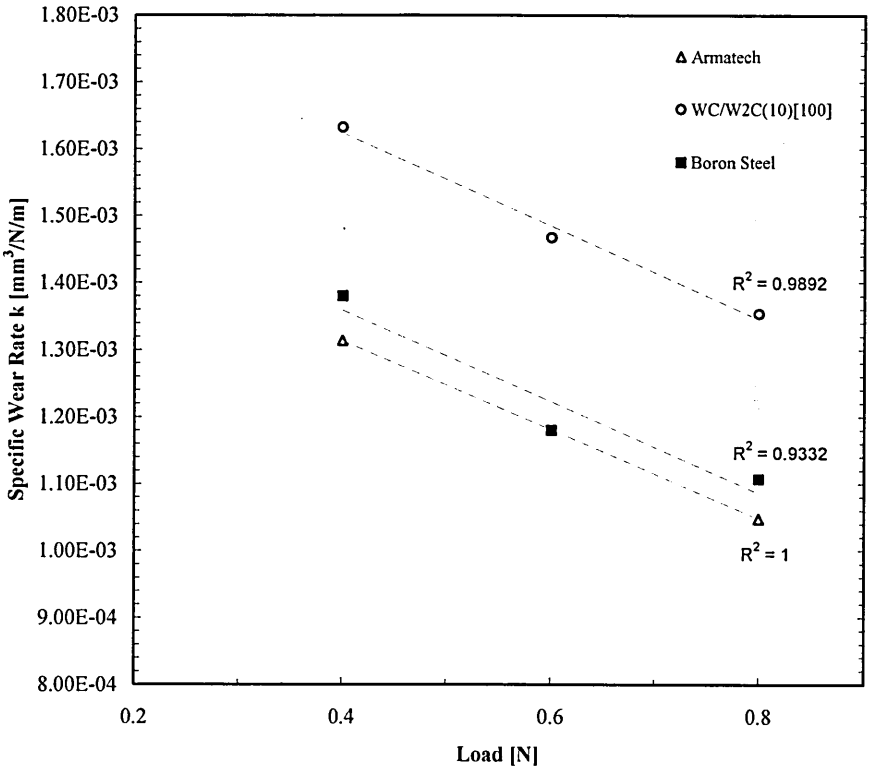

Figure 96: Plot of κ ($mm^3/N/m$) vs. load (N) at a sliding distance of 50 m using 7 μm SiC abrasive between 0.4 and 0.8 N.

In theory there should be no variation of the specific wear rate with load (within a set wear mode). The observed deviation of κ from the theoretical flat straight line, shown in Figure 95 and Figure 96, (excluding the lower and higher loads where the wear is mixed mode), may be attributable to several factors. It has been found previously that the onset of ridging can reduce the wear rate due to the shape of the scars becoming less spherical, (the limited ingress of abrasive and reduced load caused by contact between ball and sample)[102]. Another issue is the possible incorrect assumption that the wear scar has the spherical geometry of the wear ball[72].

A further factor for consideration involves the error associated with the applied load for the MSAW test. Other researchers have quoted the accuracy of the applied load to be ±0.01 N[71,72]. However, Jones estimated the uncertainty in balancing the load arm to be ~0.02 N[102]. If this error remains constant then as applied load is increased the uncertainty as a percentage of the applied load would decrease. Increasing the load above 2N, however, has been shown to introduce wear mode effects such as ridging, so using very high loads to reduce error is not straightforward and applied loads have to be selected carefully.

In the case of both abrasive types, wear surfaces were examined for microstructural cracking or extensive pullout of the hard phases and none of these effects were observed.

From the results above further MSAW testing using SiC abrasive was limited to using loads 0.2, 0.4, 0.6 and 0.8 N. Although the 0.2 N loads showed some signs of a mixed wear regime,

(Figure 97), the volume of material removed per unit distance appeared to fit the trend for higher loads and so was used in calculation of the wear rate.

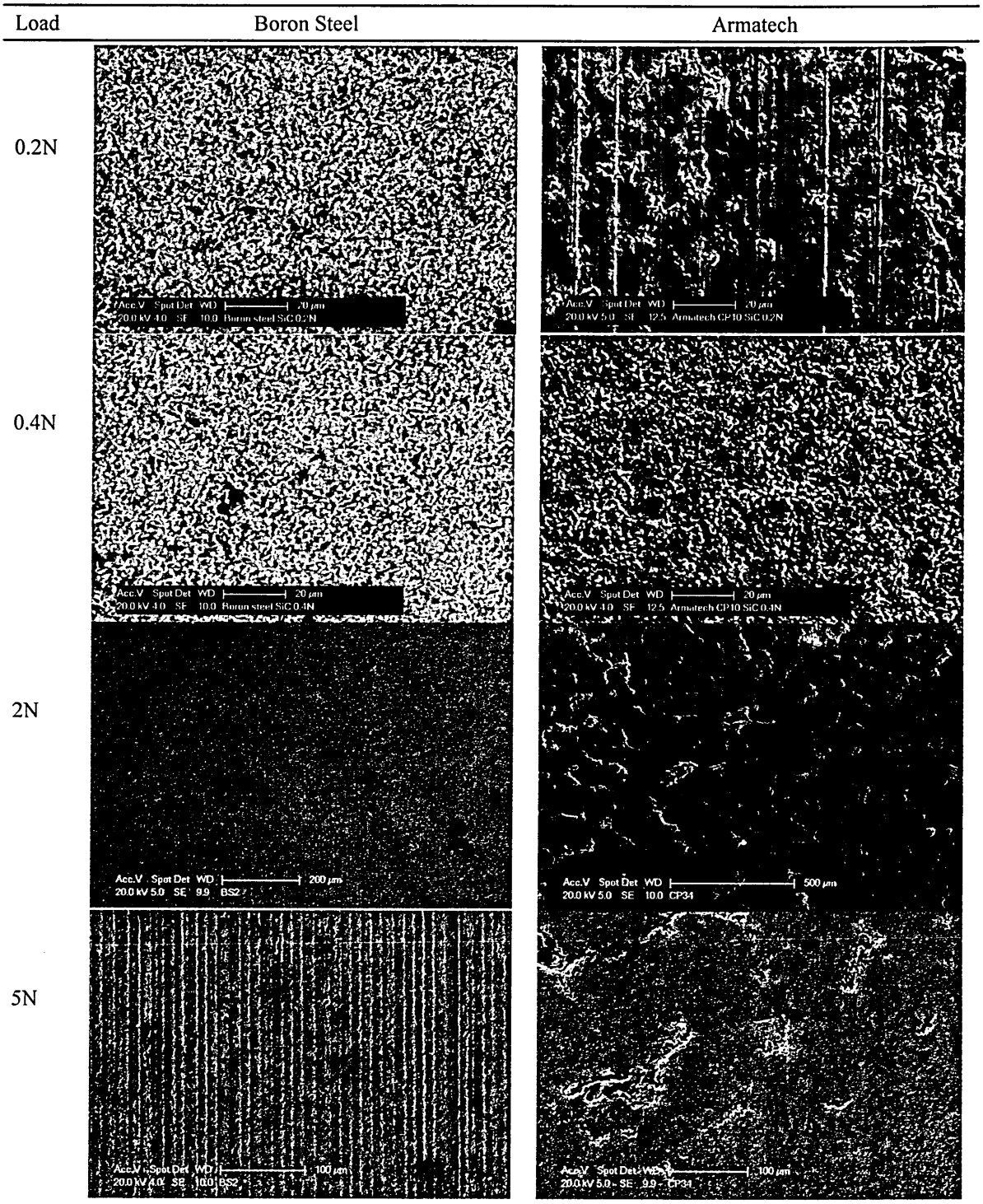

Figure 97: SEM micrographs of MSAW mechanisms for Boron steel and Armatech as a function of applied load using 7 μm SiC abrasive over a sliding distance of 50 m. The 0.2 N load shows signs of a mixed wear mode on Armatech which ceases as the load is increased, at 2 N the introduction of ridging on both materials can be seen.

6.3.2 *Tests with SiO_2 abrasive*

The wear scars produced using the SiO_2 slurry were much smaller in diameter than scars produced using SiC and at low applied loads did not have clearly definable crater edges. The major wear mechanism was two-body grooving wear as oppose to three-body rolling wear seen with SiC, SEM micrographs of the wear scars are provided later in Figure 103. To enable accurate measurement and reduce error, the sliding distance was increased to 100 m to produce a larger wear scar.

The plot below in Figure 98 shows the average crater diameter as a function of applied load over a sliding distance of 100 m using SiO_2 abrasive (abrasive information provided in Table 19). Comparing these results to the SiC results shows that the average crater diameter is smaller and the errors larger. This was due to the difficulties and uncertainty in the measurement of SiO_2 wear craters that existed even when using the increased sliding distance.

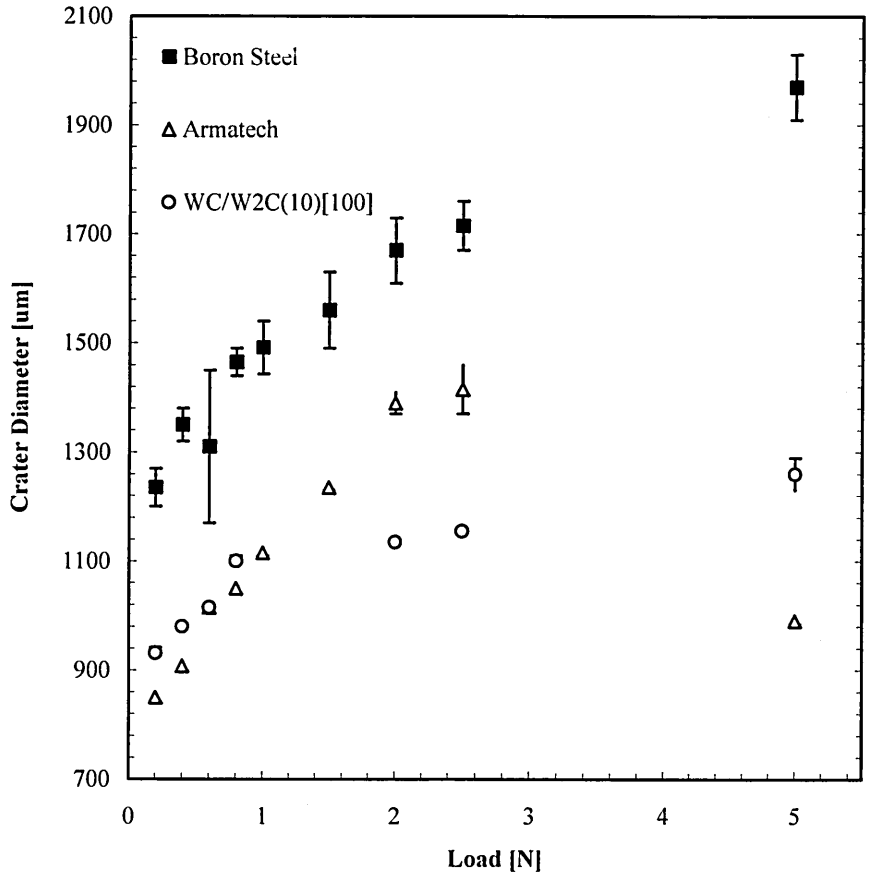

Figure 98: Average crater diameter (μm) vs. load (N) over a sliding distance of 100 m using 2.5 μm SiO_2 abrasive.

Plotting wear volume per unit sliding distance as a function of applied load, reveals an increasing linear relationship for boron steel that does not pass through the intercept (which is in contradiction to simple theory, e.g. at zero load there should be zero wear), Figure 99. This also appears to be true for the other two materials at applied loads of <1 N, when plotting the wear volume removed as a function of load, Figure 100.

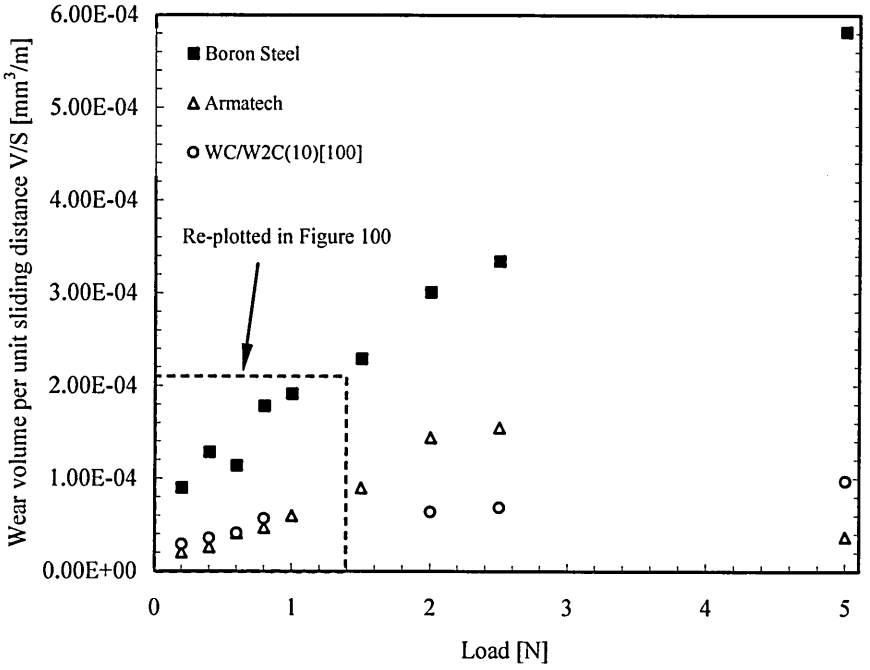

Figure 99: Variation of wear volume per unit sliding distance (mm^3/m) as a function of load (N) using 2.5 μm SiO_2 abrasive at a sliding distance of 100 m.

The linear region of Figure 99 between 0.2 and 1 N applied load is re-plotted below in Figure 100.

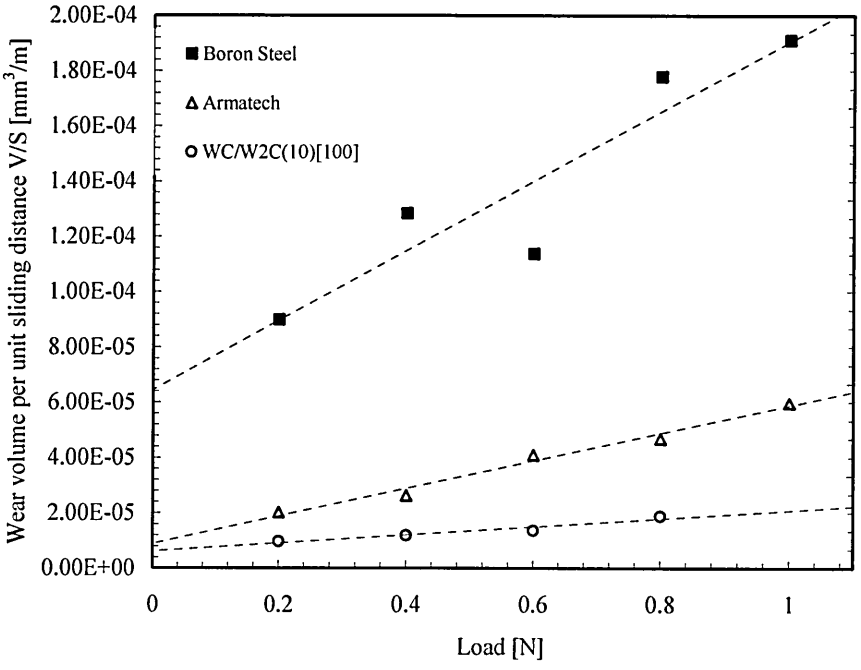

Figure 100: Variation of wear volume per unit sliding distance (mm^3/m) as a function of load between 0.2 and 1 N using 2.5 μm SiO_2 abrasive at a sliding distance of 100 m.

Research carried out by Trezona *et al.*[71] showed that for three-body abrasion, the relationship between wear volume and load was linear but obeyed a power law for two-body abrasion, which in this study has been the reverse. He noted however, that the linear relationship observed for

three-body rolling abrasion did not pass through the intercept which was the case in this research.

The plot below in Figure 101 shows κ as a function of applied load. The overall wear rate decreases as the applied load increases, as was also observed with SiC abrasive.

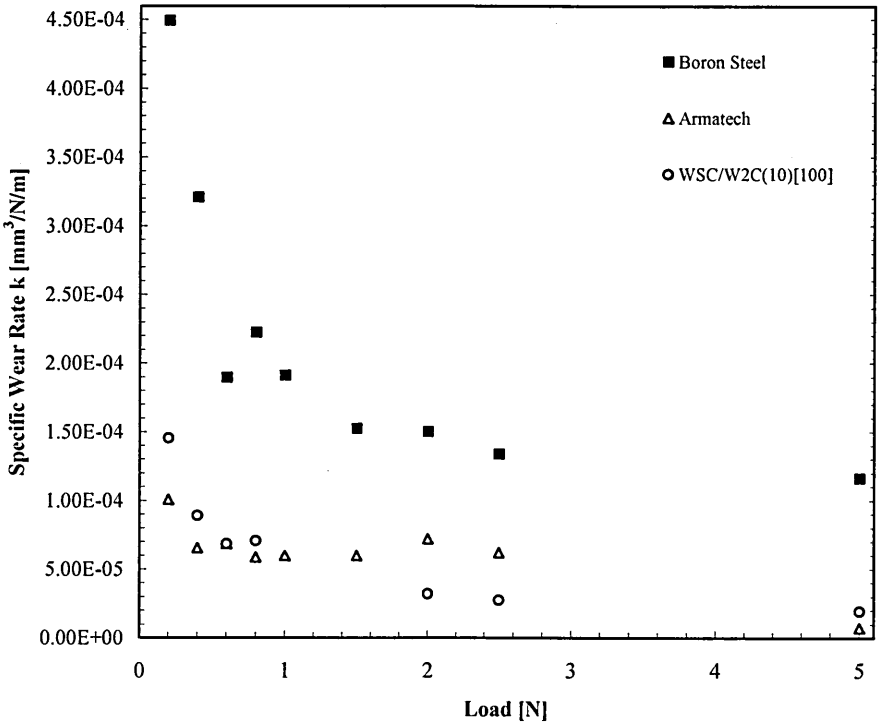

Figure 101: Variation of specific wear rate ($mm^3/N/m$) as a function of load (N) using 2.5 μm SiO_2 abrasive at a sliding distance of 100m.

Removing the data points for applied loads >1.5 N shows two relationships associated with load, between 0.2 and 0.6 N it can be seen that the wear rate appears to decrease rapidly. Above 0.6 N the rate then levels off slowly decreasing as the load is increased to 5 N, Figure 102. This is a similar to the two stage relationship observed when plotting load against κ for SiC abrasive, shown in Figure 95.

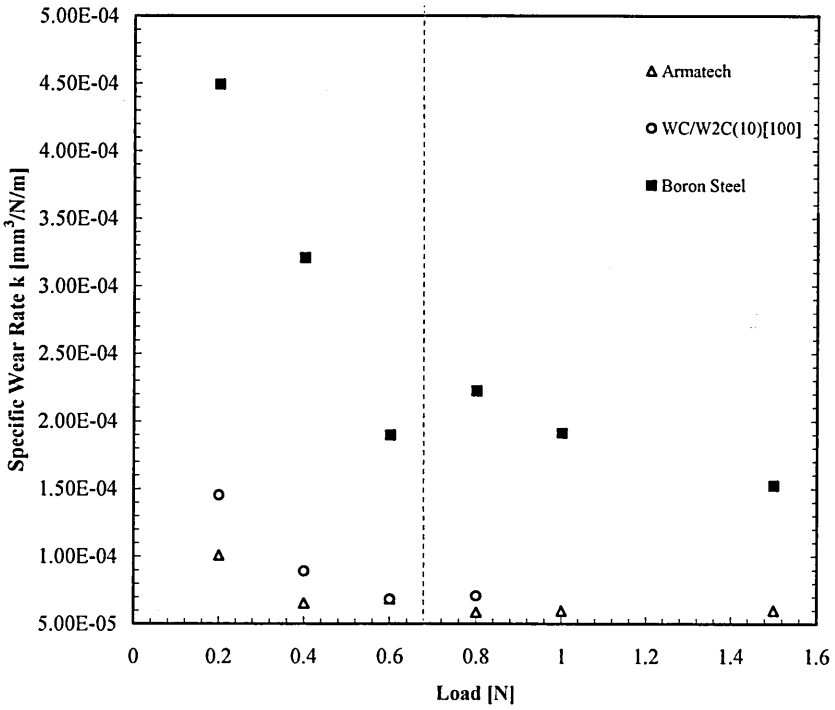

Figure 102: Plot of κ (mm^3/N/m) vs. load (N) at a sliding distance of 100 m using 2.5 μm SiO_2 abrasive between 0.2 and 1.5 N.

The exact reason for this behaviour is not known. SEM examination shows that the wear modes appear to be consistent for each applied load (Figure 103) with the severity of groove depth and width increasing as a function of the applied load.

The wear scars on the boron steel displayed predominantly two-body grooving wear mechanism with groove depth/width increasing with load, Figure 103. The Armatech and WC/W_2C modified coating however showed a mixed mode of wear at all loads, with the primary hard phases in Armatech and WC/W_2C carbides showing signs of two-body grooves and the matrix material wearing through a three-body regime.

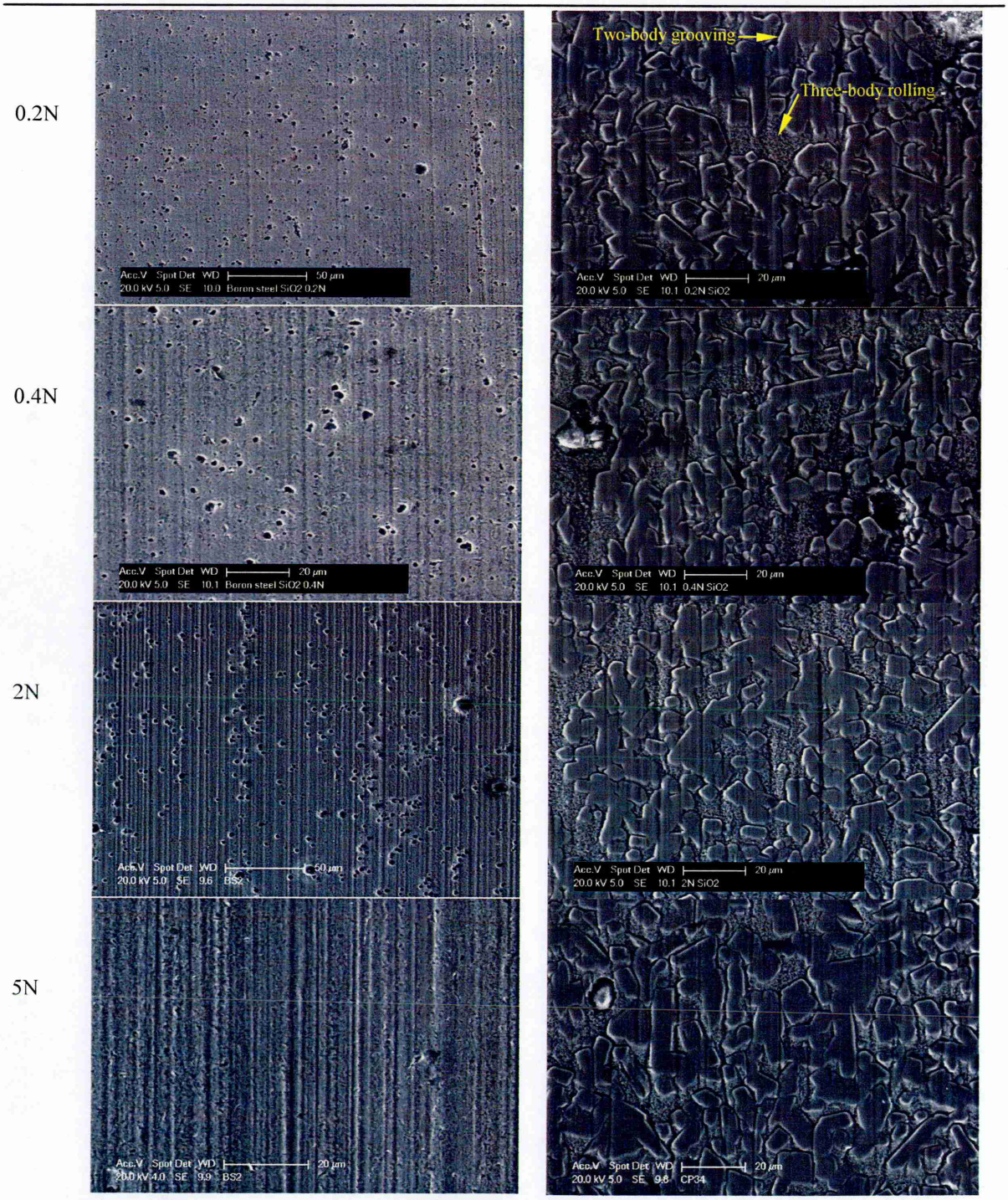

Figure 103: SEM micrographs of MSAW mechanisms for Boron Steel and Armatech as a function of applied load using 2.5 µm SiO_2 abrasive over a sliding distance of 100 m. A consistent two-body grooving wear can be seen on the boron steel surface at each load along with pitting. The wear mode on Armatech is a more complex mode, three-body in the matrix and two-body in the borides/carbides.

6.3.3 Test reproducibility

Gee *et al.* conducted an inter-laboratory exercise across fourteen organisations to assess the accuracy of wear scar measurements and the repeatability and reproducibility of the MSAW test[106]. Five different types of MSAW test were employed, nine of which were Plint TE66

testers (including Sheffield Hallam University). It was reported that the repeatability of wear rate measurement within laboratories had a standard deviation of 24% and the reproducibility between the fourteen laboratories was 26%. However, these tests were carried out using hard coated samples and the wear rates calculated were for coatings that had been penetrated by the test. This introduces uncertainties that are not present when measuring bulk materials. In this work the test is carried out on a thick coating and the wear scars do not penetrate the coating. In order to assess the test to test reproducibility in this research three tests were performed on Armatech at four applied loads using both abrasives.

The reproducibility of three-body wear modes was investigated by Adachi and Hutchings[78]. MSAW tests performed using various combinations of ball and bulk specimen materials over a range of test conditions showed that wear rates observed with three-body wear were relatively insensitive to test conditions, whereas two-body wear varied much more. They concluded that three-body wear was a more appropriate wear mechanism if reproducible test results were desired.

The results from reproducibility tests using SiC and SiO_2 abrasive for this research are shown below in Figure 104. For the SiC abrasive it can be seen that there is very little variation between the three tests showing good reproducibility. The percentage deviation measured with the SiC test was between 0.2 and 0.4%. However, for SiO_2 the variation was much higher, between 1.2 and 7.1%. The error bars shown are calculated from the error in the gradients of the MLM plots. It can be seen that data on both the SiC and SiO_2 do not pass through the intercept. This systematic error (it is similar for each series of tests in the SiC data) can be interpreted as a positive systematic error in the applied load which could be attributed to the balancing of the load arm. However, its magnitude suggests that another systematic error may also be responsible. Another possibility is a systematic over estimation in the measured wear volume.

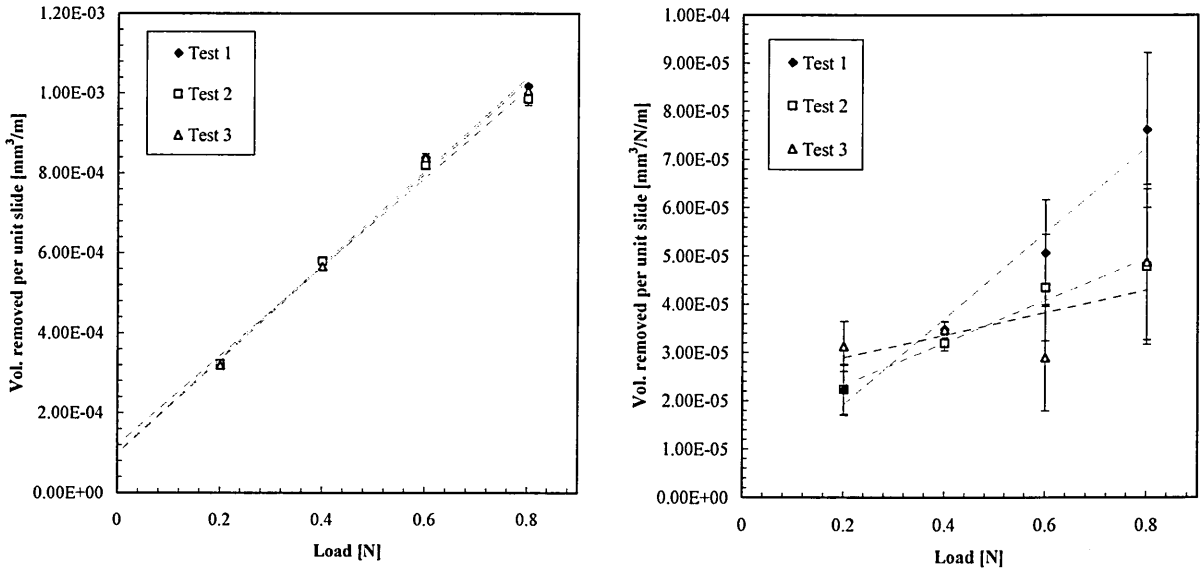

(a) (b)

Figure 104: The volume removed per unit sliding distance as a function of applied load to show test reproducibility. Three tests performed on Armatech using (a) SiC abrasive over a sliding distance of 50 m and (b) SiO_2 abrasive over a sliding distance of 100 m.

The lower reproducibility achieved with SiO_2 is primarily due to the wear scar measurement. The poor definition of the wear scars associated with the reduced aggressiveness (i.e. smaller wear scars) of the abrasive introduces error into measurements. Material microstructure may also play a role, the sample used was Armatech which has been shown to have inhomogeneous areas of residual binder.

By adjusting the data for wear volume for the SiC tests in order to make the linear relationship intercept at the origin it can be seen that the error in wear calculation highlighted by the multiple load method, re-plotted below in Figure 105.

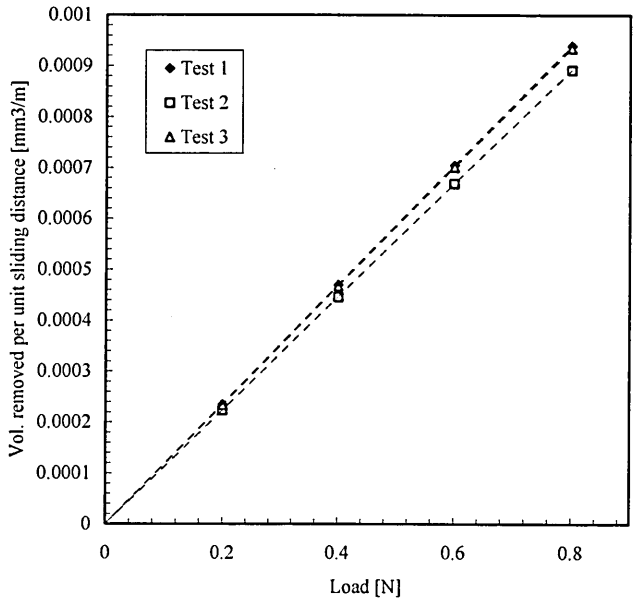

Figure 105: Corrected volume removed per unit sliding distance as a function of applied load to show test reproducibility on Armatech using SiC abrasive over a sliding distance of 50 m.

In the MLM shifting the results along the axis does not affect κ, as the gradient is not changed. However, the amount of volume removed per unit sliding distance is affected through a reduction at each of the four applied loads. If only Test 1 data is considered (Table 18) and the series is adjusted to pass through zero it can be seen that the volume removed reduces by around 27% at a 0.2 N, whereas at 0.8 N only an 8% reduction is seen. This suggests a systematic over-estimation of the wear volume which becomes less significant as the load increases.

Table 18
Corrected values of volume removed per unit sliding distance in order to make the intercept pass through zero.

	0.2 N	0.4 N	0.6 N	0.8 N
Original [mm^3/m]	3.23×10^{-4}	5.73×10^{-4}	8.38×10^{-4}	1.02×10^{-3}
Corrected [mm^3/m]	2.35×10^{-4}	4.70×10^{-4}	7.05×10^{-4}	9.40×10^{-4}
% of original	72.7	82.0	84.1	92.3

This data shows that errors in the MSAW test affect the calculation of wear volumes for the MSAW test, particularly at low applied loads. In a comparative test this would be a constant error which would be applicable to all samples tested and would not pose a serious problem. However, problems would arise if attempting to cross correlate test results with wear data from other literature. The error is most likely equipment related and also possibly user related.

6.4 Final MSAW Test Procedure

It has been shown from the test procedure development that, in order to obtain a reproducible three-body wear regime, a SiC abrasive at a sliding distance of 50 m using applied loads of 0.4 to 0.8 N should be used. At 0.2 N some signs of mixed-mode wear was observed, however, this did not appear to affect the wear volume to any great extent and as such the 0.2N data was included.

The development of the test method also revealed that to achieve a two-body wear mechanism then SiO_2 abrasive at a sliding distance of 100 m over the range 0.2 to 0.8 N applied load provided the best quality wear scars for measurement. All other test parameters such as sliding speed and slurry feed rate were kept constant and are listed in Table 19.

Table 19
Test conditions employed for MSAW testing.

Test parameters	Values
Applied load [N]	0.2 – 0.8
Speed [m/s]	0.13
Ball	25.4mm, SAE51200 bearing steel (shot blast finish) ~900H_V
Sliding distance	50m [SiC] / 100m [SiO_2]
Abrasive media	SiC [7μm], Silica [2.5μm] in deionised H_2O
Concentration	SiC [20vol.%]; SiO_2 [10vol.%]
Slurry feed rate [drops/s]	~3
Temperature/humidity	22-25°C / 35-45% RH
pH level	SiC [~4.8pH]; SiO_2 [~5.25pH];

The ball was used in the as-received shot blast condition. It was thoroughly cleaned to remove traces of debris and grease and a run-in period was carried out using a boron steel sample in several directions at a sliding distance of 50 m using a load of 0.2 N. The ball was rotated between tests to prevent any preferential wearing of the ball, although Allsopp *et al.*[74] suggested that flattening of the wear ball was insignificant.

Each wear scar was examined using SEM to allow crater diameter measurement, to identify the wear mode and to observe the contribution of the secondary hard phase additions to the abrasive wear resistance of the material.

6.5 MSAW Results with SiC abrasive

MSAW tests were performed using 7 μm SiC abrasive over a sliding distance of 50m. The data in Figure 106 shows the variation of κ, calculated for each load, as a function of applied load for a selection of materials. In all cases κ decreased with increasing load. The $WC/W_2C(10)_{[100]}$ material exhibited a slight improvement over the boron steel, Armatech and $WC/W_2C(5)_{[15]}$. The WC-Co material can be seen to show a marked improvement over all other materials.

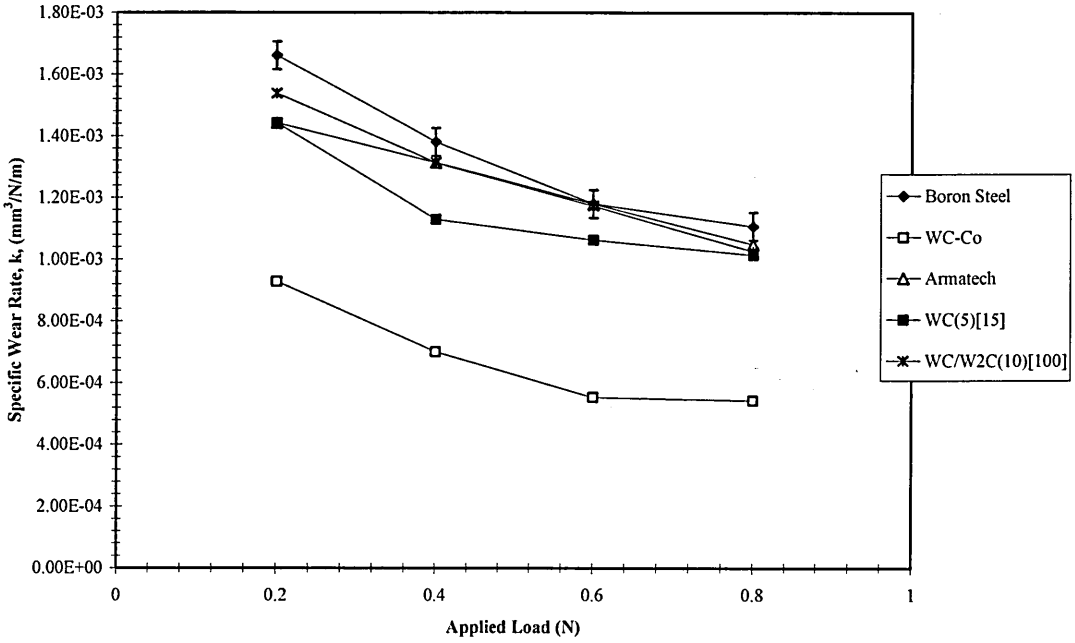

Figure 106: Plot of κ (mm^3/N/m) vs. applied load (N) over a sliding distance of 50 m using SiC abrasive.

Figure 107 shows an alternative method of plotting and calculating κ (the MLM method). Here the volume of material removed per unit sliding distance is plotted against applied load with κ being calculated from the gradient. It is clear that as applied load is increased the amount of material removed also increases linearly with all materials behaving as expected. Each trend shows very similar wear rates (i.e. gradients), except for the WC-Co tile which has lower volume removal and thus a lower gradient.

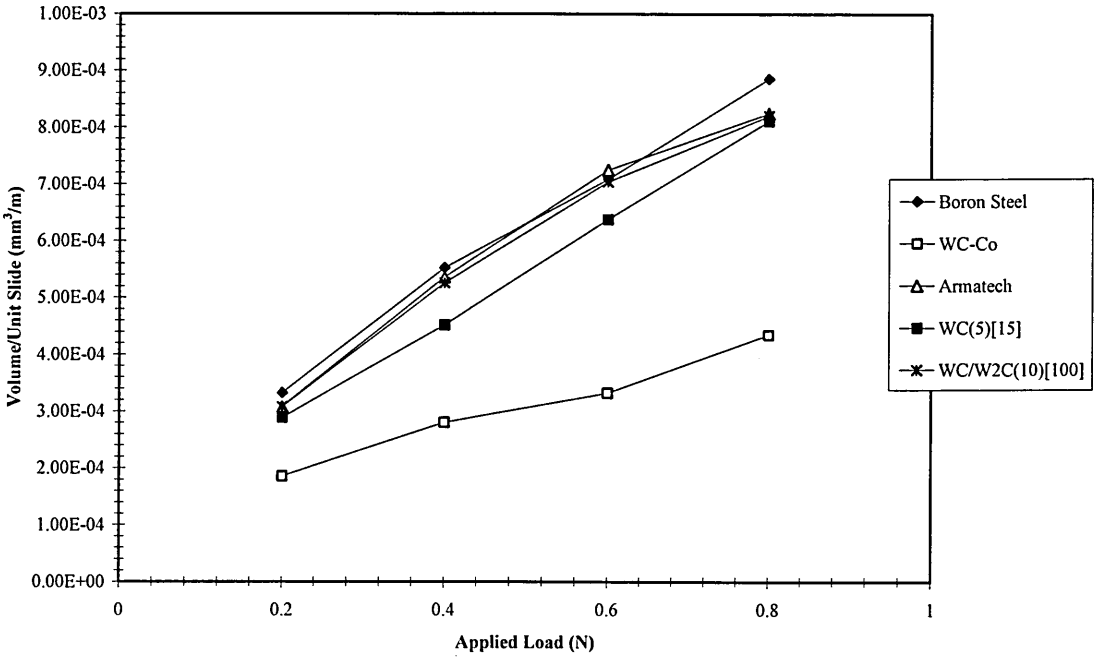

Figure 107: Plot of volume removed per unit sliding distance (mm^3/m) vs. applied load (N) over a sliding distance of 50 m using SiC abrasive.

The κ values calculated using the MLM (gradient of best fit line passing though all data points of volume removed per unit sliding distance versus load) of each material tested are summarised in Table 20 and plotted in ascending order in Figure 108, the errors bars shown are calculated S_E. Also included are the relative wear resistance values measured against boron steel ($RWR_{[Boron]}$) and Armatech ($RWR_{[Armatech]}$), the ratio of volumetric wear of the specific reference material divided by the volumetric wear of a test material.

Table 20
MSAW MLM results using 7 μm SiC abrasive over a sliding distance of 50 m.

	Hardness[H_{V20}]	S_E	κ [mm^3/Nm]	S_E	$RWR_{[Boron]}$ ‡‡‡‡	$RWR_{[Armatech]}$ §§§§
Boron	477	1	9.08×10^{-4}	4.51×10^{-5}	**1.00**	**1.01**
Armatech	485	48	9.16×10^{-4}	8.45×10^{-5}	**0.99**	**1.00**
$TiC(5)_{[75]}$	176	23	1.15×10^{-3}	1.10×10^{-4}	**0.79**	**0.80**
$TiC(10)_{[75]}$	204	53	1.68×10^{-3}	9.96×10^{-5}	**0.54**	**0.54**
$Mo_2C(5)_{[45]}$	316	23	1.00×10^{-3}	5.98×10^{-5}	**0.90**	**0.91**
$Mo_2C(10)_{[45]}$	257	20	1.23×10^{-3}	2.81×10^{-5}	**0.74**	**0.74**
$Al_2O_3(3)_{[50]}$	579	17	1.05×10^{-3}	9.76×10^{-5}	**0.87**	**0.87**
$Al_2O_3(6)_{[50]}$	406	24	1.03×10^{-3}	1.43×10^{-4}	**0.88**	**0.89**
$WC(5)_{[15]}$	583	25	8.77×10^{-4}	1.48×10^{-5}	**1.04**	**1.04**
$WC(8)_{[15]}$	340	25	9.56×10^{-4}	7.79×10^{-5}	**0.95**	**0.96**
$WC(10)_{[15]}$	240	12	1.23×10^{-3}	9.26×10^{-5}	**0.74**	**0.74**
$WC(15)_{[15]}$	203	24	1.29×10^{-3}	9.26×10^{-5}	**0.71**	**0.71**
$WC(20)_{[15]}$	256	12	1.25×10^{-3}	9.07×10^{-5}	**0.73**	**0.74**
$WC/W_2C(5)_{[100]}$	648	9	1.09×10^{-3}	2.52×10^{-5}	**0.83**	**0.84**
$WC/W_2C(8)_{[100]}$	635	2	9.55×10^{-4}	2.83×10^{-5}	**0.95**	**0.96**
$WC/W_2C(10)_{[100]}$	634	11	8.58×10^{-4}	8.11×10^{-5}	**1.06**	**1.07**
$WC/W_2C(12)_{[100]}$	589	12	9.80×10^{-4}	5.84×10^{-5}	**0.93**	**0.94**
$WC/W_2C(15)_{[100]}$	552	16	1.29×10^{-3}	7.29×10^{-5}	**0.70**	**0.71**
$WC/W_2C(20)_{[100]}$	416	29	1.34×10^{-3}	1.37×10^{-4}	**0.68**	**0.68**
$WC/W_2C(50)_{[100]}$	266	6	1.67×10^{-3}	2.32×10^{-4}	**0.54**	**0.55**
$WC/W_2C(70)_{[100]}$	130	8	1.32×10^{-3}	2.62×10^{-4}	**0.69**	**0.69**
WC-Co	1038	5	3.99×10^{-4}	3.34×10^{-5}	**2.27**	**2.29**

‡‡‡‡ $RWR_{[Boron]}$: Relative wear rate as boron steel for reference material.

§§§§ $RWR_{[Armatech]}$: Relative wear rate as Armatech for reference material.

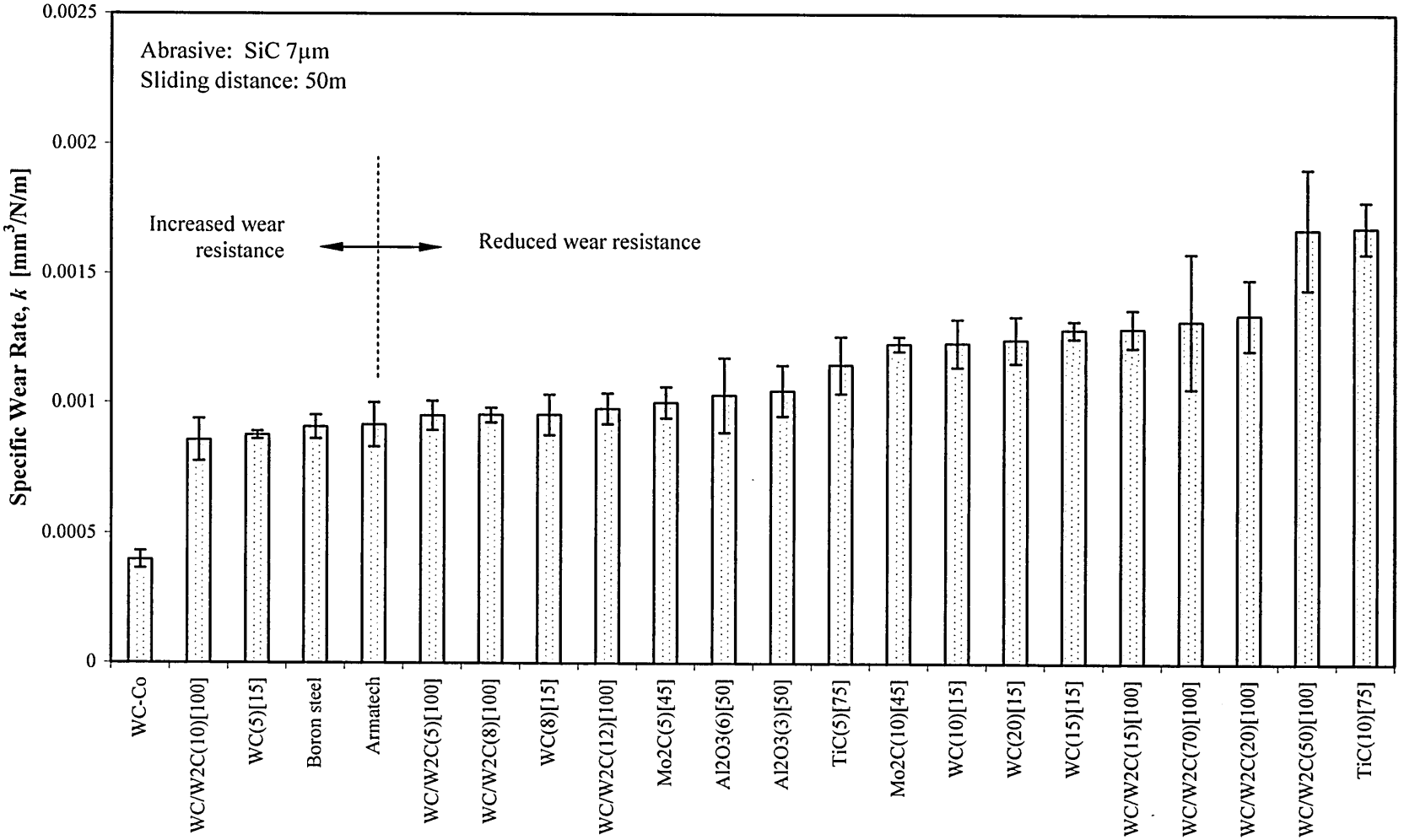

Figure 108: Specific wear rate determined by the MLM method using 7μm SiC abrasive over a sliding distance of 50 m in ascending order.

Under these test conditions Armatech did not show any significant improvement in wear resistance over boron steel, (Figure 109). The RWR values given in Table 20 show the Armatech to have the same performance as boron steel (when errors are considered). This result proves somewhat surprising as Armatech coated tools have repeatedly been shown to outlast uncoated boron steel tools (see Chapter 1) in field service and are currently mass produced for this very reason.

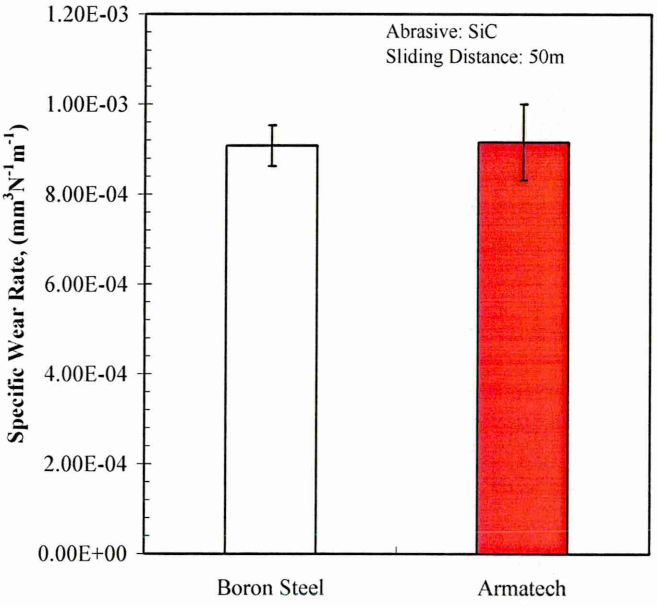

Figure 109: Specific wear rate calculated by the MSAW MLM method of boron steel and Armatech using 7 μm SiC abrasive at a sliding distance of 50 m.

The κ value of the low level addition of 15 μm WC (5wt.%) revealed a slight improvement over Armatech with an $RWR_{[Armatech]}$ of 1.07, the largest improvement of all the modified coatings, however when considering errors there is no significant difference. Further increases in the level of addition reduced κ when compared to Armatech and boron steel.

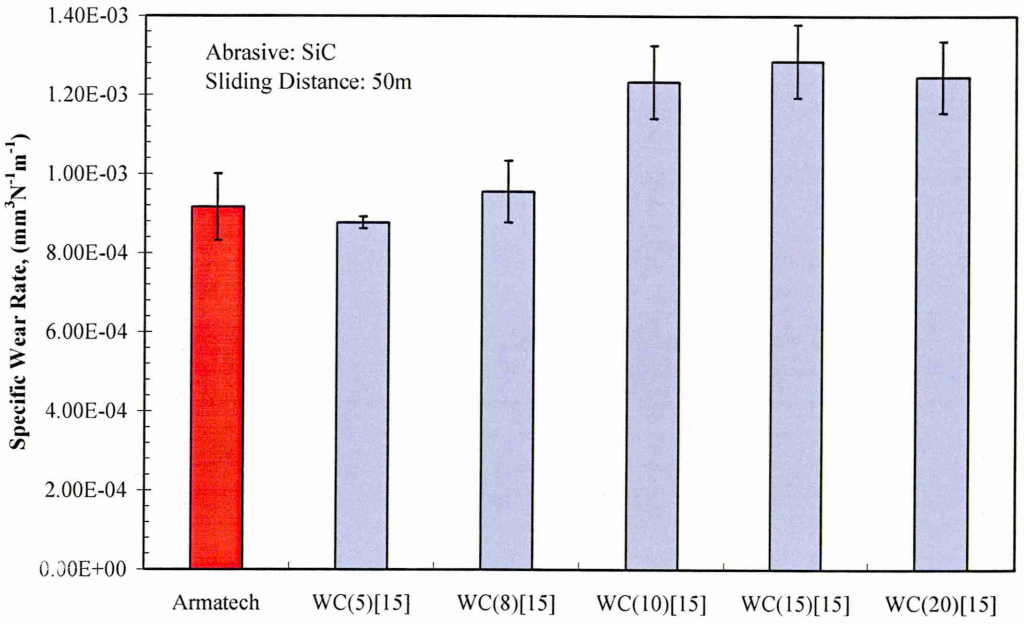

Figure 110: Specific wear rate calculated by the MSAW MLM method for Armatech and the 15μm WC modified Armatech materials (using 7 μm SiC abrasive at a sliding distance of 50 m).

The materials with additions of 100 μm WC/W_2C yielded no significant improvement in κ. All other levels of addition provided no increase, with loadings of 15wt.% and above yielding large increases in κ.

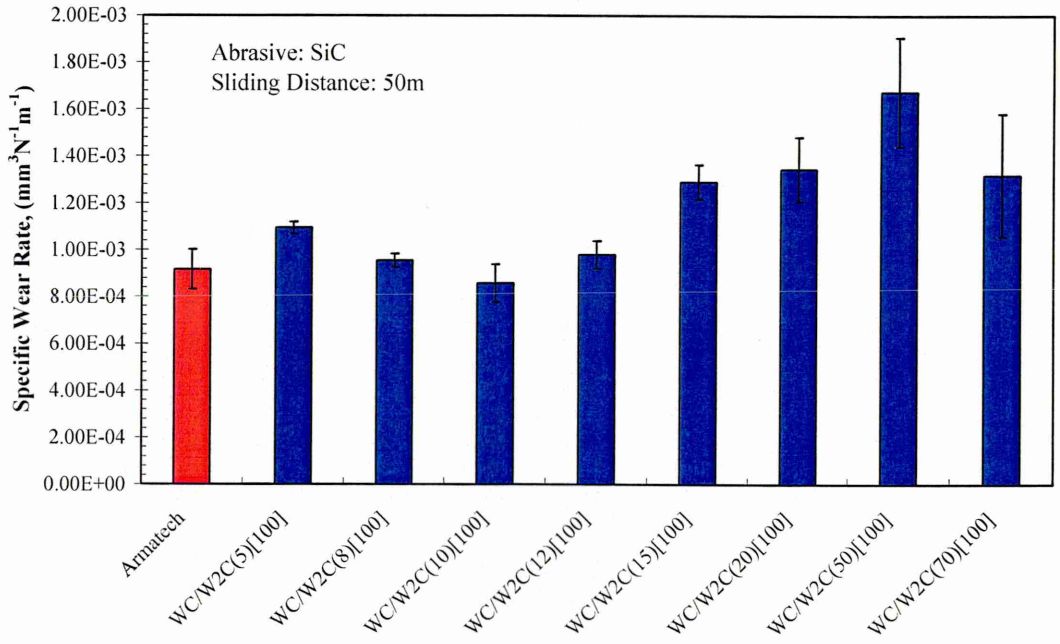

Figure 111: Specific wear rate, κ, calculated by the MSAW MLM method of Armatech and 100 μm WC/W_2C modified Armatech using 7 μm SiC abrasive at a sliding distance of 50 m.

No improvements in κ were observed under these test conditions with additions of Al_2O_3, Mo_2C and TiC as a secondary hard phase as shown in Figure 112.

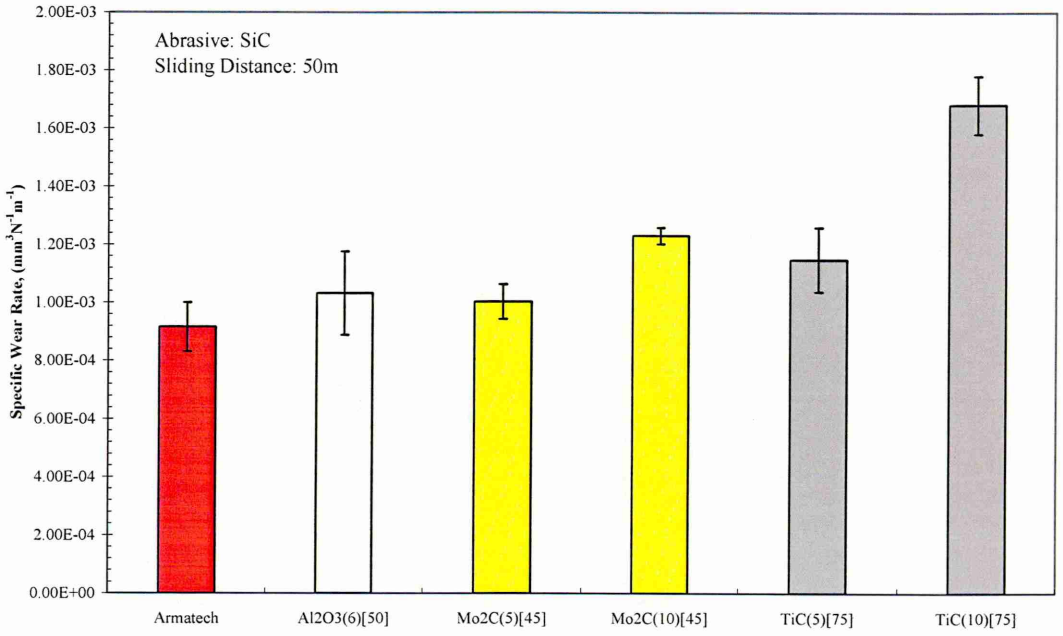

Figure 112: Specific wear rate calculated by the MSAW MLM method of Armatech and the Al_2O_3, Mo_2C and TiC modified Armatech materials (using 7 µm SiC abrasive at a sliding distance of 50 m).

The wear rate of the WC-Co was much lower than the boron steel and Armatech as was expected, with $RWR_{[Armatech]}$ values of 2.29.

6.5.1 Wear vs. bulk hardness

A commonly used approach when analysing wear results is to compare them with hardness values. Figure 113 shows volume loss per unit sliding distance (mm^3/m) plotted for each applied load as a function of Vickers hardness (H_{V20}). It can be seen that a weak correlation exists between the volume of material removed in each wear scar and the bulk hardness of the material. The correlation is stronger for the lower loads.

However, as noted previously, the hardness of an inhomogeneous material measured with high loads (e.g. 20 kg) is not necessarily representative of the behaviour of a material under tribological conditions, especially when the abrasive which is responsible for the wear is many orders of magnitude smaller than the indenter.

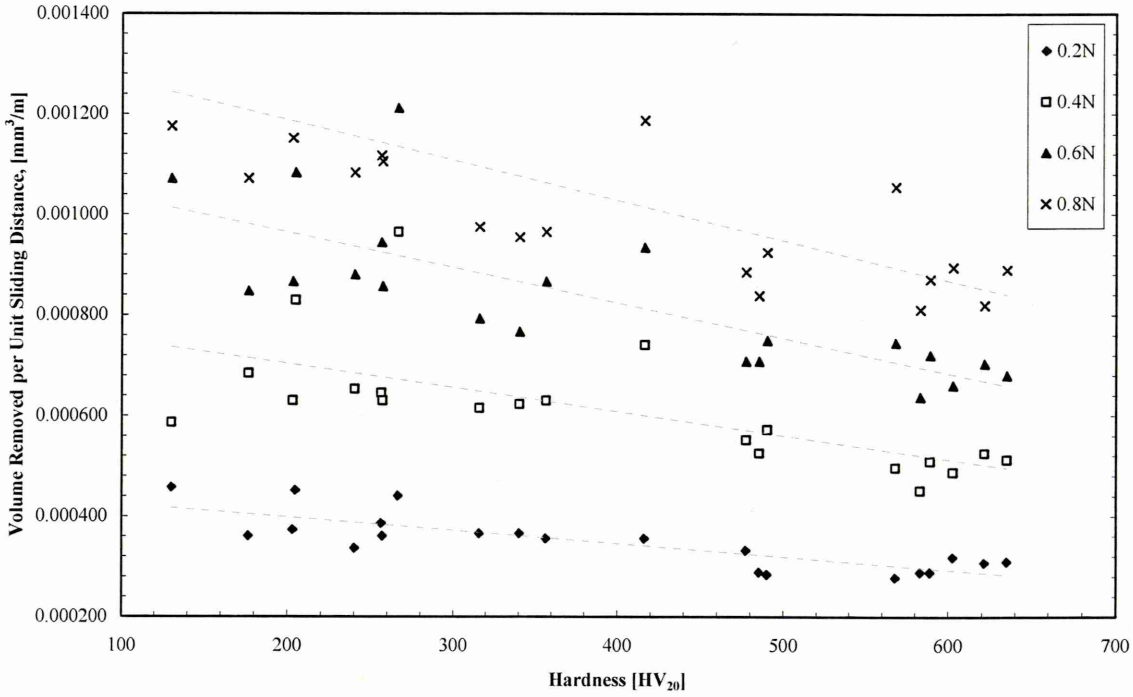

Figure 113: Volume removed per unit sliding distance versus bulk hardness (H_{V20}) for MSAW using SiC abrasive over 50 m sliding distance.

6.5.2 SEM observation of wear surface morphology (SiC)

Each wear scar produced was examined using SEM to observe wear mode and material characteristics. Each micrograph shown corresponds to the central zone of the wear scar and presents the wear direction from top to bottom of the image (demonstrated by the arrow in Figure 114).

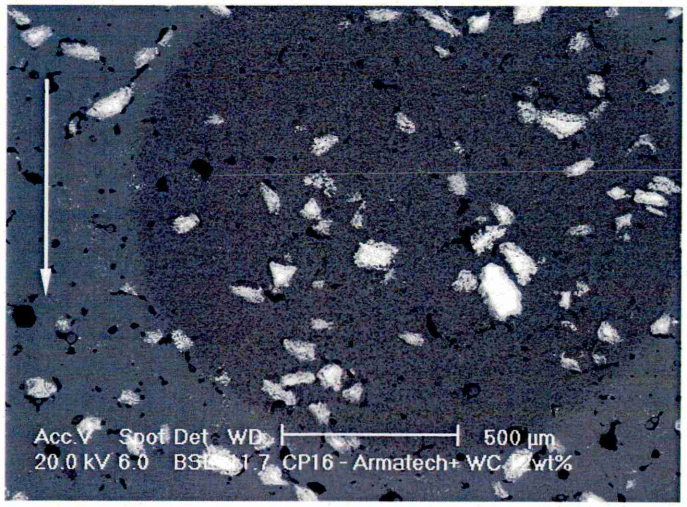

Figure 114: Typical MSAW scar using SiC abrasive and 0.8 N load on $WC/W_2C(12)_{[100]}$.

The micrographs in Figure 115 show the wear surfaces of boron steel abraded using SiC particles at applied loads of (a) 0.2 and (b) 0.8 N. The wear mode observed at each of the four applied loads was three-body rolling wear, a series of multiple, sharp indents with no directionality caused by the hard angular abrasive rolling between the sample and ball interface.

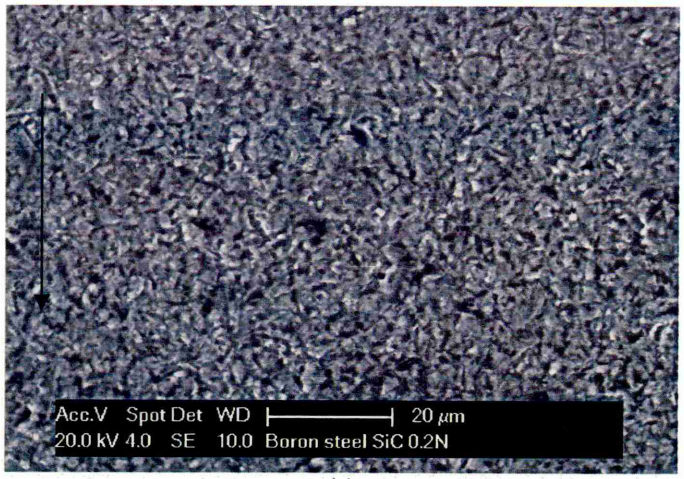

(a)

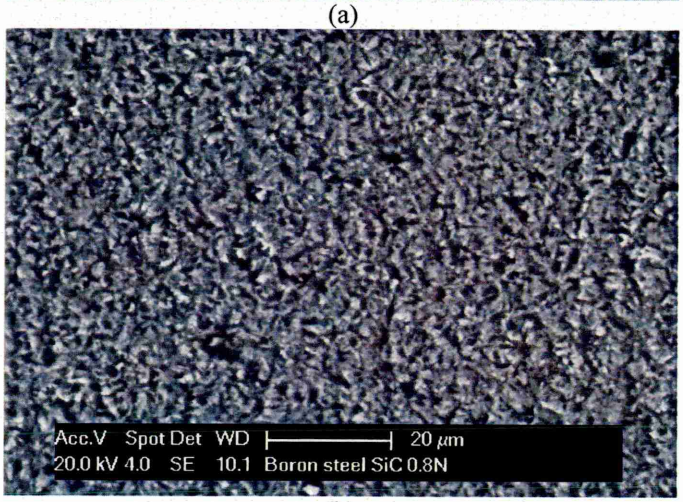

(b)

Figure 115: SEM images of MSAW test scars on boron steel using SiC abrasive over 50 m sliding distance; (a) three-body wear at an applied load of 0.2 N and (b) three-body wear at an applied load of 0.8N.

The wear scars on boron steel revealed evidence of micro-pitting. The pits were ~15 μm in diameter and concentrated within the crater bottom with a small number observed around the crater edge, see Figure 116. Pitting was also observed on boron steel tools removed from service (examined in Chapter 4).

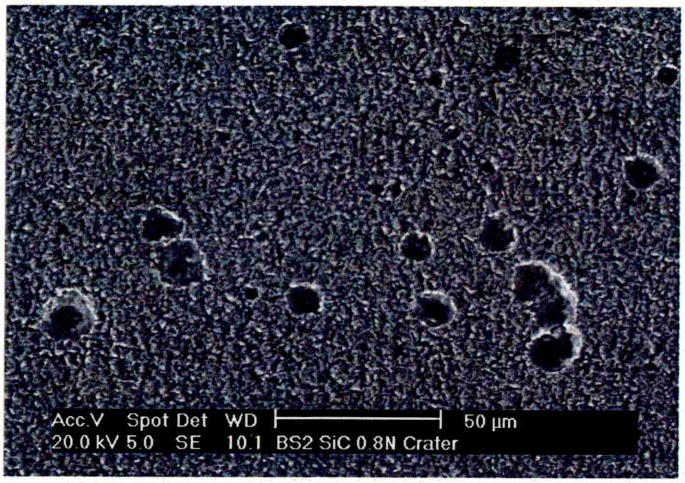

Figure 116: SEM images of MSAW test scars on boron steel using SiC abrasive showing micro pitting.

Micrographs of the Armatech surface subjected to wear using SiC are shown in Figure 117. It can be seen that under a load of 0.2 N a mixed mode of wear is responsible for material removal. Directional two-body grooving with plastic deformation creating fin edges, can be seen in conjunction with intermittent indentations caused by a three-body mechanism. Increasing the load to 0.4 N, shown in Figure 117(b), creates a uniform three-body mechanism with no signs of directional two-body grooving. This was also evident at loads of 0.6 and 0.8 N.

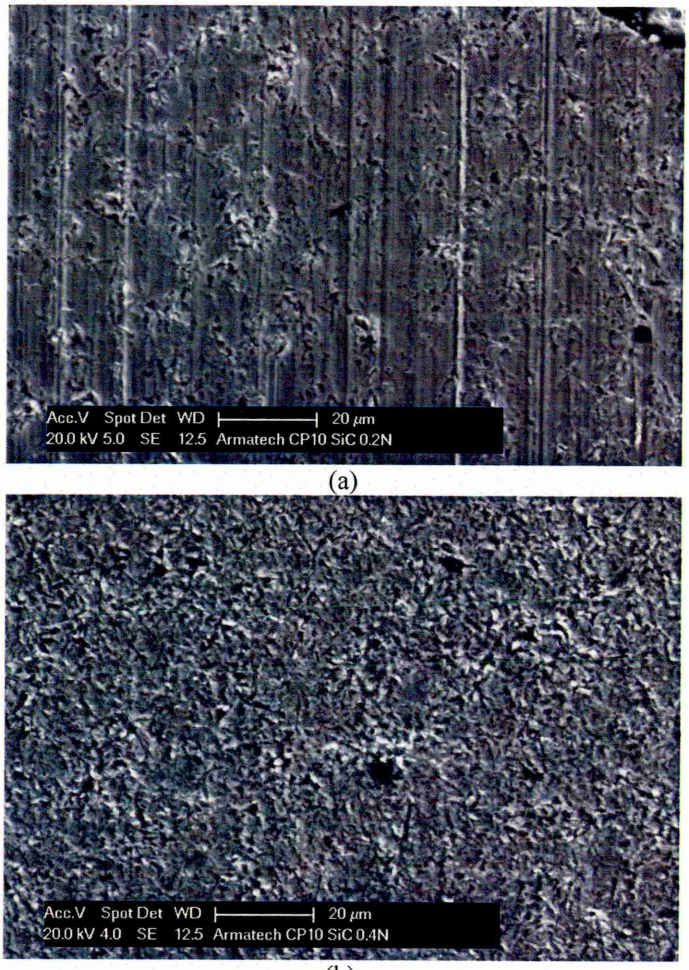

Figure 117: SEM images of Armatech MSAW scars using SiC abrasive over a 50 m sliding distance; (a) shows mixed mode wear at 0.2 N applied load and (b) shows three-body wear at 0.4 N applied load.

Due to the topographical nature of three-body wear and the severity of plastic deformation, it was difficult to determine the role of each phase within the Armatech microstructure in resisting against wear. However, inspection of areas near to crater edges (shown by the dashed line in Figure 118(a) using BSE detection to reveal elemental contrast) revealed that the indentations and hence material removal were primarily within the softer Fe-Ni matrix (Figure 118(b)) while the hard Fe-Ni-Cr borides/carbides appeared more resistant to the rolling abrasive.

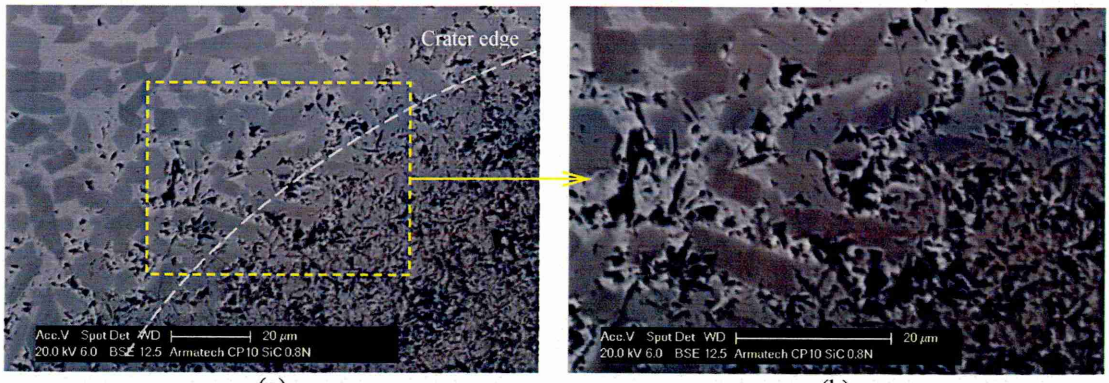

(a) (b)

Figure 118: SEM micrographs of Armatech MSAW scar edge under abrasion from SiC abrasive; (a) shows the crater edge at a load of 0.8 N and (b) high magnification showing wear resistant carbides.

Due to the level of deformation caused by the multiple indentations, it is difficult to ascertain whether the removal of the matrix material causes pullout of the boride/carbide phase or whether they remain in situ and wear by abrasion.

The micrographs in Figure 119 show the wear surface of the 15 μm WC addition at 5wt.% ($WC(5)_{[15]}$). The dominant wear mode is three-body rolling in both the Armatech matrix and WC hard phase addition. The WC did not appear to provide any significant improvement in wear resistance over the surrounding material under these test conditions. A large amount of WC phase pullout occurred at each test load as shown in Figure 119(a). The presence of extensive pullout perhaps explains why this material yielded no real improvements in wear resistance over both Armatech and boron steel.

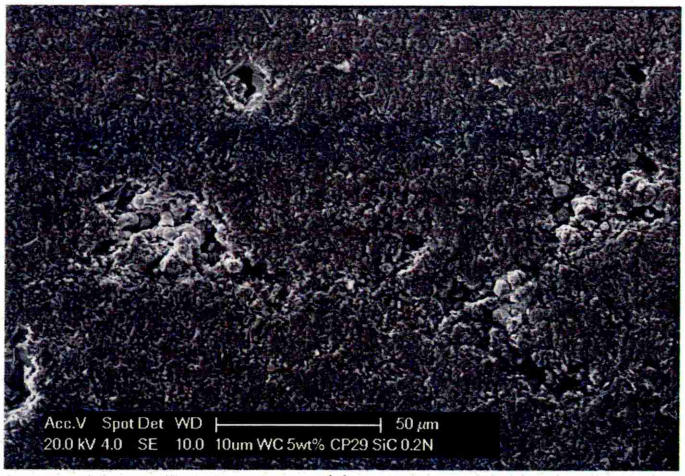

(a)

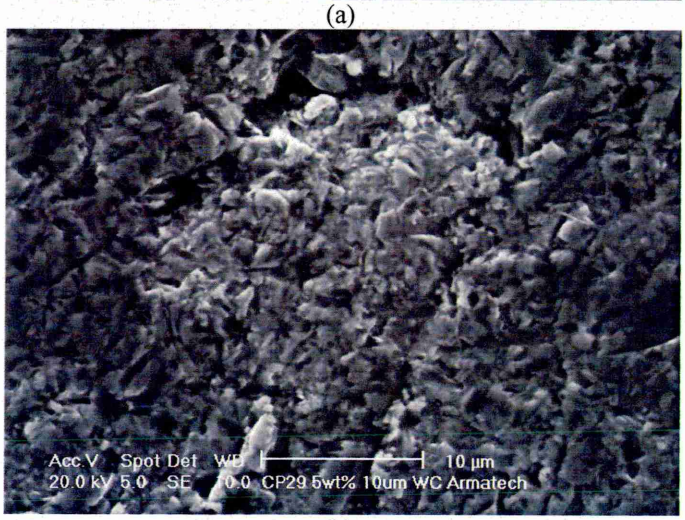

(b)

Figure 119: SEM images of MSAW test scars using SiC abrasive; (a) wear surface and (b) shows the wear of a WC carbide in $WC(5wt.\%)_{[15]}$.

The micrographs below in Figure 120 show wear regimes produced using an applied load of 0.8 N on $WC/W_2C(5)_{[100]}$ materials. It can be seen that both the Armatech and WC particles suffered wear by three-body rolling conditions. The higher magnification image in Figure 120(b) shows the three-body wear mode of the WC particles more clearly; specifically the carbide appears to be more resistant to the wear and appears to be protruding from the surrounding matrix.

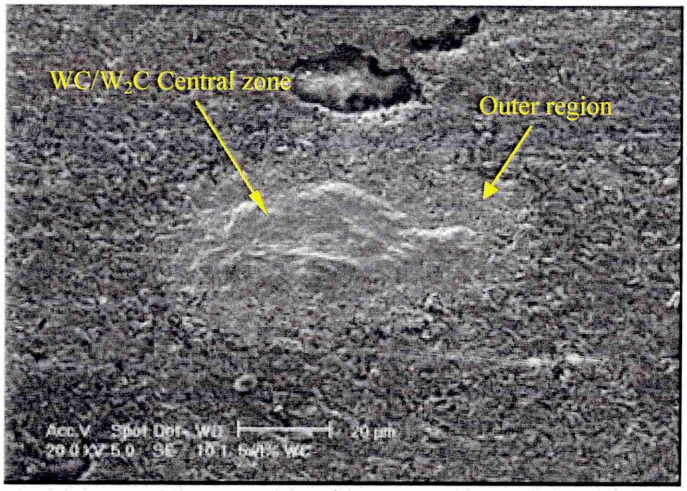

(a)

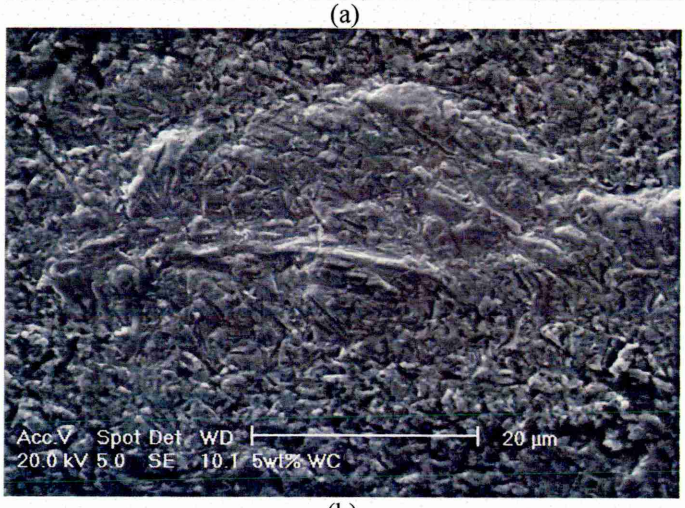

(b)

Figure 120: SEM images of MSAW test scars using SiC abrasive and 0.2N applied load on $WC/W_2C(5)_{[100]}$.

Micrographs of the 100 µm WC/W_2C at a much higher loading of 50wt.% are shown in Figure 121. At an applied of load of 0.2 N, a mixed mode of wear was present as shown in Figure 121(a) and (b), where both two-body grooving and three-body rolling indentations were observed. When increasing the load to 0.4 N a single wear mode of three-body rolling became dominant and there was no evidence of two-body grooving. Examination of the WC particles revealed that the core appeared to be suffering brittle fracture as shown in Figure 120(d). The fracture of the WC core may cause increased wear rates for two reasons; firstly, the fractured particles may act as a second abrasive and secondly the volume of material removed from the surface is increased.

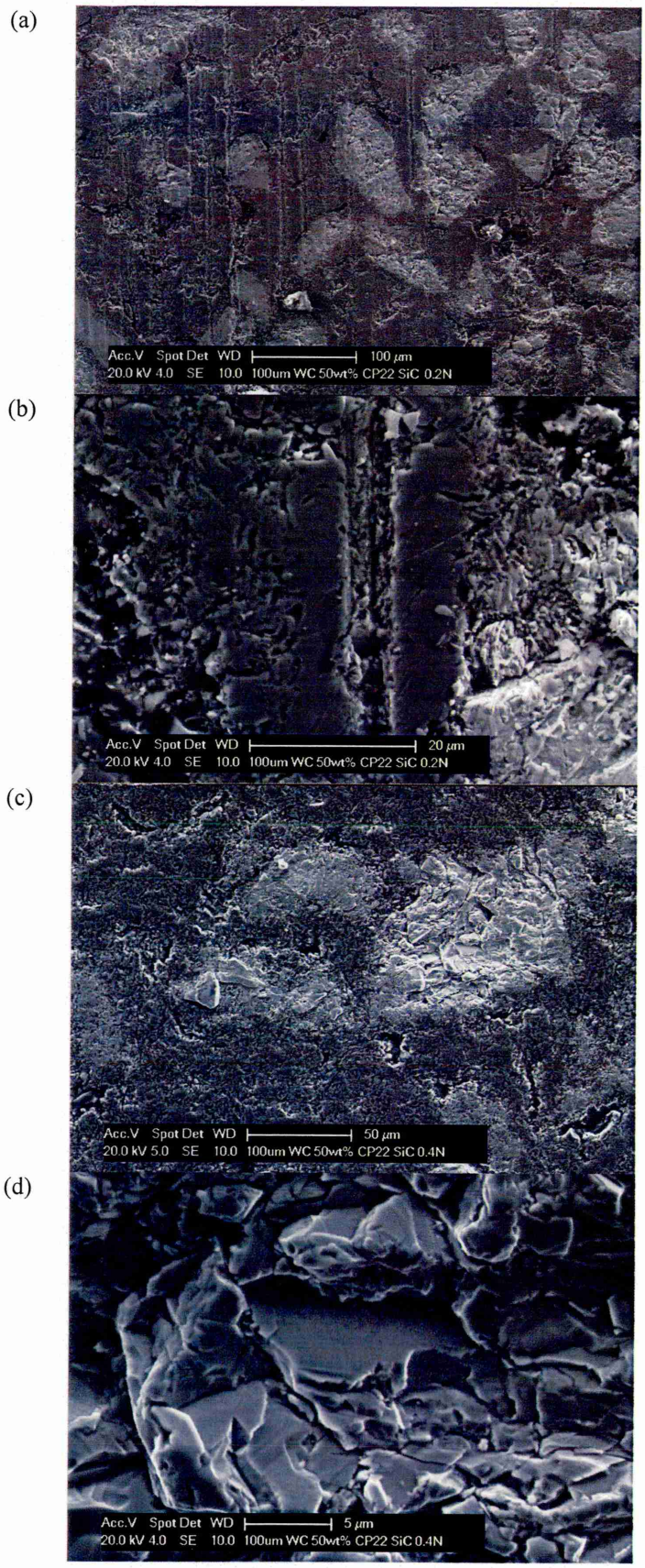

Figure 121: SEM micrographs of $WC/W_2C(50)_{[100]}$ MSAW scars using SiC abrasive over a 50 m sliding distance; (a) shows mixed mode wear at 0.2 N applied load, (b) shows three-body wear and a two-body groove 0.2 N applied load, (c) shows 'fallout' of WC core region and (d) shows high magnification of brittle fracture of WC core region.

SEM micrographs of wear surfaces of Armatech modified by the addition of 50 μm Al_2O_3 addition are shown below in Figure 122. It was evident from both the Armatech matrix and the Al_2O_3 additions (those that had not been removed from by wear), that the wear mode was three-body rolling wear. The material suffered a high degree of pullout of the Al_2O_3. Some Al_2O_3 particles which had not been pulled out exhibited evidence of three-body indentations.

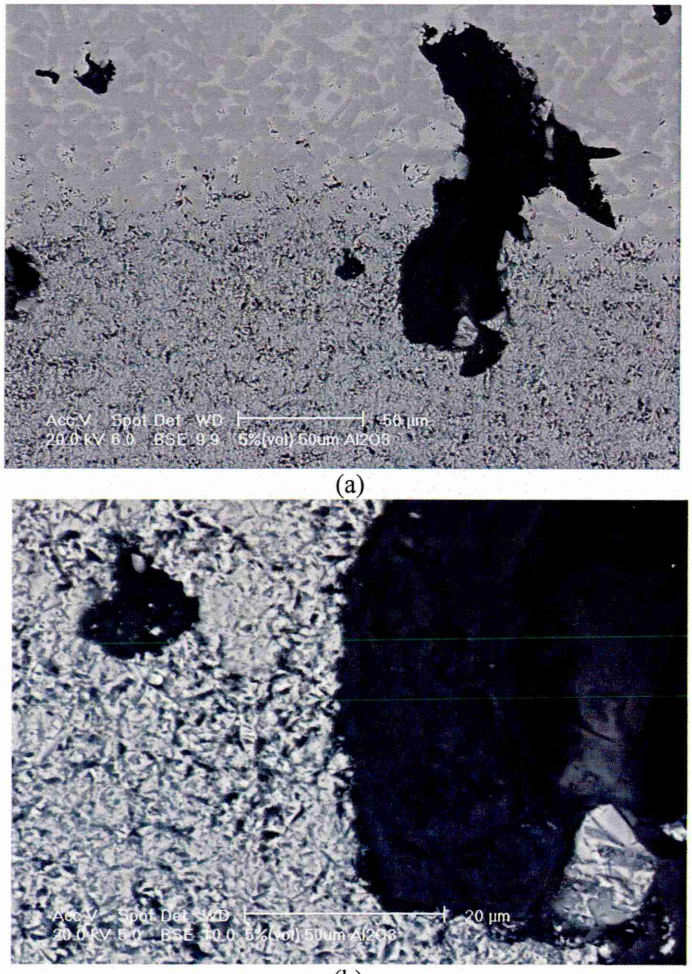

Figure 122: SEM images of MSAW test scars of $Al_2O_3(3)_{[50]}$ using SiC abrasive; (a) crater edge and (b) shows multiple indentations in matrix and Al_2O_3 particle.

The addition of Mo_2C to the Armatech coating created a well dispersed phase throughout the matrix material, discussed in Chapter 5. The carbides had a sponge like appearance and appeared to be agglomerations of nano-scale powders. The wear results from the SiC abrasive test however showed no improvement in wear resistance. Examination of the wear scar revealed a three-body rolling wear mechanism, Figure 123.

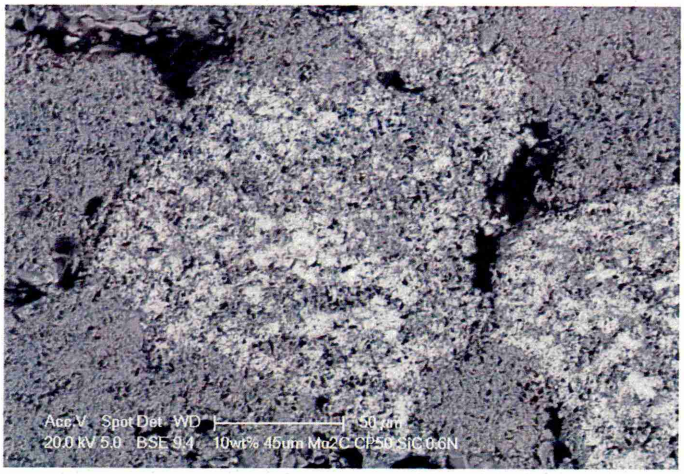

Figure 123: SEM micrograph of 10wt.% 45 μm Mo_2C addition material wear surface using SiC abrasive exhibiting three-body rolling wear mechanism.

The wear mechanism observed in wear scars created with SiC abrasive on the TiC addition materials, again showed a predominant three-body rolling wear. However, the fact that the addition had not bonded with the matrix material meant that the TiC was not improving the wear resistance, Figure 124. The TiC particles had fractured in a brittle manner and pullout had occurred. The high hardness of TiC, 3200 H_V, is much higher than that of SiC so in theory TiC should provide good wear resistance. But due to the inability to bond with the Armatech coating, no support was provided to the hard phase and much of it was removed after suffering brittle fracture.

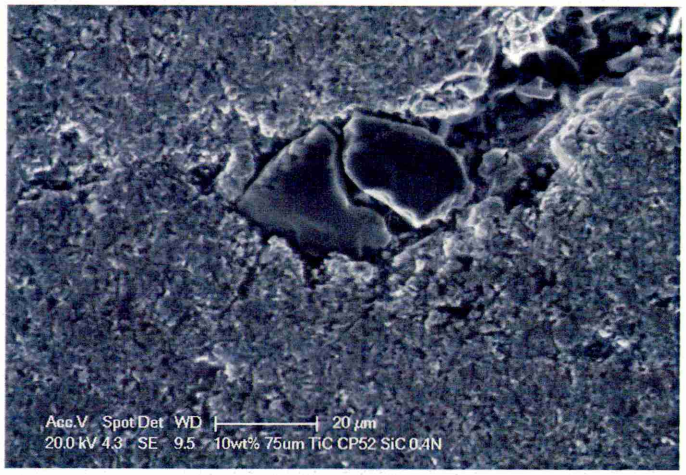

Figure 124: SEM micrograph of MSAW test scar on 10wt.% 75 μm TiC produced using SiC abrasive at a load of 0.4 N over a sliding distance of 50 m. A TiC particle is visible which has not bonded with the matrix material and has suffered brittle fracture in the process of wear.

SEM examination of the WC-Co tile showed that the mechanism of material removal was that of three-body indentations preferentially removing the cobalt binder phase around the carbide particles, Figure 125, a similar mechanism of material removal to that seen with Armatech. This mode of wear would then probably lead to carbide pullout as opposed to direct wear of the

particles. However the rounded appearance of the carbides suggests that some of the in-situ carbides were resisting wear by the abrasive particles.

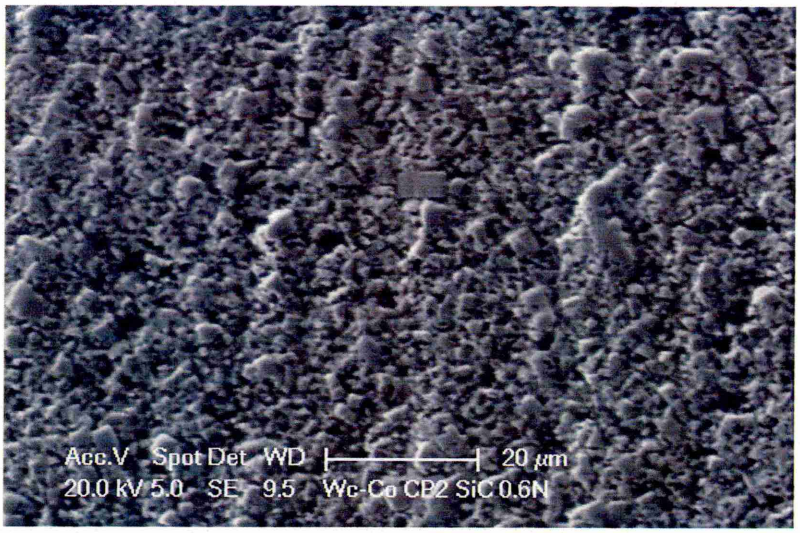

Figure 125: SEM micrograph of MSAW scar on WC-Co tile subjected to wear with SiC abrasive under a load of 0.6 N. The Co binder can be seen to be suffering material loss with the carbides standing proud of the surface.

6.5.3 Summary of MSAW with SiC

SiC abrasive particles are very aggressive in nature and possess an angular morphology and a very high hardness. This type of abrasive is used throughout industry and academia as a standard test abrasive for the MSAW test and as such it was deemed important to carry out a series of tests using this standard abrasive.

Using SiC abrasive under the conditions listed resulted in good reproducibility in results and the aggressiveness of the abrasive provided a well defined crater, reducing any errors associated with measurement of wear scar diameters. However, the properties of the abrasive affects the severity of wear, which may be determined by the H_a/H_m ratio, discussed later in *6.6.2*.

The H_a/H_m ratios of all the materials with respect to SiC are shown in Table 22 in section *6.6.2*. It can be seen that each ratio is >2.0 for each material except for the additions of 100 µm WC/W_2C additions at 50 and 70wt.%. All material/abrasive combinations however would be considered as experiencing very severe wear.

If only the results from the testing using SiC are considered it appears that no real improvements in wear resistance were achieved compared to Armatech or boron steel. Its also appears that Armatech shows no great improvement over boron steel. However, in-service experience suggests that Armatech does have a significant advantage over boron steel.

The results using SiC are still useful in being able to compare the performance of these materials with others tested by other laboratories using similar tests.

As previously discussed, replicating soil wear is very difficult to achieve in a laboratory test and prospective coatings should not be assessed simply on the basis of one laboratory test using one abrasive type. It was also apparent from wear scar examination that the regime produced was not predominant two-body sliding wear as is commonly found in ground engaging tools but three-body rolling wear.

6.6 MSAW results with SiO_2 Abrasive

The use of SiO_2 as an abrasive to assess wear resistance of soil working tools is an attempt to reproduce one aspect of field working conditions. SiO_2 is chemically typical of the main constituent of common soils and possesses a relatively high hardness (1050 H_V).

Figure 126 shows the variation of κ as a function of applied load for a selection of materials tested using 2.5 μm SiO_2 abrasive over a sliding distance of 100 m. With the exception of boron steel; κ **decreases** with an increase in applied load.

The wear resistance of the WC-Co tile could not be measured under these test conditions, the material yielded poor quality wear scars (small and with ill-defined edges) and accurate measurement was not possible.

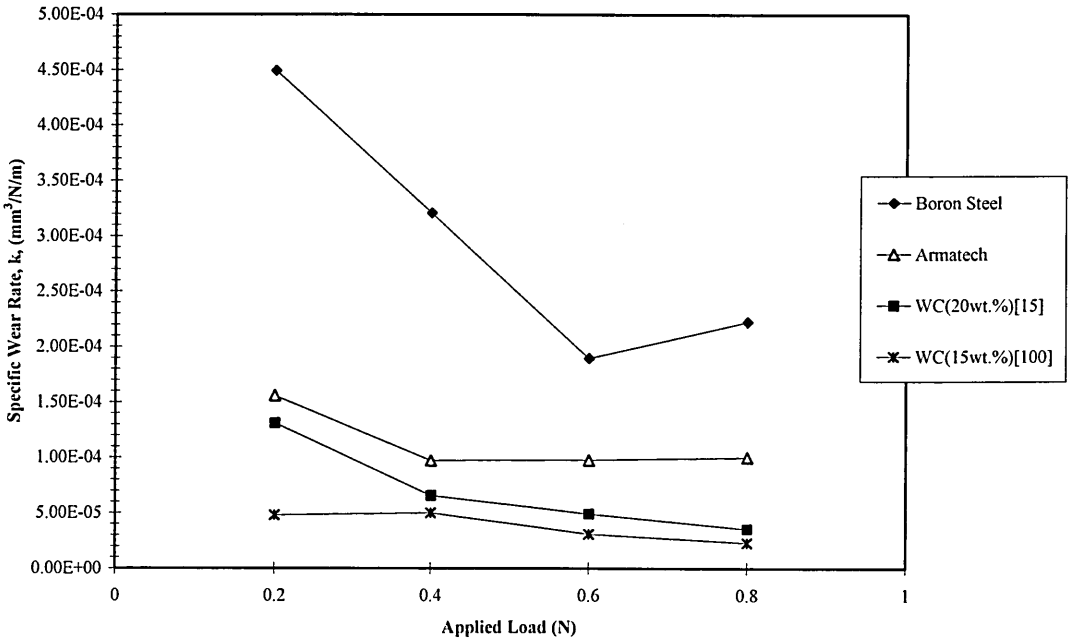

Figure 126: Plot of κ (mm^3/N/m) vs. applied load (N) over a sliding distance of 100 m using SiO_2 abrasive.

The data in Figure 127 revealed that the volume removed per unit sliding distance **increased** as a function of load for the both the boron steel and Armatech material. However, the load appears to have little or no measurable effect on the volume of material removed for the Armatech with 15 μm WC and 100 μm WC/W_2C added as a secondary phase. The wear scars

made on the $WC(20)_{[15]}$ material, whilst appearing round, were all similar in size which yielded a very low gradient under MLM conditions that was not representative. In these circumstances, where there was no gradient that could be accurately measured in MLM plot the wear resistance was calculated from the 0.6 N load measurements.

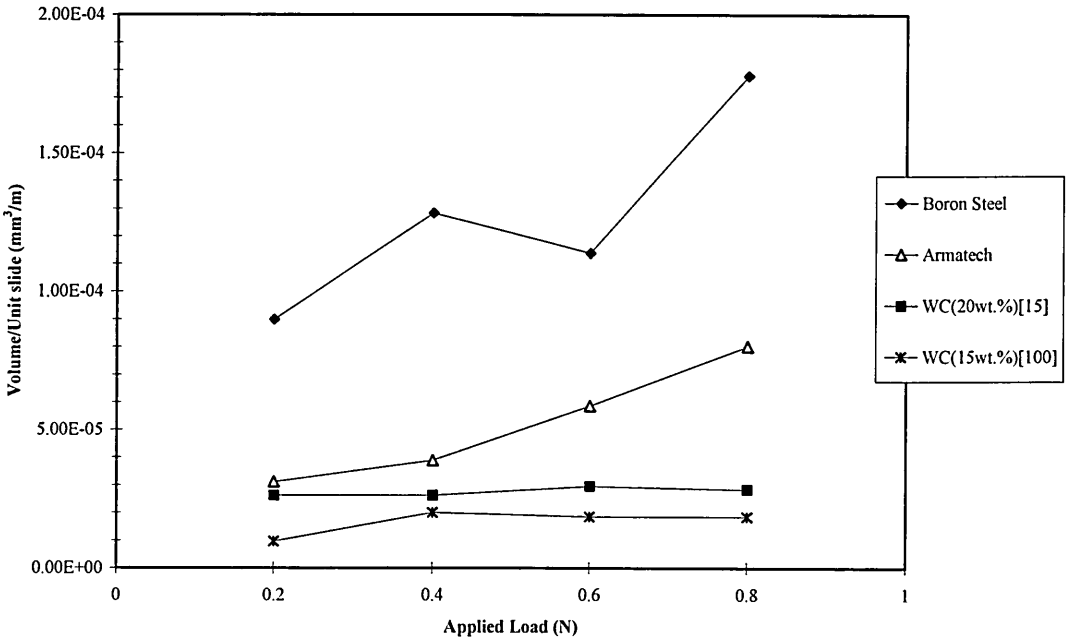

Figure 127: Plot of volume removed per unit sliding distance (mm^3/m) vs. applied load (N) over a sliding distance of 100 m using SiO_2 abrasive.

The results of all the materials tested using SiO_2 are summarised in Table 21 and presented in Figure 128 in ascending order. The data shows κ calculated using the MLM method and the errors bars are the S_E.

It is clear from the results that when comparing the SiO_2 abrasive with SiC that κ is reduced overall by a factor of approximately ten. It was also clear that the error bars associated with the SiO_2 abrasive, as a percentage of the wear rate, were much larger. This is most likely due to factors concerning the geometry of the wear scar; the less aggressive nature of the SiO_2 abrasive and hence reduced wear rate produced a much smaller wear crater which inherently increases error associated with crater measurement. Secondly the nature of the wear mode generated by the abrasive (predominantly two-body) does not produce a crater edge as clearly definable as the more aggressive three-body wear regime from SiC abrasive. Another factor concerns scars that contained areas of residual binder phase. The wear scars are much smaller using SiO_2 but the residual binder is the same size and as such can make up a larger proportion of the worn volume. Higher binder content would effectively increase the wear by reducing the wear resistance of that area. Examination of all wear scars was carried out using SEM to observe the level of residual binder within each wear scar. However, this can only provide information as to whether residual binder was present in the crater bottom and it is impossible to determine

whether a wear scar was affected by any residual binder in the volume of material removed during the test.

Table 21
MSAW MLM results using 2.5 μm SiO_2 over a sliding distance of 100 m.

	Hardness [H_{V20}]	S_E	κ [mm^3/Nm]	S_E	$RWR_{[Boron]}$	$RWR_{[Armatech]}$
Boron	477	1	1.25×10^{-4}	5.08×10^{-5}	**1.00**	**0.38**
Armatech	485	48	4.76×10^{-5}	6.23×10^{-6}	**2.62**	**1.00**
$TiC(5)_{[75]}$	176	23	6.82×10^{-5}	8.02×10^{-6}	**1.83**	**0.70**
$TiC(10)_{[75]}$	204	53	6.37×10^{-5}	1.88×10^{-5}	**1.96**	**0.75**
$Mo_2C(5)_{[45]}$	316	23	4.67×10^{-5}	1.78×10^{-5}	**2.67**	**1.02**
$Mo_2C(10)_{[45]}$	257	20	6.21×10^{-5}	1.02×10^{-5}	**2.01**	**0.77**
$Al_2O_3(3)_{[10]}$	490	43	2.20×10^{-5}	1.16×10^{-5}	**5.69**	**2.17**
$Al_2O_3(3)_{[50]}$	579	17	4.93×10^{-5}	1.01×10^{-5}	**2.53**	**0.97**
$WC(5)_{[15]}$	583	25	4.70×10^{-5}	2.68×10^{-5}	**2.66**	**1.01**
$WC(8)_{[15]}$	340	25	2.93×10^{-5}	6.53×10^{-6}	**4.26**	**1.63**
$WC(10)_{[15]}$	240	12	2.44×10^{-5}	5.39×10^{-6}	**5.12**	**1.95**
$WC(15)_{[15]}$	203	24	1.23×10^{-5}	8.17×10^{-6}	**10.17**	**3.88**
$WC(20)_{[15]}$ *****	256	12	4.92×10^{-5}	2.84×10^{-6}	**2.54**	**0.97**
$WC/W_2C(5)_{[100]}$	648	9	7.64×10^{-5}	1.04×10^{-5}	**1.63**	**0.62**
$WC/W_2C(8)_{[100]}$	635	2	6.94×10^{-5}	1.83×10^{-5}	**1.80**	**0.69**
$WC/W_2C(10)_{[100]}$	634	11	6.58×10^{-5}	2.08×10^{-5}	**1.90**	**0.72**
$WC/W_2C(12)_{[100]}$	589	12	1.94×10^{-5}	9.14×10^{-6}	**6.45**	**2.46**
$WC/W_2C(15)_{[100]}$	552	16	1.25×10^{-5}	9.54×10^{-6}	**9.95**	**3.79**
$WC/W_2C(20)_{[100]}$	416	29	2.40×10^{-5}	2.26×10^{-5}	**5.19**	**1.98**
$WC/W_2C(50)_{[100]}$	266	6	5.65×10^{-5}	7.46×10^{-6}	**2.21**	**0.84**
$WC/W_2C(70)_{[100]}$	130	8	1.61×10^{-5}	1.40×10^{-5}	**7.77**	**2.96**
$WC(1\&4)_{[15\&100]}$	513	20	7.49×10^{-6}	3.32×10^{-6}	**16.67**	**6.35**
$WC(3\&7)_{[15\&100]}$	428	21	4.94×10^{-5}	1.09×10^{-5}	**2.53**	**0.96**
$WC(5\&5)_{[15\&100]}$	361	26	3.67×10^{-5}	9.61×10^{-6}	**3.40**	**1.30**
$WC(7\&3)_{[15\&100]}$	380	19	1.40×10^{-6}	9.96×10^{-6}	**89.35**	**34.06**

***** Not MLM value, 0.6N load result used due to poor wear data analysis associated with scar measurement producing a linear series.

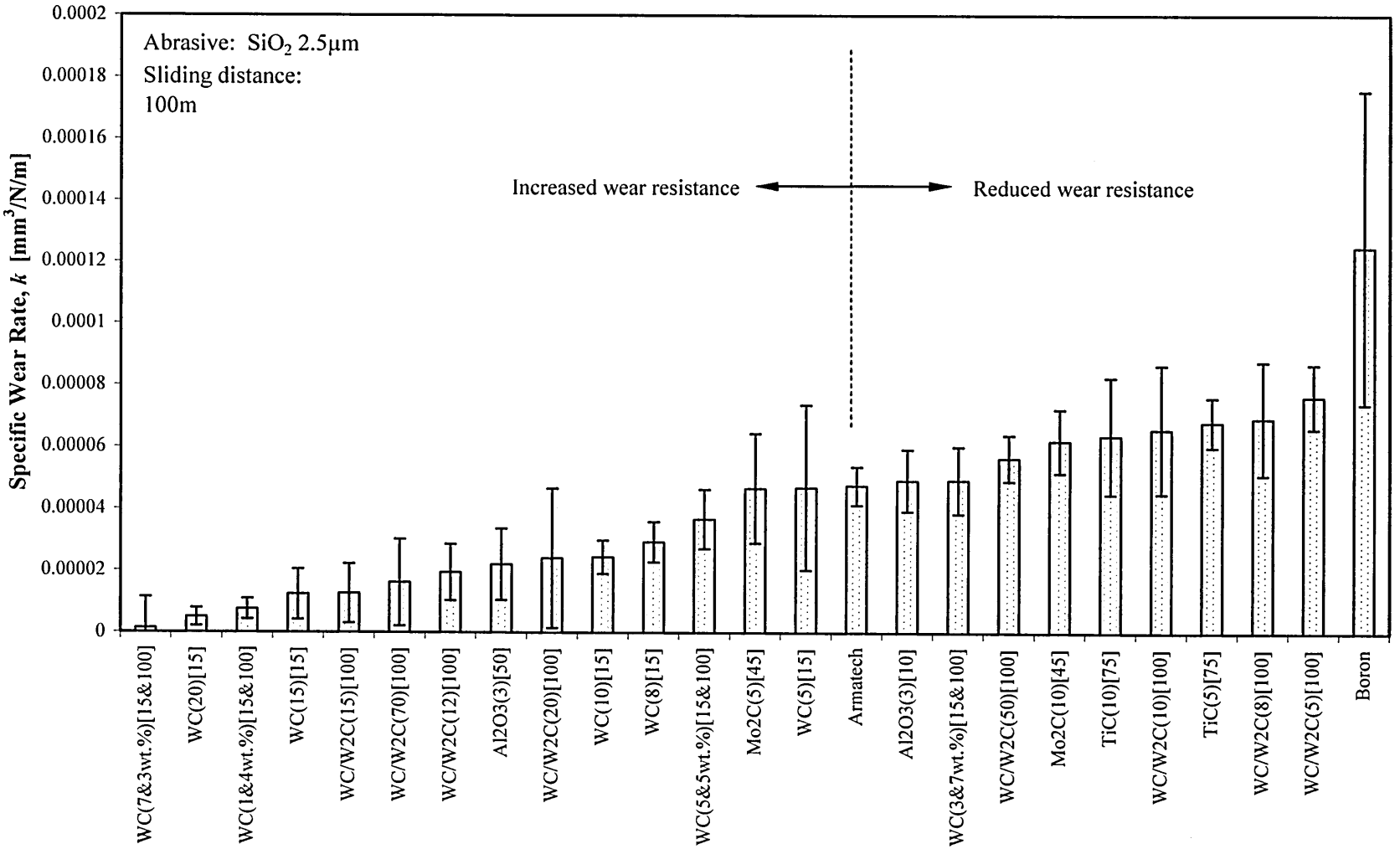

Figure 128: Specific wear rates determined by the MLM method using (1 & 2.5µm) SiO_2 abrasive over a sliding distance of 100 m.

Under these test conditions the Armatech performs much better than boron steel with an average specific wear rate nearly 75% lower and an $RWR_{[Boron]}$ of 2.62. There is also a large error bar associated with the boron steel. This was due to a very low gradient, i.e. the applied load did not affect the size of the crater significantly. This result confirms the feedback received from Chapmans and field observations from farmers that Armatech outperforms boron steel up to several times.

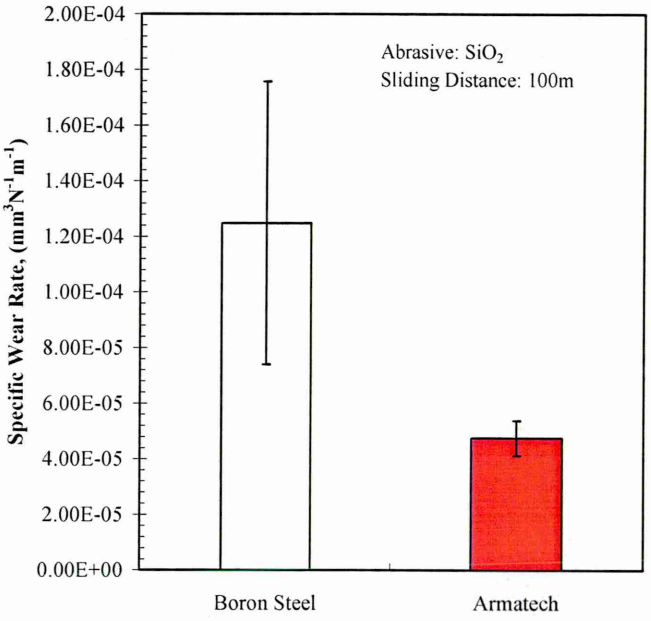

Figure 129: Specific wear rate calculated by the MSAW MLM method of boron steel and Armatech using SiO_2 abrasive at a sliding distance of 100 m.

The materials with 15 μm WC additions showed improved κ with respect to Armatech, which increased with levels of addition from 5wt.% to an optimum of 15wt.%, with 3.88 $RWR_{[Armatech]}$ (Figure 130).

Results for the 20wt.% addition are plotted using the 0.6 N applied load due to a very low gradient from the MLM analysis on this material, the 0.6 N scar showed a uniform wear regime and had a small error in crater measurement. The low gradient was caused by the four craters possessing similar diameters. It can be seen that increasing the addition from 15 to 20wt.% decreases κ, providing a similar value to Armatech, 0.97 $RWR_{[Armatech]}$.

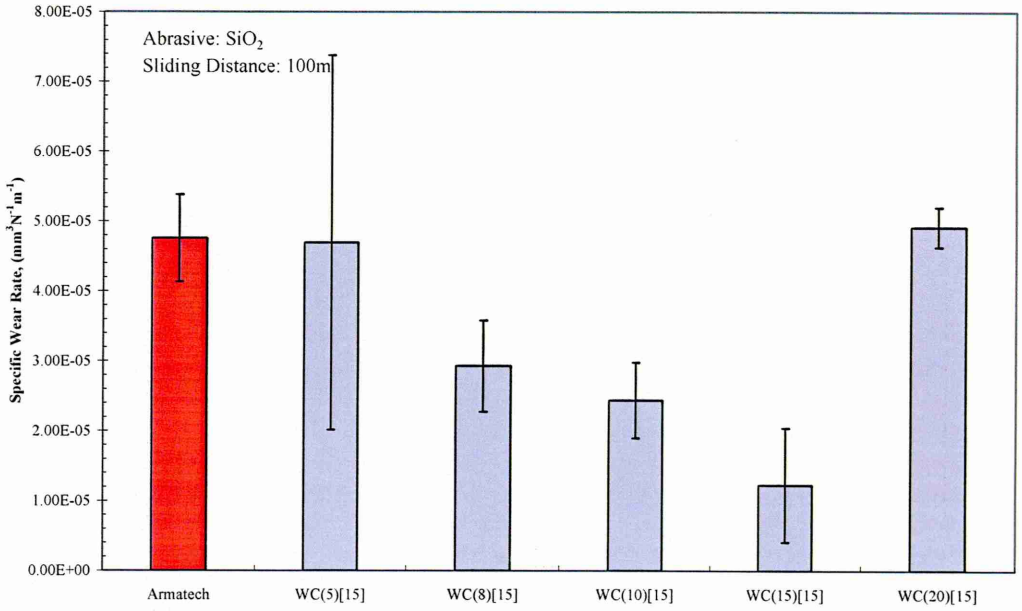

Figure 130: Specific wear rate calculated by the MSAW MLM method of Armatech and 15 μm WC modified Armatech using SiO_2 abrasive at a sliding distance of 100 m.

The addition of the larger 100 μm WC/W_2C resulted in a different trend. No improvements in wear resistance were observed until an addition of 12wt.% was reached. The lower additions of 5, 8 and 10wt.% resulted in a reduction in κ when compared to Armatech. The optimum level of addition was a loading of 15wt.% (3.79 $RWR_{[Armatech]}$) with further increases in addition reducing the wear resistance. The 20wt.% addition also provided improved wear resistance but also possessed a large error. The addition of 50wt.% showed a slight reduction in wear resistance compared to Armatech (0.84 RWR) and the 70wt.% addition showed an improvement in wear (2.96 RWR) similar to the optimum level of 15wt.%.

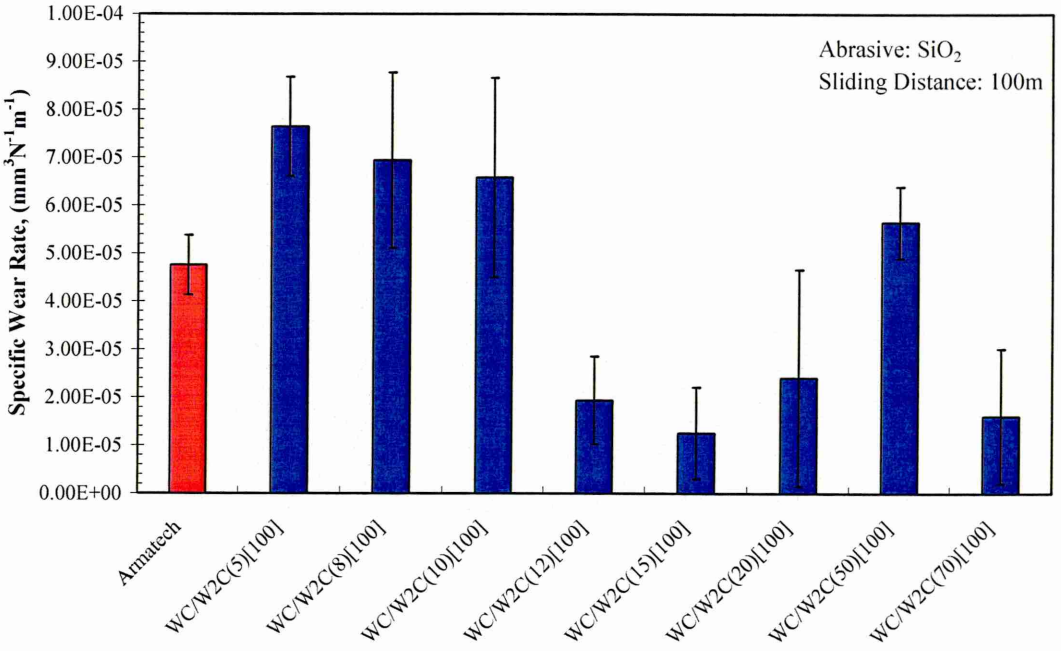

Figure 131: Specific wear rate calculated by the MSAW MLM method of Armatech and 100 μm WC/W_2C modified Armatech using SiO_2 abrasive at a sliding distance of 100 m.

The series of materials produced with mixed ratios of 15 μm WC and 100 μm WC/W_2C revealed a trend when ordered according to the quantity of the larger particle size addition. The material produced using 7wt.% 15 μm plus 3wt.% 100 μm WC/W_2C showed a significant improvement in wear resistance, 34.06 $RWR_{[Armatech]}$. As the loading level of the 100 μm WC/W_2C increased, the wear resistance decreased.

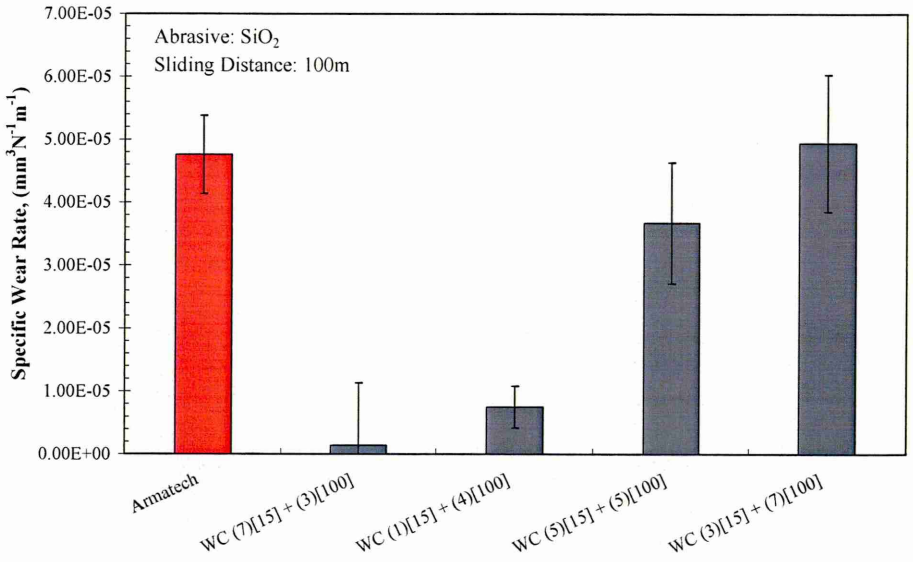

Figure 132: Specific wear rate calculated by the MSAW MLM method of Armatech and mixed ratios of 15 μm WC and 100 μm WC/W_2C modified Armatech using SiO_2 abrasive at a sliding distance of 100 m.

The addition of Al_2O_3 with two particle sizes at the same level of loading (3 wt%) yielded different results suggesting the particle size played a role in wear resistance. The smaller 10 μm addition at a loading of 3wt.% had a much improved wear resistance, $RWR_{[Armatech]}$ of 2.17 but the larger addition of 50 μm Al_2O_3 at 3wt.% had a reduced $RWR_{[Armatech]}$ of 0.97.

A slight improvement (but within errors) in wear resistance is seen when adding 45 μm Mo_2C at 5wt.% but an addition of 10wt.% showed no improvement.

The addition of 75 μm TiC at both 5 and 10wt.% provides no improvement in wear resistance.

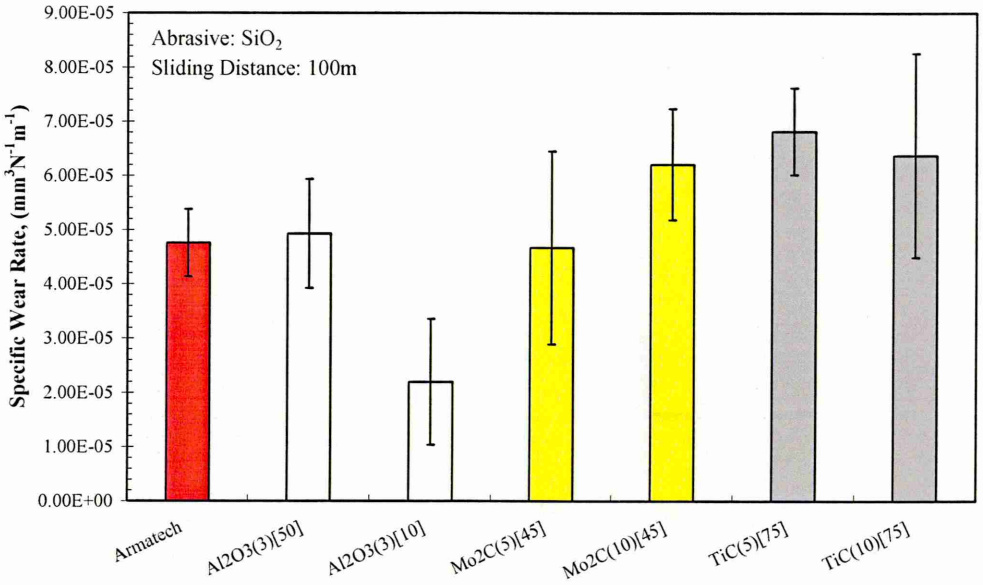

Figure 133: Specific wear rate calculated by the MSAW MLM method of Armatech and Al_2O_3, Mo_2C and TiC modified Armatech using SiO_2 abrasive at a sliding distance of 100 m.

6.6.1 Wear vs. bulk hardness

It was found with SiO_2 wear test data that plotting hardness as a function of both volume removed per unit sliding distance and as a function of RWR (for both boron steel and Armatech) did not result in a correlation as was seen for the SiC abrasive (see Figure 113).

6.6.2 H_a/H_m Ratios

One method that has been employed by other researchers for calculating wear test severity is to determine the H_a/H_m ratio[34]. However, when the materials in question contain small hard phases or additions it is not appropriate to use bulk hardness. As discussed previously bulk hardness provides a lower hardness value due to it being an average of the constituent phases in the microstructure. Microhardness is a more representative measurement when considering indentation of small phases in the microstructure by small abrasive particles. In order to do this measurements were performed on each of the phases; Armatech matrix, Armatech carbides/borides, secondary addition phases along with phase proportions allow a theoretical average microhardness of each material to be calculated.

For example, the matrix phase in Armatech was measured at around 35% with a hardness of 715 $H_{V0.1}$ and the two primary phases 65% with a hardness of ~1550 $H_{V0.1}$. The WC/W_2C additions were ~2050 $H_{V0.1}$. This therefore equates to an average microhardness of 1007 MH_V. The hardness used for the remaining secondary phases were obtained from the CRC handbook due to measurement issues.

It was suggested that the volume of wear removed should be constant at values <0.8 and >1.2 the wear volume should reduce due to deterioration of the abrasive particle.

It can be seen initially from the ratios that the SiC values are much higher than the SiO_2 values due to the higher hardness of the abrasive. As the average hardness of Armatech additions increases with an increase in addition level, this has been shown to not be the case from bulk hardness measurement.

Table 22
Average micro hardness values and H_a/H_m ratios for SiC and SiO_2 abrasive.

	Average MH_V	H_a/H_m ratio	
		SiC	SiO_2
Boron steel	477	5.24	2.22
Armatech	1007	2.48	1.05
$WC(5)_{[15]}$	1059	2.36	1.00
$WC(8)_{[15]}$	1091	2.29	0.97
$WC(10)_{[15]}$	1112	2.25	0.95
$WC(15)_{[15]}$	1164	2.15	0.91
$WC(20)_{[15]}$	1216	2.06	0.87
$WC/W_2C(5)_{[100]}$	1059	2.36	1.00
$WC/W_2C(8)_{[100]}$	1091	2.29	0.97
$WC/W_2C(10)_{[100]}$	1112	2.25	0.95
$WC/W_2C(12)_{[100]}$	1132	2.21	0.94
$WC/W_2C(15)_{[100]}$	1164	2.15	0.91
$WC/W_2C(20)_{[100]}$	1216	2.06	0.87
$WC/W_2C(50)_{[100]}$	1529	1.64	0.69
$WC/W_2C(70)_{[100]}$	1737	1.44	0.61
$WC(7\&3)_{[15\&100]}$	1112	2.25	0.95
$WC(1\&4)_{[15\&100]}$	1059	2.36	1.00
$WC(5\&5)_{[15\&100]}$	1112	2.25	0.95
$WC(3\&7)_{[15\&100]}$	1112	2.25	0.95
$Al_2O_3(3)_{[50]}$	1059	2.36	1.00
$Al_2O_3(6\%)_{[50]}$	1110	2.25	0.95
$Al_2O_3(3\%)_{[10]}$	1059	2.36	1.00
$Mo_2C(5)_{[45]}$	1054	2.37	1.01
$Mo_2C(10)_{[45]}$	1102	2.27	0.96
$TiC(5)_{[75]}$	1117	2.24	0.95
$TiC(10)_{[75]}$	1227	2.04	0.86

Whist H_a/H_m ratios have been explored here, due to the nature of the coatings used in this research being inhomogeneous, other elements need to be considered to assess the severity of wear, for example abrasive particle properties and subsequent wear modes created.

6.6.3 SEM observation of wear surface morphology (SiO_2)

A SEM micrograph showing a typical MSAW scar produced using 2.5 μm SiO2 is provided below in Figure 134.

Figure 134: Typical wear scar from MSAW testing using SiO_2 over 100 m sliding distance on $WC/W_2C(10)_{[100]}$. Arrow denotes direction of ball rotation.

Micrographs from the wear surfaces of boron steel at 0.2, 0.4, 0.6 and 0.8 N applied loads using SiO_2 abrasive are shown in Figure 135. The wear mode transformed from a mixed two/three-body mechanism at 0.2 N applied load, with the intensity of two-body grooving **increasing** and three-body indentations **reducing** as the load was increased to 0.8 N. Furthermore, some areas within the wear scars suffered some degree of micro pitting, suggesting a tribo-corrosion mechanism taking place, this was also observed in the SiC abrasive tests but to a lesser extent.

(a)

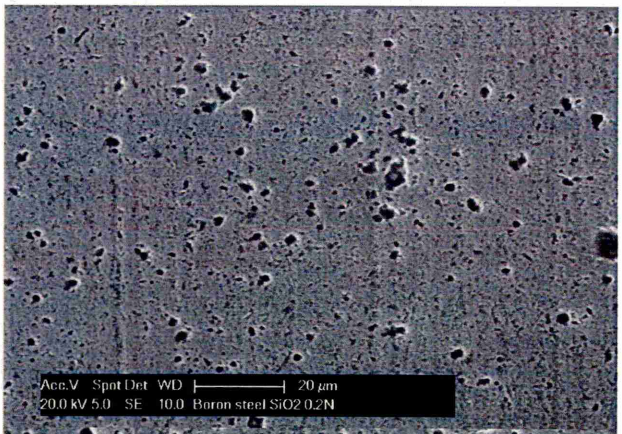

(b)

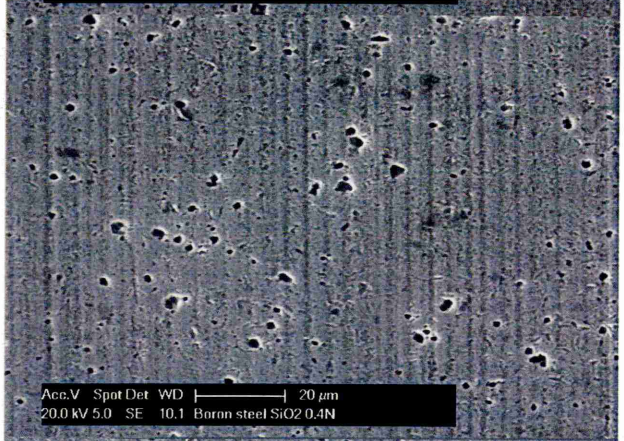

(c)

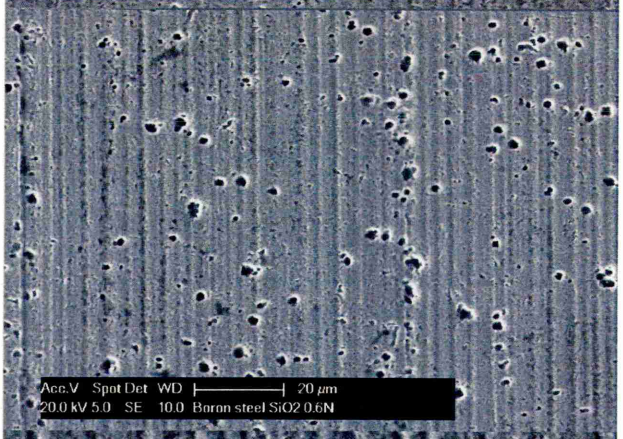

(d)

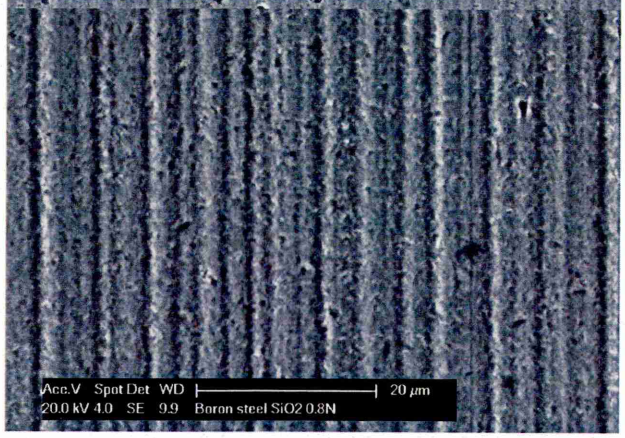

Figure 135: SEM images of MASW scars on boron steel using SiO_2 abrasive; (a) shows mixed mode wear and pitting at 0.2 N load (b) mixed mode wear at 0.4 N load (c) mixed mode wear at 0.6 N and (d) two-body grooving wear at 0.8 N load.

Examination of the Armatech wear scars revealed that a more complex wear regime was taking place than the predominant three-body rolling mechanism observed under SiC abrasive tests. Interestingly, the SiO_2 abrasive produces a mixed mode wear regime within the different phases of the Armatech microstructure as shown in Figure 136. The predominant mode was two-body grooving wear mode as observed in actual field conditions, acting on the Fe-Ni-Cr carbide phase with the softer Fe-Ni matrix suffering three-body rolling wear.

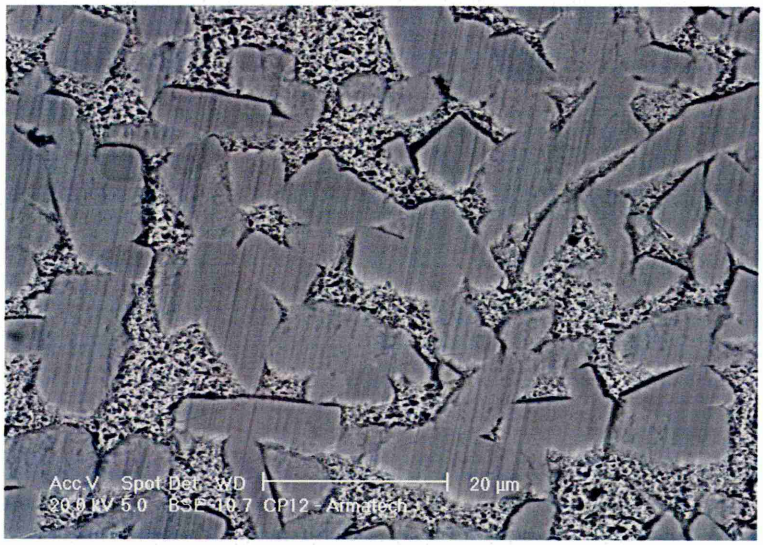

Figure 136: SEM micrograph of MSAW scar on Armatech using SiO_2 abrasive at an applied load of 0.8 N over a sliding distance of 100 m.

The nature of this mechanism may be a result of the softer Fe-Ni matrix phase allowing the SiO_2 particles to dig into the matrix and roll, whereas the carbides are sufficiently hard to prevent this. The path of an abrasive particle would alternate between the two wear modes as it passed over each phase, sliding over the carbides and rolling over the matrix regions causing intermittent indentations. The protrusion of the borides/carbides from the surrounding matrix suggests that these are the dominant phase contributing to wear resistance.

Examination of the wear scars on a material with the addition of 15 µm WC is shown in Figure 137. The addition of the secondary hard phase does not appear to affect the mode of wear within the surrounding Armatech microstructure, a mixed wear regime is still evident. It was also clear that some pullout of the 15 µm WC had occurred. In cases where pullout had not occurred the WC appeared to be protecting the matrix material against wear and showing signs of some plastic ploughing, as shown by back scattered contrast in Figure 137(b). The light coloured phase seen at the centre of the micrograph is the small WC phase sintered within the Armatech structure. The WC phase acts in a similar manner to the primary hard phase of

Armatech, suffering two-body wear while the Fe-Ni matrix wears through three-body indentations.

Increasing the applied load to 0.8 N appeared to increase the severity or depth of the two-body grooving scars, Figure 137(c). It also gave the wear surface an appearance of directional plastic deformation. Furthermore, Figure 137(d) shows two-body grooves, micro-cracking is apparent in the Armatech boride/carbides at the highest (0.8 N) loads.

The micrographs from the $WC/W_2C(10)_{[100]}$ material show how the large WC particle addition does not affect the wear mode occurring on the Armatech structure, and a mixed mode occurring in the hard phase and softer matrix was again apparent.

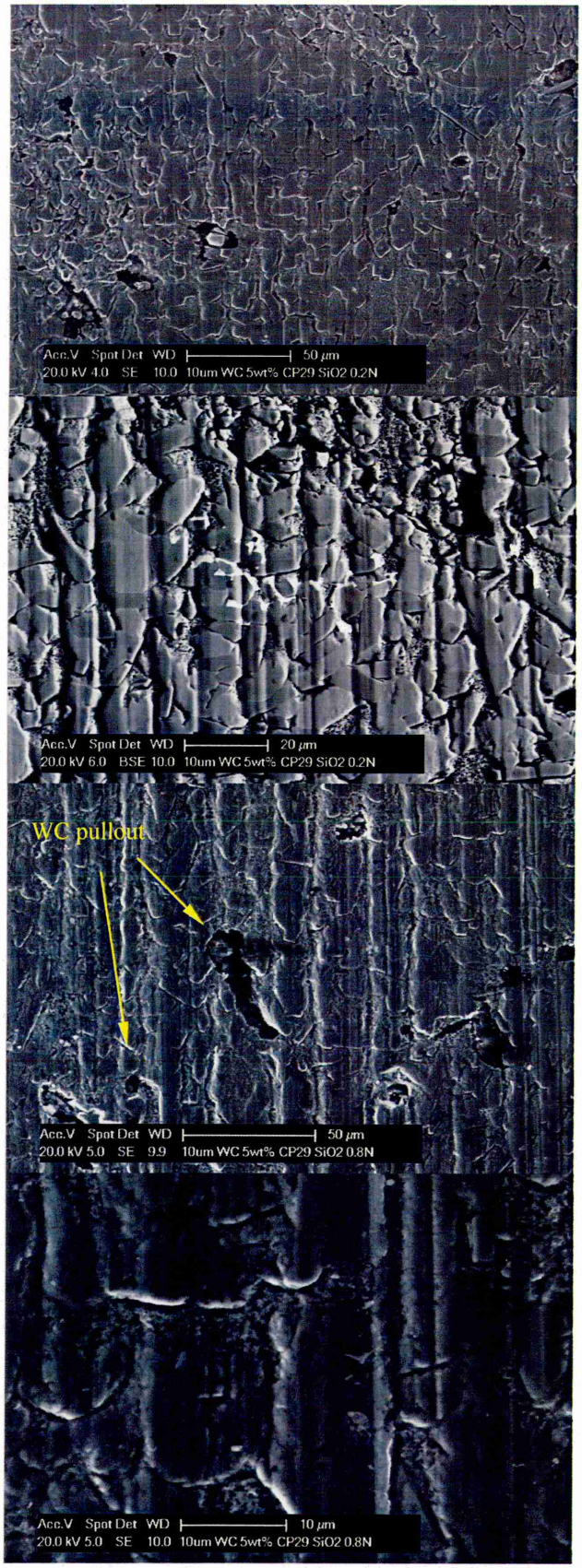

Figure 137: SEM micrographs of MSAW scars produced using SiO_2 abrasive over a sliding of 100 m at a) and b) 0.2 N loads and c) and d) 0.8 N load.

(a)

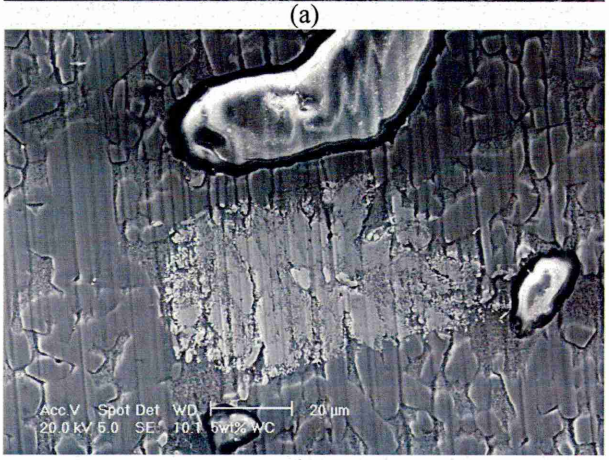

(b)

Figure 138: SEM images of MSAW scars on 10wt.% 100 µm WC/W_2C coating using SiO_2 abrasive over a sliding of 100 m

The large WC particles showed signs of the two-body sliding wear regime as observed in the primary hard phase of Armatech, Figure 138. The WC particles did not appear to affect the wear path of the abrasive particles or the groove widths, a continuous groove can be seen.

Increasing the level of addition to 50wt.% resulted in the wear mode of the surrounding Armatech structure still being a mixed but the Armatech boride/carbides appeared to be suffering from micro-cracking as shown in Figure 139(c). The continuous appearance of the two-body grooves across the Armatech boride/carbide phases and the WC particles observed in the lower level additions appeared to be less common and a more discontinuous appearance prevailed. The appearance of cracking within the Armatech and also within the central region of the WC carbides probably promoted material pullout, reducing the wear resistance.

Examination of the WC particles revealed that the dominant wear mode in this phase was two-body grooving wear, however, it was also clear that as the applied load increased the amount of fracture and pullout of the core WC region increased, as shown in Figure 139 (b) and (d). It may be the case that the increased loading of WC into the Armatech structure affects the chemistry of the existing microstructure increasing brittleness, leading to micro-cracking when subjected to wear testing.

(a)

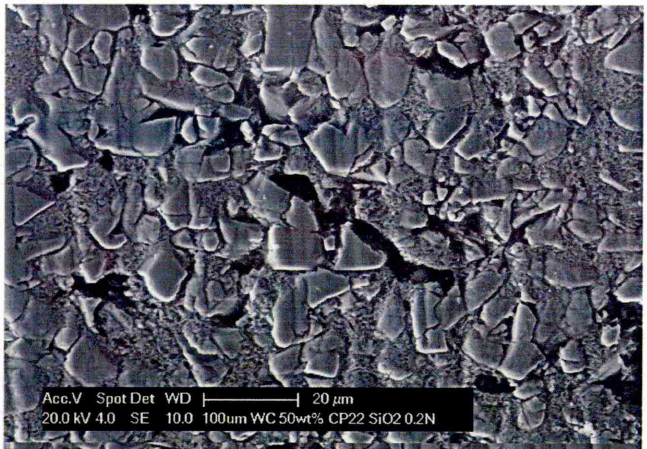

(b)

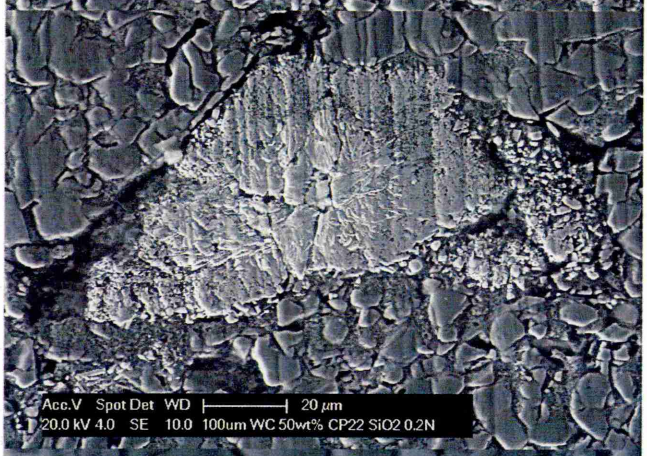

(c)

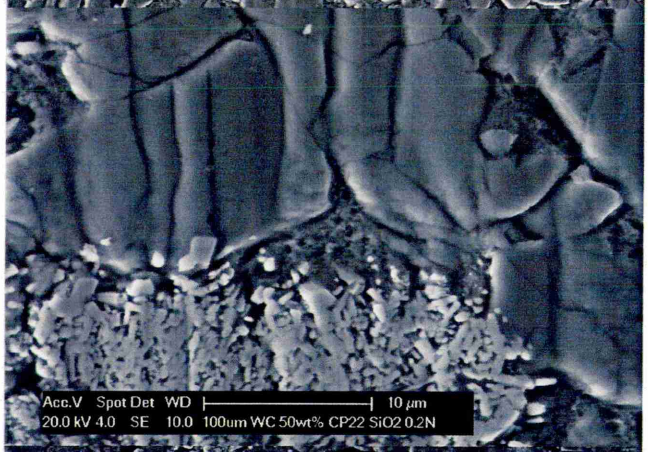

(d)

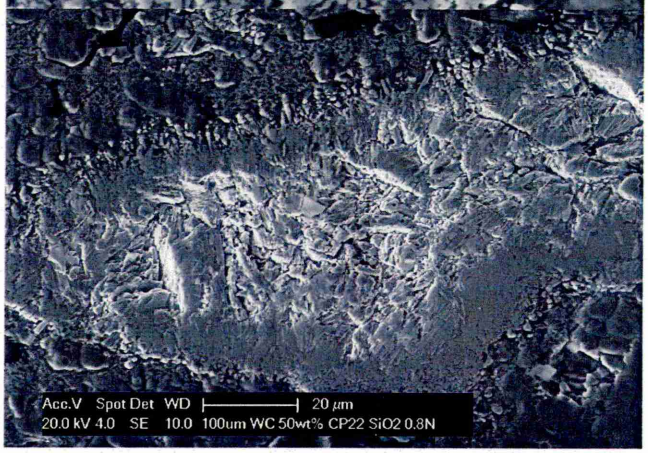

Figure 139: SEM micrographs MSAW scars on $WC/W_2C(50)_{[100]}$ using SiO_2 abrasive; (a) shows mixed mode wear at 0.2 N load, (b) shows a WC particle suffering two-body wear, (c) shows micro-cracking of Armatech boride/carbides and (d) shows 'fallout' of WC particle centre region.

The micrographs presented in Figure 140 show the wear scars of materials with additions of both 15 μm WC and 100 μm WC/W_2C additions at different ratios tested with the SiO_2 abrasive. Both small and large additions exhibited the same wear characteristic described previously and the addition of one or the other did not affect the wear regime. It was observed however in the [5wt.% 15 μm plus 5wt.% 100 μm WC] $(WC(5\&5)_{[15\&100]}$ material that, where an agglomeration of the smaller 15 μm particles had occurred, a 'comet tail' like area of Armatech could be seen to be protruding behind this area of WC. The WC particles having been protected the area by resisting wear, see Figure 140(d).

(a)

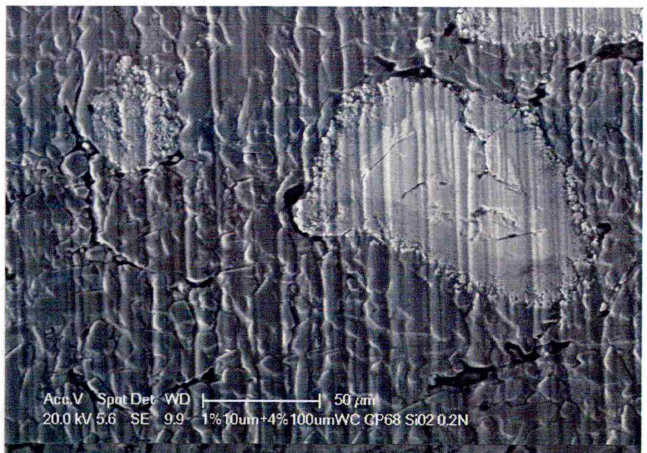

(b)

(c)

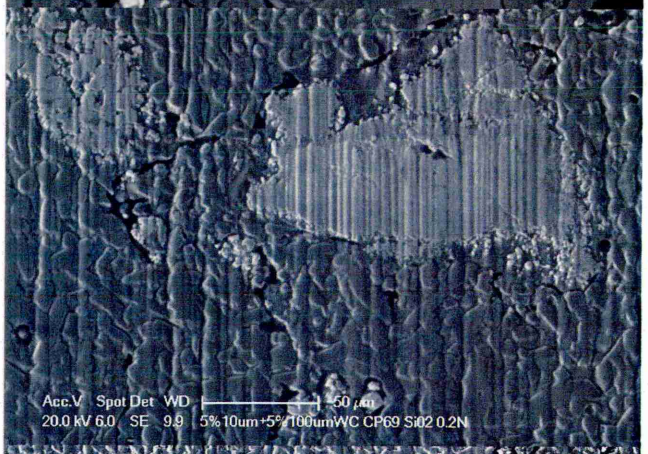

(d)

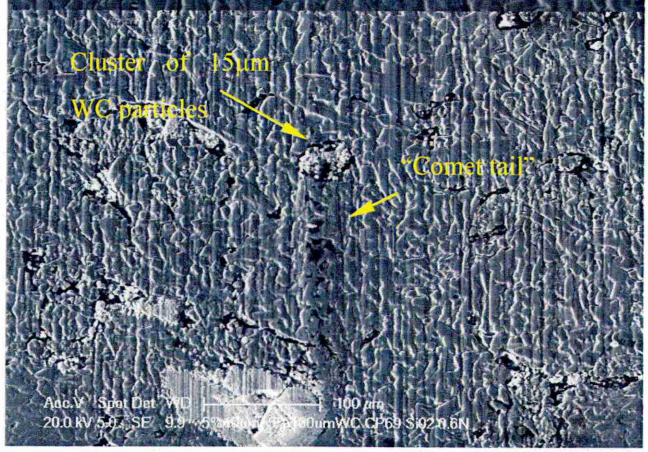

Continued…

(e)

(f)

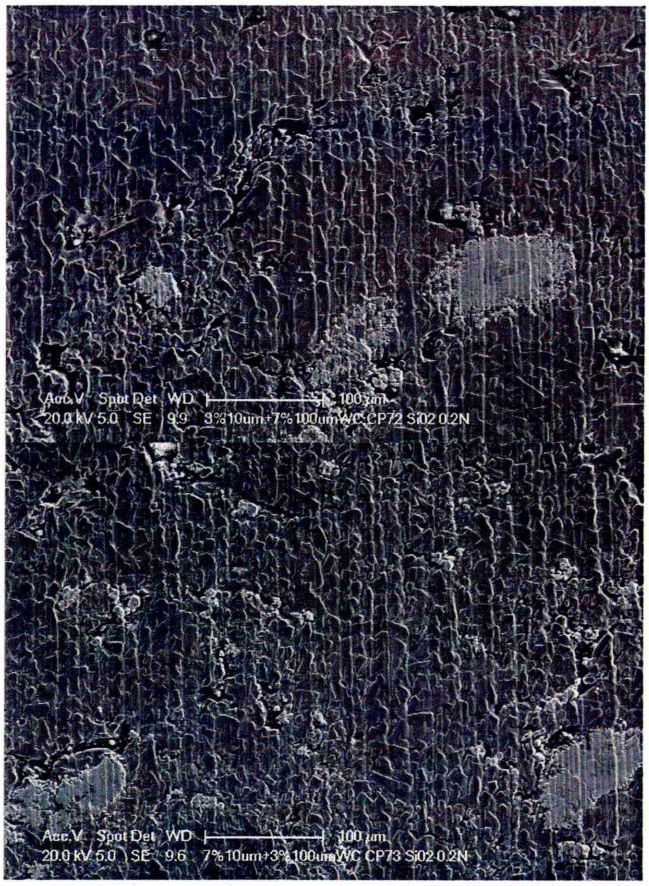

Figure 140: SEM micrographs MSAW scars on mixed ratios of 100 µm WC/W_2C and 15 µm WC using SiO_2 abrasive over 100 m sliding distance.

Examination of the wear scars on the Mo_2C addition materials indicated that the areas of Mo_2C were acting in a similar manner to the boride/carbides of the Armatech structure as shown in Figure 141. They appeared to be experiencing a two-body grooving wear mode with the Fe-Ni matrix showing three-body indentations. However, the 45 µm agglomerates had dispersed into clusters of smaller particles. It is suspected that the powder was supplied as 45 µm agglomerates which were porous in nature and that the sintering process had allowed the Fe-Ni phase of Armatech to penetrate into the agglomerates.

(a)

(b)

Figure 141: SEM micrographs in MSAW scar on 45 µm Mo_2C 10wt.% addition using SiO_2 abrasive and sliding distance of 100 m.

As seen from the wear scars of the TiC addition in Chapter 5, the TiC particles had not fused with the Armatech material so no real protection from wear resulted as evident from Figure 142. It was evident from the wear scars that a high level of TiC pullout had occurred. This may explain the similar wear resistance values to Armatech as the TiC particles were not contributing to wear resistance.

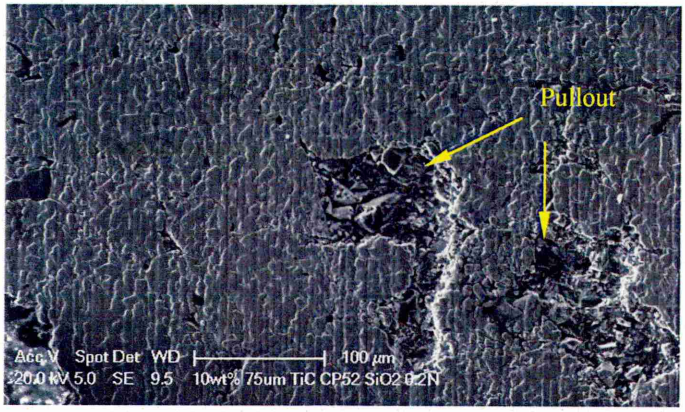

Figure 142: SEM micrographs in MSAW scar on 75 µm TiC 10wt.% addition using SiO_2 abrasive and sliding distance of 100 m.

Examination of the WC-Co tile wear surface showed that the wear regime appeared to be by preferential removal of the Co binder phase around the carbide particles through characteristic three-body multiple indentations with some directionality, suggesting two-body grooving was also occurring. The carbide phase appears not be greatly affected by the wear mechanism but some areas of pullout were evident.

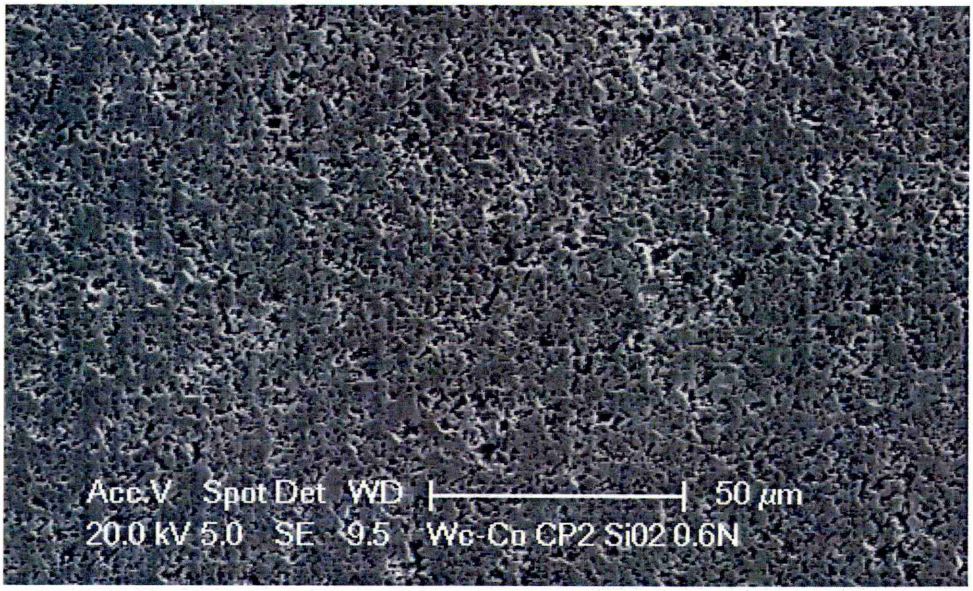

Figure 143: SEM image of MSAW scar of WC-Co tile, SiO_2 abrasive, 100 m sliding distance and applied load of 0.6 N.

6.6.4 Summary of MSAW Results

It has been shown that by using different abrasives, wear rates and wear regimes can be manipulated. The results from the MSAW test using SiO_2 abrasive have simulated, to some extent, the wear mechanism observed in actual field conditions. This suggests that the use of the MSAW test can be a useful technique for the development and comparative measurement of future soil working tool materials. However, due to the nature of the test, the amount of material removed is relatively small and hence results cannot be directly compared to other wear tests or field trials, but can allow a good comparison test under these specific conditions.

A few key points must be considered when performing MSAW tests. Firstly the effect of sample microstructure can play an important role in results due to the relatively small test area. Any hard phases or particles that have been added may constitute a large area of the scar. The abrasive size is also an important factor, with both SiC and SiO_2, the abrasive particle size was considerably smaller than the Armatech carbides and additions and, in the case of SiC, very much harder. The more aggressive SiC abrasive yielded higher material losses and produced a three-body wearing pattern while the SiO_2 produced yielded less material loss with a two-body wearing mechanism. The wear rates differ greatly between the two abrasives and the change in primary wear mechanism resulted in different trends.

Whilst RWR values calculated provide some comparative indication of material performance in this specific test, they should not be considered or used as a lifetime prediction model.

It is also worth noting that the Archard equation which MSAW relies heavily upon is a model for sliding wear and not lubricated abrasive wear. It does not take wear mode into consideration or the effect of contact area and hence test pressure, which can promote abrasive particle fracture or dry abrasives. These results have shown that different wear mechanisms have different material removal rates, with three-body wear being the more aggressive regime (particularly with SiC abrasive). Contact pressure has also been shown to affect wear rate particularly at low loads and increases in pressure can lead to abrasive fracture thereby creating smaller faceted particles.

6.7 Dry Sand Rubber Wheel Results (Modified ASTM G65)

Wear data was obtained from a test based on the standard ASTM G65 under two conditions; dry sand and wet sand, as previously described in Chapter 6. The results from the dry abrasive environment are presented first followed by the results from the wet abrasive environment Examination of the resultant wear scars and determination of the wear mechanisms via SEM in both environments is then presented

6.7.1 Dry Environment, DSRW

The results for tests using dry sand 260 μm abrasive are summarised in Table 23 (page 186). The measured weight loss from each test is given along with the calculated volume losses and relative wear resistance values (compared with both boron steel and Armatech). The total volume loss, calculated using the mass loss measurements and the theoretical densities of the materials, are also shown graphically in Figure 144 to Figure 147, where the standard error, S_E, is used for the error bars.

The results from the dry environment show that under these test conditions the Armatech coating performs better than boron steel, with an $RWR_{[Boron]}$ of 1.26, around a 25% improvement.

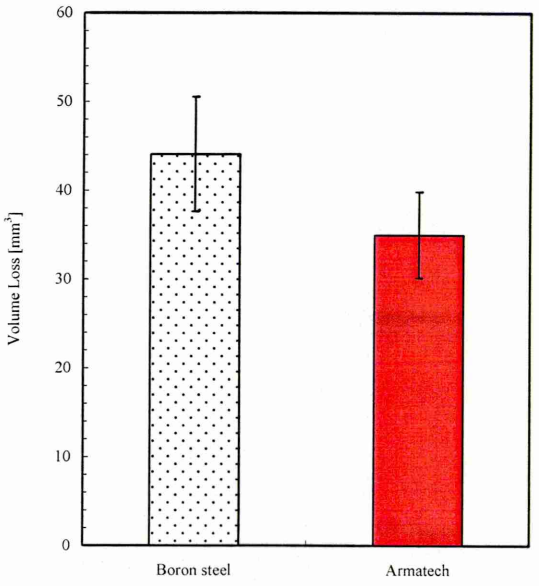

Figure 144: Average volume loss of boron steel and Armatech from DSRW testing at 130 N load over a sliding distance of 942 m with 260 μm silica sand.

For the modified materials, improvements over Armatech were observed with 15 μm WC additions of 5 and 10wt.%, with $RWR_{[Armatech]}$ of 2.8 and 1.8 respectively (see Figure 145). It appears that 5wt% of 15μm WC is an optimal addition as the higher level of 15wt.% yielded similar performances to boron steel with an $RWR_{[Armatech]}$ of 0.8.

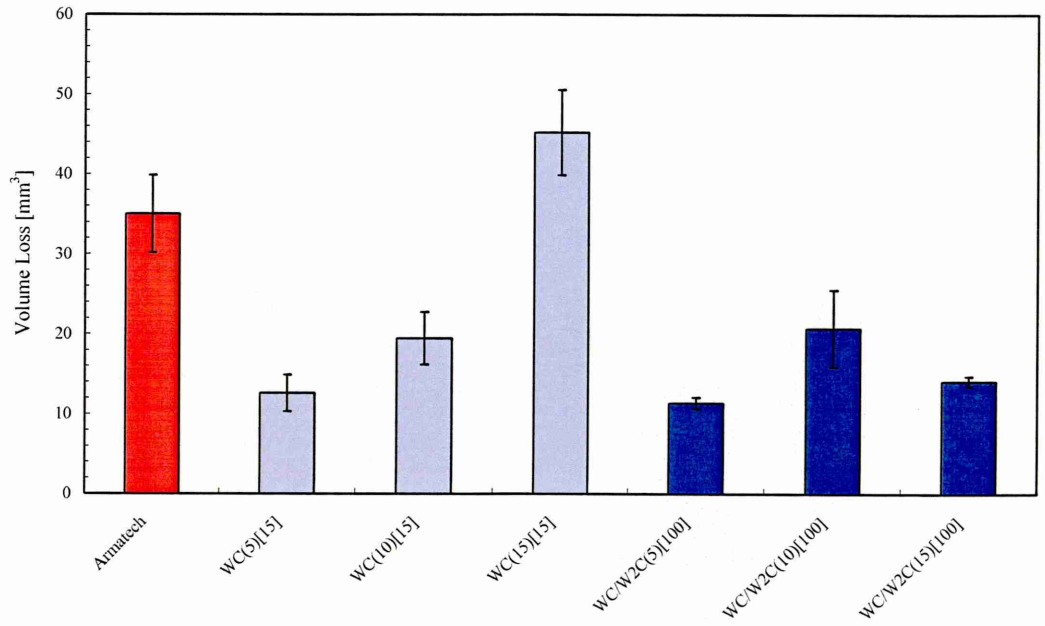

Figure 145: Average volume loss of Armatech, 15 μm WC series and 100 μm WC/W_2C modified Armatech from DSRW testing at 130 N load over a sliding distance of 942 m with 260 μm silica sand.

Figure 145 also shows the results for the additions of 100 μm WC/W_2C. All levels of addition showed improvements over Armatech, with the optimum again being at 5wt.%, yielding an $RWR_{[Armatech]}$ of 3.1.

Improvements were also apparent with the mixed size additions of 15 μm WC plus 100 μm WC/W_2C, having $RWR_{[Armatech]}$ figures ranging from 1.8 and 2.2, as shown in Figure 146.

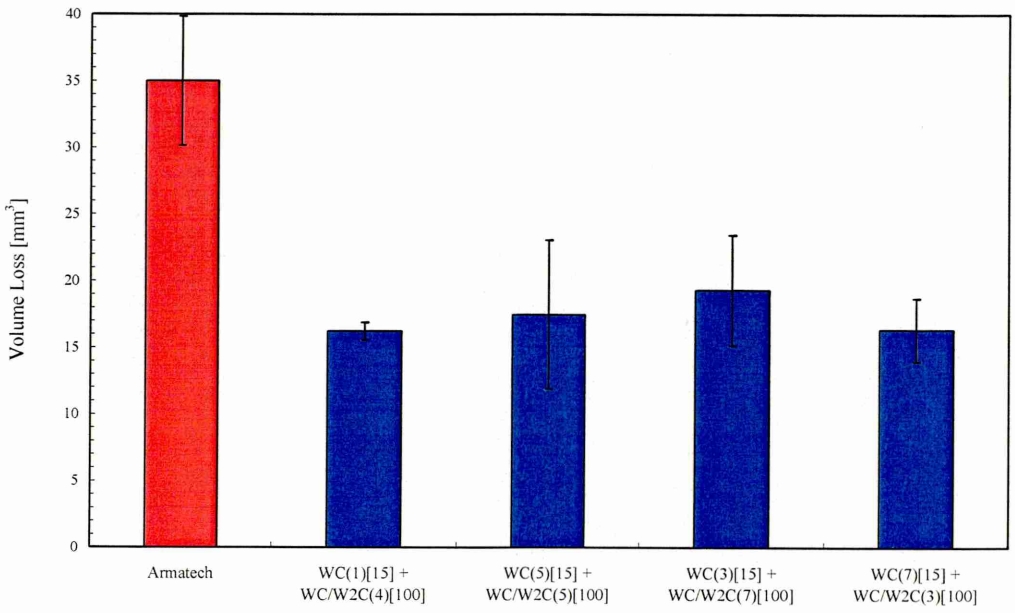

Figure 146: Average volume loss of Armatech containing mixes of 15 μm WC and 100 μm WC/W_2C tested using DSRW at 130 N load over a sliding distance of 942 m with 260 μm silica sand.

The addition of 3wt% 50μm Al_2O_3 resulted in a material which was not as wear resistant as the unmodified Armatech coating. Note, however, the large error bar associated with this particular

result. The material containing 3wt.% 10μm Al_2O_3, provided an improvement in wear resistant compared with Armatech with $RWR_{[Armatech]}$ = 1.52. The addition of 5wt.% 45 μm Mo_2C also showed an improvement in wear resistance with $RWR_{[Armatech]}$ = 2.17.

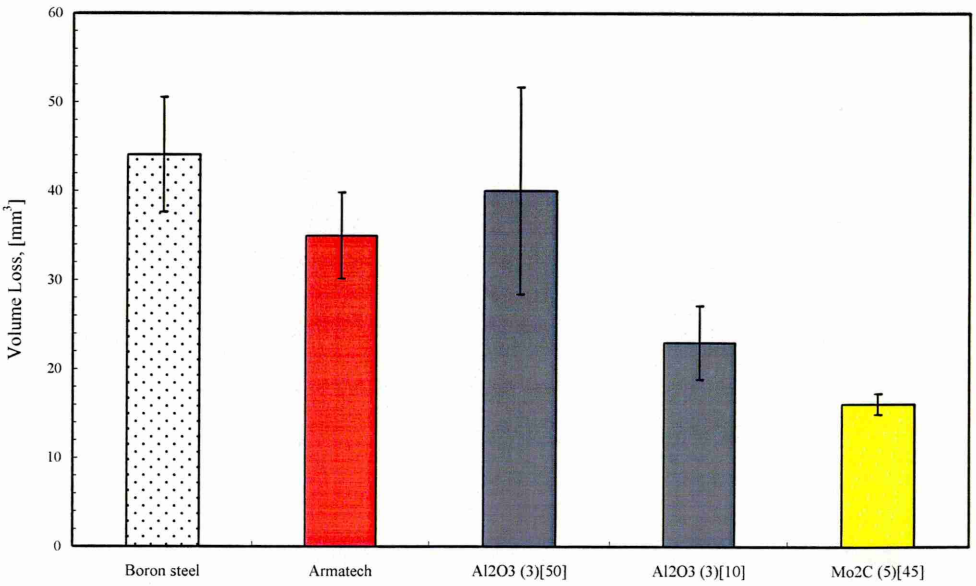

Figure 147: Average volume loss (3 tests) of boron steel, Armatech, Al_2O_3 and Mo_2C modified Armatech from DSRW testing at 130 N load over a sliding distance of 942 m with 260 μm silica sand.

Table 23
Results from ASTM G65 dry abrasive test.

Test No.	Material loss [g] 1	2	3	Ave wt loss [g]	St Err [±]	Volume loss [mm^3]	**$RWR_{[Boron]}$**	**$RWR_{[Armatech]}$**
Boron steel	0.25	0.42	0.32	0.33	0.05	44.09	**1.00**	**0.79**
Armatech	0.26	0.20	na††††††	0.23	0.03	34.99	**1.26**	**1.00**
$WC(5)_{[15]}$	0.06	0.12	0.07	0.08	0.02	12.59	**3.50**	**2.78**
$WC(10)_{[15]}$	0.13	0.18	0.10	0.14	0.02	19.45	**2.27**	**1.80**
$WC(15)_{[15]}$	0.29	0.40	0.28	0.32	0.04	45.19	**0.98**	**0.77**
$WC/W_2C(5)_{[100]}$	0.08	0.09	0.07	0.08	0.004	11.34	**3.89**	**3.09**
$WC/W_2C(10)_{[100]}$	0.21	0.11	0.11	0.14	0.03	20.70	**2.13**	**1.69**
$WC/W2C(15)_{[100]}$	0.10	0.11	0.09	0.10	0.01	14.10	**3.13**	**2.48**
$WC(1)_{[15]} + (4)_{[100]}$	0.11	0.10	0.12	0.11	0.01	16.22	**2.72**	**2.16**
$WC(5)_{[15]} + (5)_{[100]}$	0.10	0.20	0.07	0.12	0.04	17.46	**2.53**	**2.00**
$WC(3)_{[15]} + (7)_{[100]}$	0.13	0.09	0.19	0.13	0.03	19.31	**2.28**	**1.81**
$WC(7)_{[15]} + (3)_{[100]}$	0.09	0.10	0.15	0.11	0.02	16.34	**2.70**	**2.14**
$Al_2O_3(3)_{[10]}$	0.40	0.18	0.18	0.15	0.03	22.97	**1.92**	**1.52**
$Al_2O_3(3)_{[50]}$	0.14	0.11	0.20	0.26	0.07	40.01	**1.10**	**0.87**
$Mo_2C(5)_{[45]}$	0.11	0.12	0.09	0.11	0.01	16.09	**2.74**	**2.17**

†††††† 3rd test with Armatech sample disregarded due to poor surface finish.

6.7.2 *Wet Environment, WSRW*

The results of the wet environment tests are summarised below in Table 24 (page 189), and the results for volume losses are shown in Figure 148 and Figure 149. It can be seen from Table 24 and Figure 148 that the boron steel suffers the highest material loss, with Armatech having $RWR_{[Boron]} = 1.27$, virtually the same value obtained in the dry environment.

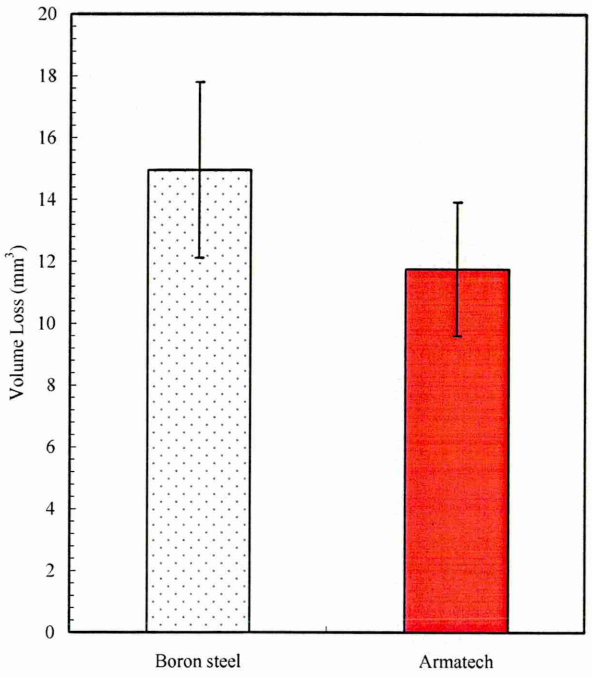

Figure 148: Average volume loss of boron steel and Armatech from WSRW testing at 130 N load over a sliding distance of 942 m with 260 µm silica sand.

The addition of **15 µm** WC resulted in a modest improvement over Armatech with the addition of 15wt.% providing the best result with $RWR_{[Armatech]} = 1.87$ (Figure 149). The **100 µm** WC/W_2C additions all showed a much greater improvement with $RWR_{[Armatech]}$ values ranging between 5 and 23.

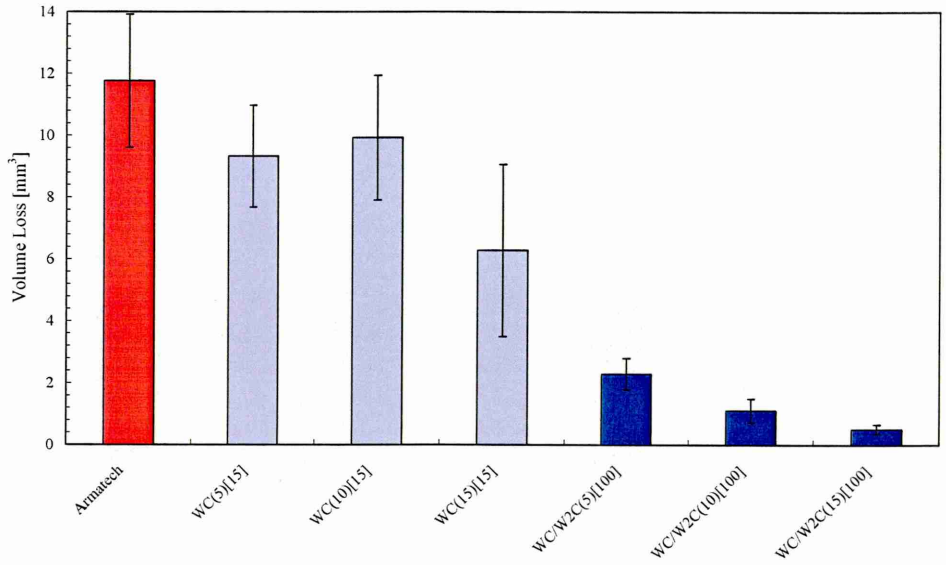

Figure 149: Average volume loss of Armatech, 15 μm WC series and 100 μm WC/W_2C modified Armatech from WSRW testing at 130 N load over a sliding distance of 942 m with 260 μm silica sand.

The mixed size additives of 15 μm WC plus 100 μm WC/W_2C materials showed very little improvement in wet environments. The most improved material was the 5wt.% addition of both particles showing a $RWR_{[Armatech]}$ of 1.63. The other three combinations of hard phase additions yielded no significant improvements.

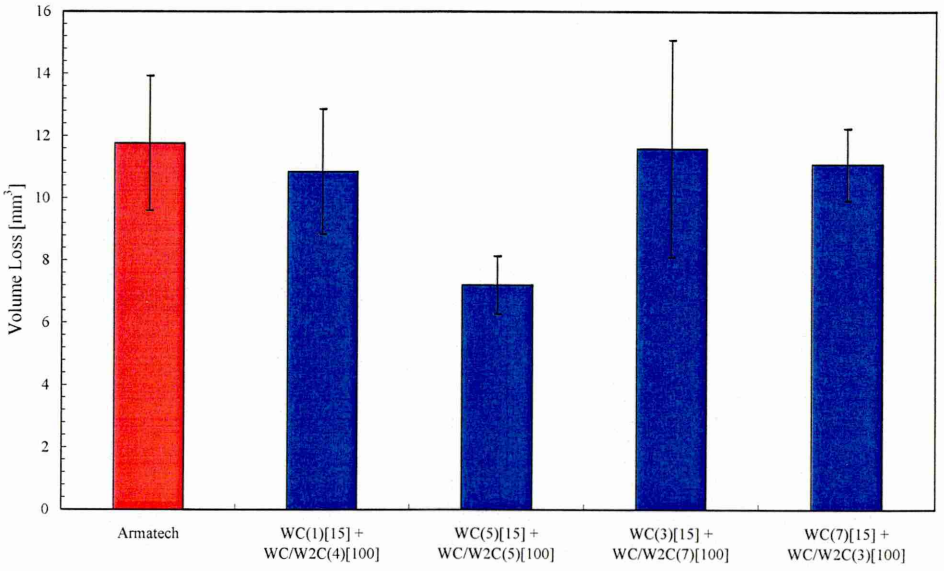

Figure 150: Average volume loss of Armatech mixed ratios of 15 μm WC 100 μm WC/W_2C modified Armatech from WSRW testing at 130 N load over a sliding distance of 942 m with 260 μm silica sand.

Table 24
Results from ASTM G65 wet abrasive test.

	Weight of Material loss [g]			Ave wt loss [g]	St Err [±]	Volume loss [mm^3]	$RWR_{[Boron]}$	$RWR_{[Armatech]}$
Test No.	1	2	3					
Boron steel	0.15	0.09	0.10	0.11	0.02	14.96	**1.00**	**0.79**
Armatech	0.09	0.10	0.05	0.08	0.01	11.76	**1.27**	**1.00**
$WC(5)_{[15]}$	0.06	0.09	0.05	0.06	0.01	9.33	**1.60**	**1.26**
$WC(10)_{[15]}$	0.10	0.06	0.05	0.07	0.01	9.92	**1.51**	**1.19**
$WC(15)_{[15]}$	0.03	0.02	0.08	0.05	0.02	6.28	**2.38**	**1.87**
$WC/W_2C(5)_{[100]}$	0.02	0.02	0.01	0.02	0.003	2.29	**6.53**	**5.14**
$WC/W_2C(10)_{[100]}$	0.01	0.01	0.01	0.008	0.003	1.10	**13.57**	**10.67**
$WC/W_2C(15)_{[100]}$	0.002	0.01	0.004	0.004	0.001	0.51	**29.15**	**22.92**
$WC(1)_{[15]} + (4)_{[100]}$	0.06	0.10	0.06	0.07	0.01	10.85	**1.38**	**1.08**
$WC(5)_{[15]} + (5)_{[100]}$	0.04	0.04	0.06	0.05	0.006	7.21	**2.08**	**1.63**
$WC(3)_{[15]} + (7)_{[100]}$	0.13	0.05	0.07	0.08	0.02	11.59	**1.29**	**1.02**
$WC(7)_{[15]} + (3)_{[100]}$	0.07	0.08	na‡‡‡‡‡	0.08	0.008	11.09	**1.35**	**1.06**
$Al_2O_3(3)_{[10]}$	0.07	0.06	0.07	0.06	0.01	10.45	**1.43**	**1.13**
$Al_2O_3(3)_{[50]}$	0.08	0.04	0.07	0.07	0.001	9.76	**1.53**	**1.21**
$Mo_2C(5)_{[45]}$	0.08	0.07	0.05	0.06	0.01	9.79	**1.53**	**1.20**

‡‡‡‡‡ 3rd test not performed on $WC(7wt\%)_{[10]} + (3wt\%)_{[100]}$ due to poor sinter quality of sample.

The volume losses of the materials with additions of 10 and 50 μm Al_2O_3 and 45 μm Mo_2C are shown below in Figure 151. It can be seen that the 50 μm Al_2O_3 additions at 3wt.% provides some improvement ($RWR_{[Armatech]}$ = 1.21) with the 10 μm addition at the same weight percentage possessing an $RWR_{[Armatech]}$ of only 1.13.

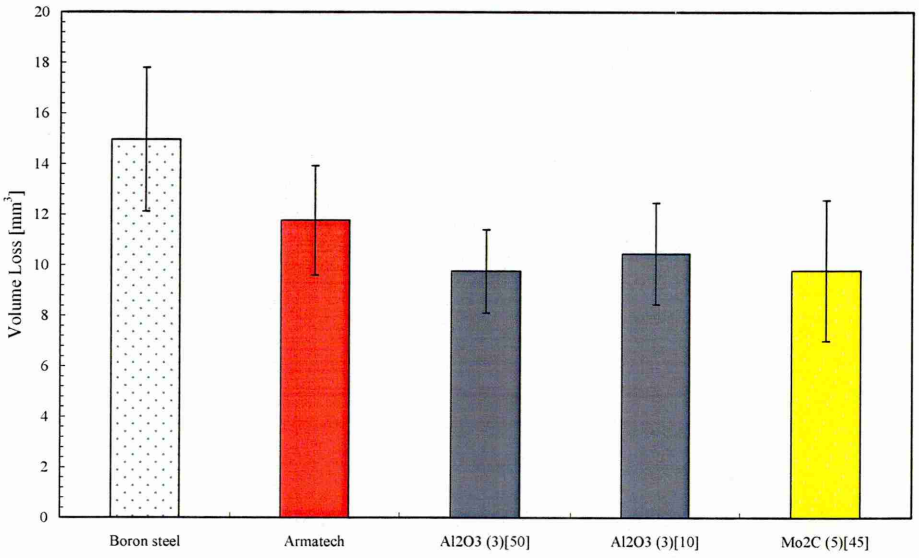

Figure 151: Average volume loss of boron steel, Armatech, Al_2O_3 and Mo_2C modified Armatech from WSRW testing at 130 N load over a sliding distance of 942 m with 260 μm silica sand.

The Mo_2C addition again showed some signs of improvement in volume loss and yielded an $RWR_{Armatech}$ of 1.2.

6.7.3 Comparison of wet and dry abrasive test results

When comparing the dry environment to wet environment, using the same sliding distance and applied load, it is clear that overall the rate of material loss is substantially lower in wet conditions. This trend was also observed in research by Swanson[107] when assessing typical materials used for agricultural implements. It can be seen from the standard errors listed in Table 23 and Table 24 that the reproducibility between the 3 tests carried out on each material in both environments was good.

Figure 152 shows that the volume loss of the boron steel and Armatech was ~66% lower than values obtained under dry conditions.

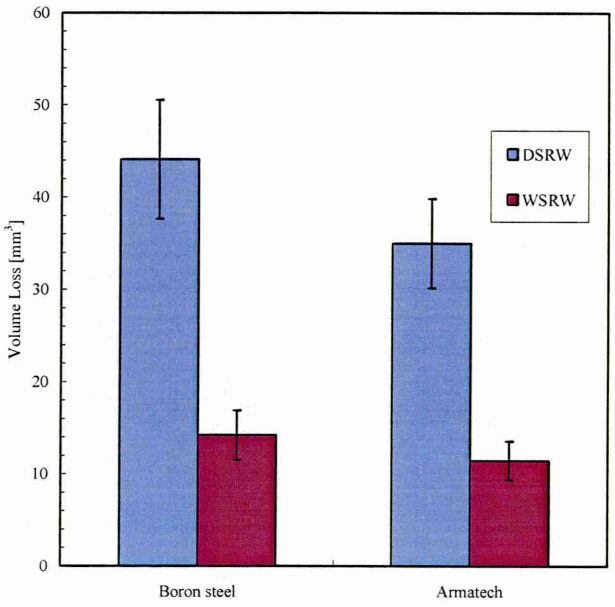

Figure 152: Effect of dry and wet environment on the volume loss of boron steel and Armatech using the ASTM G65 test rig.

Figure 153 below shows a comparison of volume losses under dry and wet environments for Armatech and the 15 μm WC additions. The 5 and 10wt.% materials suffered 26 and 50% lower volume losses respectively under wet conditions with the 15wt.% addition material having a significant 86% lower volume loss in the wet condition.

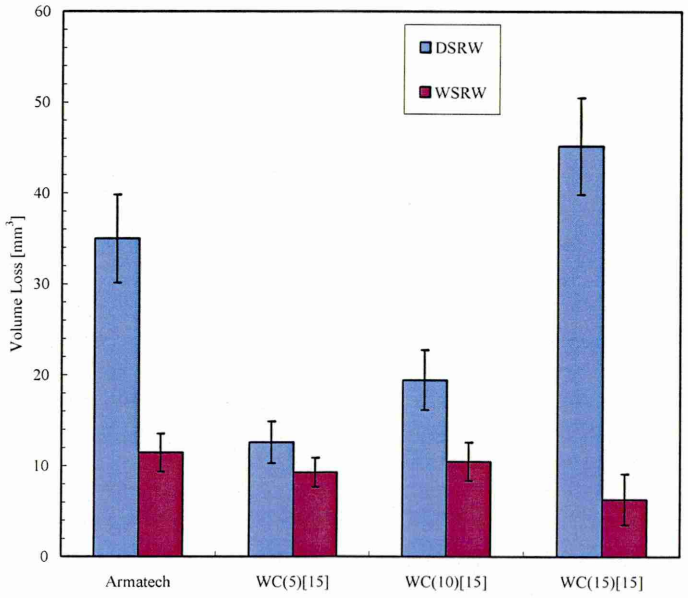

Figure 153: Effect of dry and wet environment on the volume loss of Armatech and 15 μm WC modified Armatech using the ASTM G65 test rig.

Even greater reductions in volume loss under wet conditions were seen for the 100 μm WC/W_2C materials. The 5wt.% material experienced 80% lower volume loss while the 10 and 15wt.% was ~95% lower.

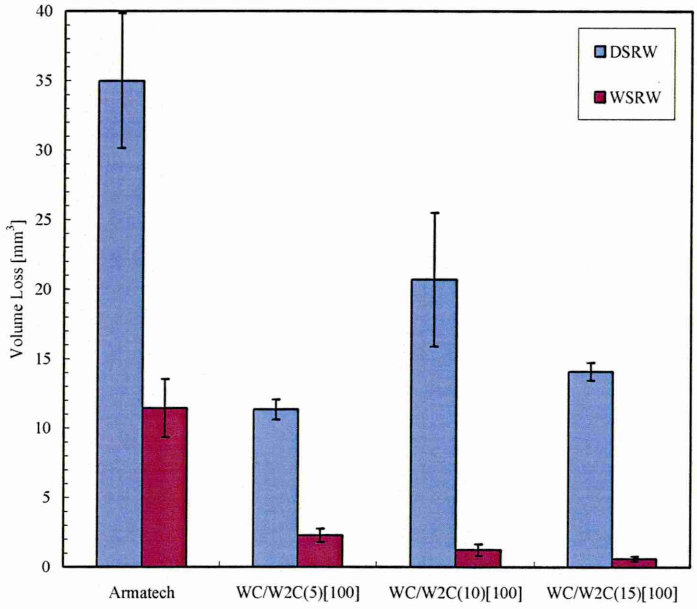

Figure 154: Effect of dry and wet environment on the volume loss of Armatech and 100 μm WC/W_2C modified Armatech using the ASTM G65 test rig.

The results from the four mixed WC and WC/W_2C material showed overall lower volume losses when compared to the individual additions, ranging from 32 to 60%.

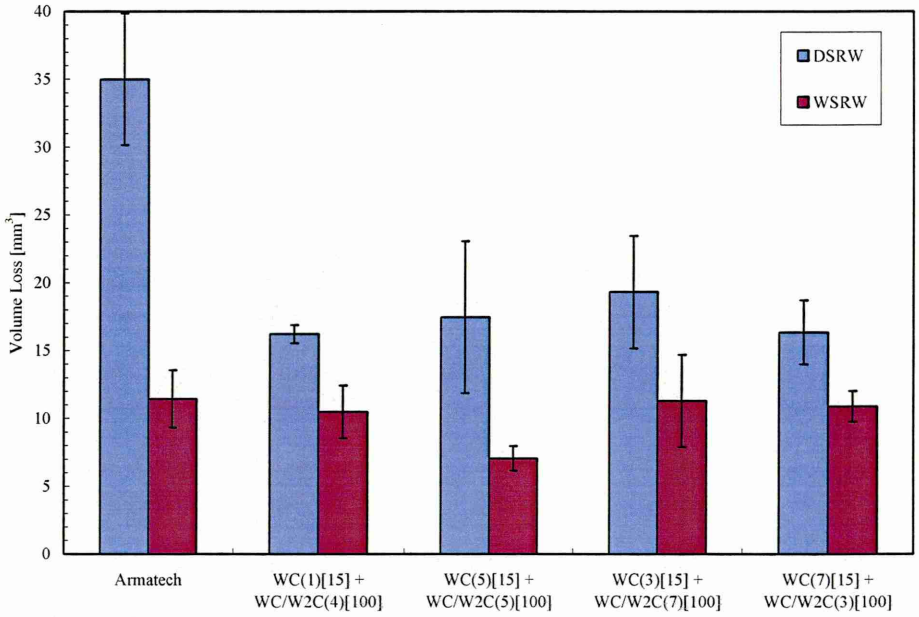

Figure 155: Effect of dry and wet environment on the volume loss of Armatech and mixed ratios of 10 μm WC and 100 μm WC/W_2C modified Armatech using the ASTM G65 test rig.

A large reduction in volume loss was observed with the 50 μm Al_2O_3 material, 75% lower in the wet when compared with the dry environment. The 10 μm Al_2O_3 addition was slightly lower at 55% less volume removal and the Mo_2C material was around 40% lower.

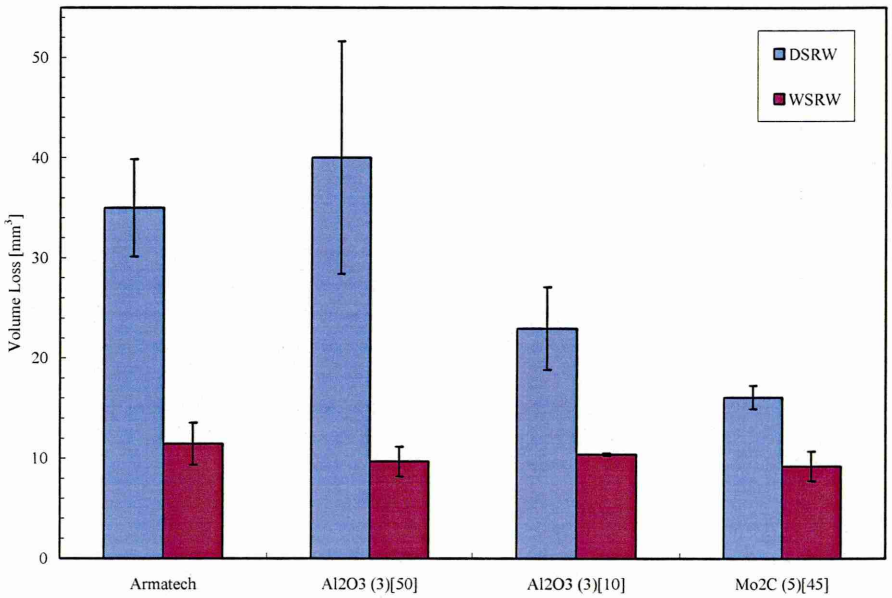

Figure 156: Effect of dry and wet environment on the volume loss of Armatech and 10 and 50 μm Al_2O_3 and 45 μm Mo_2C modified Armatech using the ASTM G65 test rig.

The likelihood for the reduction in material loss is most likely due to the water acting as a lubricant, reducing friction and therefore the amount of abrading energy the wear surface experiences. It may also be that case that the water acts in a flushing manner, washing out abrasive from the wear interface which reduces the severity of wear. A further consideration is that the water acts as a hydrodynamic film separating the wearing surfaces to a greater extent, reducing the degree of indentation from the abrasive particles, however, this would possibly lead to three-body indentations as the abrasive would be free to roll along the surface, which were not present on the wear surfaces.

The graphs below in Figure 157 and Figure 158 represent the values of $RWR_{[Boron]}$ for all materials in both wet and dry environments, plotted in ascending order. Note that for RWR results the larger the number the better the wear resistance.

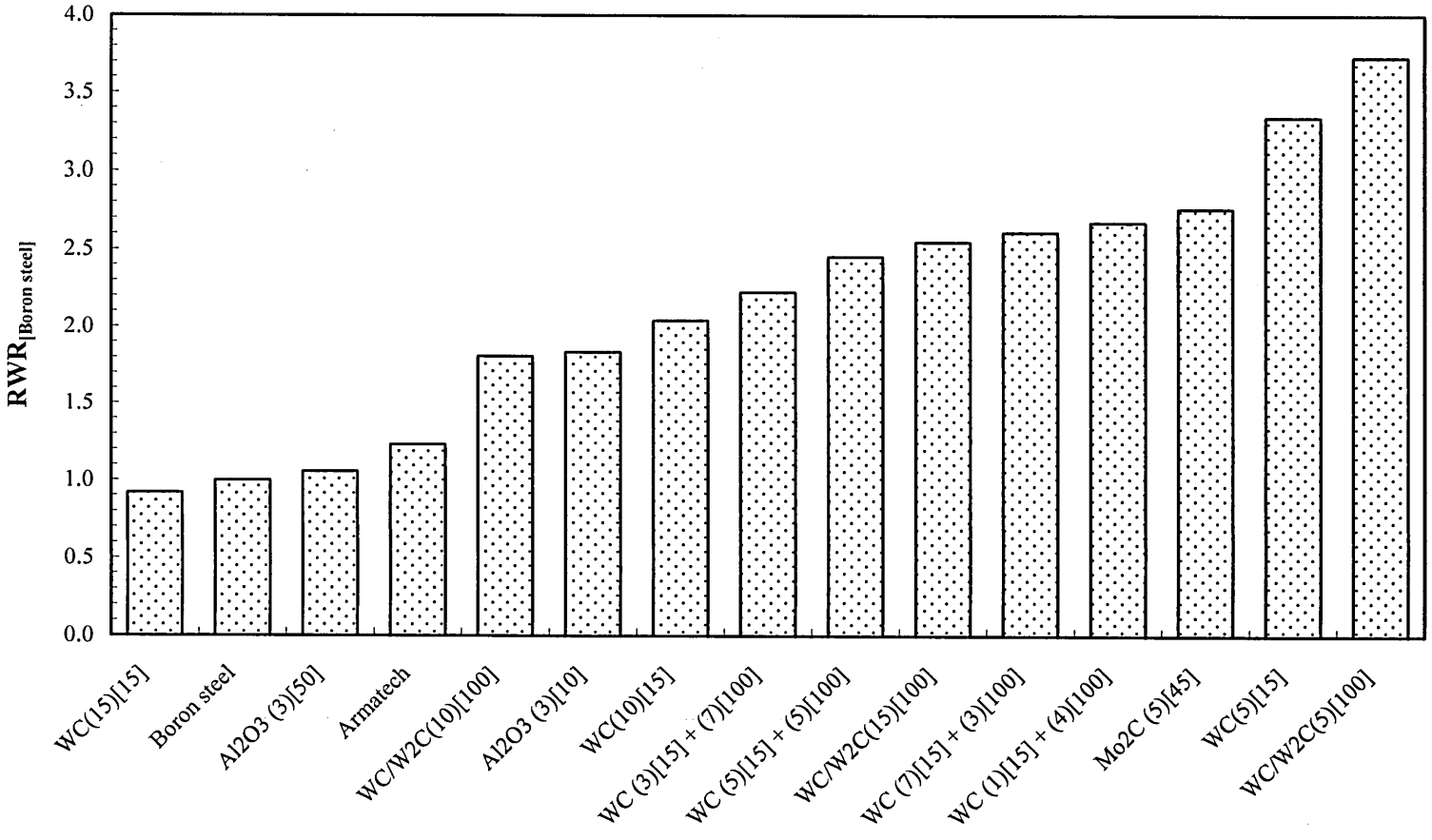

Figure 157: Relative wear resistance values with respect to boron steel for DSRW test.

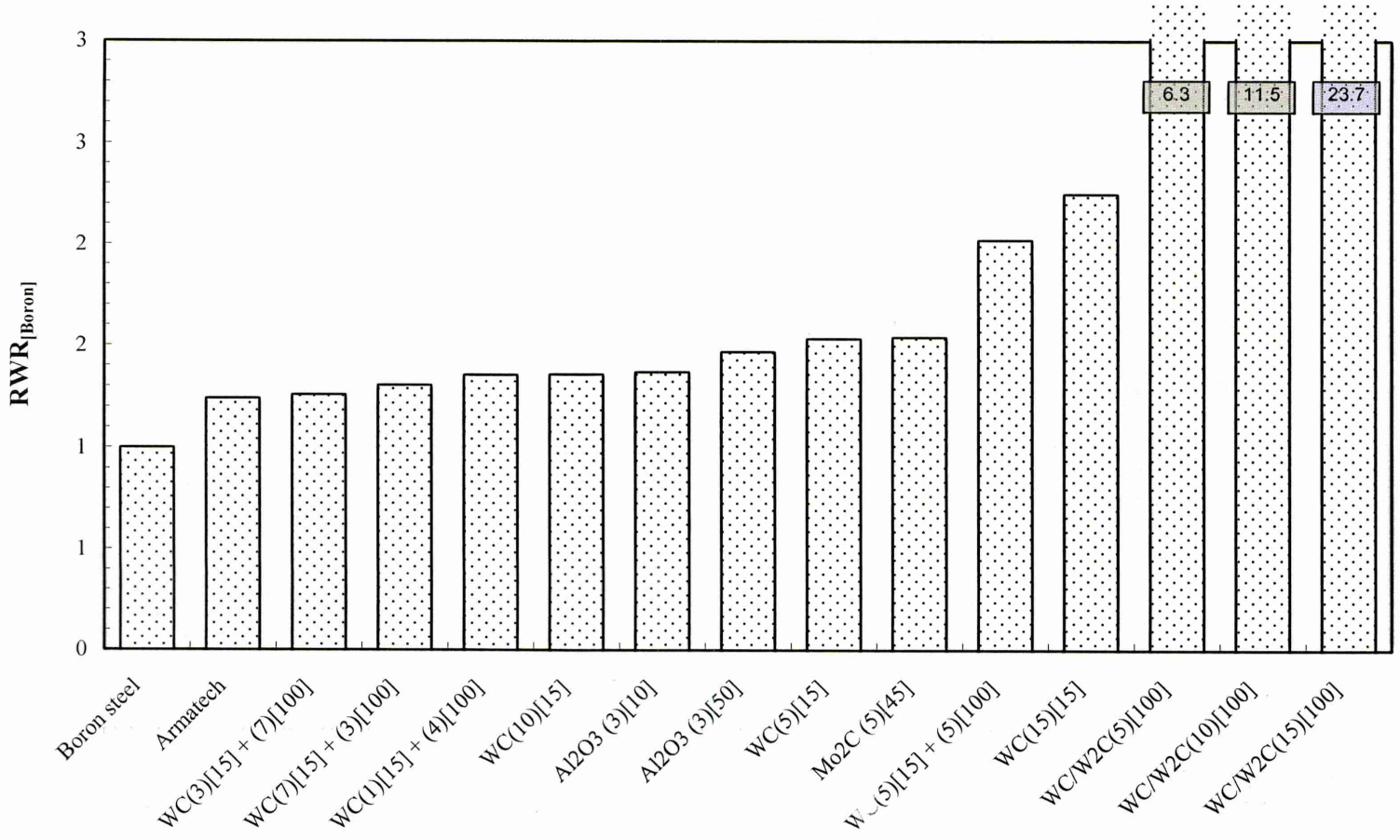

Figure 158: Relative wear resistance values with respect to boron steel for WSRW test.

6.7.4 *SEM observation of wear surface morphology*

Optical images of typical wear scars produced using both dry and wet 260 μm silica sand on boron steel ((a) and (b)) and $WC/W_2C(5)_{[100]}$ ((c) and (d)) are shown below in Figure 159.

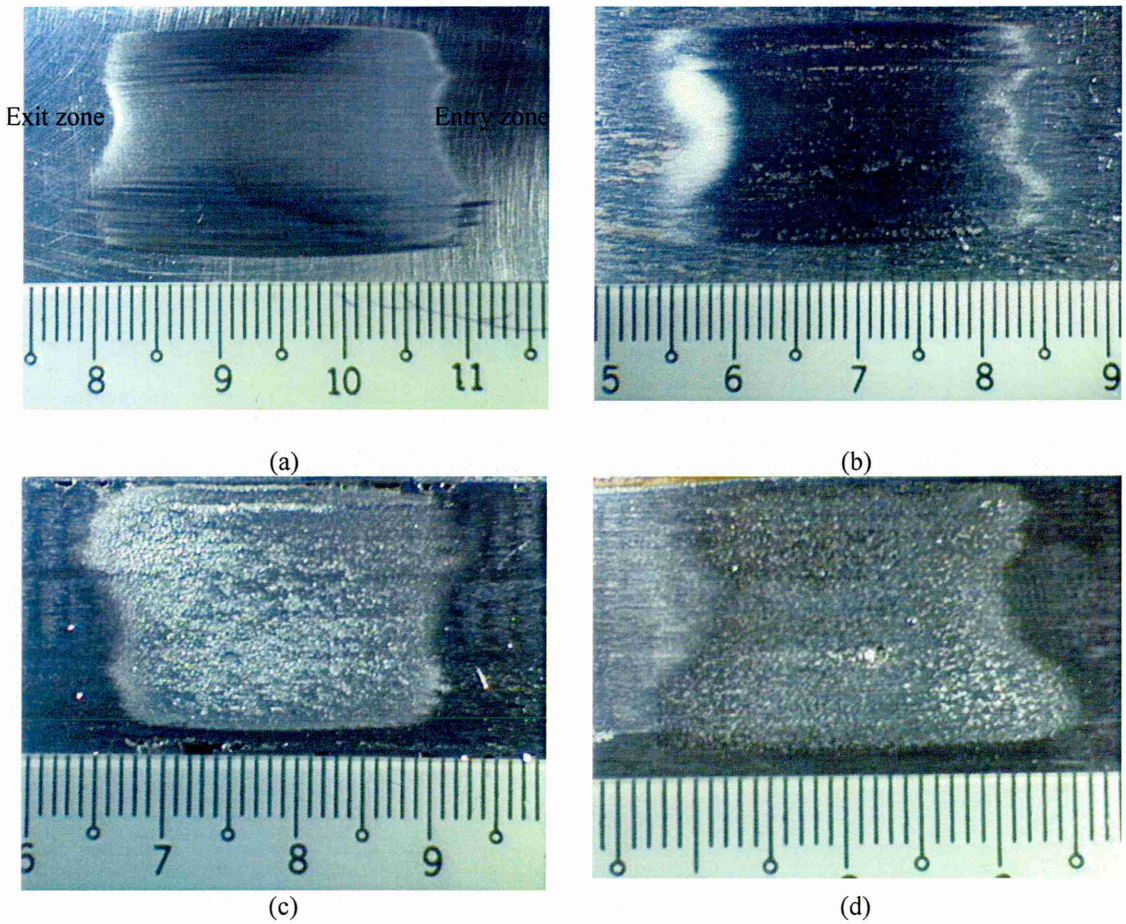

Figure 159: Typical rubber wheel wear scars using 260 μm sand; a) dry abrasive boron steel; b) dry abrasive $WC/W_2C(10)_{[100]}$; (c) wet abrasive boron steel and (d) wet abrasive $WC/W_2C(10)_{[100]}$.

It can be seen from Figure 159 that the abrasive entrance and exit regions of the wear scars exhibit irregular features. The scars can often exhibit an unevenness caused by a slight misalignment of the wheel.

The centre of the wear scars show parallel grooves. The images of the $WC/W_2C(10)_{[100]}$ surfaces in Figure 159(c) and (d) show that in both wet and dry environments, some pullout has occurred, these areas of pullout can be seen to have 'comet tails' in the direction of wear.

Surface profile analysis of sample DS8 ($WC(5)_{[15]}$) shows that the crater is asymmetrical, Figure 160.

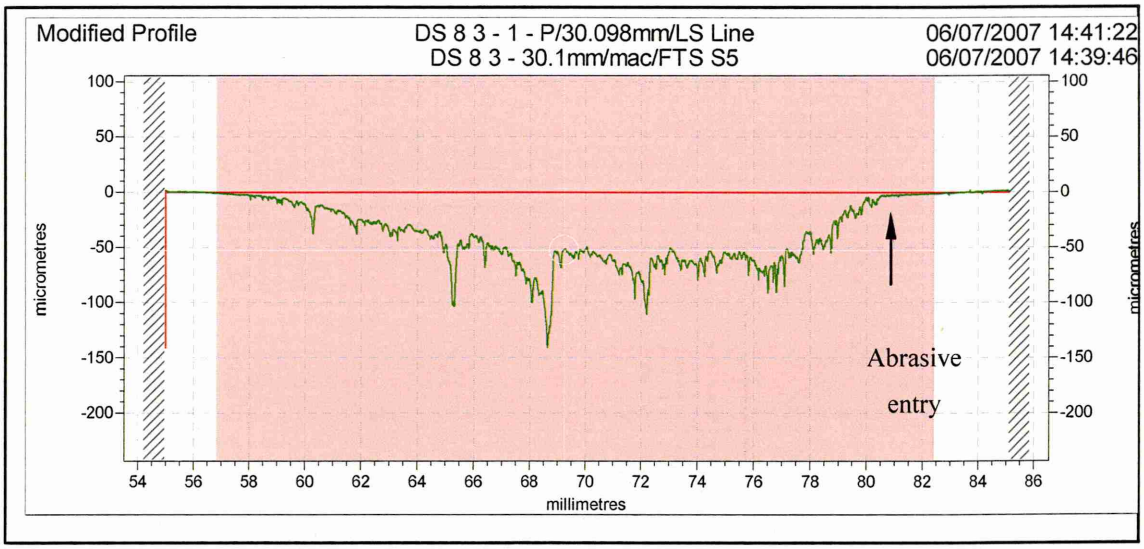

Figure 160: Profilometry of a typical DSRW wear scar

It can be seen that the entry region for the abrasive (right hand side) appears to have a steeper profile than the exit region. This can be attributed to the way the abrasive feed works. The abrasive particles are fed onto the rubber wheel just before the wheel/sample interface where some of the abrasive is lost over the wheel edges and the remaining abrasive is fed into the sample interface. This can cause a slight build up of abrasive at the first point of entry creating a higher rate of material removal at this point. It can also be seen from the trace that the crater appears to have a maximum depth of around 50 µm. The sharp valleys seen in the centre of the wear scar may be caused by regions of hard phase pullout.

6.7.5 SEM of wear morphology; Dry environment

An area from a sample of each material tested using the DSRW was examined by SEM to observe the wear mode.

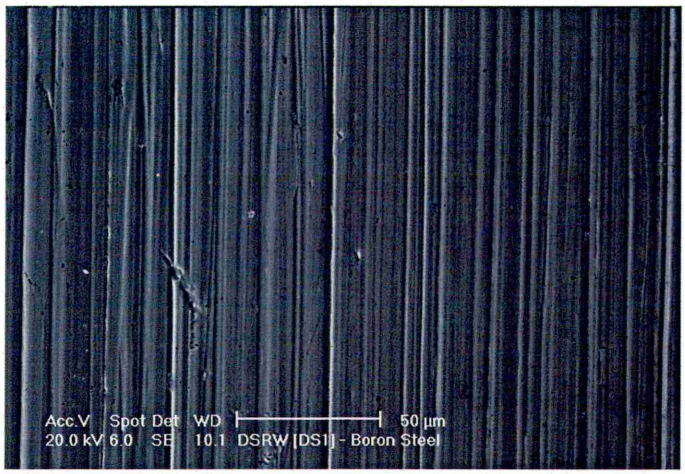

Figure 161: Wear surfaces of boron steel at 130 N applied load, 260 µm silica sand; modified ASTM G65 dry environment.

Examination of the wear scar on boron steel produced using the a dry environment shows very clear two-body directional wear grooves as shown in Figure 161. The grooves show little signs of interruption.

Polished cross-sections of the wear scars, sectioned 90° to the direction of wear were examined to assess the surface topography and the extent of subsurface damage. A cross-section through a boron steel sample abraded under dry conditions is shown below in Figure 162. It can be seen from the cross-section that the wear surface actually has a very smooth appearance with no obvious deep wear grooves visible or any detectable subsurface damage or cracking.

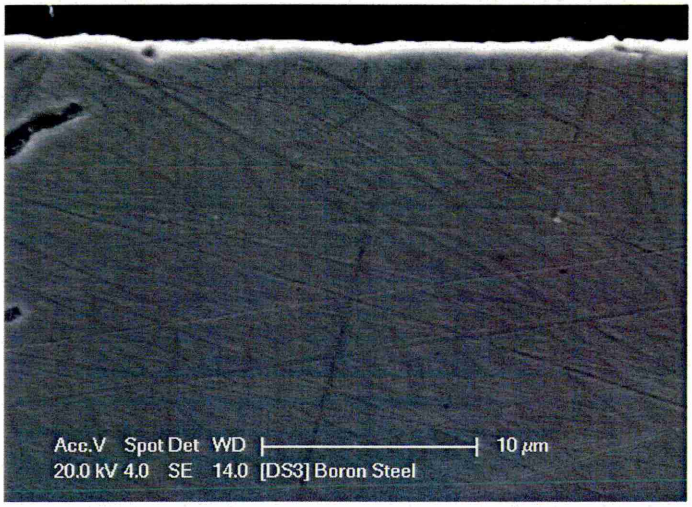

Figure 162: Cross-section of DSRW scar on boron steel 90 degrees to the rolling direction.

(a)

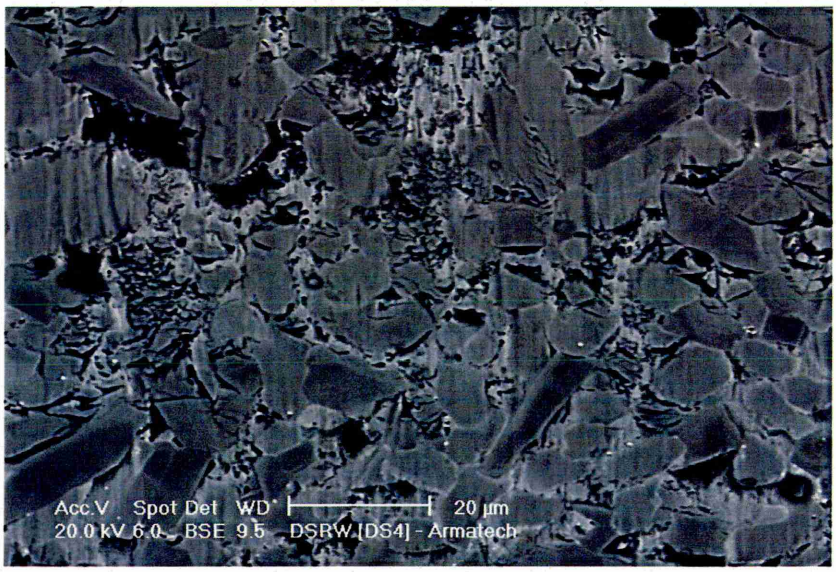

(b)

Figure 163: Wear surfaces of Armatech at 130 N applied load, 260 µm silica sand; modified ASTM G65 dry environment.

Figure 163 shows the wear scars produced on Armatech with some evidence of two-body grooving observed but in this case it had a more rounded and smooth appearance when compared to the morphology of the scars on boron steel (Figure 161). The grooves are much less pronounced and it appears that the Fe-Cr borides/carbides appear to stand proud of the surface with the softer Fe-Ni matrix being preferentially worn away. Higher magnification of the wear scar, shown in Figure 163(b), shows both two-body grooves on the Fe-Cr hard phase but also reveals that the hard phases have cracked laterally and there is also a high degree of hard phase/matrix interface cracking or de-bonding. The Fe-Ni matrix does not suffer three-body rolling wear in this test as seen with the MSAW test.

The wear mechanism is most likely due to the abrasive particles becoming embedded in the surface of the rubber wheel and passing across the surface of the sample without rotating. Note

that this is analogous to the two-body sliding wear which occurs in the MSAW test but with much larger abrasives.

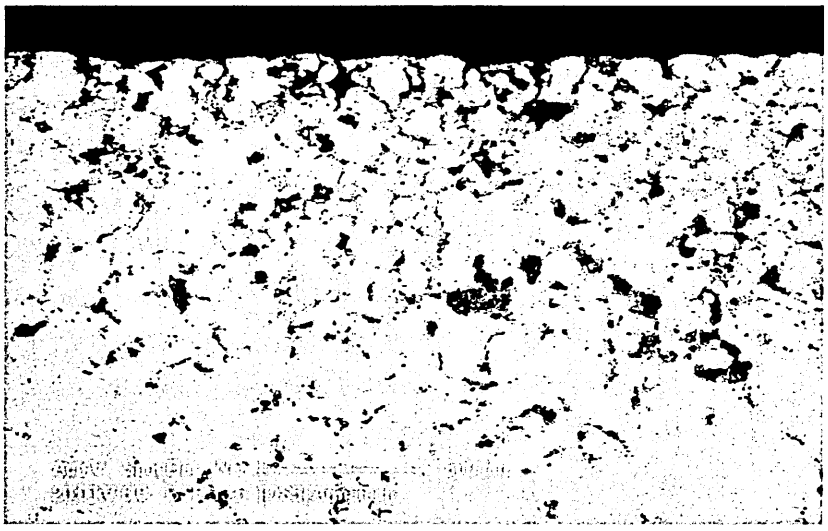

Figure 164: Cross-section of DSRW scar on Armatech 90 degrees to the rolling direction.

Examining the cross-section of the wear scar of Armatech the degree of porosity and content level of residual binder can be seen by the dark areas. Again close inspection of the wear surface did not reveal any clearly definable wear grooves, but the level of porosity made this difficult to confirm.

Examination of materials with 15 μm WC additions revealed regions of pullout as shown in Figure 165. Higher magnification inspection of these areas, Figure 165(b), revealed evidence of micro-cracking. It was also clear that the WC addition, where fully bonded with the matrix, acted as a hard phase that resisted wear by the silica sand abrasives.

A similar mode of material removal and the presence of micro-cracking could be seen with an addition of 10wt.% but a higher level of fallout was observed as shown in Figure 165(c).

(a)

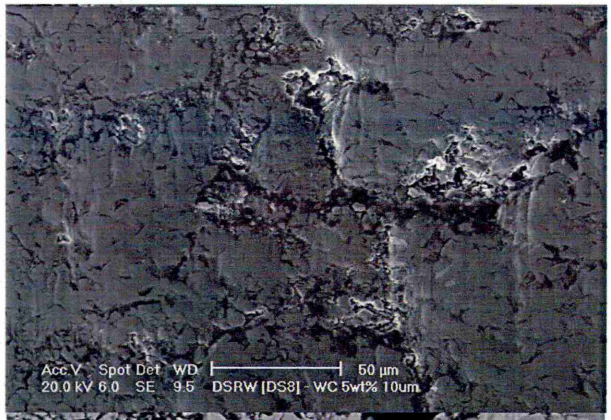

(b)

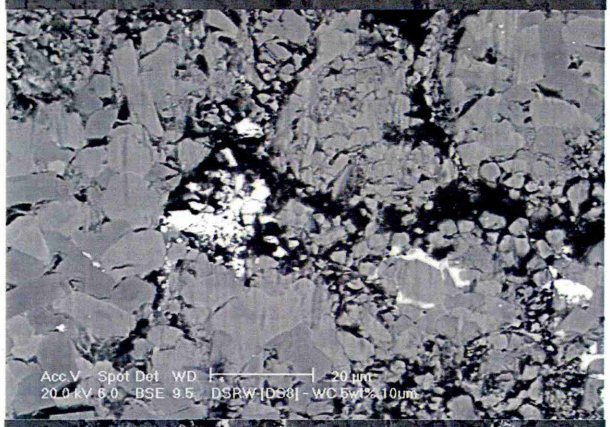

(c)

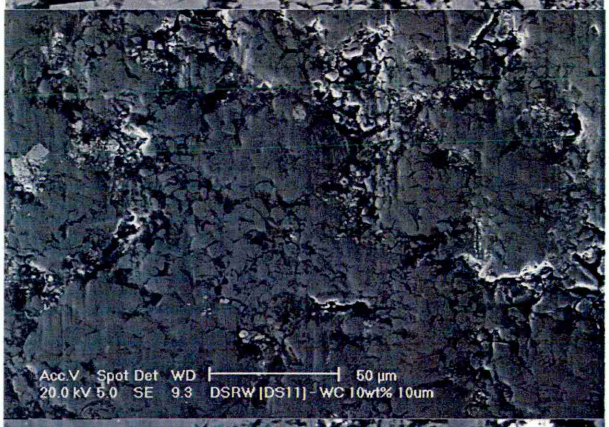

(d)

Continued…

(e)

(f)

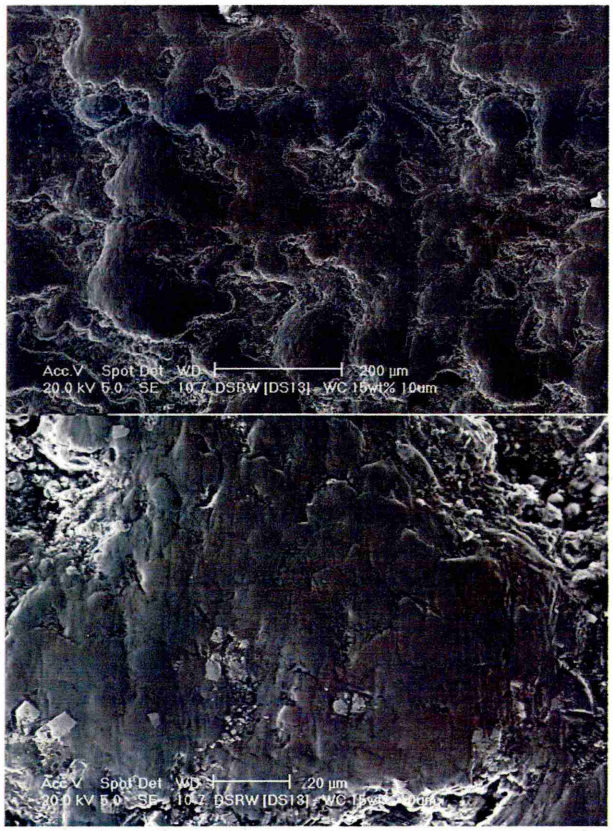

Figure 165: Wear surfaces of (a) 5wt.% 15 µm WC; (b) high magnification; (c) 10wt.% 15 µm WC; (d) high magnification; (e) 15wt.% 15 µm WC and (f) high magnification at 130 N applied load, 260 µm silica sand; modified ASTM G65 dry environment.

A cross-section through the wear scar of a material containing WC additives ($WC(10)_{[15]}$) revealed that sub-surface cracking had occurred in the Armatech material immediately above a WC particle to a depth of several microns of the surface as shown in Figure 166(a). Where a WC particle intersected the surface it was also observed that the 15 µm WC particles appeared to be contributing to the overall wear resistance as they were observed to stand proud of the Armatech as shown in Figure 166(b).

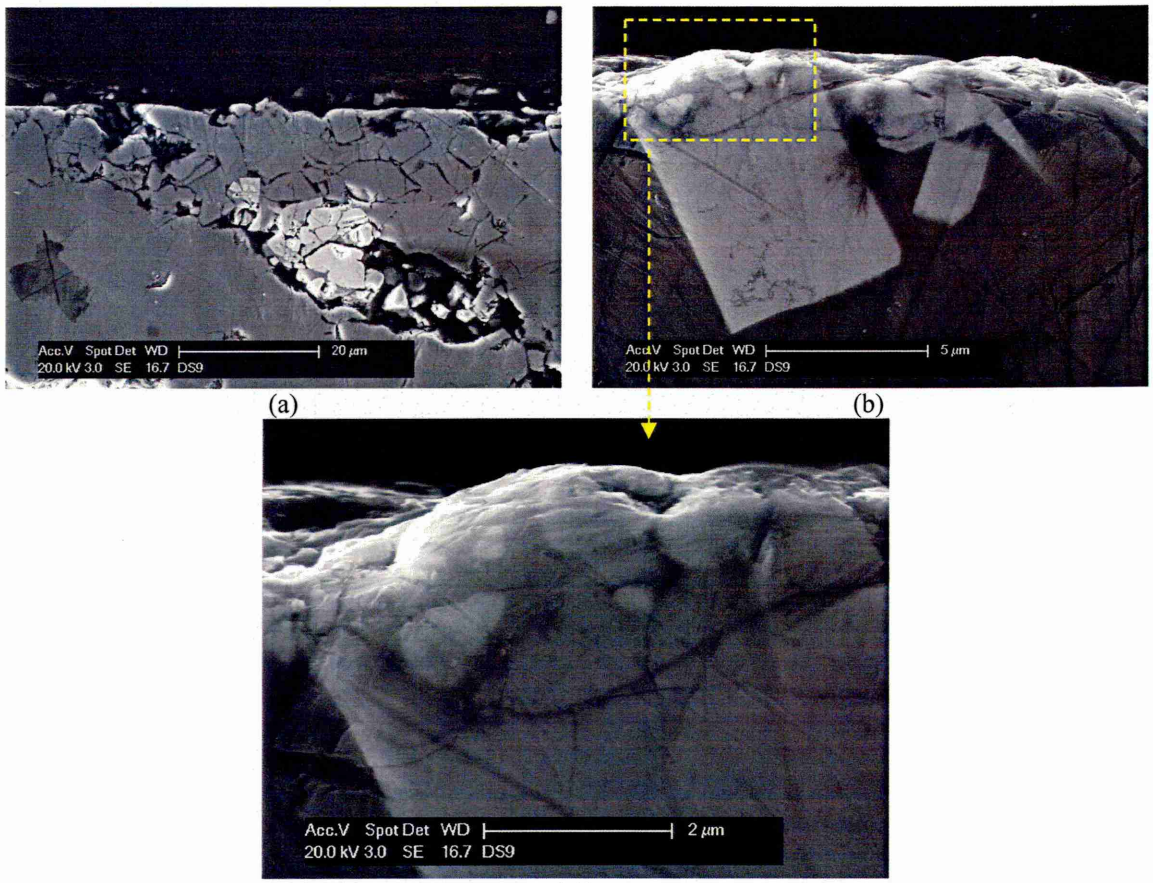

Figure 166: Cross-section of DSRW scar on 10wt.% 15 µm WC 90 degrees to the rolling direction.

SEM examination of Armatech with additions of 100 µm WC/W_2C show that the added hard phase had sintered well within the existing microstructure and could be seen to be protruding from the surface after the test The additions had a rounded appearance confirming that they had resisted wear without cracking. While in general, the addition appeared to be contributing to the wear resistance, some evidence of WC fallout was observed. Inspection of the surrounding Armatech microstructure showed the same wearing mechanism observed with Armatech alone (Figure 163(b)). The major wear mode seen was two-body grooving. It was also apparent that the WC particle appeared to have a surrounding zone where the Armatech matrix suffered a higher extent of cracking. This suggests that the WC affects the chemistry in this region rendering the Armatech more brittle and prone to this phenomenon, evident in Figure 163(b) and (d).

(a)

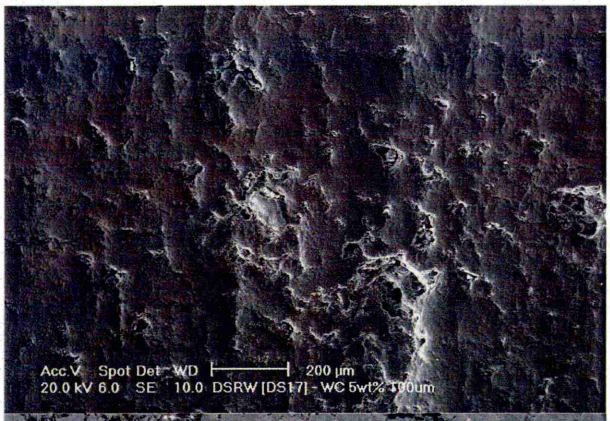

(b)

(c)

(d)

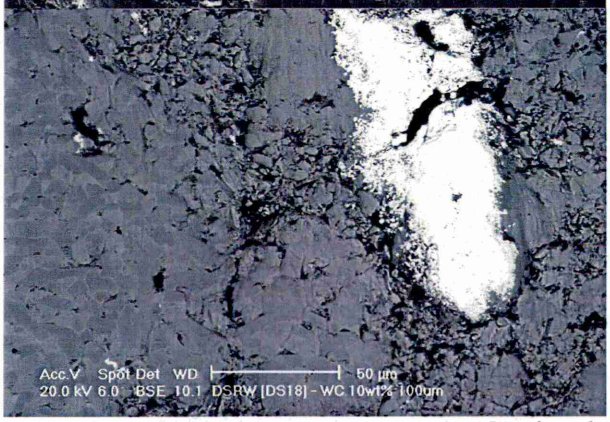

Continued…

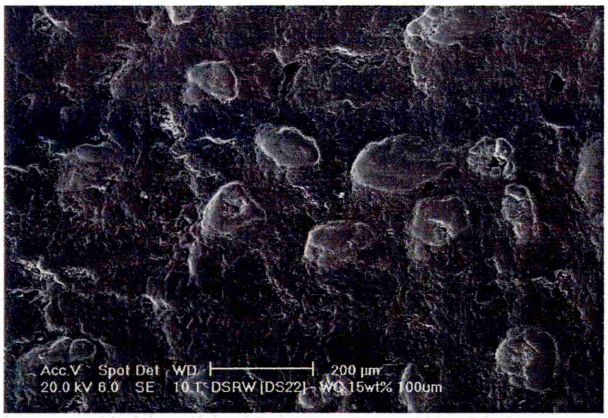

(e)

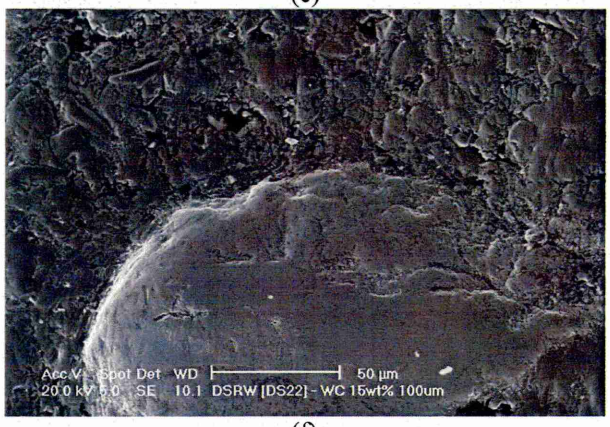

(f)

Figure 167: Wear surfaces of (a) 5wt.% 100 µm WC/W_2C; (b) high magnification; (c) 10wt.% 100 µm WC/W_2C; (d) high magnification; (e) 15wt.% 100µm WC/W_2C and (f) high magnification at 130 N applied load, 260 µm silica sand; modified ASTM G65 dry environment.

Examination of the cross-section of wear scars on a material containing 100µm WC particles ($WC/W_2C(10)_{[100]}$) revealed that a large degree of pullout had occurred (Figure 168). The surface topography in Figure 168(a) shows where a WC particle has resisted wear and is standing proud of the surface. Higher magnification images (Figure 168(b) and (c)), show the surface and hence wearing mechanism of a WC particle. The micrograph in Figure 168(d) shows one mechanism of material loss from a WC/W_2C particle. It can be seen that the particle has fractured and a large quantity was in the process of breaking away.

(a)

(b)

(c)

(d)

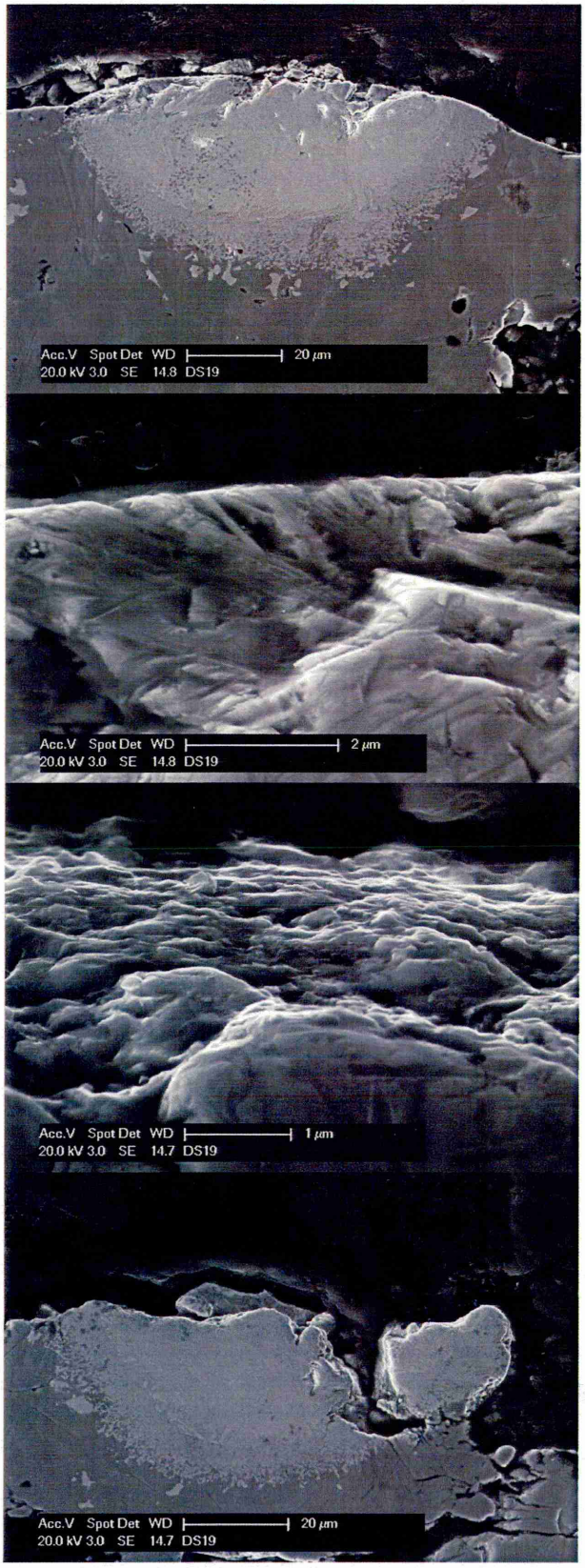

Figure 168: Cross-section of DSRW scar on 10wt.% 100 µm WC/W_2C 90 degrees to the rolling direction; (a) shows fallout of WC particle (b) shows WC particle standing proud of surface, (c) shows wear of WC particle and (d) shows fracture mechanism of WC particle.

Examination of the materials with mixed size additions of 15 μm WC plus 100 μm WC/W_2C revealed that the wear mechanisms observed above were combining in these materials. The larger 100 μm WC/W_2C particles were protruding from the surface with a rounded appearance, Figure 169(a), and the smaller 15 μm particles can be seen dispersed among the existing structure with some cracking present, Figure 169(b). The effect of the 100 μm WC particles on the sinter quality of the surrounding Armatech can still be seen, with a higher degree of cracking around each particle. The addition of both sizes of particulate WC did not appear to affect the way in which the existing Armatech microstructure wears. It was observed that some degree of pullout had occurred.

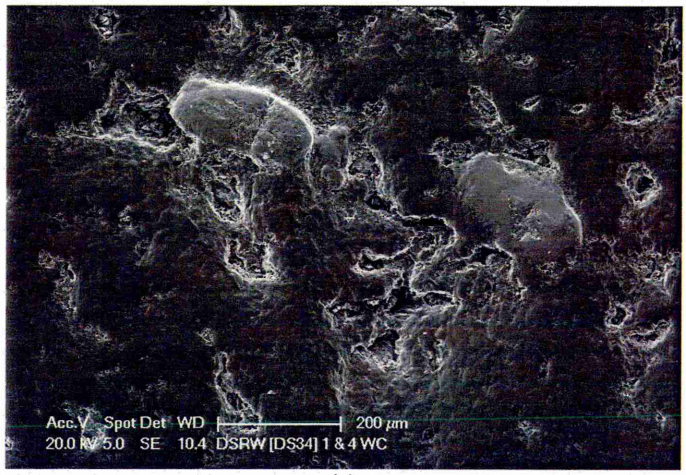

(a)

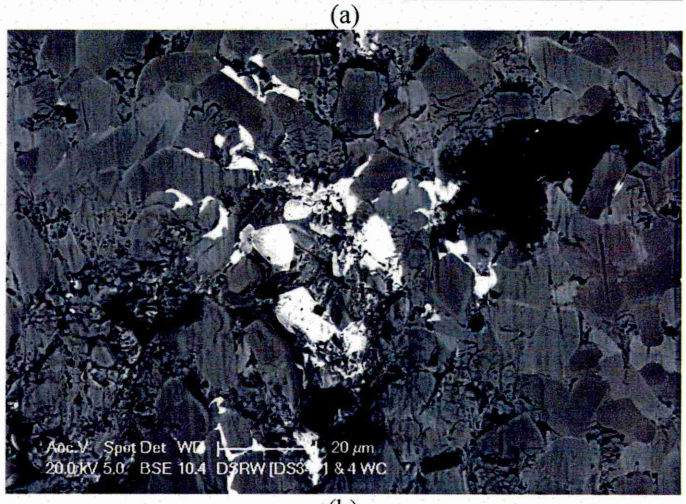

(b)

Figure 169: Wear surfaces of (a) 1wt.% 15 μm and 4wt.% 100 μm WC/W_2C and (b) high magnification at 130 N applied load, 260 μm silica sand; modified ASTM G65 dry environment.

The addition of 10 μm Al_2O_3 at 3wt.% did not appear to have any effect on the wear mode when compared to Armatech. It is clear from Figure 170(a) that the Al_2O_3 addition had not fused with the Armatech and offered little improvement wear resistance.

The wear scar of the 50 μm Al_2O_3 material, shown in Figure 170(c), had a very different appearance to the 10 μm addition. Two-body groves were more definable with very clear

plastic deformation creating fins at the groove edges. The larger particle size addition appeared to have sintered within the microstructure better. High magnification of the addition, Figure 170(d), revealed two-body grooves with material pushed up to create fin edges, but also showed cracking radiating out from the particle.

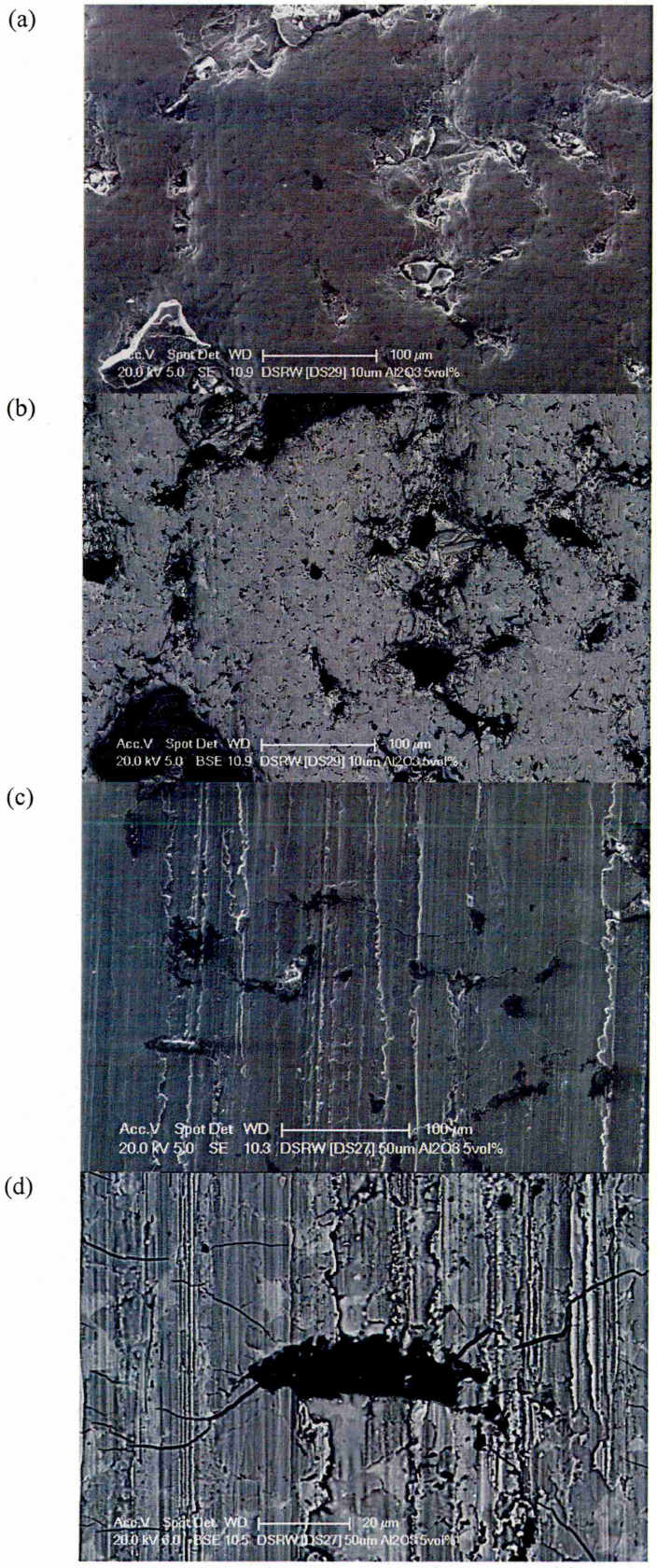

Figure 170: Wear surfaces of (a) 3wt.% 10 µm Al_2O_3; (b) high magnification; (c) 3wt.% 50 µm Al2O3 and (d) high magnification at 130 N applied load, 260 µm silica sand; modified ASTM G65 dry environment.

It can be seen from Figure 171 below that the 50 μm Al_2O_3 addition was prone to pullout due to the poor bonding of the addition and matrix phase. This poor bonding is shown in Figure 171(a) with the matrix around the Al_2O_3 particles has not bonded with the particle. The micrograph in Figure 171(b) shows where a particle has been removed.

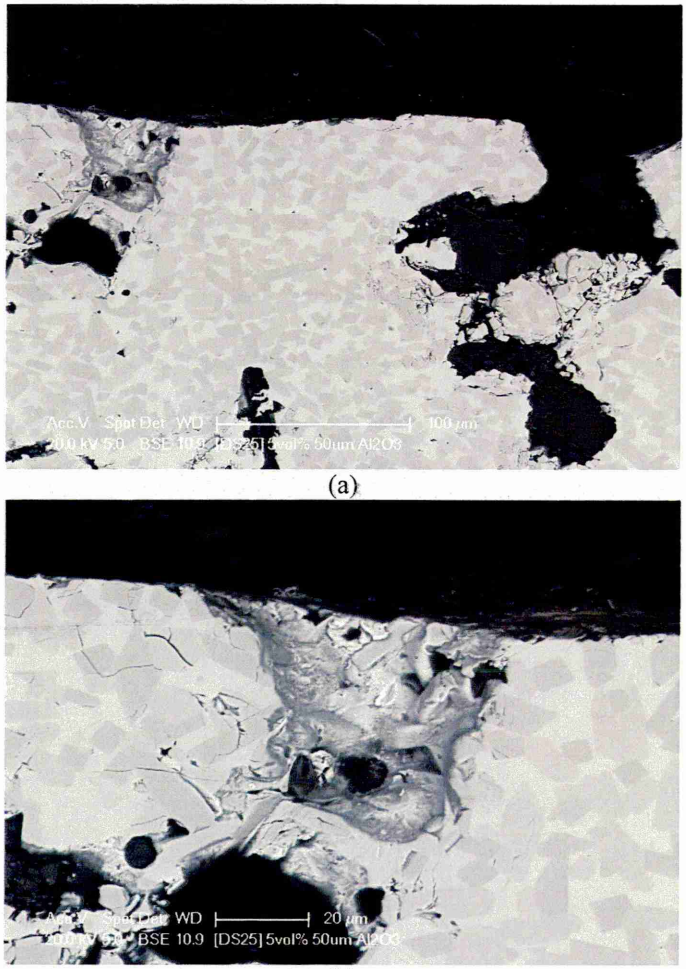

Figure 171: Cross-section of DSRW scar on mixed 3wt.% 50 μm Al_2O_3 90 degrees to the rolling direction.

The micrographs in Figure 172 show the wear scars of the 45 μm Mo_2C material. It can be seen in Figure 172(a) that the surface is very similar in appearance to standard Armatech but with some pullout. Closer inspection of the addition in Figure 172(b) and (c) shows that the 45 μm particles actually consist of smaller particles of Mo_2C. For this reason the material acts in a manner more akin to the wear process observed with 15 μm WC rather than the manner seen with larger particle size additions.

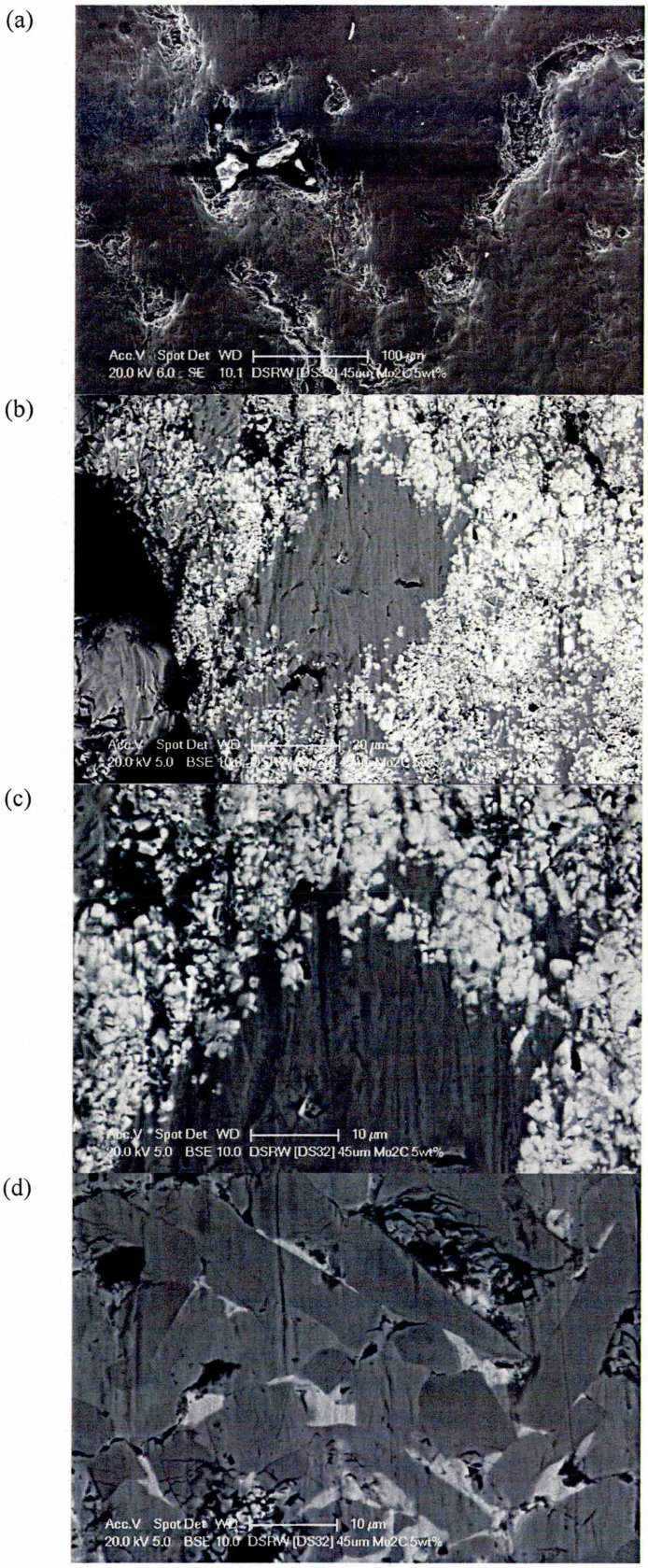

Figure 172: Wear surfaces of (a) 5wt.% 45 µm Mo_2C; (b) and (c) high magnification at 130 N applied load, 260 µm silica sand; modified ASTM G65 dry environment.

6.7.6 *Wet Environment*

Results from the test using the wet sand can be seen in the following SEM micrographs of the wear scar surfaces in Figure 173 to Figure 185.

The appearance of the wear scar on boron steel following wear using a wet environment is very similar to that seen in the dry environment, two-body grooving can be clearly distinguished, Figure 173.

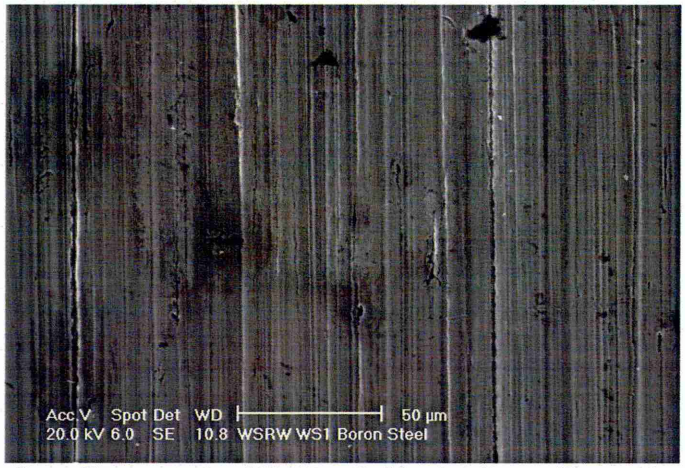

Figure 173: Wear surface of boron steel at 130 N applied load, 260 µm silica sand; modified ASTM G65 wet environment.

It can be seen from the cross-section of the wear scar that the severity of damage to the surface layers is minimal and no abrasive embedment was observed, Figure 174.

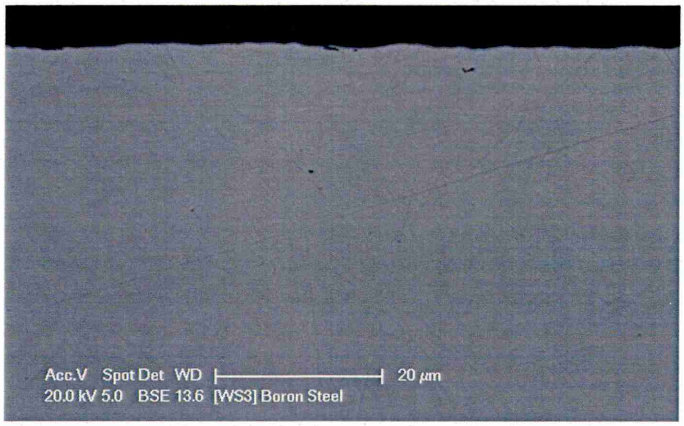

Figure 174: Cross-section of WSRW scar on boron steel 90 degrees to the rolling direction.

Figure 175(a) shows that whilst the wear mode consists of two-body grooving, the appearance, when compared to boron steel under wet conditions and the surface appearance of Armatech produced under a dry environment, was much smoother.

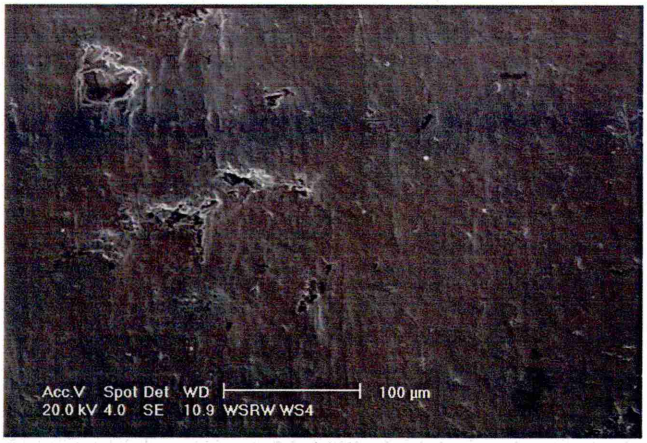

(a)

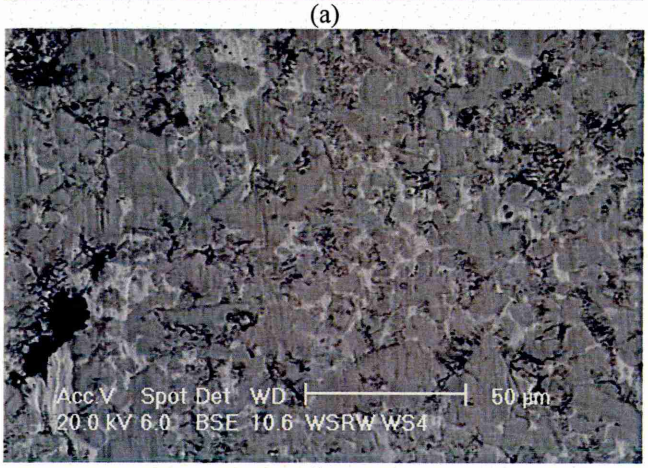

(b)

Figure 175: Wear surface of Armatech at 130 N applied load, 260 µm silica sand; modified ASTM G65 wet environment.

It was observed that the cross-section of the Armatech wear scar exhibited shallow (5-10 µm) sub-surface cracks parallel to the wear surface. These appeared intermittently along the width of the wear scar and.

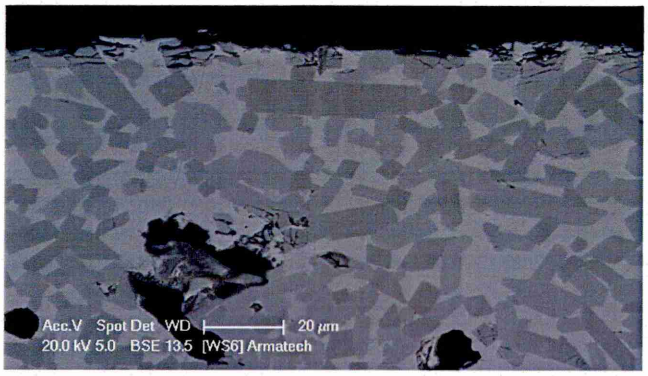

Figure 176: SEM micrograph of WSRW scar cross-section scar on Armatech 90 degrees to rolling direction.

The appearance of the wear scar on $WC(5)_{[15]}$ under wet conditions shows two-body grooving but also a degree of plastic deformation, Figure 177(a). The 10wt.% addition shows two-body grooving also and some evidence of fallout is apparent. It can also be seen that, as for the dry

sand test, micro-cracking has occurred in the areas around the small WC addition, (Figure 177(b)). Increasing the addition of 15 μm WC to 15wt.%, Figure 177(c), appears to increase the level of micro-cracking within the microstructure.

(a)

(b)

(c)

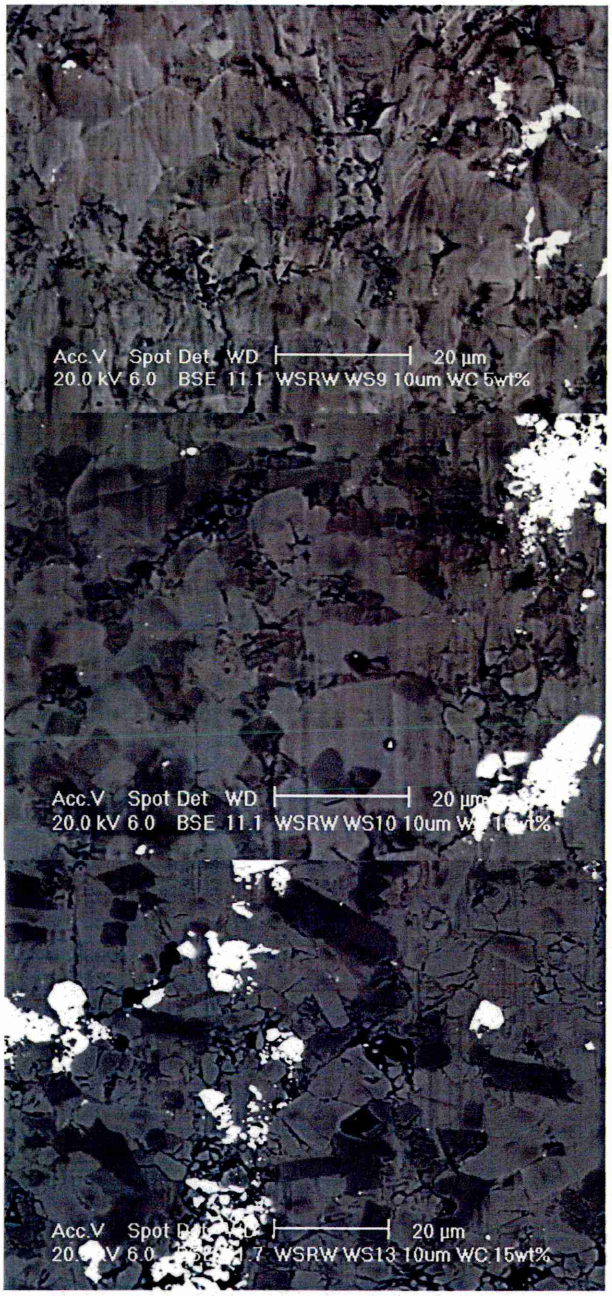

Figure 177: Wear surface of (a) 5wt.% 15 μm WC; (b) high magnification; (c) 10wt.% 15 μm WC; (d) high magnification; (e) 15wt.% 15 μm WC and (f) high magnification at 130 N applied load, 260 μm silica sand; modified ASTM G65 wet environment.

Examination of the cross-section of the wear scar of $WC(10)_{[15]}$ showed that the WC particles were, in areas, contributing to the wear resistance of the material. Figure 178 below shows a collection of WC particles standing slightly proud of the surface of the wear scar surface having been worn and appearing to resist against wear.

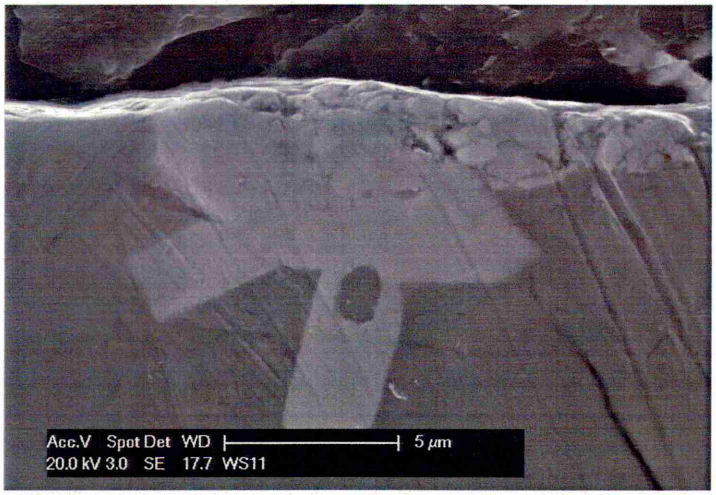

Figure 178: SEM micrograph of cross-section of WSRW scar on 10wt.% 15 μm WC 90 degrees to the rolling direction.

The appearance of the wear scar on a material with 100μm WC particles ($WC/W_2C(5)_{[100]}$) revealed a smoothed two-body grooving wear mechanism, (Figure 179(a)). Inspection of the particles, Figure 179(b), revealed two-body grooving wear but the central core of the particles had suffered from fracture and pullout. The role of the particles in resisting wear appeared to be less dominant than in dry conditions. The WC particles were not standing proud of the surface but appeared to be wearing at a similar rate.

(a)

(b)

(c)

(d)

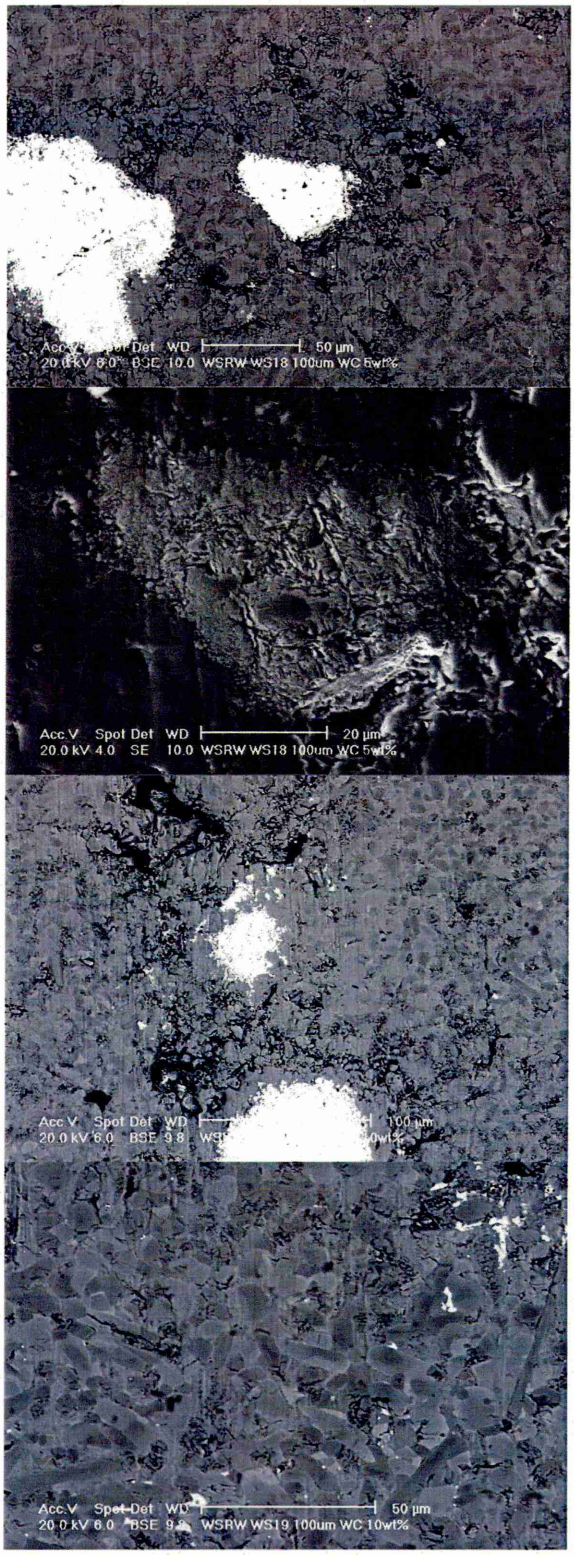

Figure 179: Wear surface of (a) 5wt.% 100 µm WC/W_2C; (b) high magnification; (c) 10wt.% 100 µm WC/W_2C; (d) high magnification, 130 N applied load, 260 µm silica sand; modified ASTM G65 wet environment.

It can be seen from the cross-section of the 10wt.% addition scar that the 100µm WC particles do not appear to be standing proud of the surface and in fact some degree of fallout was observed (Figure 180(a)). The WC particle present at the surface appeared to have suffered from cracking, the most likely cause of hard phase removal, Figure 180(b).

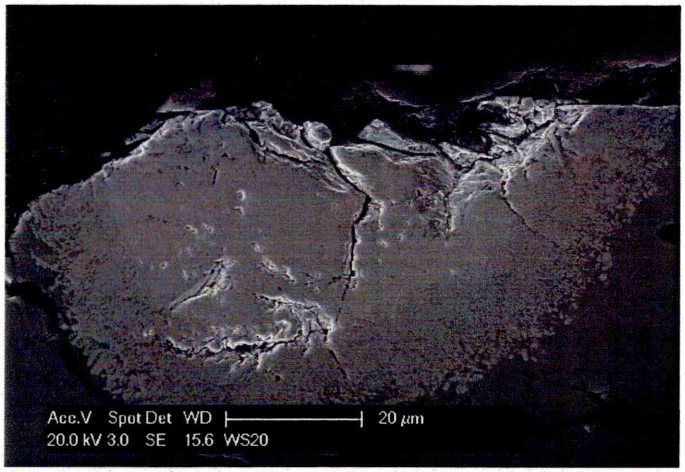

(a)

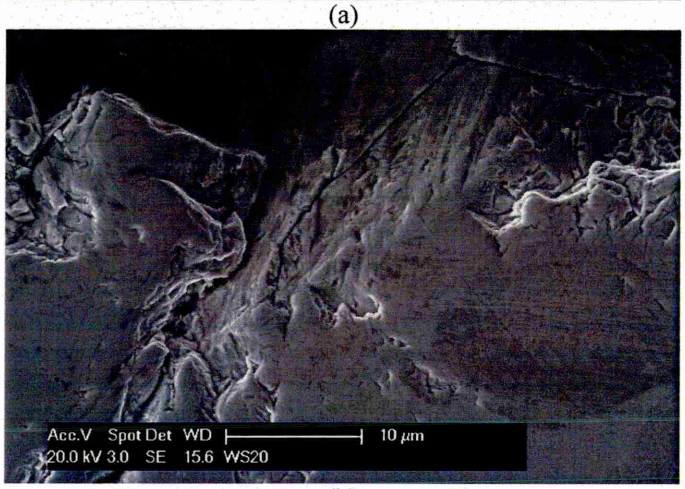

(b)

Figure 180: SEM micrographs of cross-section of WSRW scar on 10wt.% 100 μm WC/W_2C 90 degrees to the rolling direction.

Figure 181 shows a wear scar produced on a mixed particle size WC material, (1wt.% 15 μm and 4wt.% 100 μm). The overall appearance of the wear scar was an undulating two-body wear mode. Inspection of the WC additions showed the same wearing mode as observed with individual additions.

(a)

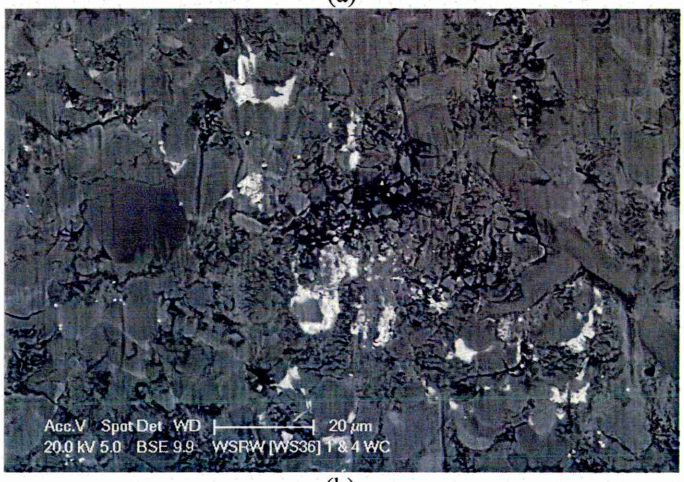

(b)

Figure 181: Wear surface of (a) 1wt.% 15 µm and 4wt.% 100 µm WC and (b) high magnification at 130 N applied load, 260 µm silica sand; modified ASTM G65 wet environment.

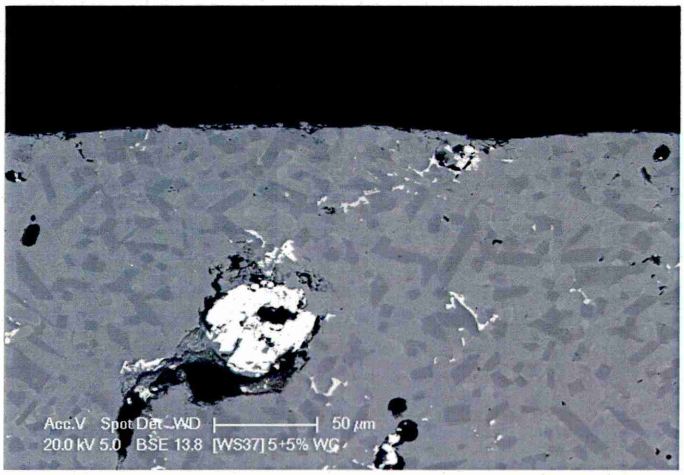

Figure 182: SEM micrograph of cross-section of WSRW scar on mixed 5wt.% 15 µm and 5wt.% 100 µm WC 90 degrees to the rolling direction.

(a)

(b)

(c)

(d)

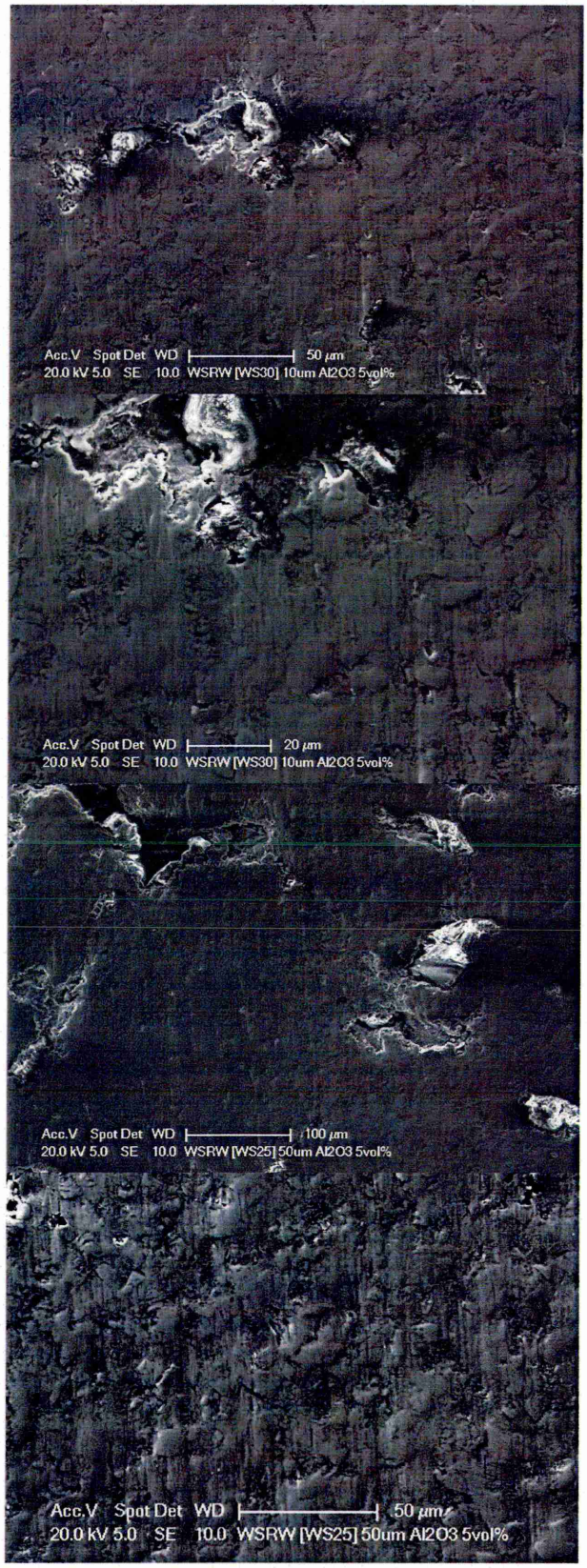

Figure 183: Wear surfaces of (a) 3wt.% 10 µm Al_2O_3; (b) high magnification; (c) 3wt.% 50 µm Al_2O_3 and (d) high magnification at 130 N applied load, 260 µm silica sand; modified ASTM G65 wet environment.

Examination of the Al_2O_3 materials showed that the 10 μm particle addition possessed a similar two-body wear mode appearance to that of the dry environment but somewhat smoother in appearance.

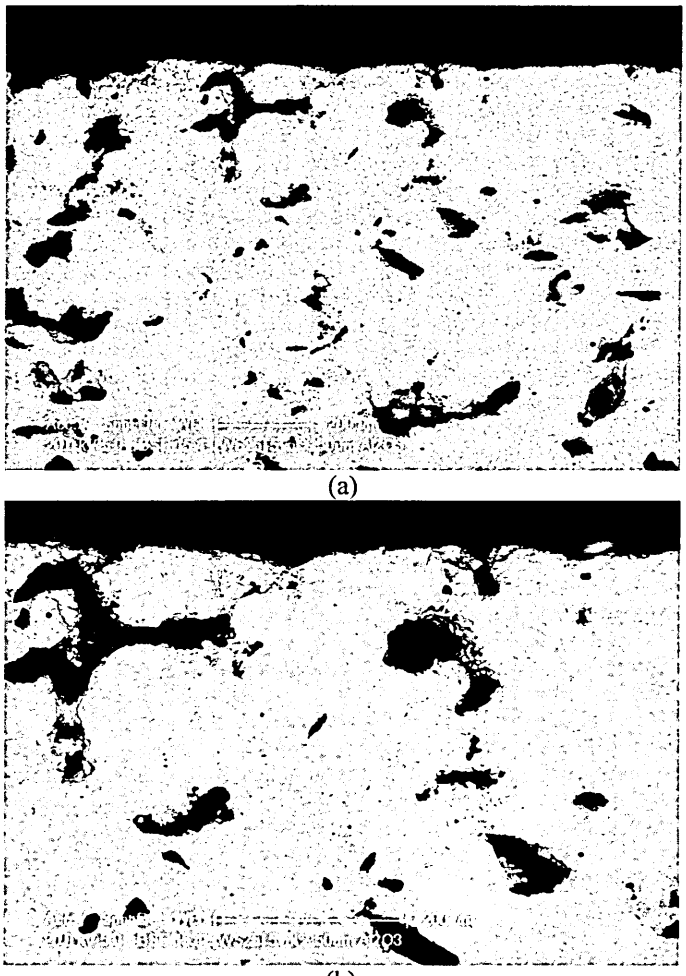

(a)

(b)

Figure 184: SEM micrographs of cross-section of WSRW scar on mixed 3wt.% 50 μm Al_2O_3 90 degrees to the rolling direction.

Figure 185: Wear surfaces of 5wt.% 45 µm Mo_2C addition at 130 N applied load, 260 µm silica sand; modified ASTM G65 wet environment.

The overall appearance of the Mo_2C addition material was very similar to that for standard Armatech with a smoothed two-body wear mechanism, Figure 185(a). Closer inspection of the addition shows that they had dispersed throughout the microstructure and were resisting wear in a two-body manner. It is also clear that some pullout of the addition had taken place, shown in

Figure 185(c). It was also observed that cracking of the Armatech microstructure was taking place.

6.7.7 Summary

Comparison of the wear mode produced using the ASTM G65 test with post service tool surfaces (Chapter 4) revealed that a similar mechanism was active. It was observed that the wear surfaces from the ASTM G65 test differed greatly between the wet and dry environments. The extent of damage is more pronounced in tests performed in the dry environment whereas the wet environment tests have a much smoother appearance.

The DSRW test on 100 μm WC/W_2C materials exhibited wear modes that were very similar to those from tools used in service (shown below in the next section on field testing). The carbides were seen to stand proud of the surface resisting against wear. It was expected that WSRW would replicate soil wear to a higher degree due to the moisture found in soil being replicated in the test conditions. Wear surfaces from the WSRW test however, all had a smoother appearance with no carbides standing proud of the surface. It may be the case however; that the process of the carbides standing proud of the surrounding material is quicker in the dry environment due to the level of wear severity, and longer test durations may eventually show this mechanism in the wet environment also.

It is also clear from weight loss measurements that the severity of damage is reduced in the presence of water indicating that the water acted as a lubricant between the wearing surface and abrasive, although the motion of the particle appears to not have changed, with two-body wear being the predominant wear mode. The presence of water may reduce the likelihood of particle fracture and embedment which suggests the stress experienced by abrasive particles is reduced. The presence of water may also reduce friction and hence impact energy of the particles on the wear surface.

6.8 Field Testing

While it was not intended that field trials be a significant part of this study, the opportunity was taken to carry out a small number of field trials with local farmers to assess the performance of the materials under real conditions and to allow the study of the wear modes active, at least in local soils.

6.8.1 Trial A - September 2006

The data presented below in Table 25 and Table 26 lists the weight loss and calculated volume loss for each component over a ploughed area of 110 acres. The RWR values listed in Table 25 and Table 26 are with respect to boron steel and Armatech tools which were present on the corresponding furrow side.

It should be noted that test samples used were coated in the usual manner employed by Chapmans. This meant that only the leading edges of tools were coated and inevitably some of the exposed boron steel substrate would have been lost due to wear.

The extent of boron steel loss was impossible to determine on the coated parts, it is however the leading edges of the tools that suffer the most wear in the initial stages and the amount of boron steel lost has been considered low or negligible for analysis purposes and more emphasis should be given to the weight loss measurements. Furrow 1 was not used for material testing as this is the most aggressive position. A photograph of the samples following removal from the plough after testing can be seen below in Figure 186 and in the Appendix. The photograph shows that most of the coating was worn away.

Figure 186: Photographs of ploughshares following 110 acres of testing, some patches of coating material can be still seen.

It can be seen that overall the points suffered higher material losses than the shares as was expected due to the points being subject to a more severe environment. The boron steel share and point suffered the highest material loss, followed by the Armatech coated tools, with the $WC/W_2C(10)_{[100]}$ coated tools providing the lowest loss overall.

The improvements of Armatech over boron steel supports the feedback received from farmers and Chapmans and the further improvement of $WC/W_2C(10)_{[100]}$ over Armatech supports the conclusions from both DSRW and WSRW test results.

It is also worth noting that the improvement demonstrated for Armatech over boron steel occurred with Armatech tools being placed in positions on the plough that experience a more aggressive environment than boron steel.

The $WC/W_2C(10)_{[100]}$ coated tools which experienced the lowest material loss were in the least aggressive position of the three, but these results would allow boron steel to be eliminated from further testing and allow a more direct comparison of Armatech and $WC/W_2C(10)_{[100]}$.

Table 25

Measured weight loss, calculated volume loss and RWR values for boron steel, Armatech and $WC/W_2C(10)_{[100]}$ coated points.

	Furrow	Side	Weight Loss [g]	Volume removed [cm^3][§§§§§]	**$RWR_{[Boron\ steel]}$**	**$RWR_{[Armatech]}$**
Armatech	2	L	345	52.71	**1.55**	**1.00**
	2	R	567	86.62	**1.06**	**1.00**
Boron Steel	3	L	608	81.53	**1.00**	**0.65**
	3	R	683	91.59	**1.00**	**0.95**
$WC/W_2C(10)_{[100]}$	4	L	363	52.41	**1.56**	**1.01**
	5	R	473	68.30	**1.34**	**1.27**

Table 26

Measured weight loss, calculated volume loss and RWR values for boron steel, Armatech and $WC/W_2C(10)_{[100]}$ coated shares.

	Furrow	Side	Weight Loss [g]	Volume removed [cm^3]	**$RWR_{[Boron\ steel]}$**	**$RWR_{[Armatech]}$**
Armatech	2	L	550	84.03	**1.12**	**1.00**
	2	R	800	122.22	**0.88**	**1.00**
Boron Steel	3	L	700	93.87	**1.00**	**0.90**
	3	R	800	107.27	**1.00**	**1.14**
$WC/W_2C(10)_{[100]}$	4	L	500	72.20	**1.30**	**1.16**
	5	R	400	57.76	**1.86**	**1.45**

§§§§§ Calculated using 95 % theoretical density values.

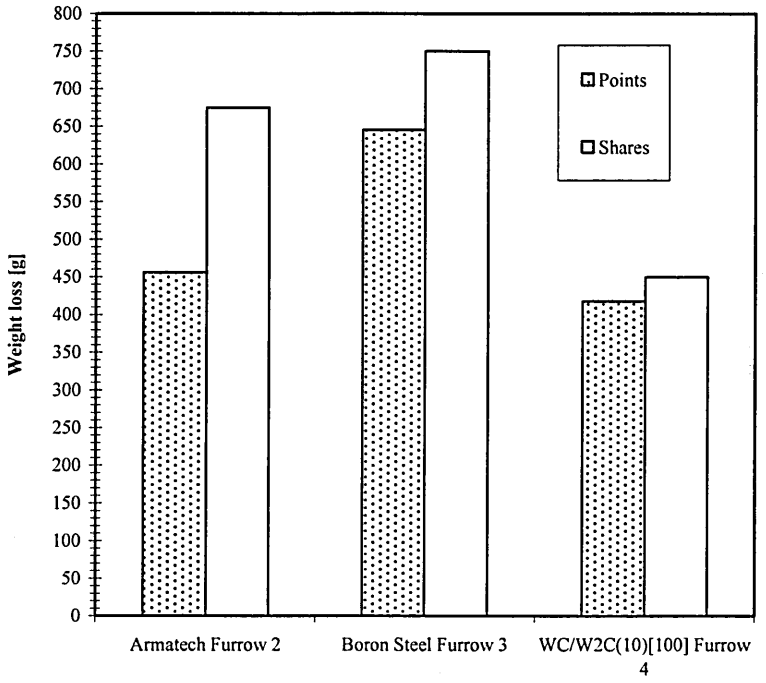

Figure 187: Measured weight loss of Armatech, boron steel and $WC/W_2C(10)_{[100]}$ points and shares after 110 acres of soil wear.

6.8.2 Trial B - March 2007

Results from tests carried out in March 2007 over a distance of 20 acres comparing only Armatech with the $WC/W_2C(10)_{[100]}$ coating are presented below in Table 27 to Table 30.

The test run was reduced from 110 acres to 20 acres to ensure that the coatings remained intact and did not wear through to the boron steel substrate beneath. Some substrate loss, albeit much lower than in the 110 acre tests, was expected in the exposed regions of boron steel substrate and was unavoidable. The adoption of this test method allowed a greater understanding of the coating performance and a more accurate measurement of volume loss to be calculated. The result revealed that both points and shares in each furrow position suffered lower material and hence volume losses when coated with $WC/W_2C(10)_{[100]}$ modified Armatech when compared to standard Armatech.

The results clearly showed the expected effect of furrow position on the rate of wear, with the amount of wear decreasing as furrow position is moved back.

Table 27
Measured weight loss on points [g]

	Furrow Position				
Coating	1	2	3	4	5
Armatech	176	146	140	139	133
$WC/W_2C(10)_{[100]}$	128	110	106	90	85

Table 28
Calculated volume loss on points[cm^3]

	Furrow Position				
Coating	1	2	3	4	5
Armatech	26.89	22.31	21.39	21.24	20.32
$WC/W_2C(10)_{[100]}$	18.48	15.88	15.31	13.00	12.27

Table 29
Measured weight loss on shares[g]

	Furrow Position				
Coating	1	2	3	4	5
Armatech	155	148	144	125	91
$WC/W_2C(10)_{[100]}$	101	86	78	53	17

Table 30
Calculated volume loss on shares [cm^3]

	Furrow Position				
Coating	1	2	3	4	5
Armatech	23.68	22.61	22.00	19.10	13.90
$WC/W_2C(10)_{[100]}$	14.58	12.42	11.26	7.65	2.45

The effect of furrow position is shown below in Figure 188 by a plot of weight loss per tool as a percentage of the starting weight. The amount of tool lost decreases with respect to furrow position. It is also clear that both $WC/W_2C(10)_{[100]}$ coated shares and points suffer a lower percentage loss at each furrow position when compared to Armatech coated tools.

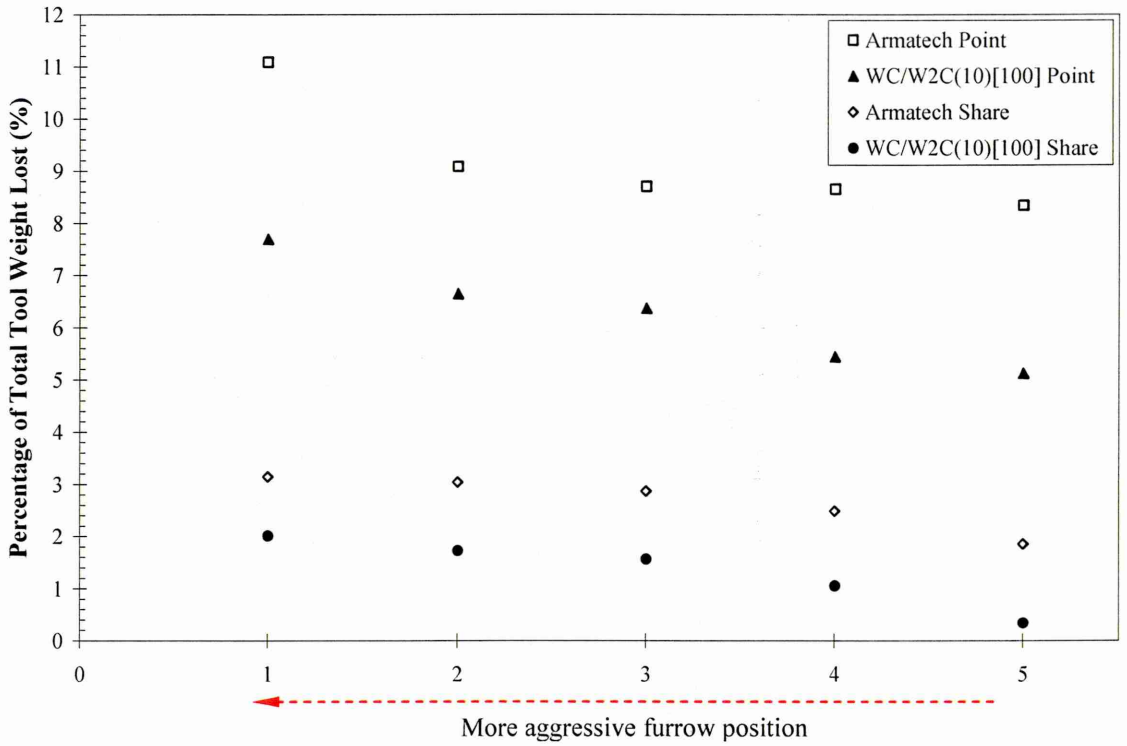

Figure 188: Percentage of tool weight loss at each furrow position for Armatech and $WC/W_2C(10)_{[100]}$ coated shares and points.

The results from these limited field trials indicate that $WC/W_2C(10)_{[100]}$ coated tools out-perform standard Armatech tools and can provide an increase in tool lifetime over the life of the coating. The RWR values of the $WC/W_2C(10)_{[100]}$ coated tools at each furrow position are provided in Table 31. If RWR values were used to estimate tool life (in the period of the coating being present on the tool), the average RWR taken across the five furrow positions shows that $WC/W_2C(10)_{[100]}$ coated tools have a 50% life improvement and the shares have very large 160% improvement.

Table 31
RWR values of $WC/W_2C(10)_{[100]}$ compared to Armatech

	Points	Shares
Furrow Position	$RWR_{[Armatech]}$	$RWR_{[Armatech]}$
1	1.44	1.56
2	1.37	1.76
3	1.37	1.83
4	1.59	2.36
5	1.63	5.48
Average	1.48	2.6

6.8.3 Wear surface examination

The wear surfaces from the field test of both boron steel and Armatech were shown in Chapter 4. The wear surface of the $WC/W_2C(10)_{[100]}$ from Trial A are shown here.

A boron steel reversible point coated with Armatech with an addition of 10wt.% 100 μm WC/W_2C having experienced some service is shown below in Figure 189.

Figure 189: Photograph of reversible point with $WC/W_2C(10)_{[100]}$ from Trial A.

Shown in Figure 190 below are micrographs from the surface of a worn $WC/W_2C(10)_{[100]}$. It can be seen from Figure 190(a) that the WC/W_2C are standing proud of the surface resisting wear in a two-body manner as observed with DSRW testing. This is also seen in Figure 190(b) at higher magnification. It can be seen that the particle has a rounded appearance and also possess a fracture across the centre. The region that appears light coloured is the bentonite binder phase.

(a)

(b)

(c)

(d)

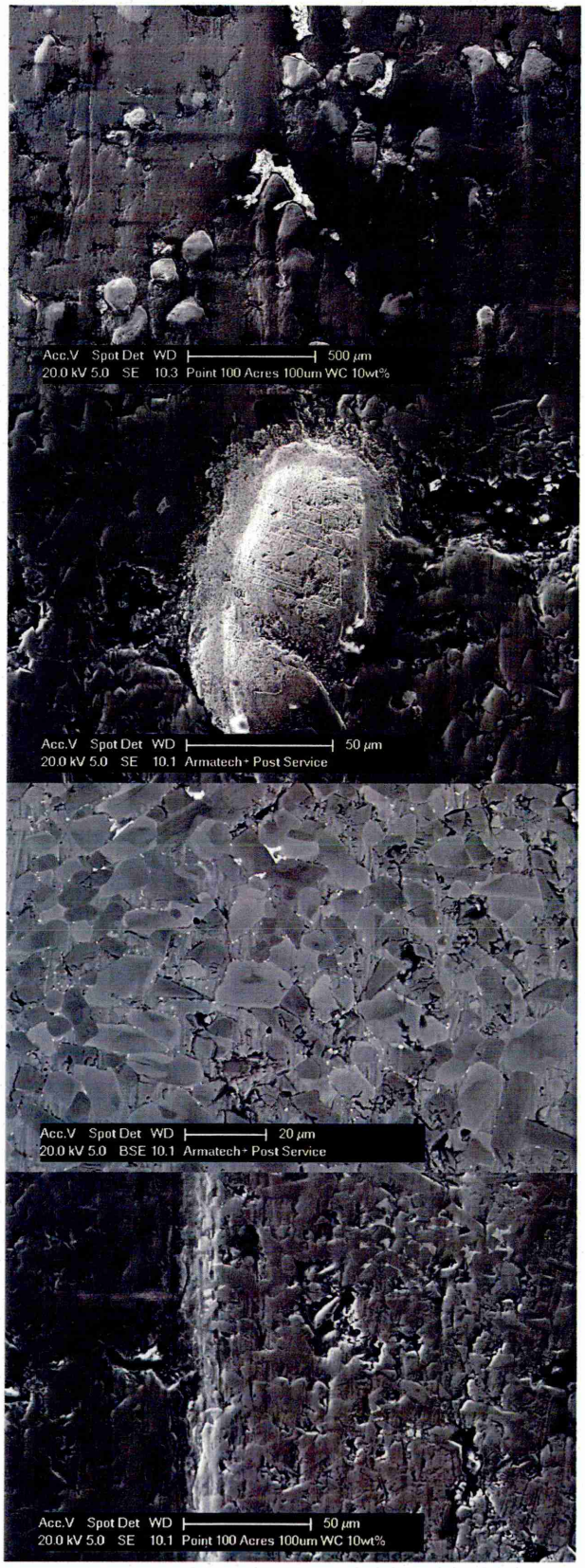

Figure 190: SEM micrographs of a $WC/W_2C(10)_{[100]}$ coated tool following field trial.

Examining the surrounding Armatech matrix material shows that the primary hard phases are resisting wear with the more ductile Fe-Ni rich matrix being worn away at a faster rate which is similar to the wear mechanism produced in the MSAW test using SiO_2. It is this combination of hard phases within a more ductile matrix that gives Armatech its improved wear resistance

properties over boron steel. Figure 190(d) shows a region of the Armatech matrix with a much larger wear groove.

Closer inspection of the WC/W_2C particle in cross-section showed that often the particles suffered from fracture, as was seen in DSRW wear scar examination. It can be seen in Figure 191(a) that the particle which is at the wear surface has resisted against wear and has a rounded appearance on the surface, however it can be seen that the particle has suffered fracture, most likely from the loading on the tool. Closer inspection of a particle wear surface shows that the mechanism of material removal is by brittle failure and hence removal.

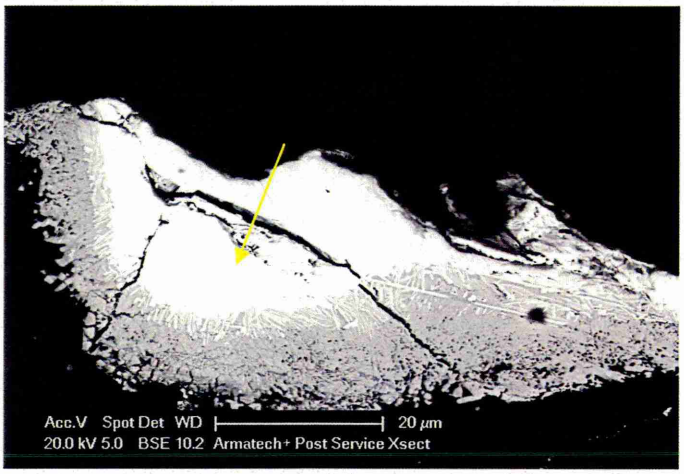

(a)

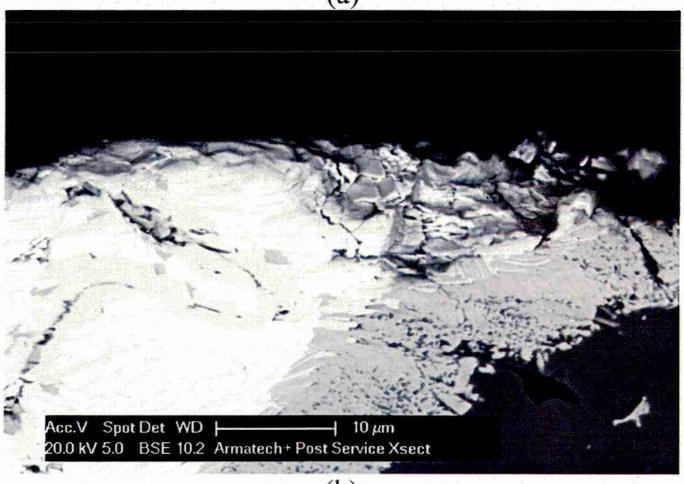

(b)

Figure 191: SEM micrographs of worn $WC/W_2C(10)_{[100]}$ particles following field trial.

6.8.4 Field test summary

The field tests provided promising results for both Armatech and $WC/W_2C(10)_{[100]}$ coated tools and provide data that suggests further development would be beneficial. The weight loss measurements in Trial A showed that both the points coated with Armatech and the modified coating performed better than standard boron steel. The results from Trial B showed that both the points and shares coated with the modified $WC/W_2C(10)_{[100]}$ tools performed considerably better than the Armatech coated tools. It was also confirmed from Trial B that plough position plays an important role in the rate of material removal, with position 1, the foremost position

suffering the highest rate of material removal, which decreased at each position towards the rear of the plough.

The field test results have shown results that confirm the conclusions drawn from the laboratory based wear tests. Both the DSRW and WSRW showed the same trend for the three materials field tested.

Whilst the standard method is to use standard production tools where the coating is only applied to the leading edges, using completely covered tools for field tests would provide increased accuracy in volume loss calculations and would eliminate the effect of substrate wear and would allow the performance of the coating only to be assessed.

7 Introduction

The extensive literature review performed in Chapter 2 emphasised the diversity of soil conditions and the effect on wear rates, and highlighted some of the approaches that have been employed in an attempt to increase tool lifetime. Literature involving field tests, dry sand rubber wheel testing and microscale abrasive wear testing was also reviewed. The resultant wear mechanisms created through field wear were explored in Chapter 4.

The findings of this work have shown that laboratory wear tests are able to replicate field wear, to some degree, and that with additions of various sized hard phases (at several loadings) to Armatech, the wear resistance can be enhanced. This was demonstrated using both microscale and macroscale laboratory wear tests and through field trials. The effect of abrasive particle type and applied load on wear mechanism and contact severity has also been highlighted along with the effect of moisture on wear rate.

This research has revealed that the current method of calculating wear volume and hence wear rate for the microscale abrasive wear test may not be as accurate and as comprehensive as previously assumed and factors such as the contact pressure, particularly at very low loads, may play a more significant role than generally assumed. It has also been shown that MSAW testing with SiC abrasive is not an appropriate wear test to assess materials for the resistance against soil wear.

The outcomes have shown that the ASTM G65 test can be confidently used as a preliminary stage to assess the wear resistance of materials proposed for use in soil.

The basic field trials performed have demonstrated that Armatech is a more wear resistant material than boron steel and that additions of WC to Armatech can further improve wear resistance. The results from the main experiments of Chapter 6 will now be discussed in detail.

7.1 Soil wear mechanisms

The examination of tillage tools removed from service allowed the wear mode present on boron steel to be compared to that present on Armatech (and with later examination of $WC/W_2C(10)_{[100]}$ coated tools). The initial reports from users of Armatech coated tools suggested that they outperformed tools manufactured from boron steel alone. It was important to examine worn tools to determine abrasive particle motion and their interaction with tool surfaces to provide an understanding of how the materials resisted wear and for comparison with laboratory tests.

It was evident that the predominant wear mechanism acting on the boron steel tools was two-body grooving with some three-body indentations (see Chapter 4). The wear morphology on the Armatech coated tools was also predominantly two-body grooving, although evidence of

microstructural cracking within the carbides and borides was seen. The carbides and borides showed lesser signs of wear when compared to the matrix indicating that they were the primary phase responsible for resistance against wear. It is possible that the microcracking observed may increase the susceptibility of material pullout, but evidence of this was not observed.

Figure 192 below shows SEM micrographs of Armatech wear morphologies from the four types of wear tests; field wear, microscale abrasive wear with SiO_2 abrasive, dry sand rubber wheel (DSRW) and wet sand rubber wheel (WSRW). The micrographs show the good correlation between field wear and the wear produced from the ASTM G65 tests, discussed in detail later. However, the MSAW test produced two-body grooving in the carbide and boride phases but three-body indentations in the matrix phase. The effect on wear mechanisms through the introduction of secondary hard phases will be discussed later.

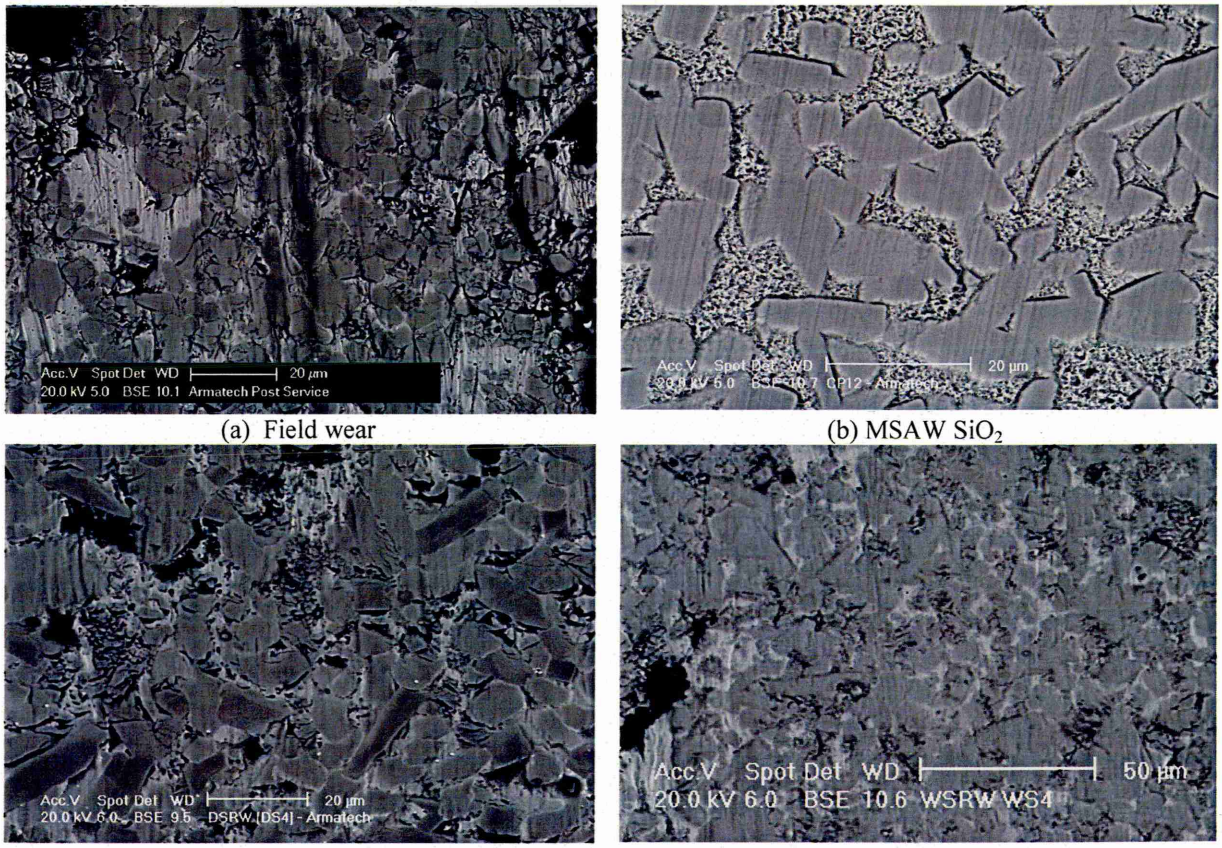

(a) Field wear (b) MSAW SiO_2

(c) DSRW (d) WSRW

Figure 192: SEM micrographs from Armatech surfaces worn by (a) soil; (b) MSAW testing with SiO_2 abrasive at a load of 0.8 N over 100 m; (c) DSRW testing with 130 N applied load and (d) WSRW with 130 N applied load. Note similarity of field worn surface to DSRW and WSRW.

Tillage tool examination revealed evidence of pitting corrosion on the boron steel material but not on the PM coatings. Pitting in this instance was most likely brought about by a lack of oxygen to the surface, creating a differential aeration cell forming an area of localised corrosion (discussed in section 7.8.5). Essentially the area with a lack of oxygen becomes anodic to the remaining cathodic surface that has higher levels of oxygen. Pitting was observed in and around the wear craters on boron steel from MSAW testing. Interestingly pitting was not seen on samples tested with the ASTM G65 test using both wet and dry abrasive.

7.2 Materials characterisation

7.2.1 Hardness

The bulk or macrohardness measurement of Armatech yielded a similar value to boron steel, 485 and 477 H_{V20} respectively. The homogenous nature of boron steel results in both similar microhardness and macrohardness values.

Due to the nature of the microhardness technique, where specific areas can be selected or avoided, (such as the residual binder phase in Armatech), different hardness values can be obtained from a heterogeneous material such as Armatech. Microhardness results revealed the Fe-Ni matrix to be ~700 H_V and the carbide and boride phases ~1500 H_V.

Therefore, although macrohardness measurements of boron steel and Armatech reveal a similar value, the harder, and suspected more wear resistant carbides and borides were expected to improve the wear resistance of Armatech over boron steel.

Modifications to Armatech made by the addition of secondary hard particles with hardness values much greater than the carbide and boride phases were expected to increase bulk hardness of the material even further.

It was highlighted from the macrohardness results that the measurement of macrohardness on Armatech yielded a large standard error, ± 48 (10%). It is possible that the randomly distributed residual binder phase contributed to the level of error, although similar errors were not observed on the modified materials, with the exception of $Al_2O_3(3)_{[10]}$ and $TiC(10)_{[75]}$ (these coatings did however suffer from fallout). The standard error in hardness of Armatech was investigated further by analysing several further samples produced over a period of time. However, a similar error was observed showing the effect to be a consistent one.

The modified materials with additions of 100 μm WC/W_2C provided macrohardness improvements of 20 to 25% over Armatech between 5 and 15wt.% loading. Microhardness measurements of the 100 μm WC/W_2C modified materials revealed no hardness change in the surrounding Armatech matrix or the carbides and borides. The core of the WC/W_2C particles possessed a hardness of ~2200 H_V, with the outer reaction zone ~850 H_V, Figure 193. Increasing the loading level above 15wt.% led to a reduction in bulk hardness, the 70wt.% addition possessed only 20% hardness of Armatech. The reduction in hardness as a function of increased WC/W_2C loading was most likely due to the Armatech becoming over saturated with WC/W_2C, reducing sinter quality which was shown in Chapter 5. SEM examination of these materials showed them to be more susceptible to WC/W_2C fallout and microstructural cracking than materials with <15wt.%. Which suggests that with the typical chemical composition of Armatech, only WC/W_2C loadings of up to 15wt.% can be made to ensure a material with a good sinter quality should be considered with a view to increasing the wear resistance.

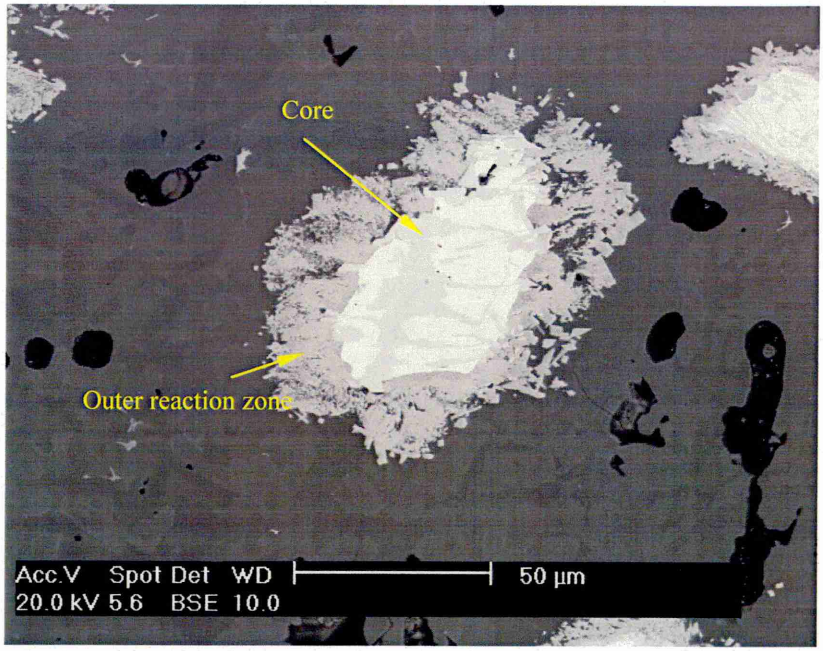

Figure 193: SEM micrograph of 100 µm WC/W_2C particle in Armatech matrix. The core of the particle and outer reaction zone are visible and possessed very different hardness values.

The hardness measurements performed on the materials with additions of 15 µm WC showed that additions greater than 5wt.% reduced the hardness by ~50% when compared to Armatech. The contributing factor may have been the degree to which the WC particles wetted and integrated into the existing structure, fallout at high loadings was observed during characterisation. The reduced particle spacing inherently reduces the volume of the tough and more ductile Armatech matrix that is responsible for 'holding' the highly wear resistant WC. Therefore, a good balance between the amount of WC and the volume of Armatech is needed.

Alternatively, the hardness of Armatech modified with mixtures of 100 µm WC/W_2C and 15 µm WC provided no increase in hardness over Armatech, except at the lowest loading level. A mixture of one and four weight percent provided an increase of 25 points ($WC(1\&4)_{[15\&100]}$).

The addition of TiC served only to reduce the hardness of the coating to less than 50% of Armatech. Examination of the microstructure revealed that the TiC additions had not fully wetted with the Armatech matrix which resulted in fracture and fallout of the TiC. The addition of Mo_2C resulted in only 30% of the hardness of Armatech, the porous nature of the Mo_2C particles provided no 'real' secondary hard phase.

The addition of two Al_2O_3 particle sizes (10 and 50 µm) at loadings of 3 and 6wt.% resulted in quite different hardness's. The 3wt.% additions provided the same hardness as Armatech with 10 µm particle size and an increase of 100 points with the 50 µm addition. The two particle sizes added at 6wt.% produced a reduction in hardness. The exact reason for the reduction in hardness with an increase in addition was not evident from examination of the microstructure. Whilst fallout was observed, it appeared to be the same degree in all Al_2O_3 modified materials.

It could be inferred from the series of hardness values that a correlation existed between the reinforcing particle size addition and the increase in hardness. Certainly six of the nine materials that provided an increase in hardness had additions using 100 μm particles (WC/W_2C at the lower loading levels) and one with a 50 μm addition (Al_2O_3). Historically wear resistance has been linked to the hardness of a material. However, it has been repeatedly shown here that microstructure (among other factors discussed in Chapter 2) plays a more important role than hardness alone. Factors such as hard phase particle spacing can be important when small particle sized abrasives come into contact with the surface, a large spacing can allow the abrasive to attack the softer matrix and pullout wear resistant phases. The interaction of the abrasive with the hard phase is also important, the hard phase may prove wear resistant but may suffer cracking from the load applied by the particle which can lead to material loss through fallout.

7.2.2 Material density

Density measurements were performed using samples of similar sizes and a wax coating was used to eradicate the problem of air bubbles and ingress of water in to any porous structure. However, despite this the density measurements were non-uniform.

It was anticipated that a material with a high hardness value, would possess a good sinter quality and hence provide a higher density value. However, the density measurements revealed that a large proportion materials with lower than anticipated bulk hardness values provided an improvement in density, i.e. the 15 μm WC additions and the mixed WC and WC/W_2C materials.

The density measurement of the Mo_2C modified materials were shown to possess higher density than Armatech, despite the theoretical density values suggesting a lower density. It is a possibility that the Mo_2C addition either increased the sinter quality of Armatech or that the repeated measurements of the Armatech sample were inaccurate.

Measurement of boron steel density provided the same result as the theoretical value. This eliminates the possibility that the method used to measure density was at fault. It is more likely that the residual binder in the PM coatings and the possibility of pores not eliminated during sintering affects density. Analysis of the residual binder phase revealed that it did not form a homogenous phase throughout the microstructure but exhibited a variation between samples (the author later recommended a mechanical stirrer should be used for the slurry in an effort to keep the binder and modifications in suspension and prevent settling which was implemented).

Due to uncertainties in the measurement of density, a 95% of theoretical value was adopted as standard in later calculations. The reduced theoretical value was used to provide a more realistic figure based on observations of the microstructure. Due to the small amounts of material removed in the laboratory wear tests and the very small difference between the

theoretical density values, the change to volume calculations by the 95% density substitution was not significant.

Whilst density and hardness are well established techniques used to characterise materials and can provide an indication of sinter quality, they are not the primary parameters that affect wear resistance. It is also worth noting that different samples were used to measure density and to measure hardness or wear resistance.

7.3 MSAW - Test procedure development

In developing the MSAW test procedure the optimum conditions were defined that resulted in reliable results, wear craters with consistent wear mechanisms and no signs of other irregularities (e.g. ridging).

Microscale wear tests were performed using two types of abrasive particle. Tests with SiC were performed on the basis of it being the 'standard' MSAW test abrasive. Previous research had shown it to provide reproducible wear results and two-body grooving wear (under certain conditions on certain materials), the dominant wear mechanism seen on soil working tools. However, the conditions used in this research resulted in only a three-body rolling wear mechanism which is not consistent with that found in soil wear.

MSAW tests were also performed using SiO_2, the abrasive particle common to soil. No published research involving MSAW testing with SiO_2 abrasive was found. The initial MSAW test development performed in this research however revealed that with a SiO_2 in water volume fraction of 0.1, two-body grooving wear could be produced. The desired wear mechanism required in order to replicate soil wear, albeit on a smaller scale.

An important aspect of the test development was to explore test reproducibility. Reproducibility using SiC abrasive yielded excellent results, with crater measurement error being calculated at only 0.2 - 0.4%. Although the SiO_2 provided a better simulant in terms of obtaining the correct wear mechanism, the reproducibility was not as good, with errors in the range of 1.2-7.1%. The lower reproducibility in the SiO_2 tests was due to measurement accuracy with the smaller and less well defined wear craters despite doubling the sliding distance to increase size.

7.3.1 Specific wear rate and contact pressure

An initial test matrix was used with loads between 0.2 and 5 N over a sliding distance of 50 m for the SiC abrasive and 100 m for the SiO_2 abrasive tests.

Plots of specific wear rate against applied load for both test abrasives revealed a two stage relationship with the wear rate decreasing with applied load but at different rates in each stage (also observed by other researchers[71,72,76]). Theoretically, specific wear rate should be independent of applied load for the same wear mechanism. According to Archard's equation V

is a function of the wear rate, the sliding distance (which under these circumstances was fixed) and the applied load. The equation however does not account for contact pressure.

The plot below in Figure 194 shows the theoretical pressure versus the increasing crater diameter, produced using a 25.4 mm ball. The relationship between the crater diameter and final contact pressure, P_f, is plotted for four test loads. The average pressure can be seen to decrease rapidly as crater size increases.

At the start of a wear test contact pressure will be high as the ball is loaded against the sample, as a test commences and a wear scar is produced test pressure will reduce as the area increases. However, in theory the load per abrasive particle will remain constant as the load is continually supported by an increasing number of particles able to enter the wearing interface.

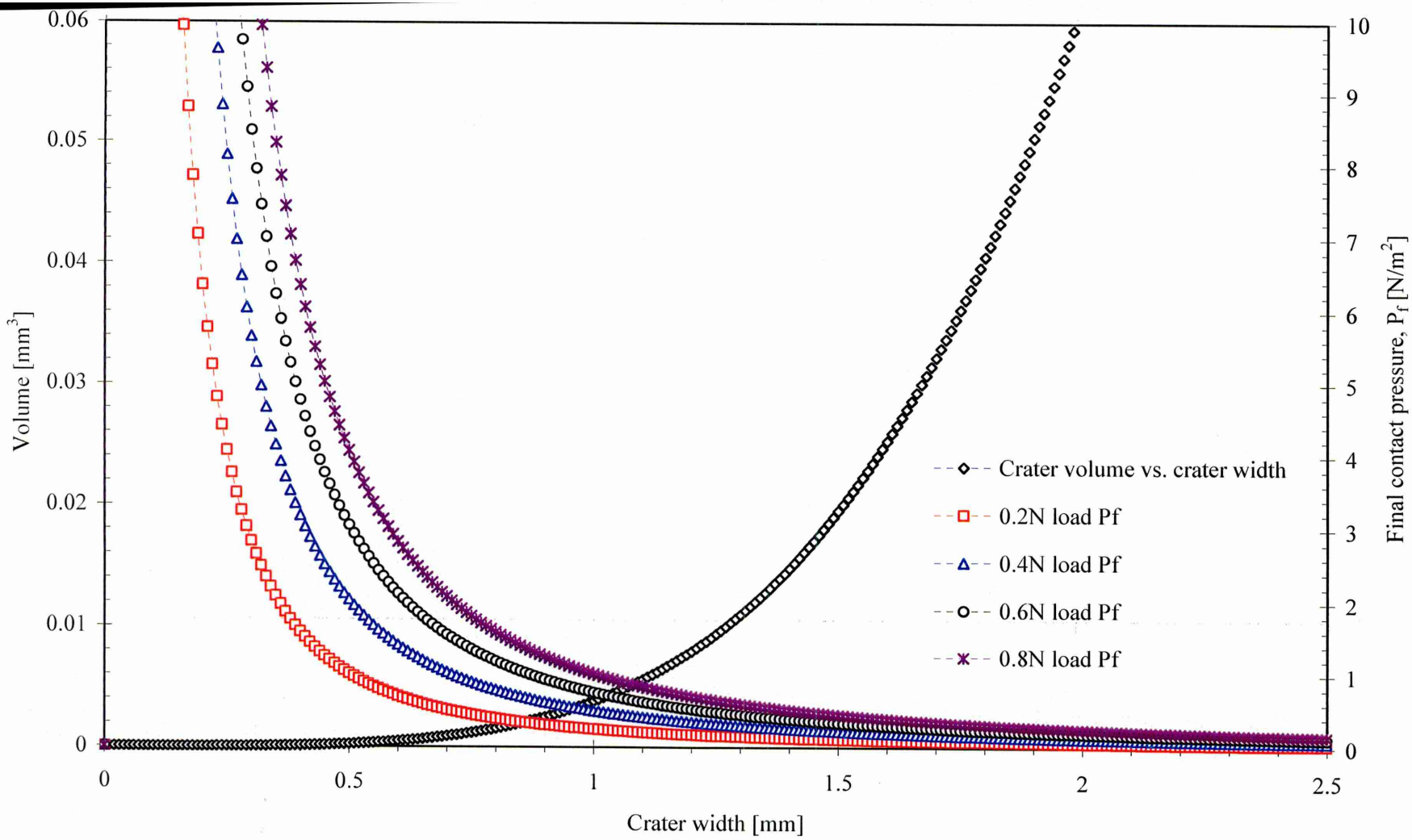

Figure 194: Plot of theoretical wear crater volume with a 25.4 mm wear ball as a function of crater width and the corresponding final contact pressures at 0.2, 0.4, 0.6 and 0.8 N load at these wear volumes.

It is most likely the effect of the contact pressure that yields a decrease in specific wear rate. A decrease in contact pressure at a crater width of around 1 mm can be seen, after this point it can be seen that the contact pressure commences to level off. If we look at the specific wear rate results obtained in Chapter 6 (re-plotted below in Figure 195), a plateau in specific wear rate was seen at ~1 N load, Figure 195(a). By reverse plotting, we can see from Figure 195(b) that the final crater width for a ~1 N load was around 1.0 mm diameter, which coincides with the plateau in contact pressure.

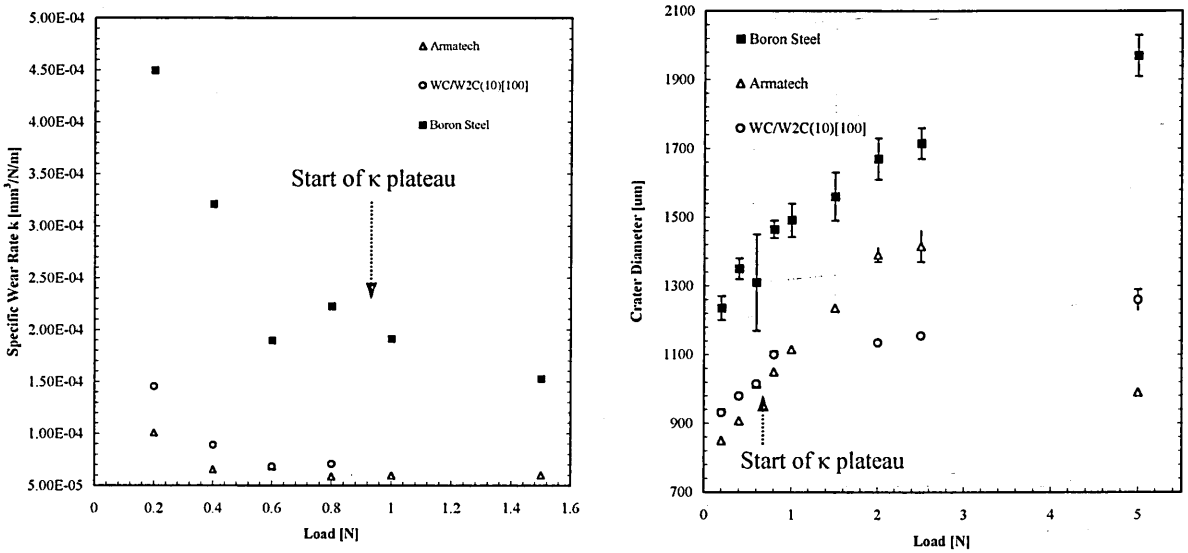

(a) (b)

Figure 195: (a) the relationship between k and applied load and (b) MSAW effect of load on crater width using SiO_2 abrasive over 100m sliding distance related to contact pressure.

It is the contact pressure that is also the cause of undesirable phenomena such as ridging. At the start of a wear test it has been shown that the contact pressure is very high due to the Hertzian contact being very small. With such high contact pressures starvation of the slurry prevents entrainment of the abrasive particle into the sample/ball interface and therefore allows direct wear ball contact creating wear grooves or ridges.

It can be seen that a wear crater at a specific size created using the same load but with separate abrasives can generate different wear mechanisms. This confirms that **wear mechanism** is dominated by load per abrasive particle and abrasive particle properties such as size and shape that affect particle motion interaction.

7.3.2 Effect of load in MSAW testing

The Archard equation predicts that abrasive wear volume should be directly proportional to the load on the wear contact. The effect of load was explored in the MSAW test development by using a range of loads from the minimum 0.2 N, to the maximum 5 N.

Loads >1.5 N using SiC abrasive produced a mixed mode wear mechanism on all test materials. The mixed mode mechanism was evident from grooves that appeared which became

increasingly dominant, and larger in size as load was increased. These grooves were not two-body wear grooves but were most likely caused by direct contact of the wear ball. Overall, a good linear relationship existed between load and wear volume removed per unit sliding distance for wear craters produced using SiC. The relationship between specific wear rate and load however, revealed a two stage relationship as discussed. A steeply declining linear relationship could be seen from 0.2 to 1 N applied load, above this load a less steep decline relationship was observed up to 5 N. At very low loads, 0.2 N, the Armatech and $WC/W_2C(10)_{[100]}$ showed signs of mixed mode wear. Two-body grooves were observed which appeared to not to be present when the load was increased to 0.4 N. These grooves, however, did not correlate to the size of the SiC abrasive and were more likely caused by direct contact from the wear ball or reduced contact pressure on the abrasive particles.

Loads >1.5 N using SiO_2 abrasive (two-body wear) revealed a deviation from a linear relationship of load against wear volume removed per unit sliding distance for Armatech and $WC/W_2C(10)_{[100]}$. This was not seen with boron steel which provided an increasing linear relationship (which did not, however, pass through the origin). The relationship between κ and load for SiO_2 revealed that loads up to 0.6 N yielded a linear decrease in κ, where upon higher loads created a plateau in κ.

Research by Trezona *et al*[71] using SiC at a volume fraction of 0.189 over a load range of 0.1 to 5 N showed that on tool steel (sliding distances between 12 and 24 m) signs of ridging (labelled grooving) were not seen until 3 N, somewhat higher than the 1.5 N in this research. It was also shown that when reducing the volume fraction of SiC to 0.015 to achieve a two-body mechanism (32 m sliding distance) signs of ridging were seen from a load 0.4 N. Interestingly, in this research the relationship between volume removed per unit sliding distance and load for two-body and three-body wear was similar to those shown by Trezona. A linear relationship for three-body wear (that also did not pass through the origin) was seen by Trezona along with a non-linear relationship under two-body grooving conditions.

It has been shown in this research that wear is proportional to load for three-body wear but obeys a power law for two-body grooving wear.

Although the Archard equation is widely used to calculate wear volume in MSAW testing, it was not observed to hold in this particular application and it has been shown that assumptions associated with the equation do not apply in certain scenarios, i.e. two-body wear is not proportional to load.

7.3.3 Wear scar volume determination

The wear volume in MSAW testing is calculated using Equation 1 in Chapter 4 with crater diameter measurements. The standard technique of measuring a MSAW crater is to use a travelling microscope or, as in this research, an SEM. Whilst using techniques such as SEM can

provide a more accurate method there is still some aspect of error involved. Rounding of the crater edges will inevitably over estimate crater volume in calculations. However, crater volume would be over estimated for each scar measured resulting in a systematic over estimation of the wear under all loads and for all materials. As such it does not pose a problem when comparatively ranking materials.

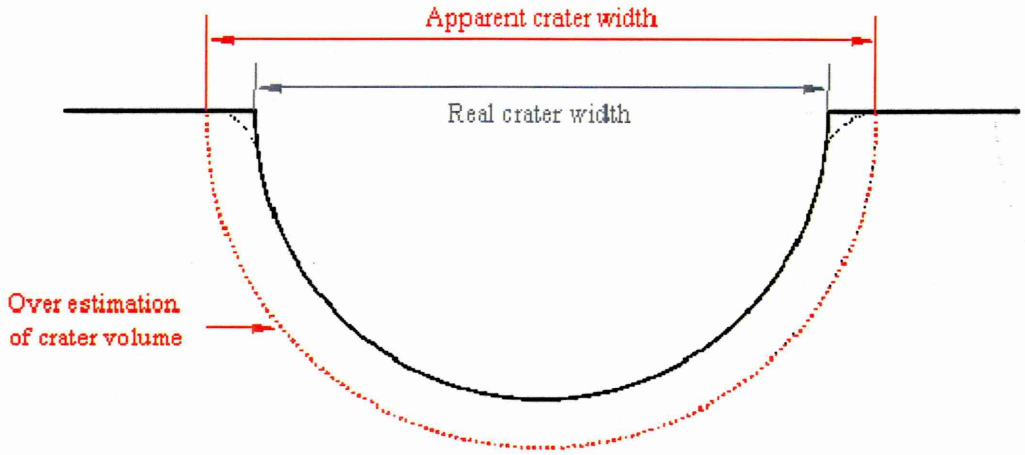

Figure 196: Schematic representation of crater edge rounding leading to over estimation of crater volume.

It is suggested that in order to avoid this error methods of volume loss calculation that do not rely on measurement of the diameter should be considered. The use of profilometry technique such the Infinite Focus Microscope (IFM) may prove to be a more accurate method (although the problem of crater edge rounding would need consideration). It is important to understand however that when MSAW testing is only used to comparatively rank materials the existing method may be adequate. Attention is required when attempting to compare results between research establishments or where crater diameter has been measured using two methods.

The MSAW test development procedure highlighted the effect of load on wear mechanism and revealed the more aggressive nature of SiC when compared to SiO_2. The excellent reproducibility achieved from SiC was also shown. A decreasing linear relationship between κ and applied load was shown and was attributed to the changes in contact pressure.

Having performed the test development and determined the optimum test conditions to achieve a consistent wear mechanism for each abrasive, each material produced was MSAW tested under these test parameters, which will now be discussed in detail.

7.4 MSAW SiC Results

As expected the WC-Co tile showed a much higher wear resistance compared to boron steel and Armatech (>200%). Morphological examination of the wear mechanism revealed preferential wear of the Co binder.

The remainder of the results of tests with SiC abrasive were somewhat contradictory to the existing feedback regarding the performance of Armatech.

The primary wear mechanism observed on all materials using SiC was three-body rolling wear with no directionality, not the typical wear mechanism seen on tillage tools. Although the density of Armatech is lower than boron steel and hardness measurements revealed little difference between the two, it was expected that the heterogeneous microstructure (including hard carbides and borides) would provide an increase in wear resistance when compared to the homogeneous microstructure of boron steel. Despite this, and the positive feedback from Armatech users, the results indicated no improvement over boron steel (RWR of 0.99). Examination of the wear mechanism on Armatech showed that the carbides and borides were providing the majority of wear resistance. The crater edges showed signs of preferential wear of the softer matrix with the carbides and borides showing little sign of indentation.

However, the nature of the test compared to the projected material use and the type of abrasive used had to be taken in to consideration. Firstly, it is important to remember that the MSAW test has been used as a comparative test and not to determine wear lifetime predictions or quantitative measurements. Secondly, the standard SiC abrasive used is a small and relatively consistent particle size with a higher hardness and is therefore not typical of soil.

Modifications made using additions of 15 μm WC did not provide any distinct improvement in wear resistance over boron steel or Armatech. A loading of 5wt.% produced a similar κ to boron steel and Armatech, but further increases in loadings up to 20wt.% reduced κ. It could be argued that the improvement seen with $WC(5)_{[15]}$ was linked to the increase in hardness over boron steel and Armatech, although other materials that showed a similar hardness increase did not show any improvements in wear resistance. It is also worth noting that the SiC abrasive was a similar size to the WC additive (5 μm and 15 μm respectively).

The wear scars of the 15 μm WC modified materials revealed that the WC particles suffered from fallout due to the action of the abrading particles. This issue was related to the degree to which the WC wetted and/or reacted with the Armatech during sintering. Particles that appeared to have fully bonded indicated signs of providing wear resistance through prominence from the surrounding material.

The addition of the larger 100 μm WC/W_2C particles did not provide any significant improvements over boron steel or Armatech with SiC abrasive. An addition of 10wt.% provided some improvement with an $RWR_{Armatech}$ of 1.07, which again was a material that provided an increased hardness value over Armatech. The wear mechanism showed that the WC/W_2C particles had been abraded through three-body wear and were standing proud of the surrounding surface, the edges of the particles had a rounded appearance showing good signs of wear resistance.

When the loading level was increased (>20wt.%), brittle failure of the particles was observed, predominantly in the core. Microcracking of the Armatech material also increased and a rise in WC pullout was seen. The increase in both microcracking and pullout is suspected to be a factor of the WC affecting the chemistry (and hence properties) of the Armatech during sintering. This potential change in properties as the amount of WC additive is increased is a possible explanation for the decrease in wear resistance.

The remaining materials of Al_2O_3, Mo_2C and TiC also provided no improvement in wear resistance over boron steel or Armatech. The 10 μm Al_2O_3 addition provided similar results to Armatech along with 5wt.% Mo_2C. The addition of 10wt.% Mo_2C and 5wt.% TiC showed a deterioration of between 20 and 30% and the higher loading of TiC at 10wt.% showed a ~40% deterioration. The Al_2O_3 additions did not wet or bond with the Armatech structure and examination of the final sintered structure revealed a high degree of fallout. Particles that remained embedded in the matrix showed good signs of wear resistance and were abraded in a three-body manner.

The reduction in wear resistance as hard phase addition was increased was also observed by Van Acker *et al.*[108] with WC/W_2C containing laser clad MMC coatings. Van Acker generated three-body rolling wear with MSAW testing using SiC abrasive and noted a decrease in specific wear rate as the carbide concentration was increased. However, it was concluded that a material with a mixture of wear resistant carbides in a less wear resistant matrix promotes three-body rolling wear and that a pure matrix material would exhibit two body grooving wear when using SiC. Whilst, three-body wear was observed on Armatech two-body grooving was not seen on boron steel under the same conditions in this research.

The results conformed to the suggestions put forward by Trezona *et al*[71] (discussed earlier and in Chapter 2) that the occurrence of two- or three-body wear is a function of applied load and slurry concentration along with abrasive size and hardness. According to the plot of wear mechanism as a function of these two parameters, a three-body wear mechanism should occur with 20% volume fraction SiC slurry, between the loads of 0.2 to 1 N, Figure 18. It was shown that increases in load above 1 N would produce mixed mode wear, as was observed in this research. A load of 1.5 N with SiC indicated the onset of grooving, most likely caused by wear ball contact.

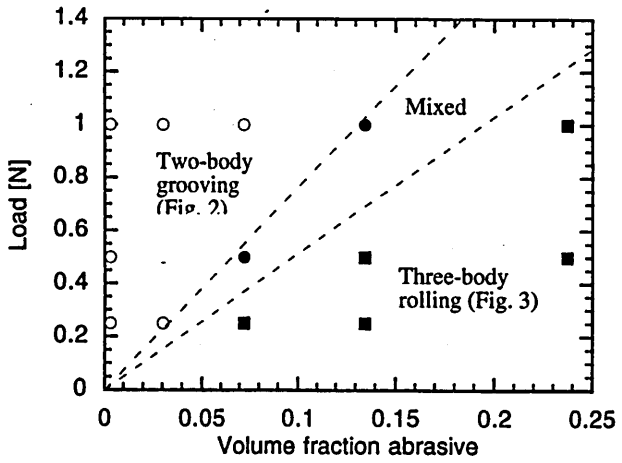

Figure 197: Wear mechanism map for MSAW test on tool steel using F1200 SiC slurry from Trezona et al[71].

It is proposed that the severity of the test with SiC renders it an inappropriate test condition to evaluate the wear of material for resistance against soil wear. A laboratory based test must present a similar correlation to the practical application, such as abrasive type and hardness as well as produce similar wear mechanisms. The results of this research recommend that MSAW with SiC abrasive should not be used to assess a materials ability to resist against soil wear.

7.5 MSAW SiO2 Results

Results from the SiO_2 abrasive tests provided very different results compared to those using SiC abrasive. The overall wear rate was reduced tenfold when compared to SiC values, an affect of the lower hardness and consequently a lower H_a/H_m ratio. An additional factor is particle size, the SiO_2 particles were smaller than the SiC (2.5 and 7 μm respectively). An increase in volumetric wear has been shown to be linked to an increase in particle size up to 100 μm, Figure 8.

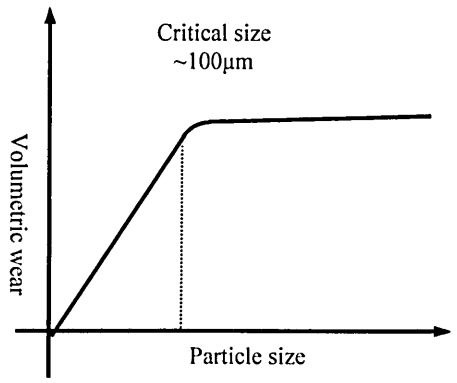

Figure 198: The effect of abrasive particle size on the volumetric wear.

Under these test conditions boron steel provided the lowest wear resistance against all other materials. The WC-Co tile was not able to be accurately assessed due to the size of wear the scars produced being too small to ensure accurate measurement.

Examination of boron steel wear scars revealed corrosive pitting in and around the wear craters, similar to that observed on boron steel tools removed from service and also on wear scars with MSAW testing using SiC abrasive, this will be discussed further in section 7.8.5.

The wear mechanism produced using SiO_2 on the Armatech coating was of a mixed mode nature. The matrix phase had worn through three-body indentation and the carbides and borides showed signs of two-body grooving. The carbides and borides stood 'proud' of the surrounding matrix providing resistance against wear. It is this combination of a ductile and tough matrix holding hard wear resistant carbides that is desirable for a wear resistant material. However, the SiO_2 and the SiC abrasive particles used were of such a size that they were able to penetrate between the network of carbides and borides and cause material removal of the matrix. Once the matrix around the carbides and borides is worn away, they then become susceptible to cracking from further wear, due to the lack of matrix support. The applied pressure or stress from the wear process will be focused on the protruding carbides and borides.

In reality, soils possess a range of particulate sizes which would result in not every abrasive particle being able to attack the matrix phase. It is also important to note that although the particles are able to penetrate between the hard phases, simply reducing the area of matrix phase by increasing the level of hard phase additions would not increase wear resistance.

The results of the test showed that the addition of 15 μm WC had a positive effect on wear resistance at each level of loading. It was seen that the wear resistance improved linearly as loading was increased from 5 up to 20wt.%.

The addition of the larger 100 μm WC/W_2C provided mixed results. The loadings of 12, 15, 20 and 70wt.% all provided improved wear resistance whilst 5, 8, 10 and 50wt.% yielded a decrease in wear resistance over Armatech. The exact reason for this variation is not known, it is suspected however that the 70wt.% material is a rogue data point and is possible that the optimum sintering conditions are achieved with an addition between 15 and 20wt.%. SEM investigation of the wear scars showed that tendency of particle fallout increased at higher additive levels, but lower levels, between 5 and 20wt.%, all possessed similar wear mechanisms despite different wear resistance values.

It can be concluded from this test that the smaller WC based powder particles perform best when resisting against wear from the small silica abrasive particles and that the larger WC/W_2C additive was not as successful as resisting wear caused by small particles.

The results from the mixture of WC 15μm and WC/W_2C 100μm materials provided interesting results. The material with 5wt.% of each particle type showed some improvement over Armatech. Lowering the amount of 15 μm WC and increasing the 100 μm WC/W_2C to 3 and 7wt.% respectively did not provide any improvement in wear resistance over Armatech. Mixtures of 1 and 4wt.% and 7 and 3wt.% however provided a marked improvement in wear

resistance. This result suggests that by adding hard phases at two particle sizes (between 3-5% 100μm WC/W_2C with an undetermined optimum loading of 15 μm WC), wear resistant properties of each particle can be combined to enhance wear resistance.

7.5.1 Relationship between hardness and wear resistance

Historically the hardness of a material, and in particularly pure metals or annealed steels, has been used to predict wear rate. This approach, however, should be used with caution, since in complex materials such as Armatech there are a multitude of factors that require consideration aside from hardness. It was shown that whilst Armatech and boron steel possessed a similar macro-hardness, different trends in the wear performance were obtained when using different abrasives.

The weak linear correlation observed between bulk hardness and wear volume removed per unit sliding distance for the SiC abrasive under three-body conditions was not observed with wear results from SiO_2 abrasive under two-body conditions. This suggests that bulk hardness plays a more significant role when under attack from either an aggressive abrasive such as SiC or three-body wear, but that with a less aggressive abrasive such as SiO_2 or a two-body mechanism the microstructure is the major factor in resisting against wear. With SiO_2 being the common abrasive found in soils it can be said the mechanism by which a material resists wear is more important than the hardness properties.

The 80% H_a figure put forward by Richardson and often quoted in other research, in relation to materials used to combat soil wear should be interpreted with caution owing to the test conditions used to determine the figure. It was based on the wear of steels and pure metals being abraded with fixed flint and glass abrasive papers. The ability to produce a cost effective monolithic material with a hardness >800 H_V whilst remaining impact resistant is difficult to achieve. And as discussed above hardness alone does not necessarily increase wear resistance.

7.5.2 MSAW Results summary

The test conditions used in this research provided good reproducibility and the aggressiveness of SiC in particular generated well defined craters reducing the errors associated with crater measurement and hence those in the wear resistance calculation. However, the aggressiveness of the abrasive and its high hardness increases the H_a/H_m ratio. Increases in the ratio lead to the wear resistant properties of the hard phases introduced to the Armatech coating to become less significant and the matrix material becomes the determining factor for wear resistance. It must be noted however that SiC is known for its hardness and aggressiveness, the primary reason for it being selected as the abrasive in the Crater Project aimed at standardising the MSAW test. For this reason, it was deemed important to perform MSAW tests using the SiC despite it not directly representing the abrasive of interest in this research. However, the results show that the

MSAW test with SiC abrasive should not be used to assess the wear resistance of tillage tool materials.

A different wear mechanism was produced with the softer and less aggressive SiO_2. The lower hardness, smaller particles size and difference in particle shape of the SiO_2 abrasive produced two-body sliding wear and generated a smaller wear crater than the SiC, despite doubling the sliding distance. The results suggested that when using a small abrasive size, materials that contain hard phases of a similar size provide the best wear resistance.

Using the MSAW test to determine the wear resistance of heterogeneous materials such as Armatech that contain hard phases and residual binder phases is more complex than assessing homogeneous materials such as boron steel. Examination of wear scars on the coatings revealed that each wear scar may contain differing amounts of particular phases, i.e. residual binder or WC/W_2C particles. It is a possible that a large amount of WC/W_2C phase may have been removed from the crater but this scenario is impossible to quantify. This problem is reduced considerably with tests such as the ASTM G65 test or field tests, as the area or volume of material tested when compared to MSAW testing is much greater. However, the MLM method of calculating wear rates reduces this error somewhat as specific wear rate is calculated from four wear scars generated using four loads.

The influence of the applied load and contact pressure on wear rate has been highlighted in this and other research, although no in-depth studies regarding contact pressure were found from the literature search (although "contact severity" has been studied by others). This is an area worthy of further work in order to obtain a more comprehensive understanding of MSAW testing.

With SiO_2 being the common abrasive particle in soil and being and the standard abrasive used in larger scale tests such as the ASTM G65 test it was anticipated that these two methods of wear test would allow the measurement of the performance of materials subject to wear by soil.

7.6 ASTM G65 Dry Sand Rubber Wheel Testing - DSRW

The results of the MSAW test with SiO_2 showed that the smaller WC particle additions provided the most improved wear resistance. It was hypothesised that materials with larger particle size hard additions (such as materials with 100 μm WC/W_2C additions) would show improved resistance against wear from a larger abrasive particle size in ASTM G65 testing.

The results from the DSRW test revealed that Armatech experienced lower losses when compared to boron steel, which confirmed feedback reports from service and also the results from SiO_2 MSAW testing. When considering error however, it may be argued that the Armatech did not show a significant enough improvement over boron steel. SEM examination of boron steel and Armatech wear scars showed a single mechanism of two-body grooving

wear. Additionally, it was evident from the Armatech wear surface that the microstructure had suffered microcracking which was also observed on field worn tools and in some MSAW tests. The cracks were predominantly intergranular and to a lesser extent transgranular in the carbides and borides. Pitting on the boron steel material seen in field service and from MSAW tests was not present in ASTM G65 testing. While both the mechanism of corrosion and microcracking is considered undesirable for a wear resistant material, in this instance it suggests that the field wear mechanism is being recreated and is therefore considered desirable.

Cross-sections taken through each wear scar revealed the groove depth to be very small. Profilometric measurements performed along the length of wear craters from both dry and wet environments showed that the abrasive entrance region exhibited irregular features and had a greater depth when compared to the exit region, indicating a higher load and a higher degree of material removal at this point. This suggests a non-uniform entrainment of particles into the wearing interface.

The modified materials with WC powders revealed that an addition of the 15 μm powder at 5wt.% provided an improvement in wear resistance of around 60% when compared to Armatech. An improvement of around 50% was measured with an addition of 10wt.% but a decrease in performance by 25% was seen with the highest addition tested at 15wt.%.

It was anticipated that the materials that showed improvement in wear resistance in SiO_2 MSAW testing, i.e. materials that had secondary hard phases that were a similar size to the abrading particles, would not perform as well when the size of the abrading particle was much larger than the secondary hard phase.

Examination of the wear surfaces of all the modified materials with additions of 15 μm WC showed they had suffered from particle fallout and that this was exacerbated with increased levels of WC. It was also apparent from cross-sections through the wear scars that sub surface microcracking to a depth of around 20 μm was present, enough to remove a WC particle.

The addition of 5wt.% 100 μm WC/W_2C provided an improvement of 60% over Armatech, with this reduced to 50% as the WC was increased to 10wt.%. The addition of 15wt.% however showed some improvement over the 10wt.% but more material loss than the 5wt.%.

Examination of the wear scars indicated that the WC/W_2C particles were resisting wear from the 260 μm sand particles. The WC particles were protruding from the material surface and had a rounded appearance very similar to the wear mechanism observed from similar materials tested in field trials (Figure 199). Close inspection of the worn WC/W_2C particles showed that the cores were suffering from microcracking.

The series of materials produced using mixtures of both 15 μm WC and 100 μm WC/W_2C showed an improvement over Armatech of around 50% collectively. Varying the ratios of the smaller addition to larger addition showed no significant differences in wear resistance. The

addition of two particle sizes provided a good improvement in wear resistance under these test conditions using a single particle size. The wear resistant properties of a mixed particle size material may prove more successful in field tests (which were not able to be tested in this research) or in a wear test that is able to use a mixture of abrasive sizes. The mixed size WC based additions showed improved wear resistance in both the MSAW and DSRW tests and it is proposed that the properties of such a material would be beneficial in an environment with a mixed abrasive particle size (i.e. soil).

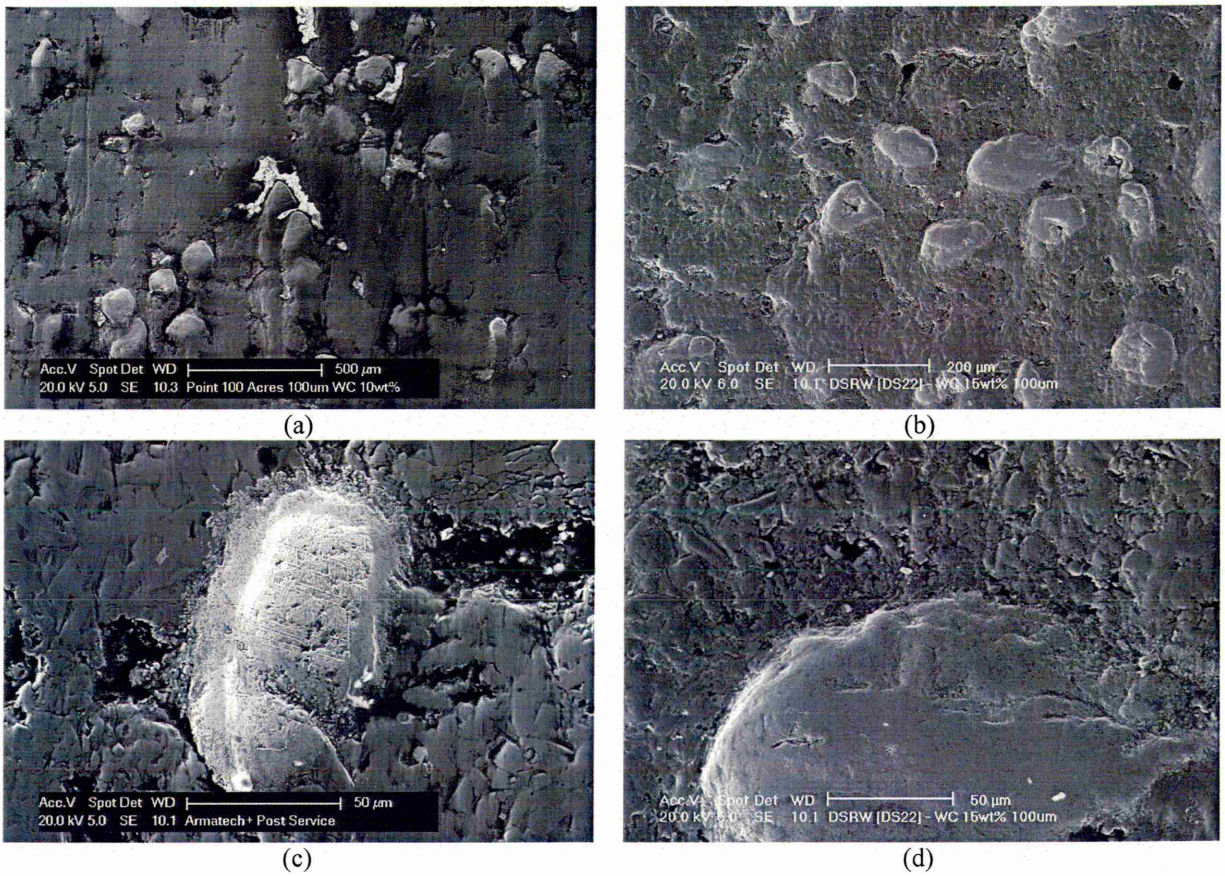

Figure 199: SEM micrographs showing similarities between wear morphologies of field and DSRW tests on 100 µm WC/W_2C modified Armatech. (a) and (c) Field wear; (b) and (d) DSRW wear.

The results from the WC based additions suggest that an optimum loading between 5 and 10wt.% using a small, large or mixture of both can provide improved wear resistance over Armatech.

The results from the Al_2O_3 materials showed that an addition of 3wt.% 50 µm particles reduced the wear resistance providing a similar result to that of boron steel. An addition of 3wt.% 10 µm particles provided an improvement of around 50%. This was an unexpected result when considering the ratio of the abrasive particle size and the particle size of the addition. It was suspected that a larger hard phase addition to Armatech would withstand wear from a large abrasive particle better than smaller additions. It was seen however from the characterisation of the material and from wear scar examination that the larger (50µm) addition of Al_2O_3 suffered a high level of fallout.

The material with 5wt.% 45 μm Mo_2C showed an improvement in volume loss over Armatech of around 60%. Examination of the final structure revealed the Mo_2C was in actual fact agglomerations of very small particles, and not single 45 μm particles. MSAW results also did not show any significant improvement in wear resistance. Examination of the wear scar from this test showed the Mo_2C exhibited two-body wear grooves.

The most improved material when considering the RWR values was that with the 5wt.% addition of 100 μm WC/W_2C at RWR = 3.09 followed closely by the 5wt.% addition of 15 μm WC at RWR = 2.78.

7.7 ASTM G65 Wet sand Rubber Wheel Testing - WSRW

Firstly, the obvious difference compared to results from the dry environment is the extent of material loss. The average weight loss for the dry environment was 0.15 g and for the wet environment 0.06 g.

The results revealed that Armatech provided some improvement in volume loss over boron steel, around 20%, a smaller effect when compared to the dry environment. This difference was mostly due to the boron steel suffering lower material losses in the wet environment as opposed to a change in the Armatech wear rate.

The boron steel wear scar had a two-body grooving mechanism, similar to the dry environment, but possessed a smoother appearance. Pitting on the boron steel material seen in field service and from MSAW tests was not present as a result of WSRW testing. The reason for this was not fully understood, it was expected that the fluid carrier would deplete oxygen at the surface and initiate pitting, as previously suggested the slurries in MASW and moisture in soil did.

Cross-sections taken through each wear scar revealed the depth of indentation to be minimal. It is likely that the aqueous carrier acts in a lubricating manner reducing the frictional forces involved and hence the energy available for material damage and removal.

Examination of the Armatech wear scar showed signs of microcracking, but to a lesser extent to that seen in the dry environment test (which may confirm a reduction in frictional forces). The cross-section through the scar revealed sub-surface cracking was to a depth of 5 μm.

An interesting result was obtained from the series of materials produced using 15 μm WC. Under dry conditions the additions of 5 and 10wt.% showed significant improvements in wear resistance over Armatech. When introducing water into the wear interface this improvement was reduced. Slight improvements in the average volume loss was seen with 5 and 10wt.% and around a 40% improvement at 15wt.%, all however were within error of the result for Armatech. The appearance of the wear scars were very similar to those produced from a dry environment.

The addition of the 100 μm WC/W_2C materials under wet conditions improved the wear resistance considerably at a loading of 5wt.% and further improved further with an increase in WC content. The exact reason for this considerable improvement in wear resistance is difficult to ascertain. It was evident from examining the wear surface of the 100 μm WC/W_2C material under dry conditions that the particles formed a network of wear resistance phases that protruded from the surface. Examination of the wear surfaces from wet conditions showed that the WC/W_2C particles were not seen to be standing proud of the surface, Figure 200. It was also evident that the core of the WC/W_2C particles showed a large of amount of cracking and fallout, a similar mechanism to that seen in the SiO_2 MSAW tests.

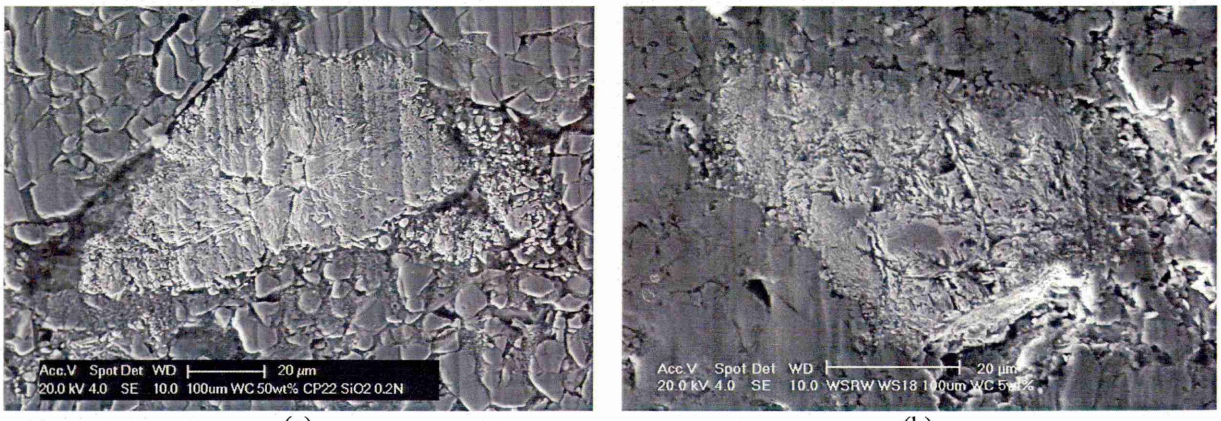

(a) (b)

Figure 200: SEM micrographs showing similar wear mechanism (core cracking) of 100 μm WC/W_2C particles in (a) MSAW tests with SiO_2 abrasive and (b) WSRW testing.

The materials with mixtures of 15 μm WC and 100 μm WC/W_2C, as for the dry conditions, showed no major improvements in wear resistance apart from the 5 plus 5wt.% material which provided a ~30% improvement.

The results from the Al_2O_3 and Mo_2C materials under wet conditions showed no significant improvements. The wear surface of the Al_2O_3 material showed signs of fallout whilst the Mo_2C appeared very similar to the appearance seen in the dry condition.

7.7.1 Results summary

The two-body wear mechanism observed on tillage tool surfaces from soil wear was able to be replicated using the rubber wheel tester with the same abrasive medium in both wet and dry conditions. An increase in wear was seen for dry tests compared to the wet tests.

Moore[109] suggested that the presence of water would lead to an increase in abrasion rate by promoting abrasive particle fracture. This proposed mechanism however was not observed in this research or in research by Wirojanupatump and Shipway[82,91] who also observed decreases in abrasion rate with wet abrasive. Although particles may fracture and become more angular in nature, the abrasive in rubber wheel testing passes through the interface only once, and it has

been shown that a smaller abrasive (under 100 μm) reduces wear rate. However, research has shown that not only particle size but also shape can affect wear rate.

It is believed that the water affects the interaction of the abrasive with the sample/wheel by providing a lubricating effect in conjunction with a reduction of the imposed forces caused by the hydrodynamic layer reducing load per abrasive particle. The presence of water may also serve to reduce, and not increase as suggested, abrasive particle fragmentation. Fragmentation may create more angular faceted particles that increase the level of attack and hence the rate of material removal, this would need to be confirmed by analysing used abrasive particles, which was not done here.

The facility to measure wheel temperature was not available when performing the tests and it is assumed that the wheel temperature was higher in dry conditions when compared to wet, as the fluid will act as a coolant, as suggested by Swanson and Klann[110]. The effect of increasing the wheel temperature would lead to a reduction in hardness of the rubber, Swanson and Klann suggested that the increase in temperature and hence reduction in hardness would reduce wear rates. Shipway and Wirojanupatump[91] measured a wheel temperature of 65°C in dry conditions and the temperature in wet was close to that of the fluid. Stevenson and Hutchings[79] stated that an increase in wheel temperature from 20°C to 70°C would reduce the wear rate of steel by 20%.

It has been seen here that when a fluid is introduced the wear rate decreases, lower material losses were seen in wet conditions where the wheel temperature is lower. The smoother wear mechanisms observed suggests that the fluid and subsequent change to wheel temperature affects the abrasive particle motion, the fluid acts in a lubricating manner and serves to **reduce** wear rate.

Aside from the overall weight loss reduction experienced in wet testing, the overall trend observed in the dry environment changed in the presence of water. It was observed that under wet conditions the majority of the test samples provided very similar values of material removal, with the exception of three materials. Arguably, a similar trend was seen with SiC and SiO_2 abrasive in the MSAW tests. Both the WSRW and the MSAW with SiO_2 were less aggressive tests and introduced a change in abrasive particle interaction when compared to DSRW and MSAW with SiC. The dry tests showed both 15 and 100 μm particles provided good wear resistance when worn by 260 μm sand. In wet conditions only the larger 100 μm additions to Armatech improved wear resistance.

The common factor to both the DSRW and WSRW tests was the improved performance of the modified materials over both boron steel and Armatech. Each modified coating performed better than the two reference materials, with the exception of $WC(15)_{[15]}$ in the DSRW test.

One option for the future could be to make further modifications to the ASTM G65 to replicate soil wear more closely by the use of additional hoppers with varying sized abrasives to feed into the wearing interface.

7.8 Field Tests

The opportunity for limited field testing allowed a conservative selection of material to be tested. Due to limitations and time constraints it was not possible to explore all the combinations of additive levels, particles size and types used to modify Armatech in the laboratory tests. The effect of plough speed and soil types on wear resistance could also not be explored. The tests allowed Armatech to be compared against the typical tillage tool material of boron steel under partially controlled conditions and later allowed a direct comparison of Armatech against a modified coating and the effect of plough position to be investigated.

7.8.1 Trial A – September 2006

Literature has shown that tools in the plough position nearest the tractor tend to suffer the greatest wear. For this reason the first position was ignored. The next position along (Position 2) was occupied by Armatech coated tools while boron steel tools were fixed in Position 3. In theory, Position 2 suffers greater wear than Position 3.

The final plough position (Position 4) used $WC/W_2C(10)_{[100]}$ coated tools as this material had shown promising results from laboratory testing. The primary intention was to obtain information regarding wear mechanism of this material in soil. The objective was not necessarily to obtain results to form a comparison against boron steel and Armatech due to the uncertainty in effect of plough position (a later opportunity allowed the comparison of Armatech against this material).

The field test provided promising results for Armatech coated tools. The Armatech tool, placed in a more aggressive position than boron steel, showed that both the points experienced around 15% reduction in weight loss when compared to boron steel points. Conversely, the Armatech share suffered ~2% higher material loss than the boron steel share. This amount of loss however may be considered negligible when considering error and plough position. Shares generally experience a less aggressive form of attack than points and have extended working lifetimes.

The $WC/W_2C(10)_{[100]}$ coated tools in Position 4 showed good results from Trial A. The point showed a very similar weight loss to the Armatech coated point and the share experienced much lower material loss than both the boron and Armatech tools, by almost a third in both cases.

The conclusion that can be drawn from Trial A is that that over 100 acres both Armatech and $WC/W_2C(10)_{[100]}$ coated points outperform tools manufactured from boron steel under the particular soil conditions. It was also shown that Armatech coated shares provided no

improvement over boron steel shares, but preliminary tests with $WC/W_2C(10)_{[100]}$ shares showed signs of improved wear resistance.

7.8.2 Trial B – March 2007

The field tests performed in March again only allowed a limited test matrix to be utilised. The results from Trial A showed improvement over boron steel for Armatech coated tools (and $WC/W_2C(10)_{[100]}$ coated tools although in a less aggressive plough position), therefore Trial B was used to compare $WC/W_2C(10)_{[100]}$ against Armatech.

Armatech and $WC/W_2C(10)_{[100]}$ coated points and shares were assessed in each of the five positions on the plough frame. The results from this trial confirmed that a higher weight loss occurs in Position 1 nearest to the tractor, and reduces in each position away from the tractor. The weight loss analysis showed that the $WC/W_2C(10)_{[100]}$ coated points suffered lower material losses in each plough position, between 1 and 4% less. This trend was also observed in the weight loss of the shares, but to a greater degree. The $WC/W_2C(10)_{[100]}$ coated share in Position 5 experienced a 90% reduction in material loss. At Position 4 a 50% reduction, and Position 2 and 3 a 40% reduction, in Position 1, the most aggressive position a 30% reduction was still seen. This large increase in performance seen with the $WC/W_2C(10)_{[100]}$ coated shares may be linked to the wear mechanisms seen from examination of the coating on points removed from service, and also from the resulting laboratory wear mechanisms. It has been shown that under certain conditions, the WC/W_2C particles suffered from cracking and hence material loss from the core due to the applied load encountered. Shares experience a lower work load and hence suffer a lower severity of wear when compared to points. The improved wear resistant properties of the WC/W_2C modified Armatech is less prominent in the more aggressive application as a ploughshare point coating.

7.8.3 Field Trial Results summary

The limited field trials confirm that an Armatech coating can increase the wear resistance of ground engaging plough points, and that a modified Armatech coating with 10wt.% 100 μm WC/W_2C addition can further increase wear resistance on points and even more so on shares.

7.8.4 Further considerations

The coatings are applied to the leading edges of the tool when manufactured for sale. This means that any exposed areas of substrate will also suffer wear and hence material loss during the lifetime of the coating. Therefore, whilst tests performed were relatively short compared to usual plough lifetimes and although the majority of wear occurred on the leading edge of the tool, any loss in weight inherently included a large amount of uncoated substrate loss. With hindsight, the design of the tool should have been modified for testing to allow the whole tool to be coated, and therefore a larger proportion of the weight loss would have been the coating. However, visually it could be seen that the coatings were protecting the tool and it was also

shown that the substrate wears at a faster rate when not coated. So while the measurements are a combination of both coating and substrate loss, it provides valuable information on the wear resistance of the 'real product'.

7.8.5 Pitting corrosion

Localised corrosion such as pitting is extremely difficult to predict and the complexities of environments required to initiate corrosion add to the problem of predicting and understanding pitting corrosion. The driving force behind pitting is often a lack of oxygen, which creates anodic and cathodic regions that lead to highly localised galvanic corrosion in the form of pits. It is a mechanism that is often associated with temperature, humidity and pH level. Pitting is often seen on metals alloys that have a passive layer such as stainless steel which tend not to suffer from general corrosion, breaks in the layer can lead to a large cathodic area and a small anodic region and hence pitting. Often this is seen in high chloride environments such as sea water where Cl^- ions aggravate the formation and growth of pits.

However, the pitting observed in this research was on boron steel which does not rely on a passive layer for corrosion resistance, also pitting was seen from field conditions, where moisture in the soil may contain chlorides, most likely at low levels. Localised pitting was also observed in MSAW tests, however using slurries with a deionised water aqueous carrier.

The role of corrosion through slurry abrasives was explored by Shipway and Wirojanupatump[91]. It was concluded that wear rate of steel increases and the wear mechanism changes when switching the aqueous carrier to an acidic from a neutral pH. The change in acidity was less significant for thermally sprayed NiCr-Cr_3C_2 coatings. Also, the effect of pH level on sintered WC-Co hardmetals has been shown to have dramatic effect on wear rate[111].

The effect of pH level was considered in these tests. The water used in the WSRW tests had pH of 7.0, the pH level of the SiC slurry was 4.95 and the SiO_2 slurry 5.23 (measured after a 1 hour settle period to allow CO_2 absorption), the average soil pH measured from the field trials was 6.04. The abrasive media in the MSAW test and field tests had lower pH values than the deionised water, it has indeed been shown with stainless steel that a reduction in pH level can increase pitting potential (and also a function of chloride ion concentration and temperature), however, it is generally decreases in pH to around 2 or 3 that increase the potential, and reducing pH from 7 to 4 often reduce pitting potential.

This said, boron steel is not a stainless steel and these conditions would not directly apply. The pitting resistance of boron steel has not been as extensively researched as stainless steels have. For this reason it is not fully understood why the boron steel suffers from pitting corrosion in field trials and in the MSAW tests whilst appearing not to pit under WSRW conditions. The coating materials did not suffer pitting under any conditions most likely due to the high nickel and chromium content which are corrosion resistant elements.

7.8.6 *The effect of hard phases in a tough metallic matrix*

The addition of hard phases to a Armatech in order to enhance wear resistance against a hard angular abrasive such as SiC resulted in no improvement. SiC imposes a severe wear testing condition.

It has been shown that simply increasing the level of addition does not enhance wear resistance with the effect on wear resistance being non-linear. Instead the optimum level of addition is dependent upon the level of bonding between the additive and the host matrix, the severity of the wear, and the abrasive type and applied load. Where abrasive particles are small they are able to penetrate between the hard phases and attack the softer matrix. It has been shown that when the material surface is abraded by a small angular abrasive (such as MSAW with SiO_2) the matrix material is preferentially worn away. Increasing the abrasive size (ASTM G65) prevented preferential attack of the matrix phase around the carbides and borides but attacked the Armatech matrix around the 100 μm WC/W_2C particles in dry sand rubber wheel testing.

It could be seen that the interaction of the abrasive particles and the hard phases can promote fracture of the hard phases. As the matrix around the carbides and borides is worn away they become exposed and further particle interactions lead to more cracking.

It has been shown here that the addition of a secondary phase with a high hardness value can increase wear resistance but the optimum size of the particle depends upon the size of the abrading particle. The increase in wear resistance is also a function of the addition level. As additive levels were increased the wear resistance began to increase up to an optimum level and further additions then reduced wear resistance. It is suspected that this effect is due to firstly the ratio of matrix phase to secondary hard phase, but also a chemical effect. High loadings will affect the chemical balance of the parent material and tend to increase susceptibility of material fallout.

7.9 Comparison of Wear tests

Since laboratory wear conditions differ greatly from the wear of tools in soil, the use of laboratory results to simulate field service is a difficult task. However, field trials to assess a new or even existing material are time consuming and expensive, more over it is difficult to keep the operating variables involved constant, which is essential to obtain valid performance comparisons.

The major variables associated with field wear are the wide size range and type of abrasives and other soil parameters such as moisture content or soil strength.

One objective of this research was to determine whether laboratory wear tests could be used to accurately assess materials for resistance against soil wear. It is not the intent to eradicate the

use of field trials to assess tillage tools, as this is the most 'realistic' method of determining how a material will perform. However, the aim was to use laboratory tests to identify the most promising candidate materials and thus reduce the extent of field tests required to assess a material.

The advantages of laboratory tests include the reduced test time needed, the amount of labour involved, the quantity of test material required and the ability to control operating variables.

One key objective of this research was to ascertain whether the laboratory test could adequately reproduce field wear by the assessment of worn tools and making comparisons to wear mechanisms produced from laboratory procedures.

Comparisons of laboratory wear tests to field wear have been performed previously by Swanson[107,88] and Richardson [18] (discussed in Chapter 2). Swanson concluded that the ASTM G65 test with dry abrasive adequately simulated sandy soil wear with a low moisture content using various alloy steels and an aluminium alloy (performed in the U.S.). The wear resistances measured from laboratory wear testing were reported to correlate well with field tests in sandy soils. However, it was reported that with heterogeneous materials, such as hardfacings, results between the laboratory and field differed significantly. It was stated that the role of the hard phase in resisting abrasion depends upon the scale of abrasion relative to the size and distribution of the hard phase particle in the supporting matrix. This has been confirmed in this study.

Both Swanson and Richardson compared field wear with pin-on-disk testing, Swanson concluded that the wear produced using pin-on-disk reproduced soil wear more closely than the rubber wheel tests. However it has been shown here that DSRW testing closely resembles wear in British soils. Literature that compared MSAW testing against field wear was not found.

Three wear tests have been assessed in order to determine their suitability to measure the wear resistance of the existing and modified coatings. The wear mechanism that tools experience from soil wear was recreated to a limited degree in each test. The abrasives used in the laboratory tests were a good model for abrasives found in soils, with small particles of silica several microns in size and larger silica particles common to the small fraction of soils.

One method of comparing the materials performance (ignoring the WC-Co tile) across all of the test methods is to list the best five from each test, Table 32. It can be seen that in each test the best performing material had an addition of 100 μm WC/W_2C at either 5, 10 or 15wt.% loading (with the exception of $WC(7\&3)_{[15\&100]}$). If a scoring system is applied to these results by giving points to each material based on ranked position, i.e. by giving 1st position five points to one point in the 5th position (from laboratory tests only), they can be ranked the materials for overall performance as shown in Table 33.

Table 32

Comparative ranking of test materials from each wear test

	MSAW SiC	MSAW SiO_2	DSRW	WSRW	Field test September 2007	Field test March 2008
1	$WC/W_2C(10)_{[100]}$	$WC(7\&3)_{[15\&100]}$	$WC/W_2C(5)_{[100]}$	$WC/W_2C(15)_{[100]}$	$WC/W_2C(10)_{[100]}$	$WC/W_2C(10)_{[100]}$
2	$WC(5)_{[15]}$	$WC(20)_{[15]}$	$WC(5)_{[15]}$	$WC/W_2C(10)_{[100]}$	Armatech	Armatech
3	Boron Steel	$WC(1\&4)_{[15\&100]}$	$Mo_2C(5)_{[45]}$	$WC/W_2C(5)_{[100]}$	Boron Steel	-
4	Armatech	$WC(15)_{[15]}$	$WC(1\&4)_{[15\&100]}$	$WC(15)_{[15]}$	-	-
5	$WC/W_2C(5)_{[100]}$	$WC/W_2C(15)_{[100]}$	$WC(7\&3)_{[15\&100]}$	$WC(5\&5)_{[15\&100]}$	-	-

From this ranking system it can be can see that $WC/W_2C(10)_{[100]}$ coatings provide the best wear resistance closely followed by $WC(5)_{[15]}$.

Table 33
Performance ranking

Test material	Wear performance points
$WC/W_2C(10)_{[100]}$	9
$WC(5)_{[15]}$	8
$WC(7\&3)_{[15\&100]}$	6
$WC/W_2C(15)_{[100]}$	5
$WC(1\&4)_{[15\&100]}$	5
$WC(20)_{[15]}$	4
$WC(15)_{[15]}$	4
$WC/W_2C(5)_{[100]}$	4
Boron Steel	3
$Mo_2C(5)_{[45]}$	3
Armatech	2
$WC(5\&5)_{[15\&100]}$	1

The result show that Armatech modified with WC can improve wear resistance, the exact level of addition and size is not directly clear, but a level between 5 and 15wt.% with either a 15 μm particle size or a 100 μm particle size, or a ratio of both appears to be the optimum addition.

7.9.1 Comparison of MSAW to Field trial results

It is not possible to draw a direct comparison between MSAW and field wear due to the abrasive and loads involved being very different. However, whilst examination of the wear mechanisms achieved from MSAW, using both SiC and SiO_2 abrasive, did not reveal a visual similarity, a two-body grooving mechanism was achieved using SiO_2.

The microstructure of many of the materials had secondary hard phases distributed in the Armatech matrix which were considerably harder than the SiO_2 abrasive. This is often the case in soil wear, soils contain abrasive particle that may not be harder than the hard phases within a coating, but the range of particle sizes means that some will be considerably larger than the hard phases in the coating.

It is however, important to understand the mechanism by which a material resists the wear induced by the fine fraction in soils, as standard wear tests do not use abrasive particulate ranges but single particle size abrasives. This means that a direct comparison of the MSAW test (singles size abrasive) to field wear (<0.002 to >2 mm abrasives) is not a straightforward comparison.

It was suggested by Moore[112] that hard particles are more effective in resisting abrasive wear from small abrasive particles under low load (MSAW). As the depth of the particle penetration increases with higher loads (ASTM G65 or field wear), the matrix or bulk properties become more important in determining wear resistance.

The results of this research support the hypothesis that the addition of hard phase particles to a material can increase wear resistance under most conditions. However, a simple relationship between the hard phase addition and the abrasive particle size is not obvious. If the tests performed using SiO_2 only are considered it could be concluded that where the applied load is low and abrasive particle size is small then a secondary hard phase with a particle size similar to the abrasive (or a mixture of small and large) provides the best wear resistance, whereas in conditions where applied load is high and abrasive particles are larger than the secondary addition, then a larger particle size hard phase (100 μm WC/W_2C) performs the best.

7.9.2 Comparison of ASTM G65 to field wear

The abrasive particles used in the ASTM G65 based tests were similar to the size range constituting the sand in the field trial soils.

A direct comparison between the laboratory and field wear results is difficult to achieve due to the wide range of abrasive particle sizes found in the field soil and also the occurrence of impacts from stones during field trials which cannot be replicated in the laboratory.

There was an increase in wear for tests carried out using dry abrasive compared to the wet abrasive test. Possible explanations for this include the cooling of the abrasive and wear surface (although previous research has shown temperature effects to be negligible), a lubrication effect and/or abrasive particle motion effects where the fluid causes the particle to either roll for more of the time in the interface or reduces the penetration of the particle during motion.

Cracks were observed in cross-sections from the ASTM G65 samples that propagated a few microns beneath the wear surface. These cracks however were not continuous across the whole wear scar width. These may be formed through a fatigue mechanism caused by the test (although no evidence was found to support this); these may cause weakening of the material which causes further fragmentation by abrasion.

7.9.3 Practical applicability

The comparison of the laboratory tests to the field trials shows that the DSRW test is probably the most practical method for determining the performance of a material against soil wear, particularly in replicating wear in a clay loamy British soil. The wear mechanisms produced were virtually the same as the wear seen on tools having been worn in service. A potential further improvement would be to further modify the ASTM G65 to incorporate the use of an abrasive with a range of sizes to replicate field wear.

Whilst MSAW testing with SiO_2 was able to produce two-body grooving wear and a rank for each material more work is needed to develop the test procedure if it is to be used for soil wear simulation.

7.10 Coating Costs

To consider the effectiveness of producing wear resistant materials the service performance has to be considered alongside the feasibility of manufacturing the coating, and the cost effectiveness.

The modifications made to the Armatech were all carried out using standard Armatech powder and were all fired using the existing conditions. The only addition to production methods involved the use of automatic stirring equipment at the factory to enable the additions to remain in suspension and increase homogeneity when made into slurry form.

The relative costs of the coatings along with boron steel are provided below in Table 34. It can be seen that boron steel is only one tenth the cost of Armatech. This suggests that with the same volume of material, Armatech would need to have an increased wear rate of at least 10 times in order to be cost effective. The largest improvement measured was from MSAW testing using SiO_2 which saw an improvement of around 2.5 times somewhat lower than 10 times. The ASTM G65 and field test results also saw improvements with Armatech over boron steel, but only in the region of 110 – 120%.

It can be seen that the cost of Armatech per kg increases with the addition of the modifications. If $WC/W_2C(10)_{[100]}$ is considered, one of the modifications that gave the overall best performance in wear resistance, increases to a cost ratio of 1.56. The coating showed improvement of around 170% from DSRW and over 10 times improvement from WSRW. Field trials however revealed an average RWR value of 1.48 for the points and 2.6 for the shares (Field Trial B). If improvements of 170% could be achieved from the modified coating then this can be deemed as a cost effective method of improving Armatech.

Table 34

Relative cost per kilogram of the coatings

Material	Relative cost per Kg******
Boron steel	0.1
Armatech	1.0
$WC(5)_{[15]}$	1.34
$WC(8)_{[15]}$	1.54
$WC(10)_{[15]}$	1.56
$WC(15)_{[15]}$	2.02
$WC(20)_{[15]}$	2.36
$WC/W_2C(5)_{[100]}$	1.28
$WC/W_2C(8)_{[100]}$	1.45
$WC/W_2C(10)_{[100]}$	1.56
$WC/W_2C(12)_{[100]}$	1.67
$WC/W_2C(15)_{[100]}$	1.84
$WC/W_2C(20)_{[100]}$	2.12
$WC/W_2C(50)_{[100]}$	3.79
$WC/W_2C(70)_{[100]}$	4.90
$WC(7\&3)_{[15\&100]}$	1.64
$WC(1\&4)_{[15\&100]}$	1.29
$WC(5\&5)_{[15\&100]}$	1.62
$WC(3\&7)_{[15\&100]}$	1.59
$Al_2O_3(3)_{[50]}$	1.91
$Al_2O_3(6)_{[50]}$	2.87
$Al_2O_3(3)_{[10]}$	1.15
$Al_2O_3(6)_{[10]}$	1.31
$Mo_2C(5)_{[45]}$	1.84
$Mo_2C(10)_{[45]}$	2.68
$TiC(5)_{[75]}$	1.45
$TiC(10)_{[75]}$	1.90

****** The cost of Al_2O_3, Mo_2C and TiC powders were from scientific supply companies, the cost would reduce if bought in bulk at a lower quality grade.

Chapter

8

Conclusions and Recommendations

8 Conclusions

In assessing the production method used to manufacture the Armatech coating it was found that the optimum furnace conditions were a temperature of 1083°C (±2°C) at a belt speed of 5 m/hr (over 18 meters).

The method of ensuring optimal mixing of the PM coating slurry was also assessed. It was recommended that an automatic mixer should be used to ensure an even distribution of the binder phase within the slurry; this recommendation was implemented by Chapmans Agricultural.

8.1 Conclusions from the materials development and characterisation:

- The existing coating system known as Armatech consisted a Fe-Ni-Si rich matrix (~700 H_V) with two hard phases; an Fe-Cr carbide phase (M_7C_3) along with an Fe-Cr boride phase (M_2B) which both possessed hardness values ~1500 H_V.
- TiN, TiB_2, TiC and TaC was not wet by the matrix phase of the Armatech and thus resulted in highly porous materials that were prone to pullout. For this reason further testing using these modifications was not performed.
- The Mo_2C addition wetted well with the Armatech. Examination of the microstructure revealed that the individual Mo_2C particles (45μm) were in fact agglomerates of much smaller particles.
- The two particle size additions of Al_2O_3 revealed that whilst this addition did not fully wet with the Armatech the sintering process held the addition in-situ and pullout was significantly reduced compared to the Ti based additions.
- The most promising additions were the various grades of WC. Two particle sizes were used, of which the larger particles were made up of both mono (WC) and di-tungsten carbide (W_2C). Both additions integrated well with Armatech, with the larger addition forming a reaction zone with the Armatech matrix. Some pullout of the smaller addition was observed, albeit at very low levels, the majority of the particles integrated well within the structure forming a network of small hard phase.

The measurement of bulk hardness (using loads >1kg) is not an appropriate technique for assessing the true or effective hardness of a heterogeneous material such as Armatech when considering its performance as an abrasive resistant material.

Due to the fact that the individual events causing wear damage are of the same order, or smaller, than the individual phases it is the hardness of these phases which is of greater relevance. Thus a micro-hardness test needs to be employed.

The established criteria, that the materials should possess a hardness of at least 80% of the abrasive ($80\%H_a$) cannot be relied upon as a predictive tool when considering the facts above.

8.2 Microscale Abrasive Wear.

The major conclusions drawn from the development and use of the MSAW test are:

- No relevant published research involving MSAW testing with small (2.5 μm) SiO_2 abrasive was found.
- Under the conditions used here the maximum applied load was limited to 1.5N, above which a central groove was produced, indicating slurry starvation.
- SiC was a significantly more aggressive abrasive than SiO_2.
- MSAW tests using SiC abrasive yielded well defined craters and was shown to possess excellent reproducibility. However, the wear mode created was three-body rolling which is not the dominant mechanism observed in soil induced wear.
- SiO_2 abrasive resulted in two-body grooving for the carbide and boride phases whilst three-body rolling indentations were observed in the softer metallic matrix phase of Armatech. Wear scars however were relatively small and had less well defined edges thus increasing crater measurement error.
- The wear mechanism induced in the MSAW test is dependant upon abrasive hardness, size and shape. However, wear resistance appears to also be dependant upon the relative size of the abrasive to the hard phase within the microstructure. The results suggest that when using a small abrasive particle size (2-5μm), materials that contain hard phases of a similar size (~5μm) provide the best wear resistance.
- The Archard equation, widely used to calculate wear volume in MSAW testing, was not seen to hold for this particular application. The equation assumes wear to be directly proportional to load. Whilst this was observed for three-body wear, it was shown that two-body wear obeys a power law which does not pass through the intercept.
- Phenomena, such as edge rounding, in MSAW testing have been highlighted, whereby over estimation of crater volume may occur. Edge rounding occurs when the crater edge definition is reduced through wear by a build up of abrasive particles in the meniscus slurry at the ball/sample interface. The problem of over estimation however is

eradicated when comparatively ranking materials in a single research project (assuming that each material behaves in a similar fashion).

The fundamental conclusion to be drawn from the MSAW test, used as a method of evaluating the wear resistance of tillage material against soil, is that the use of SiC as a test abrasive is inappropriate due to the severity of wear created.

8.3 Conclusions on the use and results of the ASTM G65 rubber wheel test.

- The 260 μm silica sand abrasive possessed a similar morphology to the small particulates found in the field trial soil in South Yorkshire, UK.
- Examination of the wear surfaces generated from the ASTM G65 test in both wet (WSRW) and dry (DSRW) conditions revealed excellent correlation with field wear morphology, with clear two-body grooving in both environments.
- Test results from dry conditions produced a higher material weight loss when compared to wet conditions (average weight loss was 0.15 g for the dry environment was and 0.06 g for the wet). The reduction was due to a lubricating effect from the fluid which affects particle motion at the sample/wheel interface.
- The lubricating effect seen in the presence of water created a smoother appearance to the wear surface.

The use of both types of wear test indicated a significant improvement in abrasive wear resistance for materials containing WC additives. The optimum material under these test conditions was found to be an addition of 15 μm WC at 10wt.% in MSAW testing and an addition of between 5 ands 15wt.% of 100 μm WC in ASTM G65 testing.

8.4 Conclusions from the Field Trials.

- The field trial results showed that a higher weight loss occurs in the position nearest to the traction unit, and wear is reduced in those points further away from the traction unit.
- The addition of an Armatech coating significantly increases the wear resistance of boron steel tools. Furthermore, a modified Armatech coating with 10wt.% 100 μm WC/W_2C addition can further increase wear resistance on points and is particularly effective on shares.

- The comparison of the laboratory tests with the field trials indicates that the DSRW test is the most practical method for determining the performance of a material against soil wear, particularly in replicating wear in a clay loamy British soil. The wear mechanism produced was virtually the same as the wear seen on tools having been worn in service.

8.5 Recommendations for Further Work.

The results of this research have indicated the following areas as recommendations for further work.

- Perform further work to assess the large variations associated with the macrohardness measurement of Armatech.
- Use alternative methods, such as 3D profiling methods, to measure wear crater volume in MSAW tests.
- The effects of real soil may be simulated more accurately by using the ASTM G65 with abrasives with a particle size distribution similar to that found in the soil of interest.
- Tungsten Carbide powders are relatively expensive and further work is recommended on the use of cheaper forms or WC (e.g. scrap) or on cheaper carbide additives.
- The results indicate that the use of a hard additive with a range of particle sizes may be the most beneficial in terms of resisting soil wear and this work needs to be extended.
- The field trials performed as part of this research were carried out in one geographical location, and it has been shown that soil properties differ widely around the globe. In order to gain a better understanding the wear resistance of the modified coatings, and to assess the wear resistance of the coatings as a function of soil type it would be beneficial to perform field trials in other locations with different soil classifications or, through the use of test tracks such as the one based in the at the University of Southern Australia, Adelaide.

[1] M.J. Neale and M.G. Gee, "*Guide to wear problems and testing industry.*" Professional Engineering Publishing Ltd, London; Editors: M.J. Neale, T.A. Polak, C.M. Taylor, First edition (2000).

[2] A. Natsis, G. Papadakis and J. Pitsilis, *J. Agric. Eng. Res.* **72**, 171 (1999).

[3] S.A. Ferguson, J.M. Fielke and T.W. Riley, *J. Agric. Eng. Res.* **69**, 99 (1998).

[4] H.J. Yu and S.D. Bhole, *Tribology International,* **23**, 309 (1990).

[5] M.A. Moore, *Wear* **27**, 1 (1974).

[6] M.M. Khrushchov and M.A. Babichev, "Research on wear of metals." Izdat. Akad. Nauk, Moscow. NEL Transl. (1960).

[7] R.L. Aghan, L. E. Samuels, *Wear* **16**, 293 (1970).

[8] K. Kato, *Tribology International.* **30**, 333 (1997).

[9] J. Larsen-Badse, *Wear* **11**, 213 (1968).

[10] M.F. Stroud, H. Wilman, *Brit. J. App. Phys.* **13**, 173 (1962).

[11] G.B. Stachowiak, G.W. Stachowiak, *Wear* **256,** 600 (2004).

[12] E. Rabinowicz, L.A. Dunn and P.G. Russell, *Wear* **4**, 345 (1961).

[13] J.D. Gates, *Wear* **214**, 139 (1998).

[14] J.T. Burwell, *Wear* **1**, 119 (1957)

[15] A. Misra, I. Finnie., *Wear* **60**, 111 (1980).

[16] R.C.D. Richardson, *Wear* **10**, 291 (1967).

[17] C.R. Weiss, *Iron Age*, 1166 (1932).

[18] R.C.D. Richardson. "The wear of metal shares in agricultural soil." PhD Thesis University of London (1967).

[19] B.W.E. Avient, J. Goddard and H. Wilman, *Proc. Roy. Soc.* A258 159-180 (1960).

[20] A. Misra, I. Finnie, *Wear* **68**, 33 (1981/4/15).

[21] R.C.D. Richardson, *Wear* **10**, 353 (1967).

[22] A.G. Foley and V. A. McLees, *J. Agric Engng Res.* **35**, 97 (1986).

[23] R.C.D. Richardson, *J. Agric Engng Res.* **12**, 22 (1967).

[24] M.A. Moore, *Tribology International*, **105** (1975).

[25] BS1377: 1975 Methods of test for soil for civil engineering purposes.

[26] European Commission Joint Research Centre. Institute for Environment & Sustainability, November 2004

[27] C. J. Studman, *J. Agric. Eng. Res.* **20**, 413 (1975).

[28] R.W. Fitzpatrick, T.W. Riley, M.J. Wright, J.M. Fielke, P.J. Butterworth, B.G. Richards, P.J. McThompson. M.G. Slattery, D. Chin, S.G. McClure and J.S. Lundy, *End of Grant Report (1988-1990) for the Australian Wheat Research Council* (Project No.SAIT 1W), 1990, 141.

[29] Z. Owsiak, *Soil Tillage Res.* **50**, 333 (1999).

[30] R. Gahlin, S. Jacobson., *Wear* **224**, 118 (1999).

[31] A. Misra, I. Finnie., *Wear* **65**, 359 (1981/1/1).

[32] I. Sevin, I. B. Eryurek., *Materials & Design* **27**, 173 (2006).

[33] B.W.E. Avient, J. Goddard and H. Wilman, *Proc. Roy. Soc.* A258 (1960) 159-180.

[34] R.C.D. Richardson, *Wear* **11**, 245 (1968).

[35] A. Misra, I. Finnie, *Wear* **85**, 57 (1983/2/15).

[36] R.C.D. Richardson, Journal and Proceedings of the Institution of Agricultural Engineers. **19**, 42 (1963).

[37] A. Misra, I. Finnie, *Wear* **68**, 41 (1981/4/15).

[38] J. Larsen-Badse, *Wear* **12**, 35 (1968).

[39] G.K. Nathan, W.J.D. Jones., *Wear* **9**, 300 (1966).

[40] T.O. Mulhearn and L.E. Samuels, *Wear* **5**, 478 (1962).

[41] M.A. Moore, V.A. McLees and F.S. King, *The Agricultural Engineer*, **15** (1979).

[42] V.A. McLees, F.S. King and M.A. Moore, *"The effect of the wear of hard-faced steel plates and chisel plough points of weld bead pattern and soil type."* Rep. No.DN/ER/716/1160 (National Institute for Agricultural Engineering, Departmental note).

[43] M.A. Moore, V.A. McLees, *"The effect of weld bead pattern and spacing on the wear resistance of hardfaced steel plates in a flinty soil."* Rep. No.DN/ER/602/1160 (National Institute for Agricultural Engineering, Not for publication.

[44] V.A. McLees, M.A. Moore., *"The effect on the wear of steel plates of surface patterns which disrupt soil flow."* Rep. No.DN/EN695/1160/44 (National Institute for Agricultural Engineering, Not for Publication.

[45] P.L. Hurricks, *Wear* **22**, 291 (1972).

[46] R. Angers, B. Champagne, M. Fiset and P. Chollet., International Journal of Refractory Metals and Hard Materials **3**, 79 (1984).

[47] V.A. McLees, C.J. Chisholm., *"Hard materials for soil cutting edges. Part I: Preliminary Investigations."* Rep. No.DN 1374 (AFRC Institute of Engineering Research, 1986).

[48] V.A. McLees, C.J. Chisholm., *"Hard materials for soil cutting edges. Part II: Field trials Autumn 1986."* Rep. No.DN 1442 (AFRC Institute for engineering research, , 1988).

[49] V.A. McLees, C J. Chisholm., *"Hard materials for soil cutting edges. Part III: Assessment of different grades of tungsten carbide under field conditions, 1987."* Rep. No.DN 1502 (AFRC Institute for Engineering Research 1989).

[50] S. Hiller, V.A. McLees., *"Hard materials for soil cutting edges. Part IV: Assessment of an alumina-faced tungsten carbide-tipped plough point under field conditions, 1989."* Rep. No.DN1586 (AFRC Institute for Engineering Research -1990).

[51] A.G. Foley and V.A. McLees, *J. Agric Engng Res.* **35**, 97 (1986).

[52] P.J. Lawton, A.G. Foley, *J. Agric Engng Res.* **34**, 343 (1986).

[53] American Welding Society Welding Handbook Pt. III, Cleaver-Hume, London, 5th edn., 1965, Ch 41.

[54] A. G. Foley, *Soil and Water*, **12** (1984).

[55] K. Bhakat, A. K. Mishra, N. S. Mishra and S. Jha, *Wear* **257**, 338 (2004).

[56] A.G. Foley, *"Reducing wear of soil engaging equipment."* National Institute for Agricultural Engineering, Silsoe, (1984).

[57] R. Zhou, Y. Jiang and D. Lu, *Wear* **255**, 134 (2003).

[58] V.S. Popov, P.L. Nargony and A.S. Garbuzov, *Fiz. Metal. i Metalloved* **28**, (2) 332 (1969).

[59] V.S. Popov, P.L. Nargony and A.S. Garbuzov, *Russ. Cast. Prod.* **8**, 377 (1969).

[60] M.M. Oliveira, J.D. Bolton., *J. Mat. Process Tech.* **92-93**, 15 (1999).

[61] I.V. Petrov, N.A. Grinberg, *Svarochn. Proizv* **2**, 30 (1968).

[62] V.S. Popov, *Svarochn. Proizv* **1**, 32 (1971).

[63] V.V. Levin, A.F. Tereshchenko, *Avt. Svarka* **7**, 30 (1967).

[64] R.W. Wilson, *Symp. Savings from Tribology*, P.E.R.A. (1969).

[65] N.M. Serpik, M.M. Kantor, *Friction and Wear in Machinery* **19**, 28 (1965).

[66] R.N. Shaughnessy, *J. Iron Steel Inst.* **206**, 981 (1968).

[67] Y.A. Yuzvenko, M.A. Pashenko, *Avtomat. Svarka* **3**, 24 (1969).

[68] Introduction to powder metallurgy: The process and its products. European Powder Metallurgy Association (EPMA) 2004.

[69] S.A. Ferguson and R.W. Fitzpatrick, *Studies in to the effect of intensive cultivation on the properties of the tillage test track soil* (2000).

[70] M.G. Gee, et al., *"Interlaboratory Exercise: Description and Procedure,"* Rep. No. MATC(D)170 (NPL 2003).

[71] R.I. Trezona, D.N. Allsopp and I.M. Hutchings., *Wear* **225-229**, 205 (1999).

[72] M.M. Stack, M. Matthew, *Wear* **14**, 255, (2003).

[73] M.G. Gee *et al.*, *Wear* **255**, 1 (2003).

[74] D.N. Allsopp, R.I. Trezona, I.M. Hutchings, *Tribology Letters* **5**, 259 (1998).

[75] P.H. Shipway, J.J. Hogg, *Wear* **259**, 44 (2005).

[76] J.O. Bello, R.J.K. Wood, *Wear* **258**, 294 (2005).

[77] A.J. Gant, M. G. Gee and A. T. May, *Wear* **256**, 500 (2003).

[78] K. Adachi, I.M. Hutchings., *Wear* **258**, 318 (2004).

[79] A.N. J. Stevenson, I.M. Hutchings, *Wear* **195**, 232 (1996/7).

[80] ASTM G65-94, Standard test for measuring abrasion using dry sand/rubber wheel apparatus. 1996 Annual book of ASTM standards, vol. 03.02. ASTM.

[81] A.J. Gant, M.G. Gee., *International Journal of Refractory Metals and Hard Materials* **24**, 189 (2006).

[82] S. Wirojanupatump, P.H. Shipway, *Wear* **233-235**, 655 (1999).

[83] S. Wirojanupatump, P.H. Shipway, *Wear* **239**, 91 (2000/4).

[84] N.B. Dube, I.M. Hutchings, *Wear* **233-235**, 246 (1999).

[85] L. Xu, S. Clough, P. Howard, D. Stjohn, *Wear* **181-183**, 112 (1995).

[86] L. Bourithis, G. Papadimitriou., *Wear* **258**, 1775 (2005).

[87] P.A. Swanson., *Tribology* **ASTM STP 1199**, 80 (1993).

[88] P.A. Swanson, A.F. Vetter, *ASLE Transactions* **28**, 225.

[89] O.N. Dogan, J.A. Hawk, J. H. Tylczak, R.D. Wilson and R.D. Govier., *Wear* **225-229**, 758 (1999).

[90] R.D. Haworth., The abrasion resistance of metals. Trans. Am. Soc. Met. **41** 819-869 (1949)

[91] P.H. Shipway, S. Wirojanupatump, *Tribol. Int.* **35**, 661 (2002).

[92] A.J. Gant, M.G. Gee and B. Roebuck, *Wear* **258**, 178 (2005/1).

[93] H. Chandler. "Hardness testing" Materials Park, ASM International, 1999, 2nd ed.

[94] ASTM C914. Standard Test Method for Bulk Density and Volume of Solid Refractories by Wax Immersion. ASTM International.

[95] Theoretical density and hardness values obtained from CRC Materials Science and Engineering Handbook, 3rd Edition.

[96] BS 7755-3.2 1995 Soil Quality. Part 3: Chemical methods – Section 3.2 Determination of pH.

[97] Electron microscopy and analysis. P.J. Goodhew, J.Humphreys, R. Beanland, London: Taylor and Francis, 2001 3rd ed.

[98] http://www4.nau.edu/microanalysis/Microprobe/img/InteractionVolume.jpg

[99] Chapter 7: Basics of X-ray Diffraction. Scintag. www.scintag.com

[100] Elements of x-ray diffraction / B.D. Cullity, S.R. Stock. Upper Saddle River, NJ: Prentice Hall, 2001.3rd ed.

[101] D.N. Allsopp, R.I. Trezona, I.M. Hutchings., *Tribology Letters* **5**, 259 (1998).

[102] A.H. Jones, *Wear* **258**, 942 (2005).

[103] H.C. Meng, K.C. Ludema, *Wear* **181-183**, 443 (1995).

[104] J.F. Archard, *J. App. Phys.* **24**, 981 (1953).

[105] M.G. Gee et al., *"Interlaboratory Exercise Description and Procedure," Rep. No. MATC(D)170* (NPL, 2003).

[106] M.G. Gee *et al.*, *Wear* **259**, 27 (2005).

[107] P.A. Swanson, *Tribology* **ASTM STP 1199**, 80 (1993).

[108] K. Van Acker, D. Vanhoyweghen, R. Persoons, J. Vangrunderbeek, *Wear* **258**, 194 (2005).

[109] M.A.Moore, Laboratory simulation testing for service abrasive wear environments. In: Ludema KC, editor. Wear of materials 1987. New York: ASME, 673 (1987).

[110] P.A. Swanson, R.W. Klann. Abrasive wear studies using the wet and dry sand rubber wheel tests. In: Rhee SK, Ruff AW, Ludema KC, editors. Wear of Materials. New York: ASME 379-389 (1981)

[111] A.J. Gant, M.G. Gee, A.T. May, *Wear* **256**, 954 (2004/5).

[112] M.A. Moore, *J. Agric. Eng. Res.* **20**, 167 (1975).

A.1 Typical MSAW wear calculation example from spreadsheet

A.1.1 Test parameters

	Values	Units
Ball diameter:	25.4	*mm*
Circumference (2.pi.r):	79.80	*mm*
Ball volume:	8.580	m^3
No. Rotations:	**627**	-
Sliding distance:	50.03	*m*
RPM:	**100**	*rpm*
Test time:	376.2	*s*
Sliding speed:	0.1330	*m/s*

Table A 1

A.1.2 Wear crater measurement and calculation of κ

Sample: Boron Steel (BS2)	**Applied Load (L)**				**Units**
Abrasive: SiC (80g/100ml water)	**0.2**	**0.4**	**0.6**	**0.8**	***N***
Ave diameter:	0.00144	0.001635	0.00174	0.00184	*m*
Volume removed (V):	1.66E-02	2.76E-02	3.54E-02	4.43E-02	mm^3
Volume per unit slide:	3.32E-04	5.52E-04	7.08E-04	8.85E-04	mm^3/m
Spec. wear rate (κ):	1.66E-03	1.38E-03	1.18E-03	1.11E-03	$mm^3/N/m$

Table A 2

Where:

Average diameter calculated from SEM measurements
Volume removed calculated from Equation 1 (Chapter 4)
Volume per unit slide calculated from ball diameter and number of revolutions
Specific wear rate calculated from Equation 2 (Chapter 4)

A.1.3 Regression Analysis

Analysis of the four values κ values is performed to obtain an average κ, i.e. the gradient

Gradient	0.000908017
St error	4.51167E-05
r^2	0.99508666

Table A 3

A.2 Typical MLM calculation for born steel

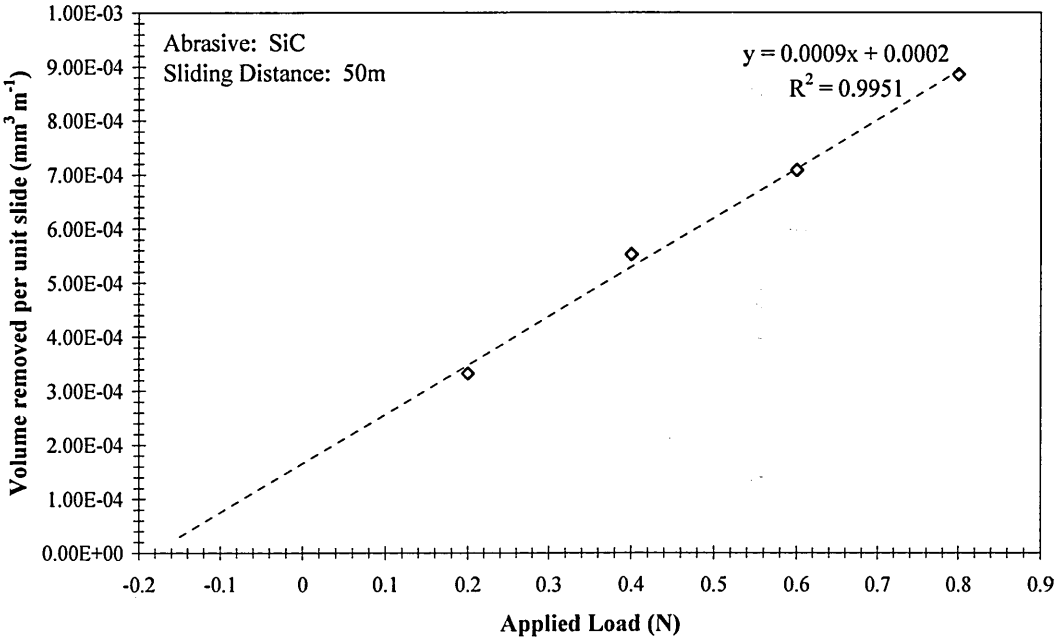

Figure A 1: Boron steel analysis MLM

A.2.1 Schematic diagrams of soil working tools used in field trials

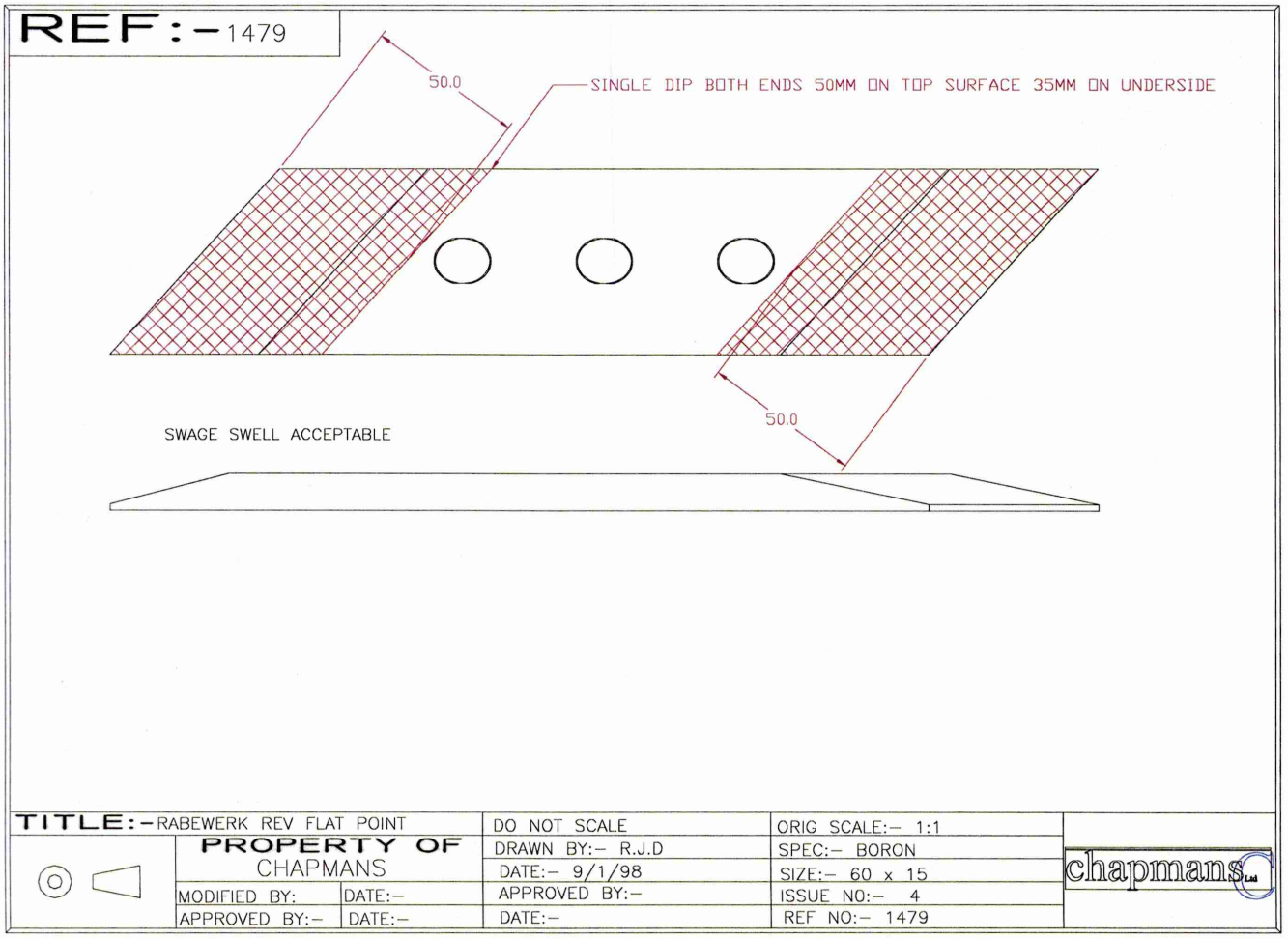

Figure A 2: Schematic diagram of reversible point.

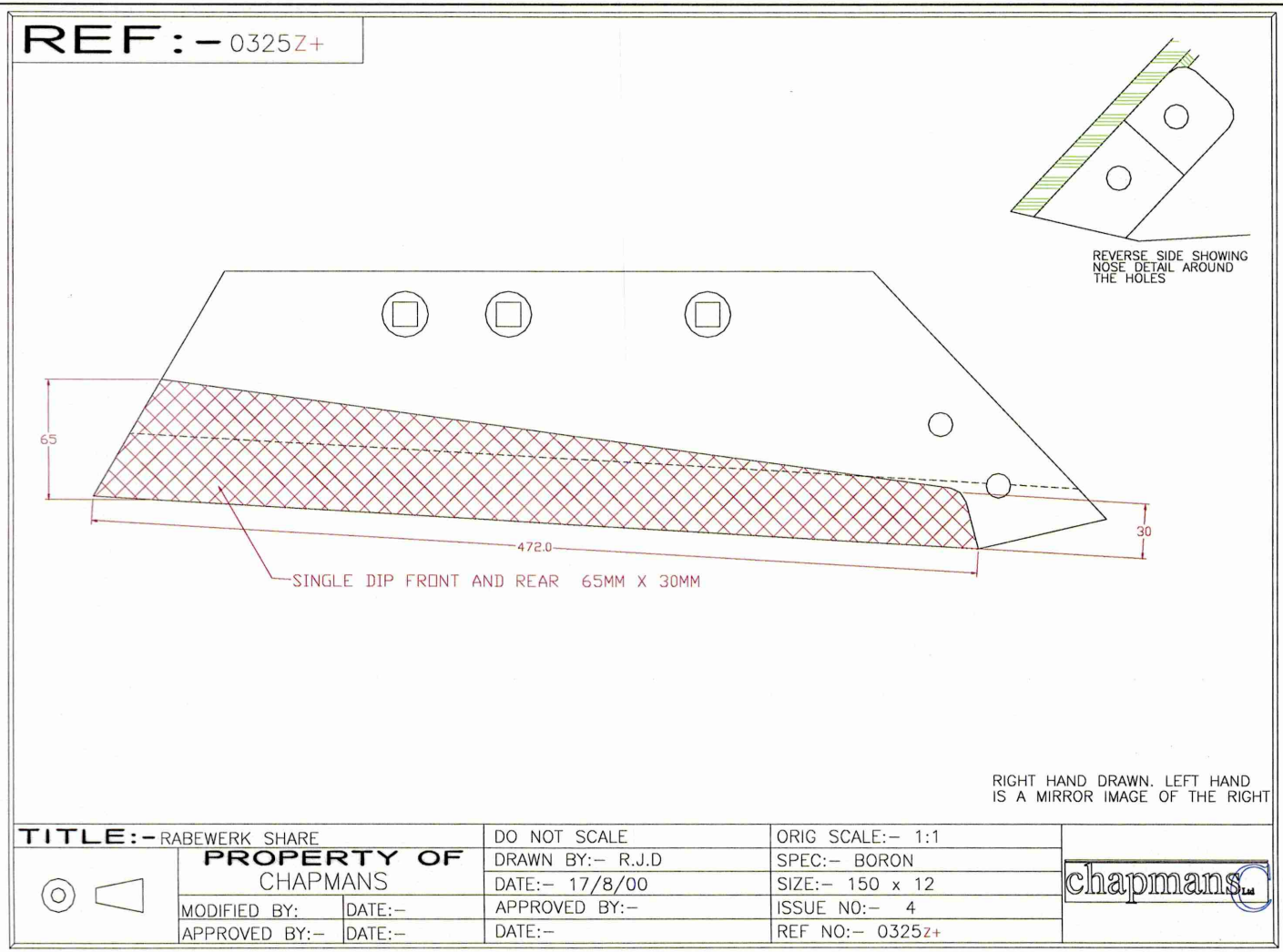

Figure A 3: Schematic diagram of a share.

A.2.2 Global soil classifications

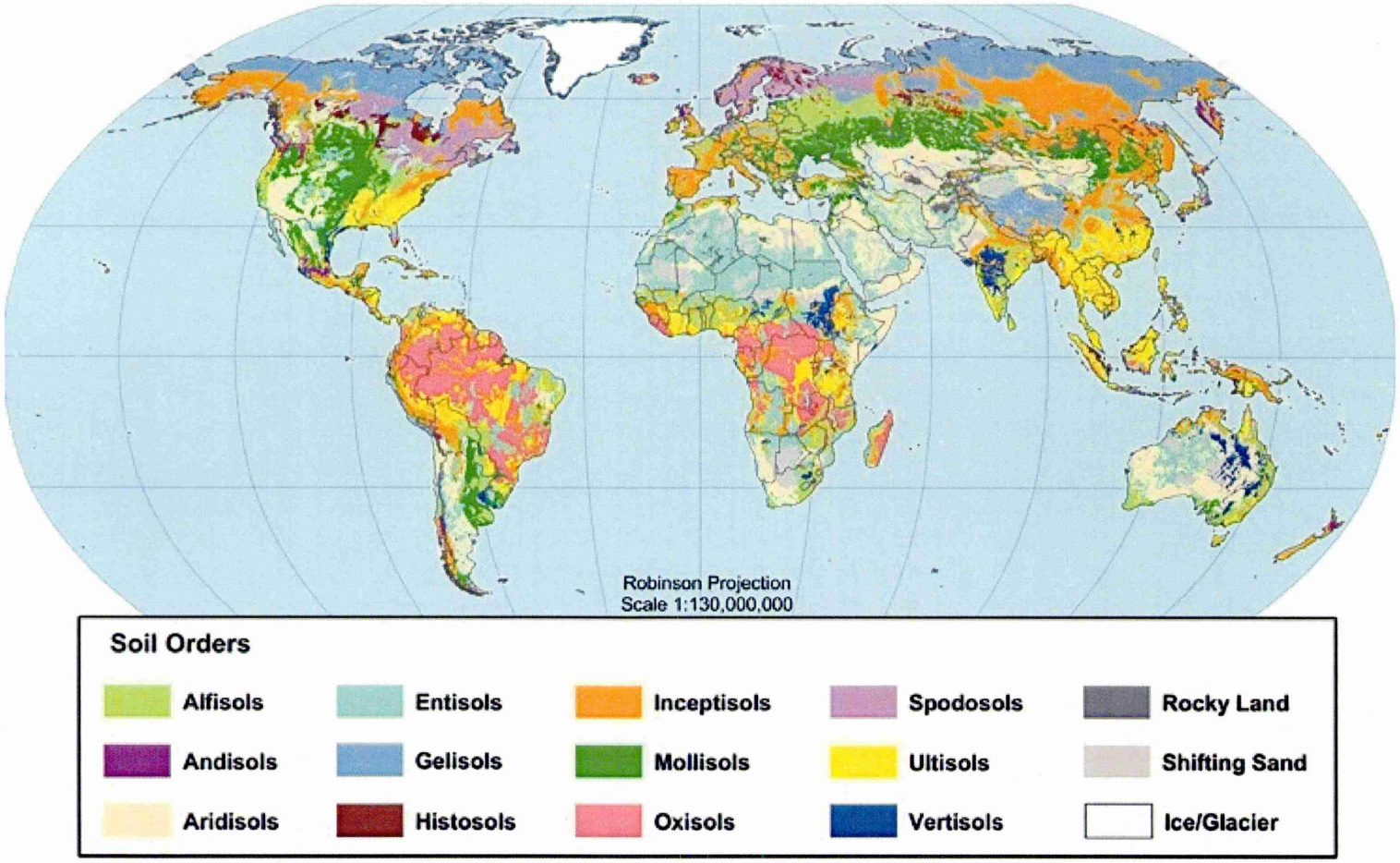

Figure A 4: Global soil classifications from US Department of Agriculture.

A.2.3 Classification of soil type by comparison of particle sizes

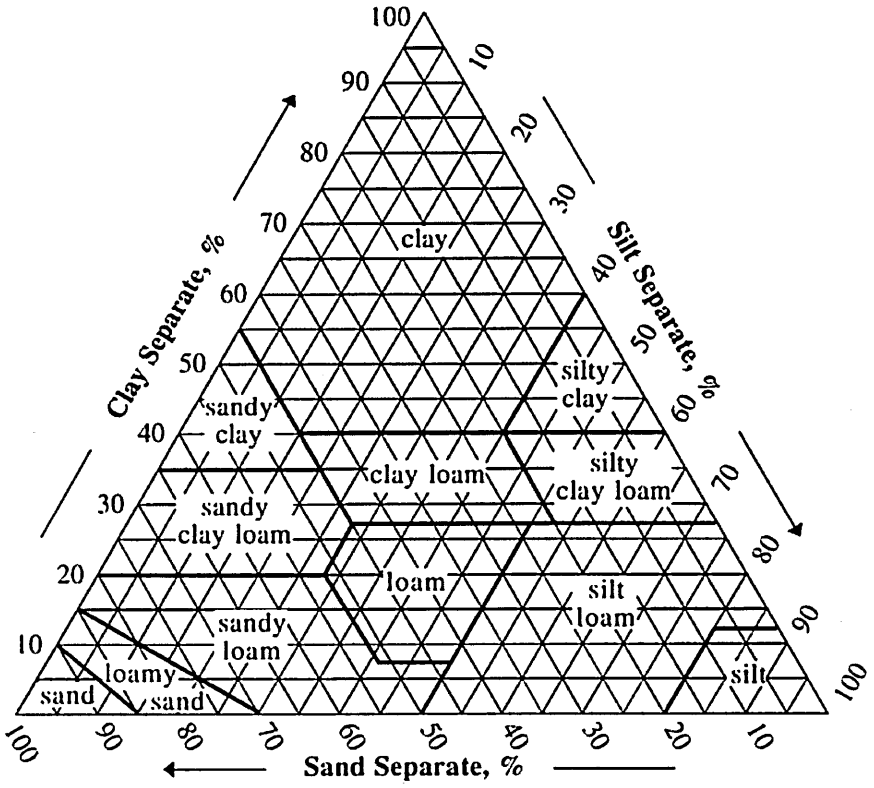

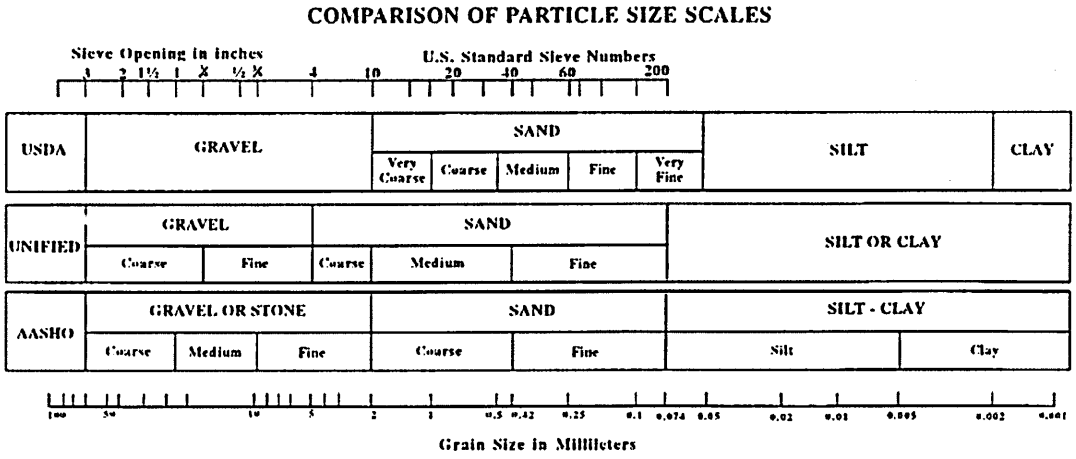

Figure A 5: Classification of soil type from US Department of Agriculture.

A.3 Typical reversible point material loss

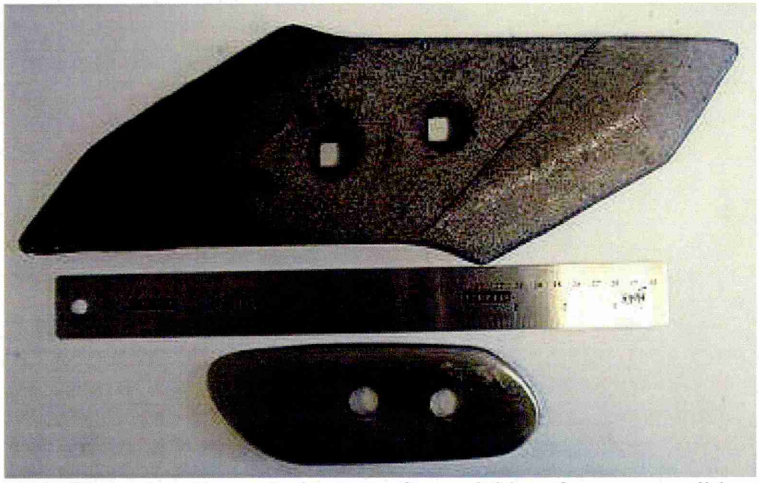

Figure A 6: Photo showing typical extent of material loss from a reversible plough.

A.4 Photographs of worn tools from September 2006 Trial

Figure A 7

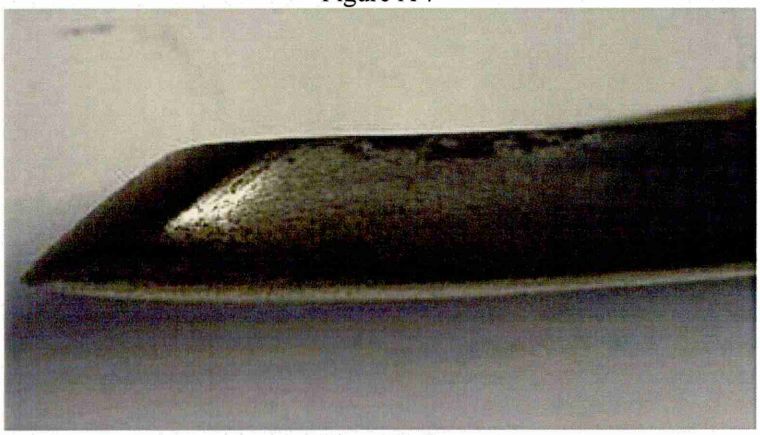

Figure A 8

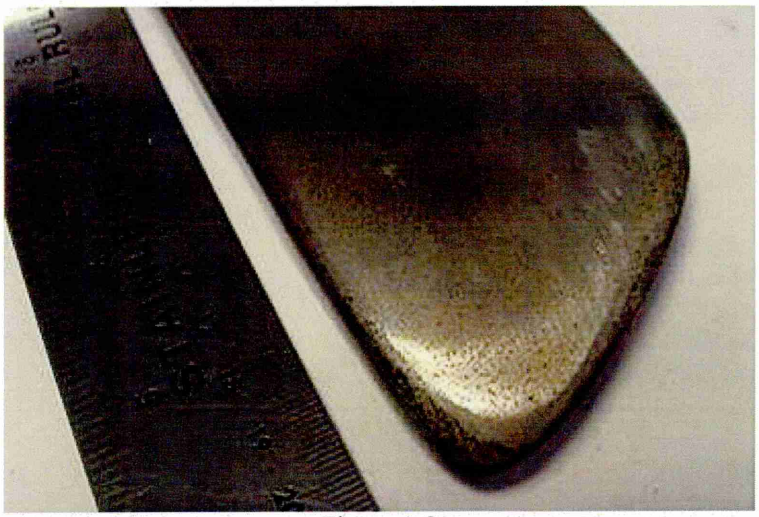

Figure A 9

Figure A 10

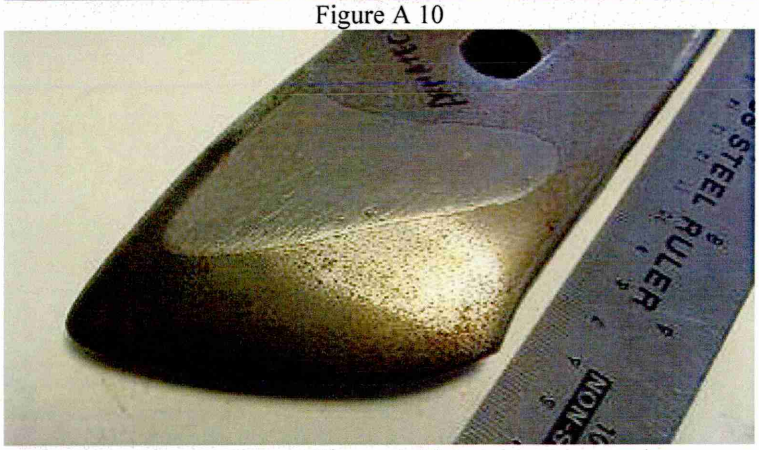

Figure A 11

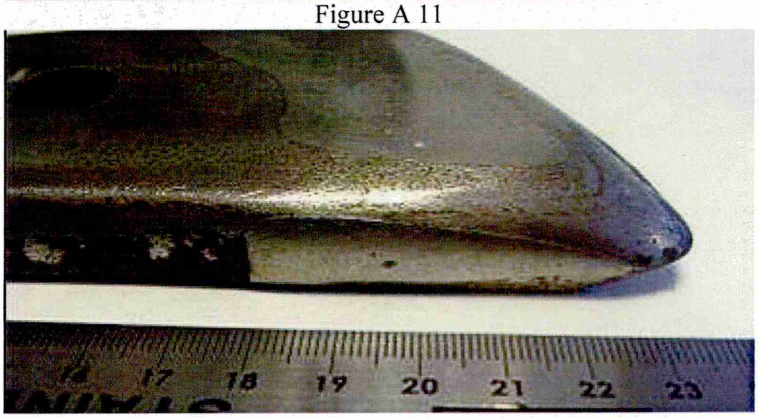

Figure A 12

Figure A 13

Figure A 14

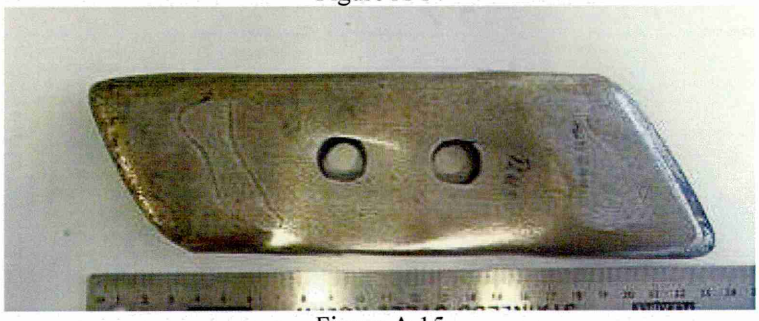
Figure A 15

Figure A 16

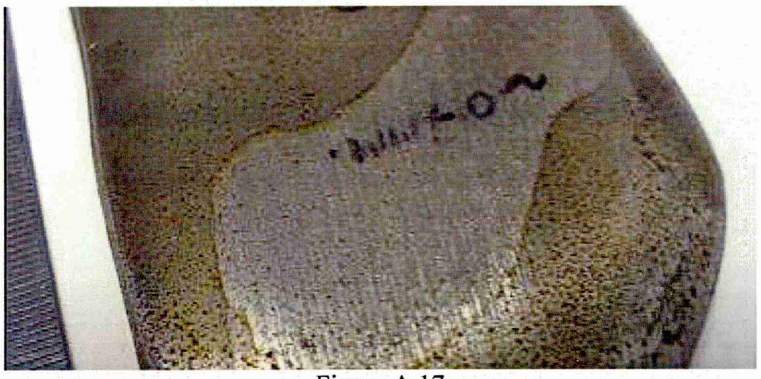

Figure A 17

Figure A 18

1.6 *Photographs of worn tools from March 2007 Trial*

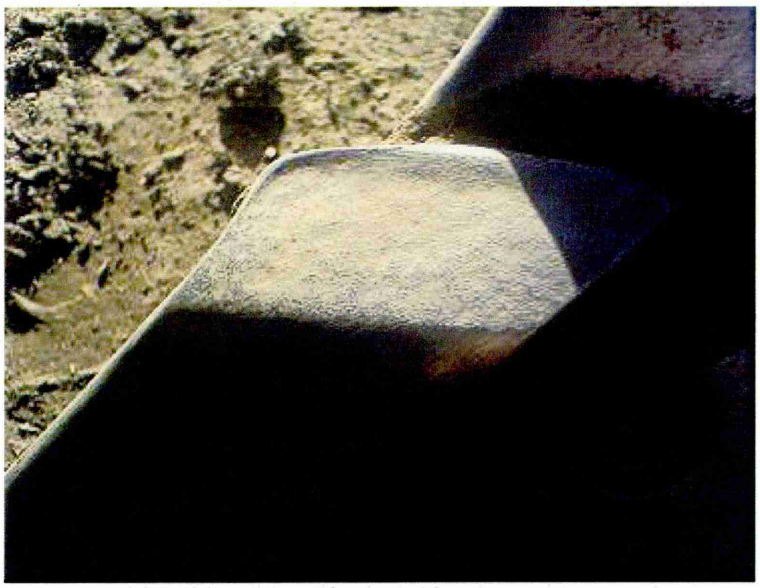

Figure A 19

Figure A 20

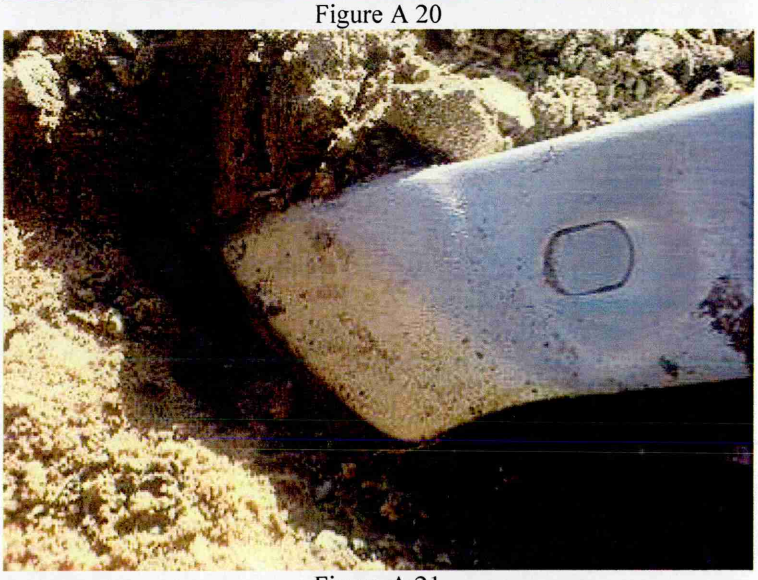

Figure A 21

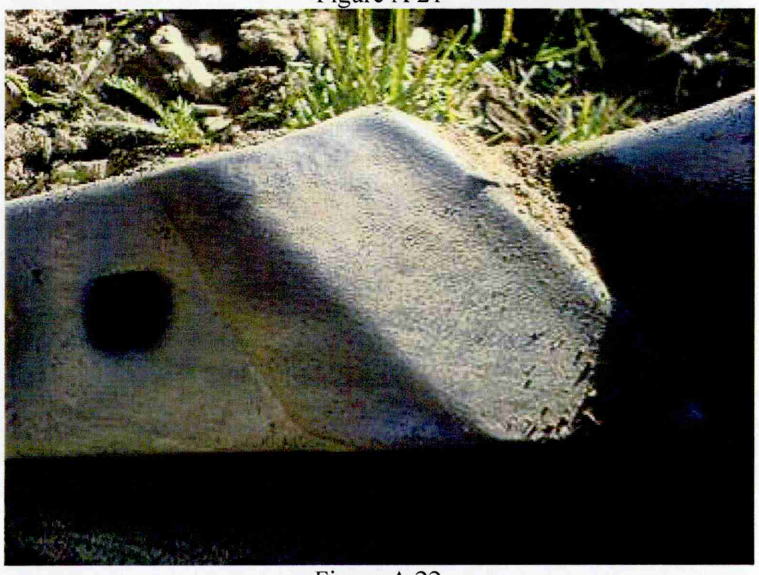

Figure A 22